Integration of the Design and Manufacture of Gradient-Index Optical Systems

by
Julie Lynn Bentley

Submitted in Partial Fulfillment
of the
Requirements for the Degree
Doctor of Philosophy

19961125 058

Supervised by
Professor Duncan T. Moore
The Institute of Optics
The College
School of Engineering and Applied Sciences

University of Rochester
Rochester, New York

1995

Curriculum Vitæ

The author was born in Jamestown, New York on March 20, 1968. She attended the University of Rochester from 1986 to 1990, and received her Bachelors degree in Science with Honors and Distinction in May, 1990. In the fall of 1990, she entered the doctoral program at The Institute of Optics of the University of Rochester. She received an Office of Naval Research fellowship in 1990, 1991, and 1992. She pursued her research in gradient-index optics under the supervision of Professor Duncan T. Moore and during the course of her doctoral research received a Master of Science degree in optics in January, 1992.

Acknowledgments

I would like to sincerely express my appreciation to the following people and organizations for their support during the course of my research:

To my advisor, Prof. Duncan Moore, for his guidance, support and constant encouragement throughout both my undergraduate and graduate years at the University of Rochester; for the speed with which he processed this manuscript, and for providing the many opportunities to travel to new places and experience new things over these past years;

To Dr. Doug Kindred for being both a valued friend and mentor from my first day as an undergraduate in the gradient-index group, for his interest and enthusiasm in my work, and for his extreme generosity with his time, advice, and general knowledge of both optics and glass science throughout my years here;

To the Office of Naval Research, the Army Research Office, the William H. Price Memorial Scholarship Fund, and the ASCO foundation for their generous financial support;

To Ray Hensler for melting several of my glass compositions and for the many insightful discussions on glass melting and glass science;

To Corning Engineering Laboratory Services, Corning Glass Works, Corning, New York, for their glass composition measurements;

To Kurt Kubath and Alex Maltsev for their knowledge and skill in the (timely) preparation of several of my samples;

To Brian McIntyre for his wide expertise in fixing computer problems and for always taking the time to help me fix mine when I really needed it;

To Sandy Anderson and Jean Conge for both their friendship and helpfulness in administrative matters;

To my fellow students in the gradient-index group, especially:

Mary Kate Crawford for graciously volunteering to proofread this thesis, for always being there during those last minute crises, and for providing such extremely helpful suggestions,

Chris Saxer for his vast knowledge of interferometry and index profile measurement and for being such a great tour guide in Switzerland,

Todd Tomkinson for the many discussions about optics and for having an incredible new story to laugh at each day,

Jennifer Rouke for her help with the experiments in the borate glasses, for being such a great office mate, and for always being there when I needed someone to eat lunch with,

Curtis Harkrider for his help with the titania silicate glasses (including a number of last minute experiments and measurements), for continuing this research, and for his infinite supply of Diet Coke,

And especially to Sarah DeJager for her help with numerous experiments which ultimately saved me a lot of time (I think everyone should have such a great undergraduate assistant);

To all the faculty, staff, and students of the Institute of Optics for their friendship and encouragement throughout my years here, especially:

My classmates, Karen Moore and Amy Bieber for always being there when I needed anything from friendship to advice in optics, and especially for sticking it out with me through all the homework, exams, and general ups and downs of research,

Abstract

Modern manufacturing incorporates fabrication constraints and quality control into the initial product design to create competitive, cost-effective products. This research offers a design-for-manufacture approach to gradient-index lens production. Fabrication parameters are coupled to a lens design program to eliminate the traditional trial-and-error manufacturing process. The new approach allows a lens designer to design a gradient-index optical system in terms of the actual fabrication parameters and then provides a set of experimental specifications to the materials scientist. The result is a more efficient and cost-effective manufacturing process for gradient-index optical systems.

Traditional gradient-index design methods were developed before many of the current gradient-index materials were available and are therefore unrelated to the material fabrication parameters. For example, the index of refraction profile is typically expressed by a polynomial expansion in optical design. Once a lens is designed with this representation, the manufacturer must guess at fabrication parameters such as time and temperature to obtain the required Δn, depth, and profile shape. As a result, the design-to-manufacture process is slow and iterative.

Therefore, a more efficient design-for-manufacture approach is offered by this research. First, a mathematical model for gradient-index fabrication by ion exchange is developed using Fickian diffusion theory. Second, an experimental procedure is developed to test this model against experimental results for several different diffusion times and temperatures in both axial and radial sample geometries. In particular, empirical diffusion models are developed for Li^+ for Na^+ and Na^+ for Li^+ ion exchange in alumina silicate glasses, alumina borate glasses, and titania silicate glasses. Third, the model is integrated with a lens design program to allow optimization on diffusion parameters and several sample designs are presented which compare the old design procedure with this new method of design. Thus, with the completion of this research, a lens designer can now choose from a realistic set of gradient-index glasses and, in turn, generate a complete set of experimental specifications for the production of the gradient.

Table of Contents

List of Tables

List of Figures

Chapter I

Introduction/Background

Preface

Industry recognizes that a design-for-manufacture approach is essential for creating competitive, cost-effective products. Modern manufacturing methods incorporate fabrication constraints and quality control into the initial product design to create a much more efficient manufacturing process. Nevertheless, few design-for-manufacture techniques exist in optics; traditional lens fabrication methods use numerous labor-intensive processing steps. Consequently, computer-integrated manufacturing of conventional lens systems is currently being explored, [1] but this process has not yet been extended to include nonconventional optical systems such as those which utilize gradient-index materials.

A gradient-index optical system contains inhomogeneous materials in which the refractive index changes continuously throughout the medium. Design studies of optical systems employing gradient-index materials indicate that a gradient can reduce the required number of lens elements or improve the system performance by providing additional optical power or aberration correction. Unfortunately, the added benefits of gradient-index lenses are often weighed against the added complexity of fabricating the material. In particular, traditional design techniques use gradient

specifications that are unrelated to the material fabrication parameters. This leads to an iterative manufacturing process which can be both difficult and time-consuming.

The research presented in this thesis offers a design-for-manufacture approach to gradient-index lens production. Fabrication parameters are coupled to a lens design program to eliminate the traditional trial-and-error manufacturing process. The new approach allows a lens designer to design a gradient-index optical system in terms of the actual fabrication parameters and then provides a set of experimental specifications to the materials scientist. The result is a much more efficient and cost-effective manufacturing process for gradient-index optical systems.

1.1 Introduction

Imaging systems incorporating gradient-index elements have been studied for over a century. In 1854, Maxwell published the first example of a lens designed with an index of refraction gradient. [2] Late in the nineteenth century, Exner observed that insect eyes were composed of tiny, naturally occurring gradient-index rods. [3] Shortly thereafter, Schott developed the first method to manufacture gradient-index materials by applying a differential cooling technique to glass. [4]

Widespread interest in gradient-index lenses emerged with the invention of the computer and the subsequent ability to efficiently trace rays through gradient-index materials. This generated several papers concerning gradient-index design, [5,6,7] but most of the early raytrace and aberration theories were based on hypothetical materials. [8,9,10] At that time, only a small number of gradient materials existed, and even fewer were completely characterized. This resulted in the development of a mathematical representation for the optical properties of the gradient that was unrelated to the fabrication process parameters. Thus, designers could determine the type of gradient needed for a particular lens configuration, but could not incorporate manufacturing constraints into the design.

Currently, the gradient-index optical systems which are commercially available include collimators, fiber couplers, endoscopes, and unit magnification lens arrays for compact photocopy or facsimile machines.

[11,12,13,14,15] Although gradient-index elements have also been incorporated into the designs of photographic objectives, binoculars, microscopes, and zoom lenses, [16,17,18,19] only a few of these systems have ever been fabricated. [20] Even with the recent development of new materials, researchers continue to use design techniques which make the implementation of these types of designs difficult and sometimes impractical.

1.2 Gradient-Index Optical Design

The index of refraction variation of a gradient-index lens is usually written as a function of spatial coordinates and then categorized according to the shape and orientation of its isoindicial surfaces. For example, the two most common types of index of refraction profiles, the axial gradient and the radial gradient, are shown in Fig. 1.1. The shading indicates both the orientation of the gradient with respect to the optical axis and the change in refractive index across the lens.

(a)   (b)
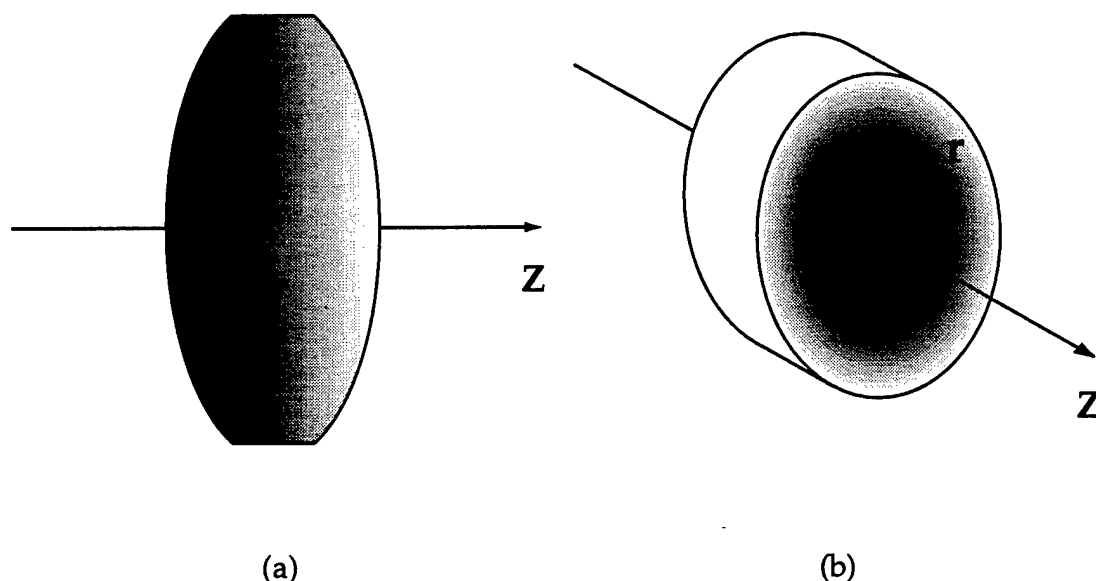
Figure 1.1 Orientation of the index of refraction gradient with respect to the optical axis, Z for (a) an axial gradient and (b) a radial gradient. The shading indicates the change in refractive index across the lens.

In optical design and third-order aberration analysis, the index of refraction profile of a gradient-index element is usually expressed by the polynomial expansion given by Sands, [21]

$$N(r,z) = \sum_{i=0}^{\infty} r^{2i} \left(\sum_{j=0}^{\infty} N_{ij} z^j \right)$$
(1.1)

where z is the distance along the optical axis (measured from a reference plane) and r is the radial distance from the optical axis. The N_{ij} coefficients of this expansion offer extra degrees of freedom to the lens designer. For example, the index of refraction gradient may contribute to the optical power of a lens system and/or help in aberration correction.

The N_{ij} coefficients of the gradient expansion also vary with the wavelength of light. Similar to a homogeneous dispersion, a gradient-index Abbe number is defined for each coefficient as [22]

$$V_{ij} = \frac{N_{ij_d}}{N_{ij_F} - N_{ij_C}} \quad \text{except for } i = j = 0$$
(1.2)

where d, F, and C refer to the spectral lines of helium and hydrogen (587.6, 486.1, and 656.3 nm respectively). For $i = j = 0$, Eq. (1.2) is replaced by the traditional Abbe number,

$$V_{00} = \frac{N_{00_d} - 1}{N_{00_F} - N_{00_C}}$$
(1.3)

where V_{00} is often referred to as the homogeneous dispersion, or V_d, and N_{00_k} is the index of refraction of the base glass at the kth spectral line.

It is sometimes more convenient to define a second gradient-index Abbe number in terms of the total change in the refractive index, or Δn, at the d, F, and C wavelengths as [23]

$$V_{grin} = \frac{\Delta n_d}{\Delta n_F - \Delta n_C} .$$
(1.4)

Each Δn is determined from the measurement of the gradient-index profile at that particular wavelength. Previous results show that the range of measured V_{grin} values (10 to ∞ and $-\infty$ to -100) extends well beyond the

range of Abbe numbers for homogeneous glasses (20 to 80). [24] Unlike designs of homogeneous lens systems, the existence of negative V_{grin} numbers allows for color-corrected gradient-index systems which contain only positive elements. [25] This reduces the power required from each individual element and can therefore significantly reduce the total aberrations of the system.

1.2.1 Axial Gradient

In an axial gradient, the surfaces of constant index are planes perpendicular to the optical axis so that all terms containing r in Eq. (1.1) are zero. The index of refraction profile may then be expressed as a Taylor series in z,

$$N(z) = N_{00} + N_{01}z + N_{02}z^2 + \ldots \tag{1.5}$$

where z is the distance measured along the optical axis. If the reference plane from which z is measured is placed in the homogeneous region of the gradient profile then in this equation, N_{00} represents the index of refraction of the base glass.

The addition of curvature to an axial gradient causes the refractive index value to change with the height of the incident ray at the surface. In terms of optical path, this type of lens resembles an asphere and many of
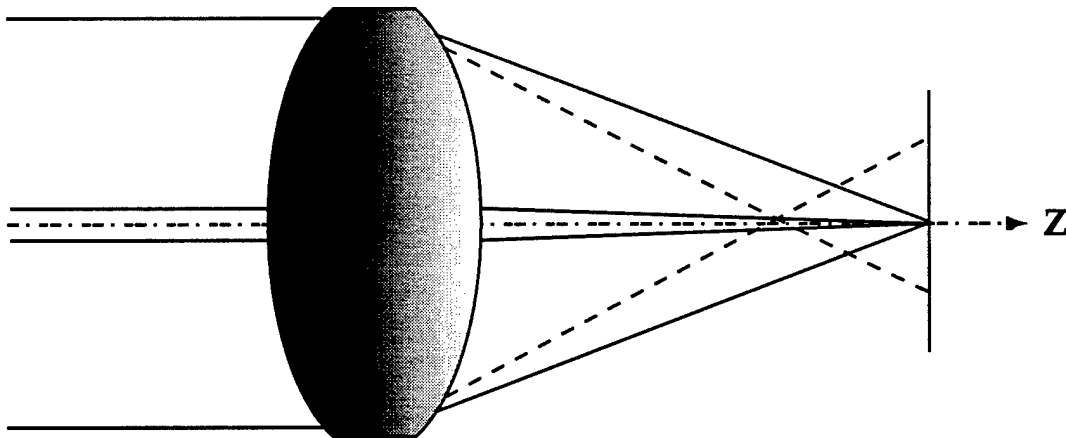
Figure 1.2 Illustration of the use of an axial gradient to correct the third-order spherical aberration of a singlet. The dashed line represents the marginal focus of the singlet without the gradient.

the design techniques applied to aspheres can be extended to axial gradients. For example, placing an axial gradient in a homogeneous singlet corrects the third order spherical aberration of the lens. Figure 1.2 illustrates the change in focus of the marginal ray with the addition of the axial gradient.

In the past, axial gradients have been incorporated into many different types of lens systems. Linear axial gradients have been used to correct the spherical aberration of single-element collimators, [26] while in more complex systems axial gradients have been used to correct other aberrations, such as distortion in eyepieces. [27] Previous designs have also shown that the total number of elements in an optical system can be reduced by including an axial gradient in the design. For example, a two element gradient-index binocular objective has been designed to replace a three element homogeneous lens in the U.S. Army M-19 binocular. [28]

1.2.2 Radial Gradient

In a radial gradient, the isoindicial surfaces are concentric cylinders about the optical axis so that all terms containing z in Eq. (1.1) are zero. The index of refraction profile is then given by the even-powered Taylor series in r, the radial distance from the optical axis,

$$N(r) = N_{00} + N_{10}r^2 + N_{20}r^4 + \dots \quad . \tag{1.6}$$

Materials with nonzero r^2 terms introduce optical power upon transfer through the lens. As shown in Fig. 1.3 (a), this allows radial gradient-index elements with only plane parallel surfaces to form images. The entire optical power is due to the gradient and for thin lenses is approximated by

$$\Phi = -2N_{10}t \tag{1.7}$$

where t is the thickness of the lens. This type of lens is commonly known as a Wood lens. [29]

Due to their unique property of having optical power without curved surfaces, small diameter radial gradient focusing rods were the first commercial application of gradient-index materials. Selfoc™ rods of this type have been available from Nippon Sheet Glass Company (NSG) for

(a)   (b)
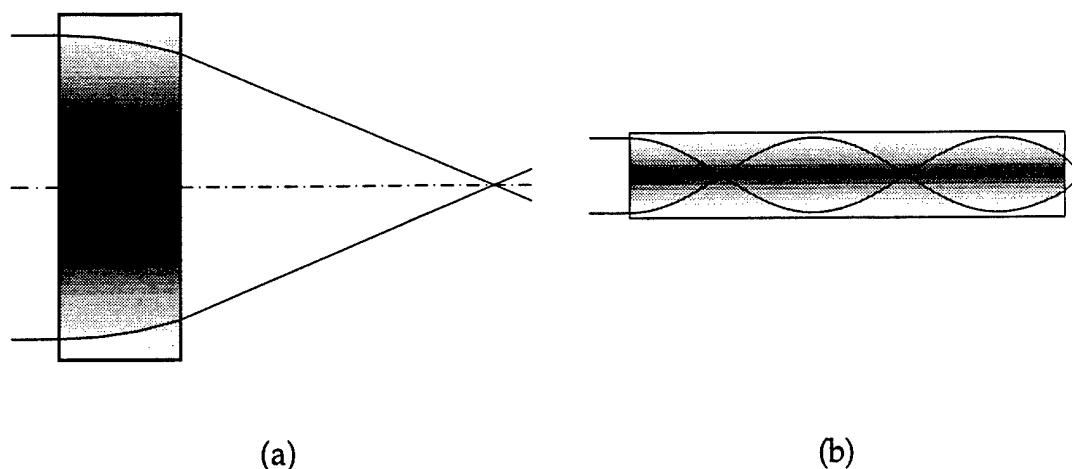
Figure 1.3 Illustration of two types of radial gradients: (a) a thin Wood lens demonstrating its ability focus light and (b) a long radial gradient-index rod showing the sinusoidal ray paths within the material.

over two decades. [30] Currently their widest application is in unit-magnification lens arrays for desktop copiers and fax machines where a wide field of view is desired for short conjugates. They are arranged in linear arrays of two rows and used to scan the document rather than image the entire document at once.

A second emerging commercial market for gradient-index materials is in the area of endoscopic instruments. [31] Many different medical procedures use a small-diameter endoscope to relay an image of the inside of the body to an outside observer. The optical system of the instrument usually consists of three separate subsystems: the objective, the relay, and the eyepiece. The objective forms an image which the relay system transfers across the length of the scope to the eyepiece. This usually requires several identical relay stages, each of which is composed of a series of homogeneous lenses that form an image at unit magnification. As illustrated in Fig. 1.3 (b), rays in long gradient-index rods traverse sinusoidal path lengths within the material, creating several intermediate image locations. Thus, a single gradient-index rod can also function as the instrument's relay system.

Shown in Fig. 1.4 is one stage of a relay system that might be used in (a) a typical endoscope and (b) an equivalent gradient index rod. For a
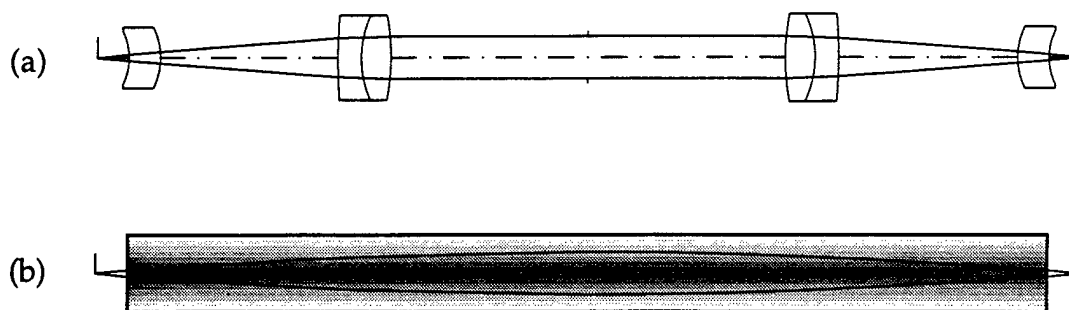
Figure 1.4 One stage of a unit-magnification endoscope relay: (a) a typical homogeneous
relay system and (b) an equivalent gradient-index relay system.

particular application, the length of the instrument determines how many
relay stages are required. Since most endoscopes have at least three of
these stages, there are a large number of small lenses to manufacture, coat,
and align in homogeneous designs. In contrast, a gradient-index relay
system consists of a single gradient-index rod and results in a much lower
fabrication cost.

In addition to their current commercial applications, radial gradients
have been incorporated into many other types of optical designs. Lens
systems which derive most of their optical power from the gradient
contribution have been shown to have significantly lower third-order,
monochromatic aberrations. For example, the aberrations of a gradient-
index eyepiece tend to be half that found in analogous homogeneous
systems. [32] In other designs, a radial gradient can reduce the number of
elements needed to meet a particular design specification. For example, a
single radial-gradient element with curved surfaces can replace as many as
three homogeneous elements and yield equivalent imaging performance.
[33] Haun has also recently developed a set of equations which utilize the
surface contribution of the radial gradient instead of relying on the
gradient's power contribution to minimize third-order monochromatic
aberrations. He then applied these equations to the design of high-speed
singlets for compact disc objectives. [34]

1.3 Gradient-Index Fabrication

Gradient-index lenses are manufactured in glass, plastic, and crystal materials using a wide variety of techniques. The most common method is ion exchange, but the diversity of the fabrication methods includes glass fusion, [35] sol-gel processing, [36, 37] chemical vapor deposition, [38] and Czochralski crystal growth. [39] Glass fusion produces gradients with large index changes (0.3) over relatively large distances (10 mm), but is limited to an axial geometry. Recent studies of sol-gel materials show promising results for radial gradients, but require a large number of delicate processing steps. Chemical vapor deposition is widely used to manufacture gradient-index fibers, but is limited to small geometries because of thermal expansion problems encountered during the fiber pulling process.

Ion exchange is a well-known process used in both the fabrication of waveguide devices for photonic applications [40] and the chemical strengthening of glass. [41] Ion exchange is also the prevailing method for commercial production of gradient-index materials. [42, 43] The manufacturing process is relatively uncomplicated and can be used for either an axial or a radial geometry. The main disadvantage is that long diffusion times are required for large penetration depths. This is one of the principal reasons why the current commercial success of gradient-index technology lies in the area of small-diameter optics.

1.3.1 Gradient-Index Glass

A wide variety of homogeneous glasses with different indices of refraction (1.5-2.0) and dispersions (20-80) are currently available to the lens designer. Unfortunately, attempts to make gradients by ion exchange in commercial optical glasses met with very limited success. [44, 45] This led to the development of special glasses specifically designed for ion exchange. For example, Nippon Sheet Glass Company of Osaka, Japan currently manufactures their own custom thallium silicate glasses in which radial gradient-index rods are fabricated by K^+ for Tl^+ ion exchange. Bausch and Lomb and University of Rochester also developed a special
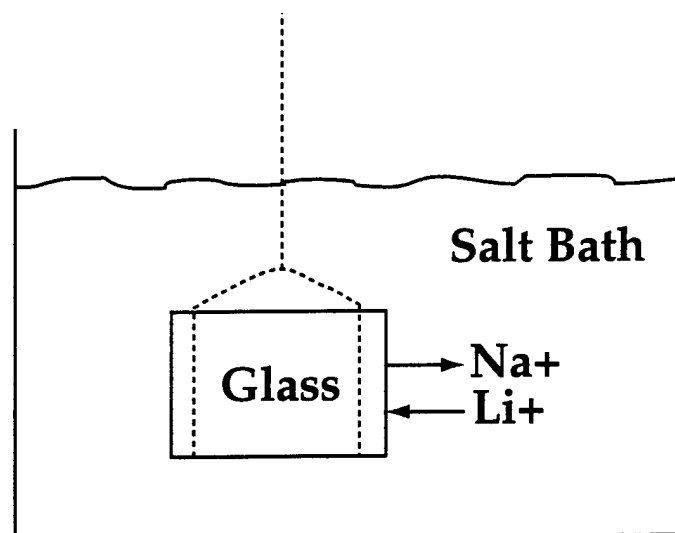
Figure 1.5 Illustration of a typical ion exchange experiment: a glass sample containing Na^+ ions is suspended in a molten salt bath which contains Li^+ ions.

alumina silicate glass that was used mainly in the fabrication of axial gradients by Ag^+ for Na^+ exchange. [46]

Thus, to take advantage of the additional degrees of freedom offered by gradient-index materials, a large number of gradient-index glasses must also be available to the lens designer. Kindred recently expanded the range of existing materials by developing several new gradient-index glasses whose compositions were specifically tailored for large exchange rates. [47] These glasses include titania silicates, alumina silicates, tantalum silicates, and silver phosphates. The large range of base glass compositions offers a wide variety of gradient properties such as Δn, gradient dispersion, and profile shape.

1.3.2 Ion Exchange Experiments

In a typical ion exchange experiment, a homogeneous glass is fabricated with a specified concentration of one of the following single-valent ions: K^+, Li^+, Na^+, Ag^+, or Tl^+. As shown in Fig. 1.5, a small sample of the glass is suspended in a molten salt bath containing another of the single-valent ions. The experiment is held at a particular temperature for a set period of time, during which an interdiffusion of ions occurs due to the

concentration gradient across the boundary. After the specified amount of time, the glass is removed from the molten salt and cooled slowly to room temperature. The exchange of ions between the glass and the salt bath produces a concentration gradient of both diffusing species in the glass sample. The concentration profile results in a corresponding index of refraction profile since the refractive index of the glass is a function of concentration.

1.3.3 Index of Refraction Profile Control

In gradient-index manufacturing, it is important to understand how to manipulate the various fabrication parameters to obtain a particular index of refraction profile. The three basic specifications for the gradient profile are the refractive index difference (Δn), the diffusion depth, and the profile shape. Each of these specifications can be related to typical ion exchange manufacturing parameters. For example, the main determinant of the maximum possible Δn is the choice of glass/salt combination [48] while the diffusion depth is a function of both temperature and time. The third specification, profile shape, is often the hardest to classify since it is affected by several experimental conditions. These include the size and geometry of the glass sample, the time dependence of the diffusant concentration at the glass/salt interface, and the concentration dependence of the diffusion coefficient of the glass/salt system.

In the past, manufacturers have had to use the results of at least one initial experiment and the relationships between profile specifications and fabrication parameters to determine the correct set of experimental conditions which would give the desired index of refraction profile. For example, if the optical design required a certain gradient profile depth and in the initial experiment the gradient depth was too shallow, then the diffusion time (or temperature) could be increased in the next experiment. Often, though, the three profile specifications become interrelated such that an attempt to change the experimental parameters to satisfy one condition changes the values of the other two. Thus, several trial-and-error type experiments are required to fabricate a particular index of refraction profile.

In addition, several of the manufacturing techniques can only be applied to very specific glass/salt systems. For example, the time-dependence of the diffusant concentration at the glass/salt interface is an important factor which can affect both the shape and the Δn of the final profile. During diffusion, the concentration of the glass cation increases in the salt bath which in turn affects the concentration of the salt bath cation at the glass surface. In some systems, this is viewed as a salt bath contamination because it results in an incomplete exchange and is often referred to as "poisoning of the melt." In other systems, the effects of outdiffusion become negligible; a large salt bath dilutes the outdiffused cations so that the actual concentration change at the surface is small, while a large equilibrium constant results in the glass having such a high preference for the salt bath cation that it is insensitive to salt bath composition changes.

Researchers have examined both types of systems by systematically changing the salt bath composition and then measuring the effect on the index of refraction profile. For example, Samuels studied the addition of several different salt bath components for a Ag^+ for Na^+ exchange in a sodium aluminosilicate glass. [49] The salt anion was shown to be a highly influential parameter for control over the index of refraction profile. In particular, her research showed that the oxyanion salts Ag_2SO_4 and Ag_2CrO_4 can be added to a AgCl salt bath to increase the equilibrium constant and therefore increase the maximum index change for this system. In contrast, both Haun and Kindred studied the effect of "poisoning" the salt bath for Li^+ for Na^+ and Na^+ for Li^+ exchange in an aluminosilicate glass. [50, 51] Kindred discovered that adding very small amounts (1-5%) of $LiNO_3$ to a $NaNO_3$ salt bath "poisoned" the bath and significantly decreased the total Δn, while Haun showed that large amounts (greater than 50%) of $NaNO_3$ must be added to a $LiNO_3$ bath before a large change in the final index of refraction profile can be obtained.

Researchers have also introduced external means to modify the index of refraction profile of a particular sample. These techniques include post annealing, field-assisted ion exchange, and microwave energy. In post

annealing, an ion-exchanged sample is held for a specified amount of time at an elevated temperature in the absence of a source of dopant concentration. [52] This effectively decreases the total Δn, increases the diffusion depth, and in some cases "smoothes" the index of refraction profile. Field-assisted ion exchange results in a larger diffusion depth over a shorter period of time since the application of an electric field to the glass-salt interface speeds the diffusion process. [53] In a similar manner, microwave energy has been applied to a glass sample during ion exchange to increase the diffusion depth in the sample. [54]

Thus, there are many different manufacturing techniques which can be used to fabricate a particular index of refraction profile, but each method requires prior knowledge of a set of experimental process parameters such as time, temperature, and glass composition. In optical design, however, the index of refraction polynomial coefficients used to characterize the gradient profile are unrelated to these parameters. This discrepancy results in a trial-and-error manufacturing process; it becomes difficult to apply the different fabrication techniques to a particular design when the fabrication parameters are not coupled into the design process.

1.3.4 *Fickian Diffusion*

A model for the gradient-index fabrication process can be developed using Fickian diffusion theory. In particular, the interdiffusion of ions which occurs during an ion exchange experiment may be described by the diffusion equation,

$$\frac{\partial C}{\partial t} = \nabla \bullet (D\nabla C) \tag{1.8}$$

where C is the concentration of the diffusing species, D is the diffusion coefficient, and t is the diffusion time. [55] Thus, the diffusion equation can be solved if the diffusion coefficient, the length of time for the diffusion, and the initial and boundary conditions for a particular sample geometry are given. The solution then describes how the concentration in the sample varies with position. Furthermore, if the index of refraction as

a function of concentration is known, the concentration profile can be related to an index of refraction profile.

The experimental process parameters are incorporated into the diffusion model through the initial condition, the boundary conditions, and the diffusion coefficient. Both the diffusion time and the ion concentration already appear as variables of the diffusion equation. The initial condition is determined by the ion concentration of the original glass sample while the boundary conditions are usually related to the salt bath concentration. Furthermore, time-dependent boundary conditions incorporate other manufacturing techniques such as "poisoning" of the salt bath and post-annealing. Finally, the diffusion coefficient is function of the temperature of the diffusion, and, for many gradient-index materials, is also a function of the concentration of the diffusing species. In particular, this concentration dependence can be related to both the original composition of the glass material and the choice of salt for the ion exchange experiment.

Solutions to the diffusion equation are strongly influenced by the concentration dependence of the diffusion coefficient. In some cases, such as diffusion in dilute solutions, D can be assumed to be constant (concentration independent), and then analytical expressions for the concentration profile may be obtained. However, for most gradient-index materials the diffusion coefficient is concentration-dependent, and, in general, the diffusion equation must be solved numerically.

Thus, Fickian diffusion theory presents a way to model the ion exchange process and predict future experimental gradient profiles when given a specific set of fabrication parameters. Furthermore, the direct integration of the experimental parameters into a diffusion model makes it easy to examine the effects of changes in those parameters on the index of refraction profile prior to performing the experiments.

1.4 Design-for-Manufacture Objectives of Thesis

It is now well-known that using gradient-index materials in optical systems gives a designer several extra degrees of freedom in the design process which are beneficial to the lens system. In addition to the

conventional parameters such as curvature and thickness, a designer can change the functional form of the index of refraction across the lens. In the past, the change in index of refraction across the lens was depicted by a polynomial in the design process. Mathematically, this representation was convenient since it allowed the simple calculation of the first- and third-order properties of the system, but it was not related to the manufacturing parameters. Consequently, it was difficult to fabricate a particular index profile that was designed with this type of representation.

The previous gradient-index design-to-manufacture process was slow and iterative. The designer asked for a particular profile and the manufacturer, after a number of experiments, obtained something similar. In most systems, the difference between the two profiles resulted in a decrease in optical performance and the lens system needed to be reoptimized. The new design usually required a slightly different profile and the entire process was repeated several times, taking several months to complete. A preferable method from a manufacturing standpoint would be to design the lens in terms of the actual fabrication parameters such as time, temperature, and salt/glass composition.

A more efficient design-for-manufacture approach is given by this research and can be divided into three sections:

- the development of a mathematical representation of the manufacturing process which uses Fickian diffusion theory to model gradient-index fabrication by ion exchange,

- a test of the model against experimental results for several different glass compositions, diffusion times, and temperatures in both axial and radial sample geometries,

- and finally the integration of the model with a lens design program to allow optimization on diffusion parameters.

With the completion of this research, a lens designer can choose from a realistic set of gradient-index glasses and, in turn, generate a complete set of experimental specifications for the production of the gradient.

The first part of this research is presented in Chapter 2 and formulates a mathematical model for the fabrication of gradient-index materials by ion exchange. An introduction into Fickian diffusion theory is given which shows how to apply this theory to ion exchange experiments. Several simple examples are used to demonstrate how manufacturing parameters can be incorporated into the diffusion equation through the initial condition, the boundary condition, and the diffusion coefficient. Then, variations in manufacturing parameters (such as diffusion time) are analyzed for their effect on the concentration/index of refraction profile. These examples also show the importance of the concentration dependence of the diffusion coefficient in determining the final concentration dependence in the sample.

In general, the concentration dependence of the diffusion coefficient must be found experimentally for each particular glass/salt pair. Thus, a discussion of the concentration-dependent diffusion coefficient is also given in Chapter 2. First, a well-known form for the concentration dependence of the diffusion coefficient is presented, but the historical treatment of this equation requires a time-consuming experimental measurement procedure. Therefore, a new analytic expression for the concentration-dependent diffusion coefficient is derived from statistical thermodynamics. This new theoretical model is called the Modified Quasi-Chemical (MQC) diffusion coefficient and can be used to determine the concentration dependence of the diffusion coefficient from a single ion exchange experiment. In particular, the new expression is shown to be very useful as a fitting function for noisy Boltzmann-Matano calculations of the diffusion coefficient.

Chapter 2 concludes with the development of a numerical routine that incorporates the new diffusion coefficient model, solves the diffusion equation, and calculates concentration profiles based on manufacturing parameters. The routine is formulated so that it is easily linked to a lens design program to allow optimization of the manufacturing process parameters for a particular design. Thus, a mathematical diffusion model has been realized which, given a set of experimental parameters, can

predict future concentration/index of refraction profiles prior to performing the experiment.

In the second part of this research, diffusion model solutions are tested against experimental results for Li^+ for Na^+ and Na^+ for Li^+ diffusions in several different types of glass. In particular, Chapter 3 gives the experimental procedure for testing the model in which glass melting, ion exchange experiments, and the measurement of index of refraction profiles are discussed. Furthermore, the mathematical diffusion model developed in Chapter 2 requires an empirical calculation of both the index of refraction and the diffusion coefficient as a function of concentration for each glass composition. Thus, Chapter 3 also gives the experimental procedure for these calculations and includes an error analysis for each step in the calculations.

Chapter 4 examines diffusions in a series of alumina silicate crown glasses with various amounts of alkali and alumina in the homogeneous glass composition. Previous results of $Li^+ - Na^+$ exchange in this type of glass show that it has favorable ion exchange properties including little or no divitrification and relatively fast diffusion rates. As a result, this type of glass is chosen to identify the parameters needed to change the mathematical diffusion model developed in Chapter 2 into a working empirical diffusion model. In particular, an empirical calculation of the diffusion coefficient and the index of refraction as a function of concentration is made for several different alumina silicate glass compositions. Ion exchange experiments are conducted in these glasses in both an axial and radial geometry for a range of different temperatures and diffusions times. Then, the measured index of refraction profiles are compared with the numerical solutions from the diffusion model.

Chapter 5 tests the diffusion model for other types of glasses to explore different regions of the glass map and to ultimately determine how well the model conforms to other glass compositions. First, $Li^+ - Na^+$ exchange in a series of alumina borate glasses is examined in axial geometry. The optical properties (such as index of refraction and dispersion) of these glasses are similar to the alumina silicate glasses. However, these glasses use boron as the glass former and there are large differences in the index of

refraction profiles. The diffusion model is tested for two different times, at the same temperature, in several different glass compositions of this series.

The second part of Chapter 5 examines two titanium silicate glass compositions which have a higher index of refraction and are more dispersive than the alumina silicates glasses. The first glass is a simple composition with only three components. The second glass has several additional components to see if the diffusion model can be applied to more complicated glass compositions. Axial diffusions in the two different glass compositions are examined over a relatively large temperature range. An empirical calculation of the diffusion coefficient as a function of concentration and temperature is made for these glasses, and then, the measured index of refraction profiles are compared with the numerical solutions from the diffusion model.

In the third part of this research, the diffusion model is integrated with a lens design program to allow optimization on diffusion parameters such as time and temperature. Preliminary research by Hoppe showed the feasibility of an optimization on diffusion parameters, but his method of solving the diffusion equation was limited to an axial geometry and experimentally he considered only one glass/salt pair. [56] Furthermore, Haun successfully investigated the radial geometry in a sol-gel material, but his model used a concentration-independent diffusion coefficient. [57]

In the first part of Chapter 6, the empirical diffusion model is linked to the lens design program, CodeV™. [58] By coupling the model with CodeV's design algorithms, a designer has access to a range of glass compositions, diffusion temperatures, and diffusion times within a particular glass/salt system. This allows the user to optimize an index of refraction profile for its Δn, depth, and shape in terms of manufacturing process parameters. Therefore, a designer can choose a particular glass composition and then explore a range of profiles without spending time developing something that cannot be manufactured. Furthermore, the new diffusion model allows for studies on the tolerances of the various diffusion parameters such as time and temperature. Typically, studies of gradient tolerances have utilized the polynomial index of refraction

coefficients and have been hard to relate to laboratory parameters. Thus, the new method gives manufacturers an idea as to what type of tolerances on the process parameters are required to fabricate specific optical systems.

In the second part of Chapter 6, several example lens designs with the diffusion model are presented. These include an axial gradient singlet, a radial gradient focusing rod, and gradient-index compact disc objective. For each lens system, the old method (using the index polynomial coefficients) and the new method (using manufacturing parameters) of design and optimization are compared and contrasted. These example designs demonstrate that the new diffusion model allows for the design of a variety of optical systems utilizing both axial and radial gradients and guarantees that the designs can be manufactured using current ion exchange technology.

References

1. Center for Optics Manufacturing, University of Rochester, Rochester, NY.

2. J. C. Maxwell, *The Scientific Papers of James Clerk Maxwell*, ed. W. D. Niven, New York, (1965).

3. K. Exner, "Zur Linsenformel. Linsenwirkung nicht homogener Korper," Annalen der Physik and Chemie **28**, 111-116 (1886).

4. H. Hovestadt, *Jena Glass and its Scientific and Industrial Applications.*, London (1902), pp. 66-70.

5. L. Montignano, "Ray tracing in inhomogeneous media," J. Opt. Soc. Am. **58**, 1667 (1968).

6. P. J. Sands, "Third-order aberrations of inhomogeneous lenses," J. Opt. Soc. Am. **60**, 1436-1443 (1970).

7. D. T. Moore, "Design of singlets with continuously varying indices of refraction," J. Opt. Soc. Am. **61**, 886-894 (1971).

8. R. K. Luneburg, *Mathematical Theory of Optics*, University of California Press, Berkeley (1966), pp. 164-195.

9. D. T. Moore, "Aberration correction using index gradients," M.S. Thesis, University of Rochester, Rochester, NY (1970).

10. E. W. Marchand, *Gradient Index Optics*. Academic Press, New York (1978).

11. Product guide, Nippon Sheet Glass America, Inc., Somerset, New Jersey.

12. D. C. Leiner and R. Prescott, "Correction of chromatic aberrations in GRIN endoscopes," Appl. Opt. **22**, 383-386 (1983).

13. Gradient Lens Corporation, Rochester, New York.

14. M. Kawazu and Y. Ogura, "Application of gradient-index fiber arrays to copying machines," Appl. Opt. **19**, 1105-1112 (1980).

15. J. D. Rees, "Non-gaussian imaging properties of GRIN fiber lens arrays," Appl. Opt. **21**, 1009-1012 (1982).

16. L. G. Atkinson et al., "Design of a gradient-index photographic objective," Appl. Opt. **21**, 993-998 (1982).

17. P. O. McLaughlin et al., "Design of a gradient-index binocular objective," Proc. Soc. Photo.-Opt. Instrum. Eng. **237**, 369-379 (1980).

18. D. P. Ryan, "Chromatic properties of index of refraction gradients in glass," Doctoral Dissertation, University of Rochester, Rochester, NY (1983), pp. 7-38.

19. D. Y-H. Wang, "Design methods for gradient-index optical systems," Doctoral Dissertation, University of Rochester, Rochester, NY (1992), ch. 6.

20. D. S. Kindred and D. T. Moore, "Design, fabrication, and testing of a gradient-index binocular objective," App. Opt. **27**, 492-495 (1988).

21. Reference 6.

22. D. P. Ryan-Howard and D.T. Moore, "Model for the chromatic properties of gradient-index glass," Appl. Opt. **24**, 369-379 (1980).

23. D. S. Kindred, "Development of new gradient index glasses for optical imaging systems," Doctoral Dissertation, University of Rochester, Rochester, NY (1990), pp. 2-3.

24. Reference 23, p. 16.

25. Reference 17.

26. D. T. Moore, "Design of a single element gradient-index collimator," J. Opt. Soc. Am. **67**, 1137 (1977).

27. J. D. Forer et al., "Gradient-index eyepiece design," Appl. Opt. **22**, 407-412 (1983).

28. J. B. Caldwell et al., "Gradient index binocular objective design," Appl. Opt. **25**, 3345-3350 (1986).

29. R. W. Wood, *Physical Optics*, Macmillan, NY (1905), pp. 71-77.

30. Reference 11.

31. Reference 13.

32. N. Haun et al., "Radial gradient-index eyepiece design," Appl. Opt. **27**, 3170-76 (1988).

33. Reference 16.

34. N. Haun, "Control of the gradient index profile using sol-gel processes," Doctoral Dissertation, University of Rochester, Rochester, NY (1992).

35. J. J. Hagerty et al., "Glass plate fusion for macro-gradient refractive index materials, " U.S. Patent 4,929,065 (1990).

36. J. B. Caldwell, "Sol-gel method for fabricating gradient index glass," Doctoral Dissertation, University of Rochester, Rochester, NY (1989).

37. Reference 34.

38. J. P. Bowen, "Radial gradient lenses for single-mode optical systems," Doctoral Dissertation, University of Rochester, Rochester, NY (1991).

39. M. T. Houk, "Fabrication and testing of index gradients in flouride materials," Doctoral Dissertation, University of Rochester, Rochester, NY (1990).

40. T. Findlaky, "Glass waveguides by ion exchange: a review," Opt. Eng. **24**, 244-250 (1984).

41. A. J. Burgraff and J. Cornelissen, "Strengthening of glass by ion exchange: I," Phys. Chem. Glasses **5**, 123-129 (1964).

42. Reference 11.

43. Reference 13.

44. S.D. Fantone, "Design, engineering, and manufacturing aspects of gradient index optical components," Doctoral Dissertation, University of Rochester, Rochester, NY (1979).

45. J.L. Coutaz and P.C. Jaussaud, "High index gradient in glass by ion exchange," Appl. Opt. **21**, 1063 (1982).

46. D. T. Moore, "Gradient index optics: aspects of design, testing and tolerancing," Doctoral Dissertation, University of Rochester, Rochester, NY (1974).

47. Reference 23.

48. Reference 44.

49. J. E. Samuels, "Influence of the molten salt bath on ion exchange in glass and the gradient-index profile," M.S. Thesis, University of Rochester, Rochester, NY (1989).

50. N. Haun et al., "Index profile control using Li+ for Na+ exchange in aluminosilicate glasses," Appl. Opt. **29**, 4056 (1990).

51. Private communications with Dr. Douglas Kindred.

52. S. N. Houde-Walter, "Field assisted ion exchange in glass," M.S. Thesis, University of Rochester, Rochester, NY (1983).

53. S. N. Houde-Walter, "Gradient index profile control by ion exchange in glass," Doctoral Dissertation, University of Rochester, Rochester, NY (1987).

54. Z. Fathi, et al., "Surface modification in a 2.45-GHz microwave field," Cer. Eng. and Sci. Proc. **15**, 1146-54 (1994).

55. J. Crank, *The Mathematics of Diffusion*, second edition. Oxford University Press, New York (1975), ch. 1.

56. M. J. Hoppe, "Design of axial gradient singlets utilizing a Fickian diffusion model," M.S. Thesis, University of Rochester, Rochester, NY (1992).

57. Reference 34.

58. CodeV is a registered trademark of Optical Research Associates.

Chapter II

Mathematical Model of Concentration-Dependent Diffusion

2.1 Introduction

The first step in a design-for-manufacture approach to gradient-index lens production is the development of a mathematical model of the fabrication process which incorporates all of the details needed to manufacture the gradient. The model must be able to take a given set of experimental parameters and calculate the index of refraction profile prior to performing the experiment. For example, in an ion exchange experiment these parameters might include time or temperature. The model must also be in a form that is easily linked to a lens design program and allow an optimization of the index of refraction profile using the manufacturing parameters. Finally, the mathematical model must have sufficient accuracy to ensure that the optical performance of the finished device meets the design specifications.

The goal of this chapter is to develop a numerical model which uses the diffusion equation to predict the results of ion exchange experiments. First, an introduction into Fickian diffusion theory is presented that includes several simple examples to demonstrate how manufacturing parameters can be incorporated into the diffusion equation through the

initial condition, the boundary condition, and the diffusion coefficient. These examples illustrate the importance of the concentration dependence of the diffusion coefficient in determining the final concentration dependence in the sample. Second, the derivation of a well-known form for the concentration dependence of the diffusion coefficient is given, but further discussion shows that the historical treatment of this equation requires a time-consuming experimental measurement procedure. Thus, an alternative technique to determine the concentration dependence from a single experiment is discussed, but the noise in this method requires a fitting function for the diffusion coefficient before it can be used in the diffusion equation. Therefore, a new analytic expression for the concentration-dependent diffusion coefficient is derived from statistical thermodynamics. This new theoretical model is called the Modified Quasi-Chemical (MQC) diffusion coefficient. Finally, a numerical routine is given that incorporates the new MQC diffusion coefficient model, solves the diffusion equation, and calculates concentration profiles based on manufacturing parameters.

2.2 Fickian Diffusion Theory

In a one-for-one ion exchange experiment, dopant cations (designated by B) from a molten salt replace the constituent cations (designated by A) of a glass sample. The interdiffusion of ions which occurs during the experiment can be written as

$$A_{glass}^+ + B_{salt}^+ \Leftrightarrow A_{salt}^+ + B_{glass}^+ \tag{2.1}$$

and under certain conditions is described by Fickian diffusion theory. [1] First, the initial glass sample must be isotropic. Second, the glass matrix must be stable and rigid at the diffusion temperature such that the cations are the only species moving during the diffusion. Finally, the boundary reaction between the salt and the glass must be fast relative to the total diffusion time. This last condition requires that the mobility of the cations in the salt is large when compared to the mobility of the cations in the glass. Under these assumptions, Fickian diffusion theory can be used to mathematically model the ion exchange process.

2.2.1 The Diffusion Equation

Fick's first law states that the rate of transfer of a diffusing substance through a surface of unit area is proportional to the concentration gradient measured normal to that surface. The flux, J, is then given by

$$J = -D\nabla C \tag{2.2}$$

where C is the concentration of the diffusing substance and the constant of proportionality, D, is called the diffusion coefficient. The negative sign in Eq. (2.2) appears because diffusion occurs in a direction opposite to that of increasing concentration. If the equation of continuity,

$$\nabla \bullet J = -\frac{\partial C}{\partial t} \, , \tag{2.3}$$

is applied to Eq. (2.2), then Fick's second law is obtained:

$$\frac{\partial C}{\partial t} = \nabla \bullet (D\nabla C) \, . \tag{2.4}$$

Equation (2.4) is often referred to as the diffusion equation where the diffusion coefficient, D, is a function of temperature and can also be a function of the concentration of the diffusing species. In some cases, such as diffusion in dilute solutions, it is reasonable to assume that D is constant, and then analytical expressions for the concentration profile may be obtained. In many cases, though, the diffusion coefficient is concentration-dependent and the equation must be solved numerically.

2.2.2 Analytical Solutions

The solution to the diffusion equation describes how the concentration in the sample varies with position. Although analytical expressions for the solution can be obtained, most require that the problem has a constant diffusion coefficient. For cases of concentration-dependent diffusion, few solutions of the diffusion equation exist which can be expressed (without approximation) strictly in terms of basic mathematical functions. Furthermore, those that can are mostly of implicit or parametric form rather than explicit relationships between the concentration, space, and time variables. In addition, most of these solutions only apply for one

particular type of concentration dependence for the diffusion coefficient and for one type of sample geometry.

Although limited to very specific problems, analytic solutions are helpful in the initial development of a diffusion model for a number of reasons. First, they can demonstrate how manufacturing parameters such as diffusion time, temperature, glass concentration, and salt concentration are incorporated into the model through the initial condition, the boundary conditions, and the diffusion coefficient of the diffusion equation. Second, variations in the experimental process parameters can then be analyzed for their effect on the concentration/index of refraction profile. The next two sections in this chapter give some simple diffusion examples for both the axial and the radial geometries usually used in gradient-index lens production.

2.2.2.1 Axial Geometry

The first example is a one-dimensional axial diffusion into a semi-infinite piece of glass. For this geometry, the diffusion equation reduces to

$$\frac{\partial C}{\partial t} = \frac{\partial}{\partial z}\left(D\frac{\partial C}{\partial z}\right) .$$
(2.5)

Given that the initial ion concentration of the glass sample is C_g, then the initial condition for the problem is given by

$$C = C_g \quad \text{for} \quad z > 0 \quad \text{and} \quad t = 0.$$
(2.6)

If the amount of ions flowing into the sample is negligible in comparison to the number of ions in the bath, then the concentration of the salt bath is assumed constant in time. The boundary conditions for this situation are then given by

$$C = C_s \quad \text{for} \quad z = 0 \quad \text{and} \quad t > 0$$
(2.7)

and

$$C = C_g \quad \text{for} \quad z = \infty$$
(2.8)

where C_s is the maximum ion concentration that the glass can acquire after diffusion and is assumed to be constant in time.
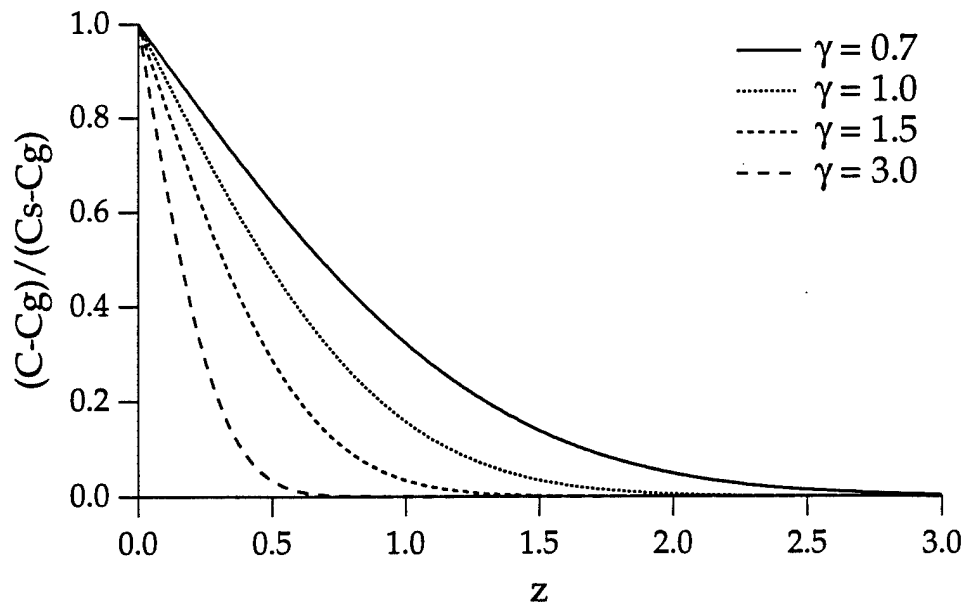
Figure 2.1 The solution for a one-dimensional axial diffusion into a semi-infinite piece of glass plotted for different values of the variable $\gamma = \dfrac{1}{\sqrt{4Dt}}$; D is the diffusion coefficient (assumed constant) and t is the diffusion time.

If the diffusion coefficient, D, is concentration-independent, then the diffusion equation can be solved with Laplace transforms. The analytical solution is given by

$$C(z) = C_g - \left(C_g - C_s\right)\mathrm{erfc}\left(\frac{z}{\sqrt{4Dt}}\right)$$

(2.9)

where the complementary error function, erfc(z), is defined as

$$\mathrm{erfc}(z) = 1 - \mathrm{erf}(z)$$

(2.10)

and the error function, erf(z), is defined as

$$\mathrm{erf}(z) = \frac{2}{\sqrt{\pi}} \int_0^z e^{\left(-\eta^2\right)} d\eta \ .$$

(2.11)

Figure 2.1 shows a plot of this solution for different values of $\gamma = \dfrac{1}{\sqrt{4Dt}}$, where D is the value of the constant diffusion coefficient and t is the time
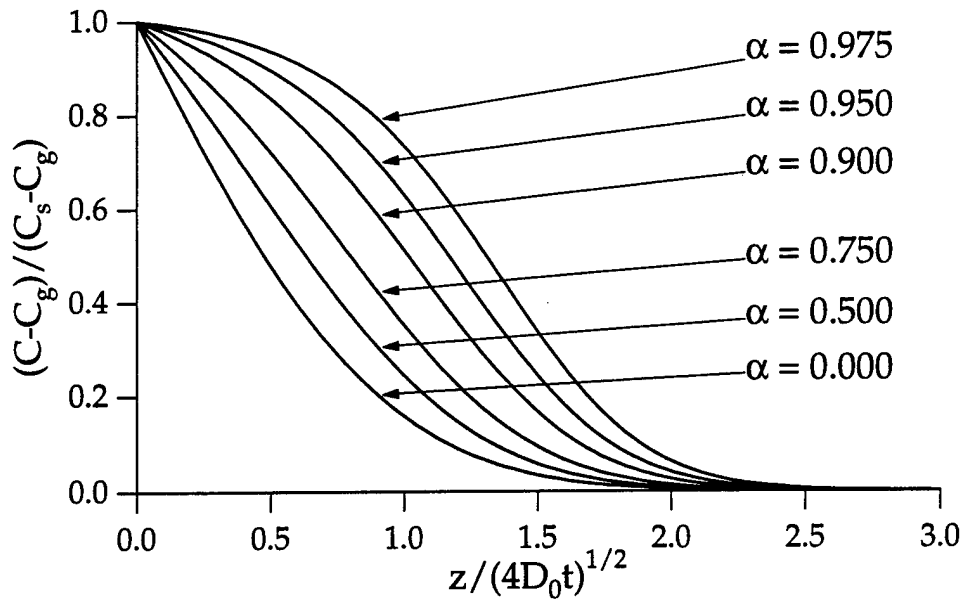
Figure 2.2 The solution for a one-dimensional axial diffusion into a semi-infinite piece of glass for the Fujita diffusion coefficient in Eq. (2.12) plotted for different values of the mobility ratio, α.

of the diffusion. As expected, increasing either the value of the diffusion coefficient or the time of the diffusion increases the depth of the diffusion.

In the same problem, if the diffusion coefficient, D, is concentration-dependent, then only a few analytic solutions exist. These solutions usually only apply for a specific form for the concentration dependence of the diffusion coefficient and many of the solutions are given in parametric form. For example, Fujita determined the solution for a diffusion coefficient with the following concentration dependence:

$$D(C) = \frac{D_0}{1 - \alpha(C/C_s)} \tag{2.12}$$

where D_0 and α are constants. [2] Although the solution is in fact analytic, it is a complicated integral solution which must be evaluated numerically.

Several solutions to the diffusion equation for the Fujita diffusion coefficient are shown in Fig. 2.2. When plotted for different values of α, they show how small changes in the concentration dependence of the diffusion coefficient have large effects on the concentration profile. Furthermore, the Fujita diffusion coefficient was important in the early

analysis of ion exchange experiments. The parameter α in Eq. (2.12) was experimentally related to the mobility ratio of the two exchanging ions. Graphical techniques then compared experimental profiles to the Fujita solutions to estimate the mobility ratio of the exchanging ions in the sample. [3]

2.2.2.2 *Radial Geometry*

The third example is given by a purely radial diffusion into a long cylinder where the effects of diffusion into the ends of the rod can be ignored. The diffusion equation in cylindrical coordinates is given by

$$\frac{\partial C}{\partial r} = \frac{1}{r}\frac{\partial}{\partial r}\left(rD\frac{\partial C}{\partial r}\right) . \tag{2.13}$$

The initial condition for the problem is written as

$$C = C_g \text{ for } r < a \text{ and } t = 0 \tag{2.14}$$

where C_g is the initial glass composition and a is the radius of the cylinder. The boundary conditions for this situation are

$$C = C_s \text{ for } r = a \text{ and } t > 0, \qquad \text{and} \tag{2.15}$$

$$\frac{\partial C}{\partial r} = 0 \text{ for } r = 0, \tag{2.16}$$

where C_s is the maximum ion concentration that the glass can acquire after diffusion, and is assumed to be constant in time.

If the diffusion coefficient is concentration independent, then the problem can be solved by separation of variables to obtain

$$C(r) = C_g - \left(C_g - C_s\right)\left(1 - \frac{2}{a}\sum_{n=1}^{\infty}\frac{\exp\left(-D\alpha_n^2 t\right)J_0\left(r\alpha_n\right)}{\alpha_n J_1\left(a\alpha_n\right)}\right), \tag{2.17}$$

where the α_n's are the roots of the equation

$$J_0\left(a\alpha_n\right) = 0 \tag{2.18}$$

and $J_0(x)$ is a Bessel function of the first kind of order zero. This solution is plotted in Fig. 2.3 for several values of $\kappa = Dt/a^2$. Equation (2.17)
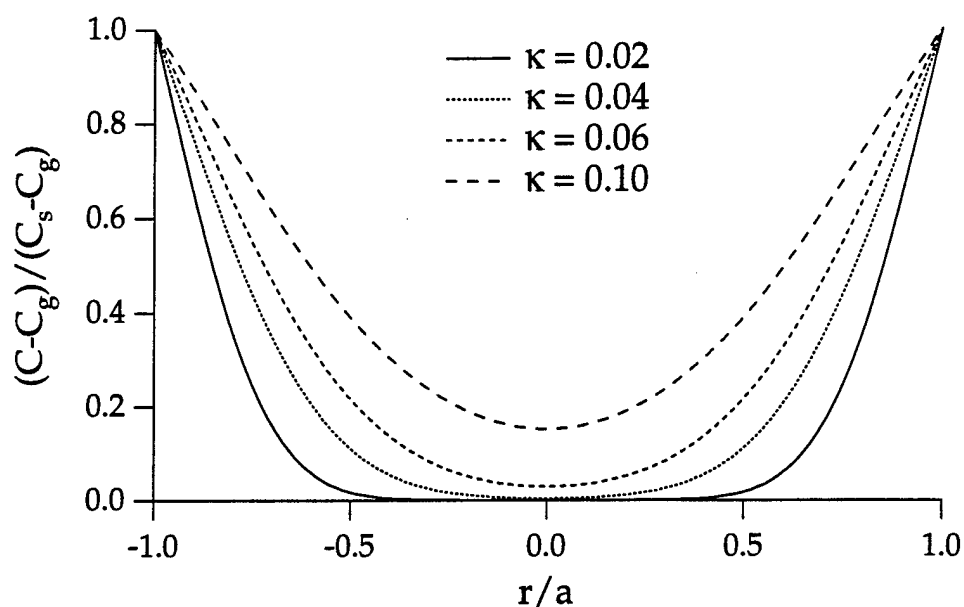
Figure 2.3 The solution for a radial diffusion into a long cylinder of glass plotted for different values of the variable $\kappa = Dt/a^2$; D is the diffusion coefficient (assumed constant), t is the diffusion time, and a is the radius of the cylinder.

shows that even for the case of a constant diffusion coefficient, the analytic solution for diffusion in more than one dimension is given by an infinite sum of Bessel functions, making it quite complicated to evaluate. As a result, the solutions for this geometry, especially for concentration-dependent diffusion, must almost always be found numerically.

2.3 The Diffusion Coefficient

2.3.1 Introduction

The results shown in the previous section demonstrate that solutions to the diffusion equation are highly influenced by the concentration dependence of the diffusion coefficient. This makes the diffusion coefficient a significant factor in determining the final concentration distribution in the sample, and, therefore, the optical performance of the finished device. Thus, an accurate mathematical model of ion exchange would require prior knowledge of the concentration dependence of the diffusion coefficient to predict index of refraction profiles for lens design.

Previous research has shown that for diffusions in which large ion concentrations are exchanged, the diffusion coefficient becomes remarkably concentration dependent. [4] However, for a specific ion exchange pair, it is currently impossible to ascertain the concentration-dependent diffusion coefficient based solely on the glass composition data, although several experimental techniques can be used to measure it. One method uses a Boltzmann-Matano technique to calculate the diffusion coefficient from the concentration profile of a single ion exchange experiment. However, this calculation tends to be very noisy and a fitting function is needed to use this data in a numerical model which solves the diffusion equation.

The main goal of this section is to develop an expression for the concentration dependence of the diffusion coefficient that can be used in the diffusion equation to predict the results of ion exchange experiments. The general expression for the diffusion coefficient for ion exchange is well-known [5], but it contains quantities which take a large amount of time and many experiments to measure. In gradient-index optics, this is not really practical, since numerous glass compositions need to be considered to identify the one most suitable for a particular application. Therefore, a new expression is presented that allows the concentration-dependent diffusion coefficient to be obtained from the concentration profile of a single experiment.

2.3.2 Background

A general expression for the concentration dependence of the diffusion coefficient can be derived from first principles in terms of the chemical potentials of the diffusing species. For a one-dimensional diffusion the flux J, or rate of transfer of a diffusing substance, is given by:

$$J = -D\frac{\partial N}{\partial x} \qquad (2.19)$$

where D is the diffusion coefficient, N is the concentration of the diffusing species, and x is the spatial coordinate. [6] At each point in the glass, the flux of each cation is also given by the rate equation,

$$J_i = N_i v_i \quad \text{for } i = A, B \qquad (2.20)$$

where N_i and v_i are the concentration and mean velocity, respectively, of cation i at that point. The mean velocity can then be written as a product,

$$v_i = F_i u_i \quad \text{for } i = A, B \qquad (2.21)$$

of a driving force, F_i, and the ionic mobility, u_i, of cation i.

If there is only one type of diffusing species, the driving force is due entirely to the concentration gradient of the diffusant and can be written as the negative of the gradient of the chemical potential, μ, [7]

$$F = -\frac{\partial \mu}{\partial x} \ . \qquad (2.22)$$

This type of situation occurs in the radiotracer experiments used to determine self-diffusion coefficients. In these experiments, the rate of diffusion of one component in a two-component system of uniform chemical composition can be observed using radioactively labeled molecules.

An additional term must be added to Eq. (2.22) when considering diffusion between two different species. In general, unlike cations will have different mobilities. During the diffusion process the difference in mobilities generates a local internal electric field; the ion with the higher mobility tends to move ahead of the other on a local scale, thereby creating a temporary electric potential. The potential acts to preserve charge

neutrality both by slowing the progress of the faster ion and by pulling the slower ion along at a faster rate. The driving force for cation i is then written as

$$F_i = -\frac{\partial \mu_i}{\partial x} + eZ_i \frac{\partial \phi}{\partial x} \quad \text{for } i = A, B \tag{2.23}$$

where e is the electric charge, Z_i is the valence of cation i and ϕ is the electrical potential set up by the unequal mobilities.

In one-for-one exchange, the flux entering the glass must be equal to the flux leaving the glass,

$$J_A = -J_B \tag{2.24}$$

so that charge neutrality is conserved across the whole sample. Following a procedure described by Jost, [8] the equation for J_A,

$$J_A = -\left(\frac{\partial \mu_A}{\partial N_A} + \frac{\partial \mu_B}{\partial N_B}\right) \frac{u_A u_b N_A N_B}{u_A N_A + u_b N_B} \frac{\partial N_A}{\partial x} \tag{2.25}$$

is obtained by using Eqs. (2.20), (2.21), and (2.23) in Eq. (2.24), solving for $eZ\frac{\partial \phi}{\partial x}$ and substituting it back into the original expression for J_A.

Comparison of Eq. (2.25) to Eq. (2.19) gives the standard expression for the diffusion coefficient

$$D = \frac{1}{kT}\left(\frac{\partial \mu_A}{\partial N_A} + \frac{\partial \mu_B}{\partial N_B}\right) \frac{D_A D_b N_A N_B}{D_A N_A + D_b N_B}, \tag{2.26}$$

where we have used

$$u_i = \frac{D_i}{kT} \quad \text{for } i = A, B \tag{2.27}$$

to relate the cation's mobility to its self diffusion coefficient where k is Boltzmann's constant and T is temperature. [9]

To explicitly see the concentration dependence, Eq. (2.26) can be rewritten in terms of a normalized dopant concentration, χ, such that

$$D(\chi) = \left\{ \frac{\chi(1-\chi)}{kT} \left(\frac{\partial \mu_B}{\partial \chi} - \frac{\partial \mu_A}{\partial \chi} \right) \right\} \frac{D_B}{1-\alpha\chi} \qquad (2.28)$$

for

$$\chi = \frac{N_B}{N_A + N_B} \qquad (2.29)$$

and the parameter α is defined as

$$\alpha = 1 - \frac{D_B}{D_A} . \qquad (2.30)$$

The term in brackets is the thermodynamic term of the diffusion coefficient, while the unbracketed term is sometimes called the Fujita term since it is similar in form to the Fujita diffusion coefficient. As expected, the Fujita term accounts for the unequal mobilities of the exchanging species since it is just a constant when $D_A = D_B$. If D_A is not equal to D_B, the mobility term is a smooth function that either increases monotonically with concentration when D_A is greater than D_B or decreases monotonically with concentration when D_A is less than D_B.

The effect of the concentration dependence of the Fujita term on the concentration profile has been known for quite awhile. On the other hand, the bracketed thermodynamic term in Eq. (2.28) has presented problems to researchers since it requires the knowledge of chemical potentials to determine its concentration dependence. In a particular system, the direct calculation of the chemical potential of a species as a function of its concentration is often difficult, and is even impossible in some cases. This made it hard to determine an explicit expression for the concentration dependence of the thermodynamic term and its corresponding effect on the concentration profile.

2.3.3 Historical Treatment

Applications which require exchanges of small dopant concentrations, such as waveguides, have often ignored the thermodynamic term or

assumed it to be equal to a constant. However, in the fabrication of gradient-index optics, large dopant concentrations (10-30 mole percent) are needed for large changes in the index of refraction. This leads to ion exchanges which are strongly concentration-dependent. [10] As a result, models which assume that the thermodynamic term is constant do not accurately predict the concentration dependence encountered in the manufacture of gradient-index lenses. Therefore the incorporation of the thermodynamic term into the model becomes very important.

In the past, the thermodynamic term has been included by defining the chemical potential of component i

$$\mu_i = \mu_i^0 + kT \ln(a_i) \tag{2.31}$$

in terms of an experimentally measurable quantity called the activity, a_i, which is equal to the product of an activity coefficient and the mole fraction of component i. The activity coefficient describes how the component interacts with its environment and is a macroscopic measure of the components ideality; in an ideal state the activity coefficient is equal to one so that the activity is exactly equal to the mole fraction. The Gibbs-Duhem relation [11],

$$N_A d\mu_A = -N_B d\mu_B \tag{2.32}$$

can then be invoked to get an equation for the diffusion coefficient, [12, 13]

$$D = \frac{\partial \ln a_B}{\partial \ln C} \frac{D_B}{1 - \alpha\chi} \tag{2.33}$$

where C is the concentration of species B and a_B is its activity.

For some glasses which exhibit "ideal behavior", the ratio of the cation activities in the glass can be approximated by the empirical equation [14]

$$\frac{a_A}{a_B} = \left[\frac{\chi_A}{\chi_B}\right]^n \tag{2.34}$$

where n is the Rothmund-Kornfeld factor. [15, 16] If n=1, the glass is said to be ideal and the activities are directly proportional to the concentration.

The equation for the diffusion coefficient can be written in terms of this factor according to: [17]

$$D = \frac{D_B}{1 - \alpha \chi} n .$$

(2.35)

Several glasses have been shown to obey this relation. [18, 19, 20, 21]

If the glass exhibits behavior which cannot be approximated by Eq. (2.34), as is the case with most glasses in the gradient index optics regime, Eq. (2.33) must be used to find the interdiffusion coefficient. The self-diffusion coefficients must then be measured by radiotracer diffusions or some other method [22] and the activities [23, 24] must be experimentally determined. This is a time-consuming process, and because of the many steps involved in making these measurements, is not really practical for the large number of glass compositions and salt melts involved in the fabrication of gradient-index optics.

2.3.4 Experimental Measurement/Calculation

Since it is currently impossible to determine the concentration-dependent diffusion coefficient based solely on the glass composition data, it must be measured experimentally. Several experimental techniques can be used to measure it, but for a design-for-manufacture approach, the goal is to use one that minimizes the number of experiments. One method uses the form for the concentration dependence given in the previous section but takes a large number of experiments and is therefore not really practical for this situation. An alternative method uses a Boltzmann-Matano technique to determine the concentration dependence of the diffusion coefficient. This method takes the concentration profile from a single diffusion experiment with certain initial and boundary conditions to calculate the diffusion coefficient.

2.3.4.1 Boltzmann-Matano Method

Under certain conditions, the diffusion equation for one-dimensional diffusion from Eq. (2.5) can be reduced to the ordinary differential equation

$$-2\eta\frac{dC}{d\eta} = \frac{d}{d\eta}\left(D\frac{dC}{d\eta}\right) \qquad (2.36)$$

in terms of a new variable, η, that has been defined as

$$\eta = \frac{z}{2\sqrt{t}} \qquad (2.37)$$

where z and t are the old variables of position and time, respectively. This type of transformation requires that the diffusion coefficient be only a function of concentration and that the boundary conditions be expressible in terms of η alone.

For a semi-infinite medium the new boundary conditions are given by

$$C = C_0 \quad \text{for} \quad \eta = 0 \qquad (2.38)$$

and

$$C = C_1 \quad \text{for} \quad \eta = \infty \; . \qquad (2.39)$$

An explicit expression for the concentration dependence of the diffusion coefficient can then be found by integrating Eq. (2.36) and then solving for D. If the resulting expression is transformed back in terms of the time and space variables, then D is given by the Boltzmann-Matano relation,

$$D(C = C_1) = -\frac{1}{2t}\frac{dz}{dC}\int_0^{C_1} z\, dC \qquad (2.40)$$

where $z(C)$ is the position versus concentration profile measured from an ion-exchanged sample and t is the diffusion time.

Thus the Boltzmann-Matano technique requires that a single axial diffusion in a sample having zero initial dopant concentration be conducted with constant boundary conditions. The concentration profile in the sample must then be measured. The derivative and integral in Eq. (2.40) are typically performed numerically to give the diffusion

coefficient as a function of concentration. The main problem with this approach is that the numerical evaluation is extremely sensitive to any noise in the concentration profile measurement. It is also clear from the behavior of typical concentration curves that problems will arise in the accuracy of the calculation near the limiting values of the concentration.

2.3.4.2 Examples

The numerical routine used throughout this thesis to calculate diffusion coefficient from a measured concentration profile is given in Appendix A.2. It uses a central difference algorithm to calculate the derivative and trapezoidal integration to calculate the integral. It also has the added option of calculating the diffusion coefficient from an index of refraction profile measurement. This thesis concentrates on Li^+-Na^+ ion exchanges, but measurements of Li^+ concentration profiles are difficult and costly. Therefore it is easier to interpolate the required concentration profile from the measured index of refraction profile according to

$$z(C) = z(n(C)) \qquad (2.41)$$

where n(C) is obtained by measuring the index of refraction from a series of homogeneous samples with different Li^+ concentrations. This procedure and its reliability are discussed in more detail in Chapter 3.

Several examples are given to show the typical concentration profiles, derivatives, integrals, and diffusion coefficients obtained using the Boltzmann-Matano technique. The first two are calculated from theoretical concentration profiles for known diffusion coefficients. One example uses a concentration-independent diffusion coefficient, while the second uses a concentration-dependent Fujita diffusion coefficient. Both of these examples show the error involved in the numerical calculation and indicate where a large portion of the error comes from. Finally, a third example gives a calculation of the diffusion coefficient from a typical experimentally measured index of refraction profile and shows the effect of the measurement noise on the calculation.

The first example shows the calculation of a constant diffusion coefficient from a complementary error function profile. A typical value

for the diffusion coefficient of 0.1×10^{-7} cm^2/s was used to generate the theoretical concentration profile shown in Fig. 2.4 where the concentration is normalized to have a maximum value of one. The numerical derivative and integral of the concentration profile are shown in Fig. 2.5. As expected, as the slope of the profile tends to zero the numerical calculation of the derivative tends to infinity such that the calculation of the derivative encounters problems near zero concentration. This leads to the error in the calculation of the diffusion coefficient which is shown in Fig. 2.6. Both the theoretical value of the diffusion coefficient and the calculated diffusion coefficient using the Boltzmann-Matano method are given. The figure shows that the error in calculating the derivative in areas near zero slope results in almost a fifty percent error in the calculation of the value of the diffusion coefficient for very small values of concentration. However, the error for the other concentration values is much smaller, approximately 1 to 2 percent.

The second example is similar to the first except that it uses a concentration-dependent Fujita diffusion coefficient with a mobility ratio, α, of 0.9 to generate the theoretical concentration profile. This profile is shown in Fig. 2.7 and is similar to the one shown in Fig. 2.2. The numerical derivative and integral of this concentration profile are shown in Fig. 2.8. Again, the derivative tends to infinity in the area near zero slope in concentration and results in a almost a fifty percent error in the calculation of the diffusion coefficient for very low concentration values as shown in Fig. 2.9. However, the error in the diffusion coefficient calculation for the remaining values of concentration is much smaller, and less than one percent.

The third example uses real data from an experimentally measured index of refraction profile. The index of refraction profile is shown in Fig. 2.10 and the interpolated concentration profile is shown in Fig. 2.11. The index of refraction profile was obtained using a Li$^+$ for Na$^+$ ion exchange in an alumina silicate glass and is typical of the profiles to be encountered in this thesis. The experimental details (including the relation for index of refraction as a function of Li$^+$ concentration) are given later in chapter 4 and the method for converting the index of

refraction profile to a concentration profile is discussed in Chapter 3. Note: the interpolated concentration profile is very similar in shape to the measured index of refraction profile since the measured index of refraction as function of concentration for this particular glass is very nearly linear.

The numerical derivative and integral of the interpolated concentration profile for this example are shown in Fig. 2.12 and the calculated concentration-dependent diffusion coefficient is shown in Fig. 2.13. The major problem with this particular method for calculating a diffusion coefficient is that any noise in the experimental measurement will cause errors in the interpolation process and then be further amplified in the numerical calculation of the derivative. Thus, very noisy diffusion coefficients are obtained with this method as shown in Fig. 2.13.

The noise in the diffusion coefficient reveals the need for an accurate fitting function for the experimental data since the noise is too large to place the diffusion coefficient directly into the diffusion equation to calculate future experimental profiles. In addition, if the expression obtained in Eq. (2.28) is to be used as fitting function the thermodynamic term must be included. This term cannot be assumed to be a constant since the concentration dependence of the diffusion coefficient obtained from the ion exchange experiment is very unlike the Fujita diffusion coefficient shown in Fig. 2.9 even having a maximum value at some intermediate value of concentration.
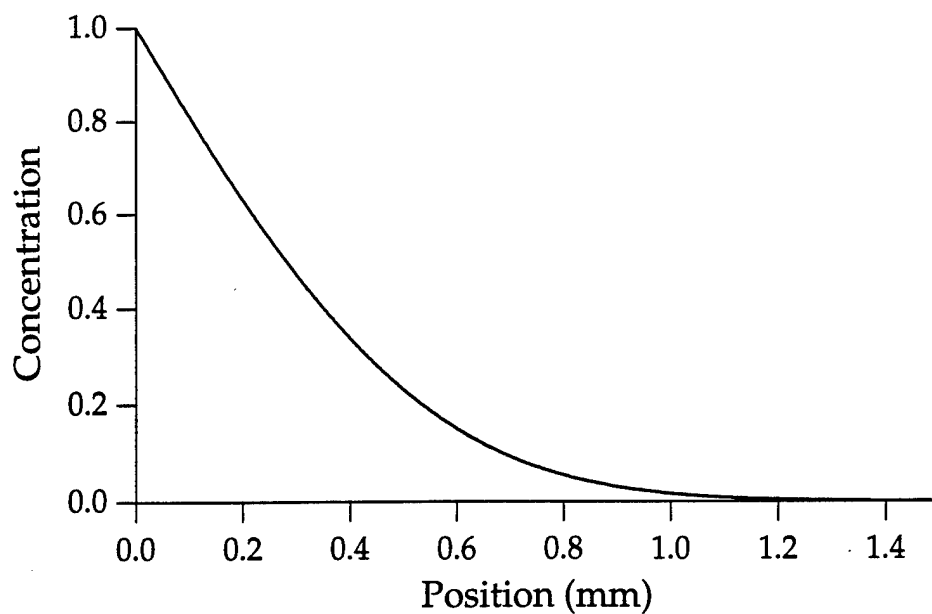
Figure 2.4 Complementary error function concentration profile generated with a constant diffusion coefficient equal to 0.1×10^{-7} cm^2/s.
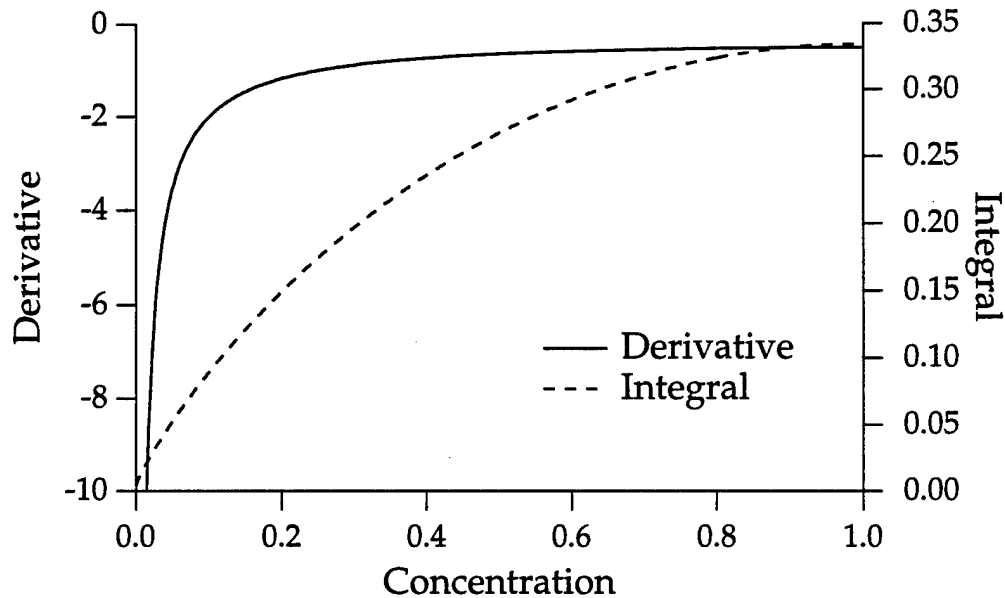
Figure 2.5 Numerical derivative and integral of the complementary error function concentration profile shown in Fig. 2.5.
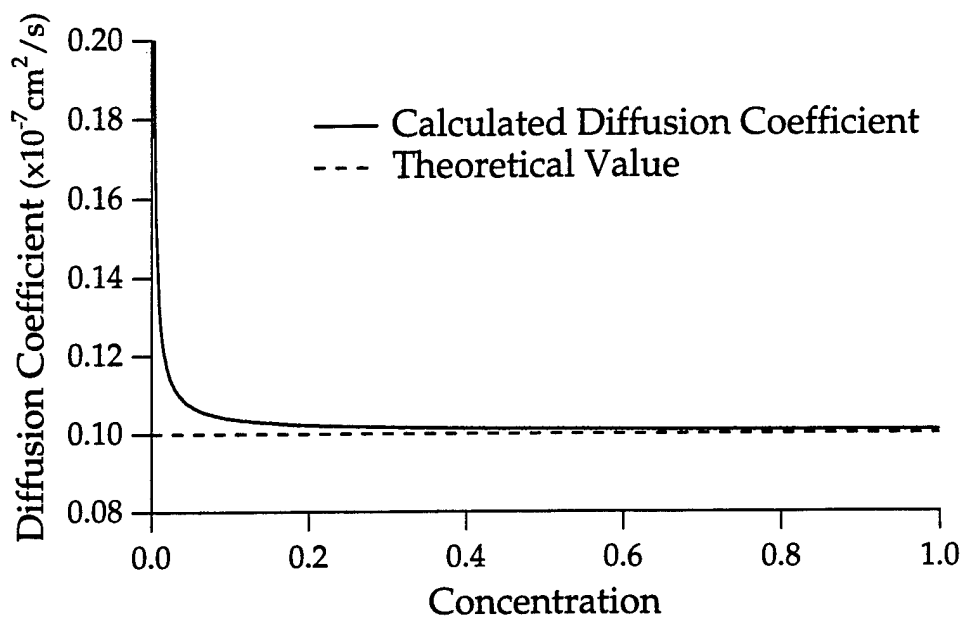
Figure 2.6 Comparison between theoretical value of diffusion coefficient and the value calculated with the Boltzmann-Matano method for a constant diffusion coefficient.
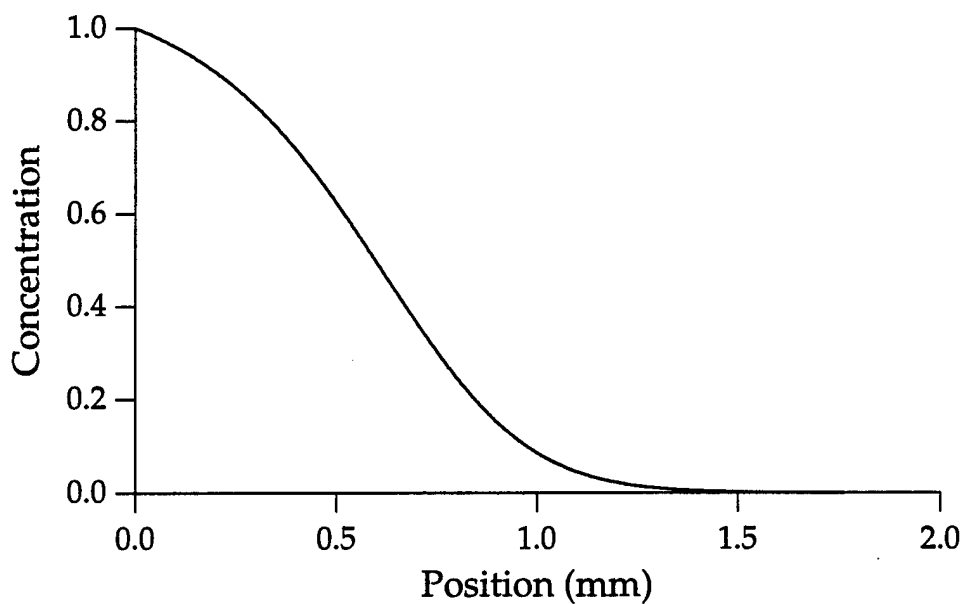
Figure 2.7 Concentration profile generated with a Fujita diffusion coefficient where D_0 is equal to 0.1×10^{-7} cm^2/s and the mobility ratio, α, is equal to 0.9.
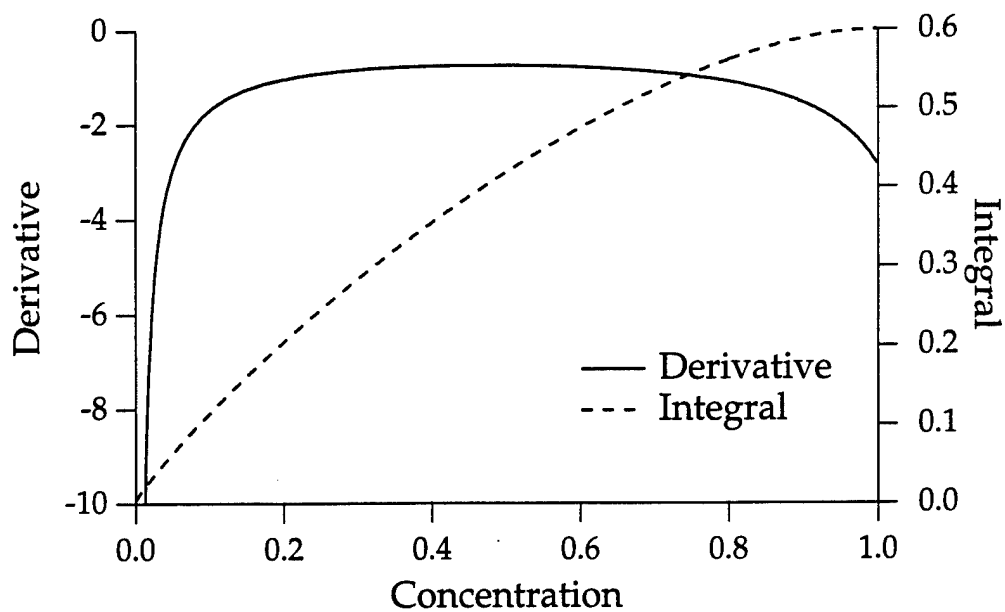
Figure 2.8 Numerical derivative and integral of the Fujita concentration profile shown in Fig. 2.7.
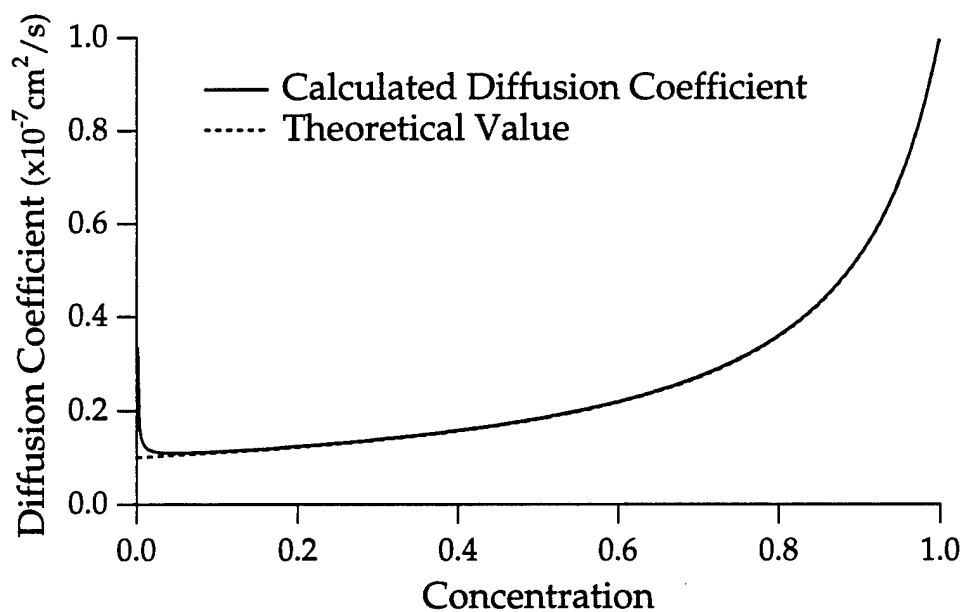
Figure 2.9 Comparison between theoretical value of diffusion coefficient and the value calculated with the Boltzmann-Matano method for the Fujita diffusion coefficient.
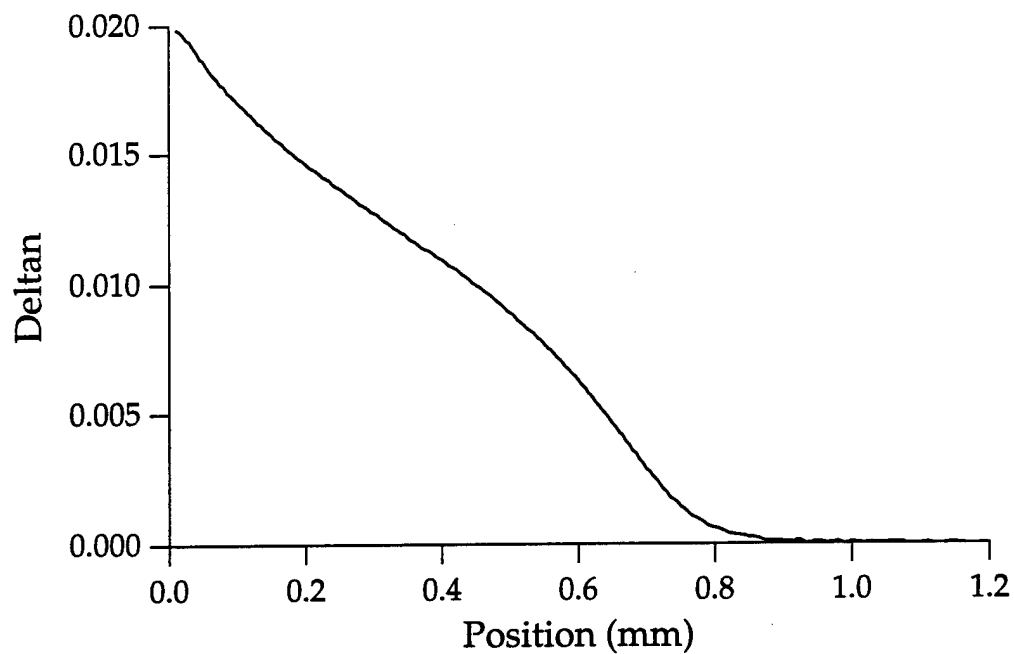
Figure 2.10 An experimental index of refraction profile representative of the type of profiles encountered in this thesis.
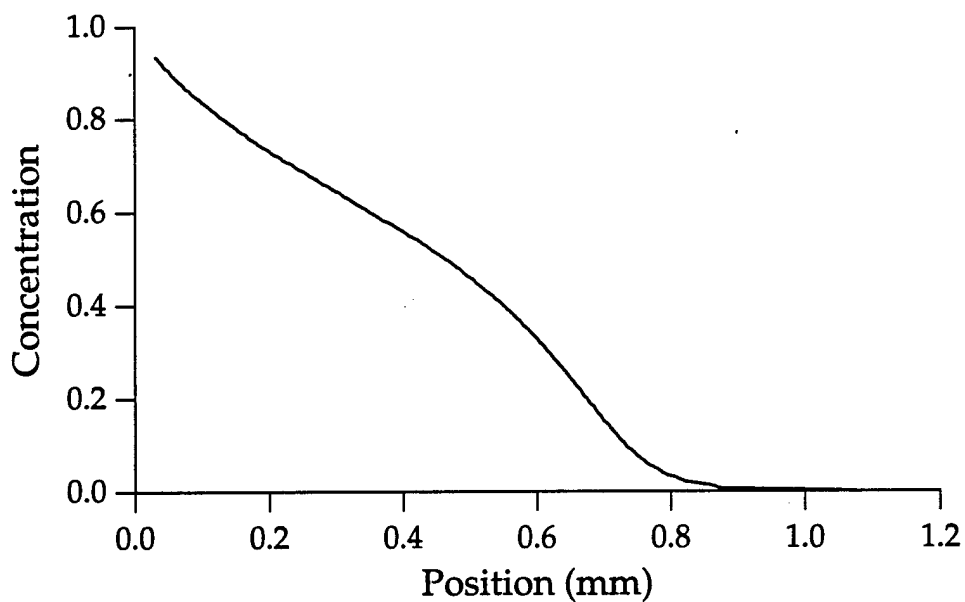
Figure 2.11 The interpolated concentration profile from the experimental index of refraction profile shown in Fig. 2.10.
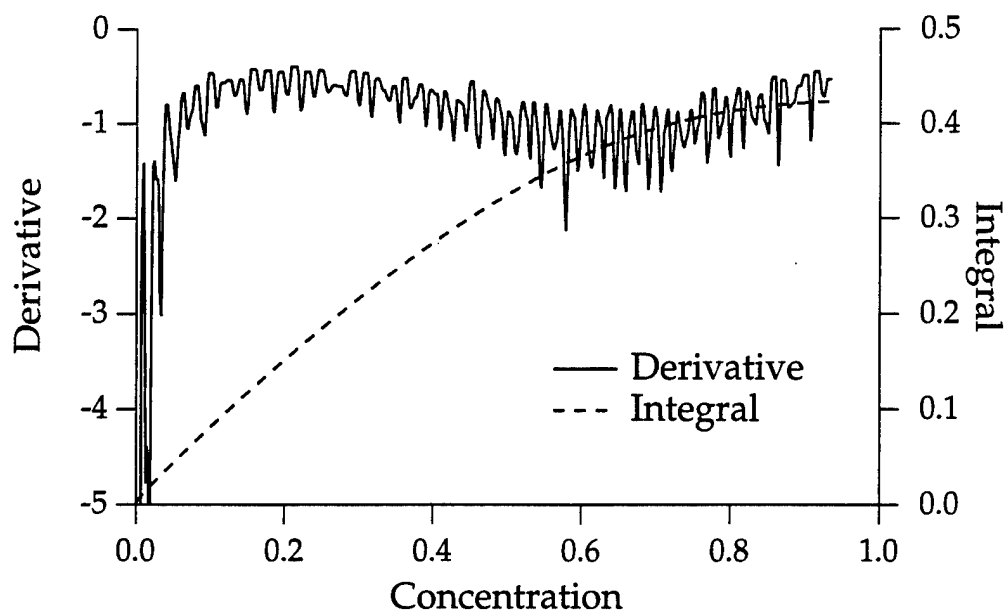
Figure 2.12 Numerical derivative and integral of the experimental concentration profile shown in Fig. 2.11.
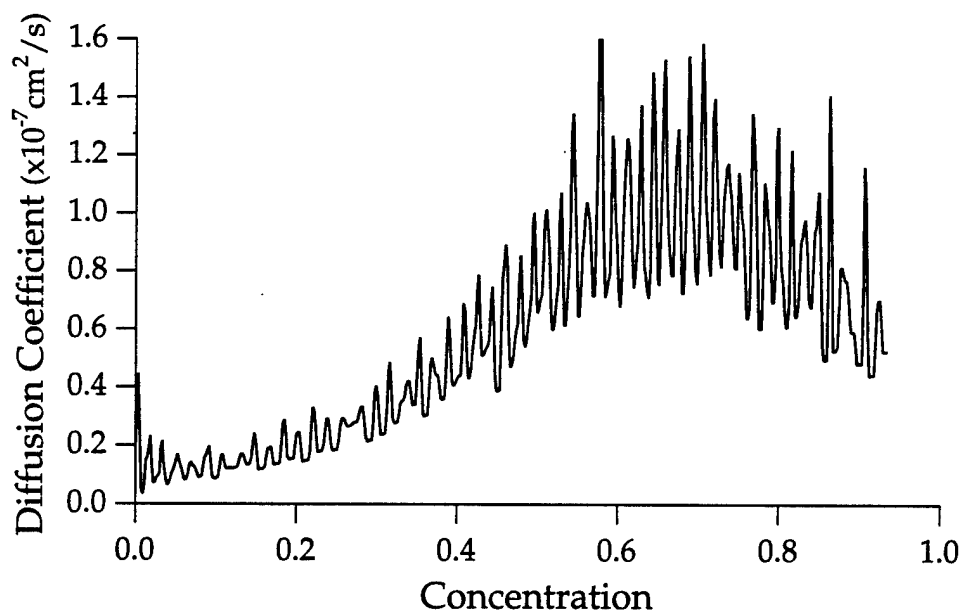
Figure 2.13 Experimental diffusion coefficient calculated from a typical index of refraction profile using the Boltzmann-Matano method to illustrate the effects of experimental noise on the calculation.

2.3.5   Quasi-Chemical Diffusion Coefficient

2.3.5.1   Introduction

In section 2.3.2 a general expression for concentration dependence of the diffusion coefficient was derived which contained the chemical potentials, μ_A and μ_B, as functions of concentration. The expression was difficult to use because the chemical potentials were unknown, and, if written in terms of activity, hard to measure experimentally. An alternative method to measure the concentration-dependent diffusion coefficient was provided in section 2.3.4 and uses a Boltzmann-Matano technique. This method of calculation was much less time-consuming since it requires only a single experiment but results in noisy data for the diffusion coefficient. Thus a fitting function is needed since the noisy data cannot be placed in the numerical routine to solve the diffusion equation.

Gaussians or high-order polynomials can sometimes be used to fit the Boltzmann-Matano data, but both usually result in a loss of accuracy in the recovery of the original index of refraction profile, and therefore in the prediction of future index of refraction profiles. In addition, no real understanding of the concentration dependence of the diffusion coefficient can be obtained when the coefficients of these fits are compared for diffusion coefficients of similar glass systems. Therefore, it was obvious that a new expression for concentration dependence of the diffusion coefficient was required for improving the accuracy of the diffusion model. The expression needed to be based in physics and not arbitrarily chosen, so that small systematic changes in the initial conditions of the ion exchange experiment, such as glass composition, could be analyzed.

In the following section, statistical thermodynamics is used to determine the concentration dependence of the chemical potentials in Eq. (2.28) to find an analytic expression for the concentration-dependent diffusion coefficient. The resulting expression is simple and in terms of meaningful physical parameters. Later in this chapter, it will be shown that it is in excellent agreement with experimental data and can in fact be

used to recover the initial index of refraction profiles. This allows the concentration dependence of the diffusion coefficient to now be obtained from the concentration profile of a single experiment and eliminates many of the experimental measurements required in the past.

2.3.5.2 Derivation

In statistical thermodynamics, the chemical potential of component i whose concentration is N_i can be written as

$$\mu_i = \left(\frac{\partial A}{\partial N_i}\right)_{T,V,N_{\alpha,\alpha \neq i}} \tag{2.42}$$

where A is the Helmholtz free energy of the system,

$$A = -TS - PV + \sum_i \mu_i dN_i \ , \tag{2.43}$$

and T is temperature, V is volume, P is pressure, and S is entropy. The Helmholtz free energy can also be written in terms of a canonical partition function, Q, where

$$A = -kT \ln Q \tag{2.44}$$

and Q is a sum over all the energy states, j, of the system,

$$Q = \sum_j e^{-E_j/kT} \ . \tag{2.45}$$

If Eqs. (2.42) and (2.44) are combined, the chemical potential of component i is given by

$$\mu_i = -kT \left(\frac{\partial \ln Q}{\partial N_i}\right)_{T,V,N_{\alpha,\alpha \neq i}} . \tag{2.46}$$

Thus, to get an expression for the chemical potential a way to determine Q must be found. Since Q is a sum over all the possible energy states of the system, it is usually estimated by making simplifying assumptions about the system and its energy states.

Recently, a theoretical paper was published by Araujo [25] in which the thermodynamic contribution to the diffusion coefficient was formulated

from statistical thermodynamics using methods from nearest-neighbor lattice statistics. He assumed that ion exchange could be represented by a 1-dimensional lattice of cation sites in which each site could be occupied by either species A or species B. In this type of derivation there is a potential energy of interaction between nearest neighbor pairs, but any interaction between higher neighbor pairs is ignored. Although the solutions were purely numerical, graphical results of the diffusion coefficient had many features which qualitatively resembled the behavior observed in many glass systems. Based on Araujo's results, a second paper was published [26] which expanded the theory to include a 3-dimensional lattice of sites and then proceeded to derive an analytical solution for the diffusion coefficient.

In the new model, nearest-neighbor lattice statistics is used to make simplifying assumptions about the system and its energy levels to find the partition function, Q. [27] First, it is assumed that the glass matrix of the ion exchange sample is rigid and unchanging and the glass is modeled as a simple three-dimensional lattice of cation sites whose most important interactions are those between the mobile cations. Second, it is assumed that the lattice is incompressible (it has a fixed volume per site) and has M identical sites, where M is a very large number. In this case the total volume, V is not an independent thermodynamic variable but is simply proportional to the total number of sites. Each of the M sites can be occupied by one of two types of mobile cation species, A or B; the two species of cations must be approximately the same size in order to occupy the same sites. Finally, it is assumed that there are no vacant sites on the lattice so that

$$N_A + N_B = M \qquad (2.47)$$

where N_i is the number or concentration of cations of type i.

The Helmholtz free energy of this system can now be written as

$$A = -ST + \mu_A N_A + \mu_B N_B \ , \qquad (2.48)$$

but to find the chemical potentials μ_A and μ_B from Eq. (2.42), Q must be found according to Eq. (2.45). This equation requires that all the energy

states of the lattice be known, each of which is the sum of the energy states of the individual cations and also the interaction energy of that state. Thus it would have been very difficult if not impossible to arrive at an analytical expression if all the components in the glass and their interaction energies were included in the model.

To simplify the model even further, only the interactions between nearest cation neighbors are considered and any interactions between higher neighbor pairs are ignored. It is assumed that each cation site has the same number, c, of nearest cation neighbors. (Again, the other components in the glass are ignored even though in an oxide glass the oxygen are actually the closest species to a cation. [28]) Under this assumption, the relationship between the number of cation species and the number of nearest neighbor cation pairs is given by,

$$cN_A = 2N_{AA} + N_{AB} \quad \text{and} \tag{2.49}$$

$$cN_B = 2N_{BB} + N_{AB} \tag{2.50}$$

where N_{AA} is the number of A-A cation pairs, N_{BB} is the number of B-B cation pairs, and N_{AB} is the number of unlike pairs of cations.

In a similar manner, an interaction energy, ε_{ij}, (assumed constant) is defined as the pair interaction energy between i and j cations. Then the energy contribution from all the i-j pairs with interaction energy ε_{ij} is $N_{ij}\varepsilon_{ij}$. Thus the contribution to the total energy of the glass from cation-cation interactions is

$$E = N_{AA}\varepsilon_{AA} + N_{BB}\varepsilon_{BB} + N_{AB}\varepsilon_{AB} \ . \tag{2.51}$$

An excess interaction term is defined according to reference [29]:

$$\varepsilon_{int} = \varepsilon_{AB} - \frac{\varepsilon_{AA} + \varepsilon_{BB}}{2} \tag{2.52}$$

which is typically negative for ion exchanges in glass. [30] Substituting Eq. (2.52) into Eq. (2.51) and using Eqs. (2.49) and (2.50) the total energy from cation-cation interactions becomes

$$E = \frac{c(N_A\varepsilon_{AA} + N_B\varepsilon_{BB})}{2} + N_{AB}\varepsilon_{int} \ . \tag{2.53}$$

If each cation vibrates about a lattice site with a three dimensional partition function $q_i(T)$ independent of the state of occupation of neighboring sites, then the canonical partition function, Q, is written as

$$Q = q_A(T)^{N_A} q_B(T)^{N_B} \sum_{N_{AB}} g(N_A, N_B, N_{AB}) e^{-E/kT} \qquad (2.54)$$

where g is the degeneracy, or the number of ways in which N_B cations can be distributed on M sites to give N_{AB} cation pairs of type A-B. [31] This degeneracy is difficult to calculate in three-dimensions, but can be estimated using a quasi-chemical approximation. If all cation pairs were independent of one another the degeneracy would be given by,

$$\omega = \frac{\left(\dfrac{cM}{2}\right)!}{\left(\dfrac{cN_A}{2} - \dfrac{N_{AB}}{2}\right)!\left(\dfrac{cN_B}{2} - \dfrac{N_{AB}}{2}\right)!\left[\left(\dfrac{N_{AB}}{2}\right)!\right]^2} \qquad (2.55)$$

However, this expression results in an over-counting of the configurations since the cation pairs are not independent; each cation is shared by c different pairs. Therefore, the degeneracy is given in the quasi-chemical approximation by $g \cong \zeta\omega$ where ζ,

$$\zeta = \left[\frac{M!}{N_A! N_B!}\right]^{1-c} \qquad (2.56)$$

is a factor that corrects for the overcounting. [32]

The chemical potentials are then calculated from partial derivatives of the canonical partition function; for example:

$$\mu_B = -kT\left(\frac{\partial \ln Q}{\partial N_B}\right)_{N_A, T} . \qquad (2.57)$$

The expression for Q in Eq. (2.54) involves a sum over all possible N_{AB}. For $M \rightarrow \infty$ the sum can be simplified by replacing Q with its maximum

term. Finally, Stirling's approximation can be used to obtain an equation for the chemical potential

$$\mu_B = -kT\ln\left(q_B e^{-c\epsilon_{BB}/2kT}\right) + kT\ln\chi - kT\frac{c}{2}\ln\left[\frac{(\beta+1)\chi}{\beta-1+2\chi}\right] \quad (2.58)$$

where

$$\beta = \sqrt{1 - 4\chi(1-\chi)\left(1 - e^{2\epsilon_{int}/kT}\right)} \quad . \quad (2.59)$$

If this is placed back into Eq. (2.28), the derivatives of μ_A and μ_B with respect to χ can be calculated and the algebraic expressions reduced to a simple equation for the diffusion coefficient,

$$D = \left[\frac{c}{2}\left(\frac{1}{\beta}-1\right)+1\right]\frac{D_B}{1-\alpha\chi} \quad . \quad (2.60)$$

Thus, the new expression for the diffusion coefficient given by Eq. (2.59) and Eq. (2.60) has four adjustable parameters: ϵ_{int}, c, D_B, and α.

One thing to note about the quasi-chemical approximation is that it is exact for a 1-dimensional lattice of sites (c=2) [33]. When c, the cation-cation coordination, equals 2, the diffusion coefficient reduces to:

$$D_{1-d} = \frac{1}{\beta}\frac{D_B}{1-\chi\alpha} \quad . \quad (2.61)$$

This is the same as the system studied by Araujo in which he assumed equal mobilities such that his numerical plots of the concentration dependence of the diffusion coefficient are essentially plots of $1/\beta$.

2.3.5.3 Graphical Analysis

A graphical analysis of Eq. (2.60) reveals some important features of the new expression for the concentration-dependent diffusion coefficient. Since there are two main terms contributing to the concentration dependence of the diffusion coefficient, the mobility term and the thermodynamic term, a separate analysis of these two terms helps to gain a full understanding of the concentration dependence of this equation.

First, the thermodynamic effects can be removed by assuming that the two particles do not interact, i.e. $\varepsilon_{int}=0$. In this case, β is equal to one, and the thermodynamic term is also equal to one, such that the diffusion coefficient reduces to the mobility term alone, or

$$\frac{D(\chi)}{D_B} = \frac{1}{1-\alpha\chi} \ .$$

(2.62)

This term accounts for the unequal mobilities of the exchanging species; when $D_A=D_B$, $\alpha = 0$, and it is just equal to a constant value. A graph of this equation is shown in Fig. 2.14 for various values of D_B/D_A. Thus the mobility expression is a smooth function that increases monotonically with concentration when D_A is greater that D_B and decreases monotonically if D_A is less than D_B.

Equation (2.62) is also the same as the expression for the Fujita diffusion coefficient and therefore the standard representation of the concentration-dependent diffusion coefficient that was used in the past. The effect of changes in the mobility ratio on the concentration profiles is well-known and was shown previously in Fig. 2.2. Furthermore, Fig. 2.14 shows that large differences in mobilities are required before the Fujita diffusion coefficient shows a marked difference in concentration dependence. However, the mobility ratios for the single valent ion pairs used in ion exchange are often close to one which leads to a minimal concentration dependence in this term. As a result, the mobility term alone cannot account for the concentration dependence observed in experimental diffusion coefficients like the one shown in Fig. 2.13.

In contrast, an analysis of the thermodynamic term shows that it gives rise to a strong concentration dependence. When $D_A=D_B$, $\alpha = 0$, and the mobility term is just equal to a constant value, D_B. Therefore, if the self-diffusion coefficients are taken to be equal, Eq. (2.60) becomes

$$\frac{D(\chi)}{D_B} = \left[\frac{c}{2}\left(\frac{1}{\beta}-1\right)+1\right] ,$$

(2.63)

and the influence of the thermodynamic interactions on the value of the diffusion coefficient can be emphasized.

The concentration dependence of Eq. (2.63) is contained in the $1/\beta$ term and will change as either the value of the interaction energy or the cation-cation coordination number changes. For a one-dimensional system, c=2, and Eq. (2.63) becomes

$$\frac{D(\chi)}{D_B} = \frac{1}{\beta} \, , \qquad (2.64)$$

so that the $1/\beta$ thermodynamic term can now be examined separately where β is given by Eq. (2.59). For χ, the normalized concentration value, between 0 and 1, this term is a symmetric function with either a maximum or minimum at $\chi = 1/2$, depending on the sign of the interaction energy. Note: the value of $1/\beta$ at each endpoint is 1, so that the endpoints of the diffusion coefficient in the original expression are the self diffusion coefficients, as desired.

The value of the interaction energy is seen to be an important factor in determining the concentration dependence of the thermodynamic term. When ε_{int} is taken to be positive, the result is shown in Fig. 2.15 where Eq. (2.64) is plotted for various values of the variable $\rho = \varepsilon_{int}/kT$. For this case, Fig. 2.15 shows that the value of the diffusion coefficient changes rapidly near concentrations of zero or one while the concentration dependence is much weaker in the intermediate ranges. Also, as either the temperature increases or the interaction energy decreases, the magnitude in the change of concentration dependence of the diffusion coefficient increases.

Plots of Eq. (2.64) are shown for negative ε_{int} values in Fig. 2.16 for various values of the variable $\rho = \varepsilon_{int}/kT$. This has just the opposite effect in that the strongest interaction effects are observed at the intermediate compositions and the weakest interaction effects are observed when either component tends to unity concentration. In addition, for a constant temperature, the magnitude of the interaction energy controls the height and the width of the peak. This is evidenced by the fact that the value of $1/\beta$ at the maximum is $e^{-\varepsilon_{int}/kT}$ while the full width at half max of β is

given by $\sqrt{3}\left(e^{-2\epsilon_{int}/kT}-1\right)^{-\frac{1}{2}}$, thereby showing that the interaction energy determines both the height and the width of the peak.

Figures 2.15 and 2.16 are similar to the numerical graphic solutions presented by Araujo. He also assumed equal mobilities and a one-dimensional system so that his plots of the diffusion coefficient are essentially plots of the function $1/\beta$. Araujo also noted that previous research showed that there exists a negative interaction between the various alkali ion pairs. This indicates that for ion exchange experiments, a maximum in the diffusion coefficient at some intermediate concentration value may be observed which is consistent with the example calculation given earlier.

If the model is now extended to three-dimensions for a cation-cation coordination number, $c \neq 2$, then Eq. (2.60) for $D_A=D_B$ becomes:

$$\frac{D(\chi)}{D_B} = \frac{c}{2}\left(\frac{1}{\beta}-1\right)+1 \ . \tag{2.65}$$

As illustrated in Fig. 2.17, for a constant interaction energy value, increasing the value of the coordination number also causes the diffusion coefficient peak to broaden and increase in height.

Finally, an examination of Eq. (2.60) as a whole shows the effects of combining the concentration dependence of both the mobility term and the thermodynamic term. For example, Fig. 2.18 illustrates how changing the ratio of D_B/D_A (changing D_A with D_B held constant) for a fixed interaction energy disrupts the symmetry of the diffusion coefficient, eventually causing a local minimum to occur when the self diffusion coefficients, and therefore the mobilities, of the exchanging cations greatly vary.
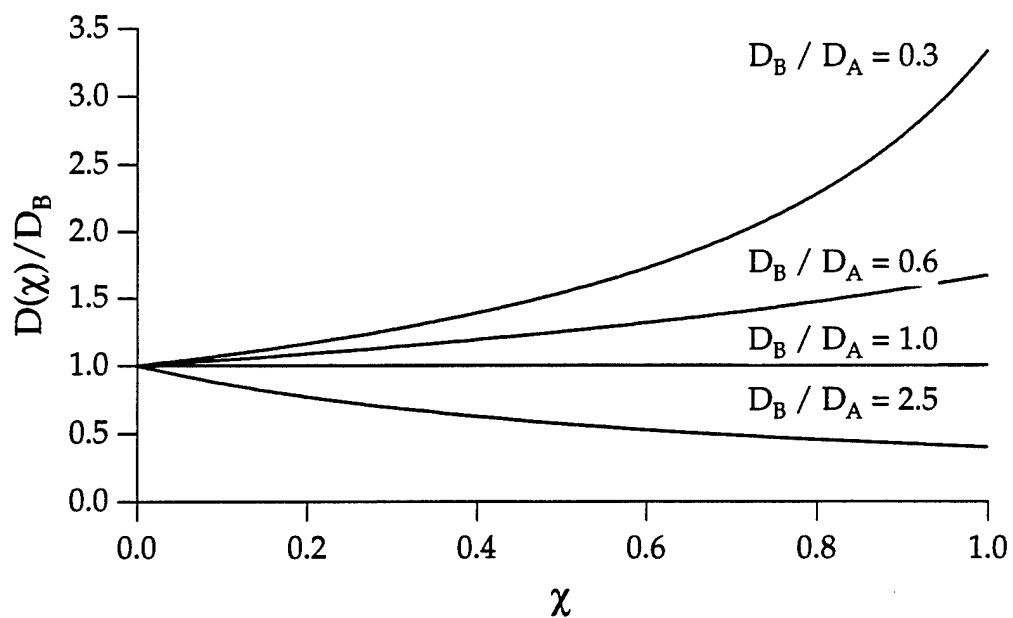
Figure 2.14 The mobility term of the Quasi-Chemical Diffusion Coefficient is plotted for different ratios of the self diffusion coefficients, D_B and D_A.
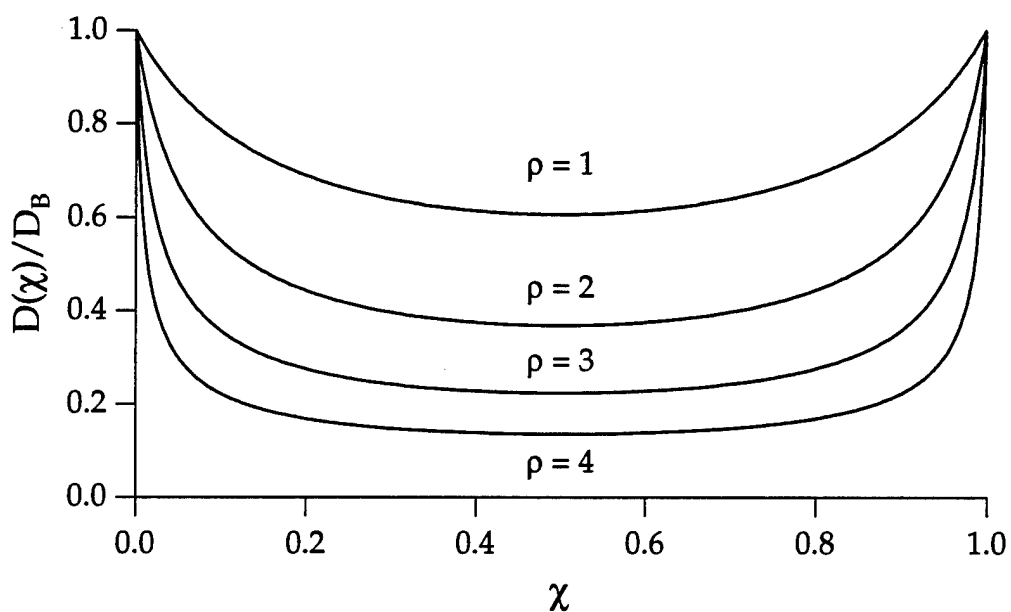
Figure 2.15 The $1/\beta$ term of the Quasi-Chemical Diffusion Coefficient is plotted for different values of the variable $\rho = 2\varepsilon_{int}/kT$ where ε_{int} is assumed to be positive.
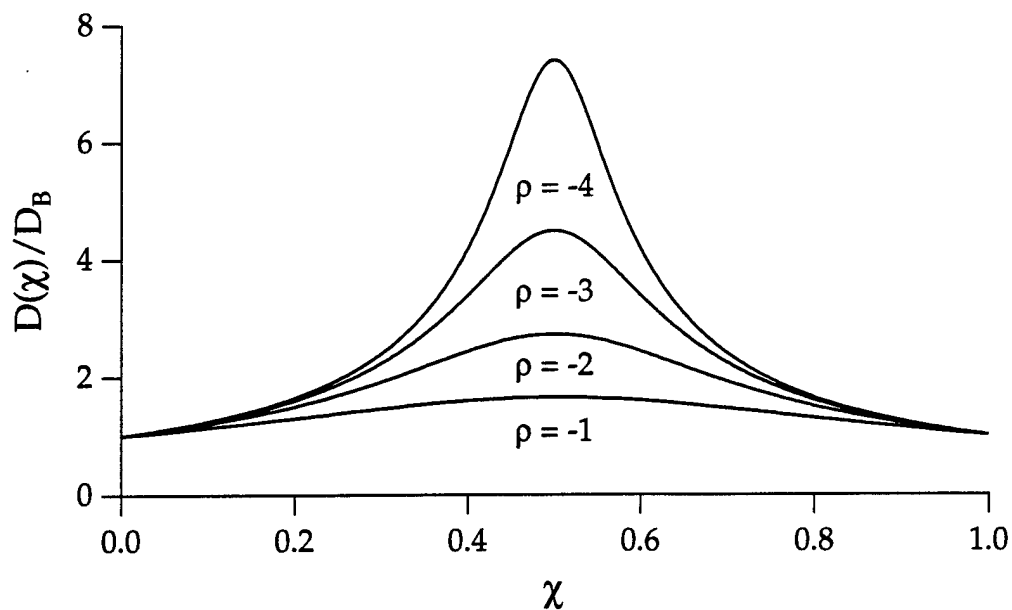
Figure 2.16 The 1/β term of the Quasi-Chemical Diffusion Coefficient is plotted for different values of the variable $\rho=2\varepsilon_{int}/kT$ where ε_{int} is assumed to be negative.
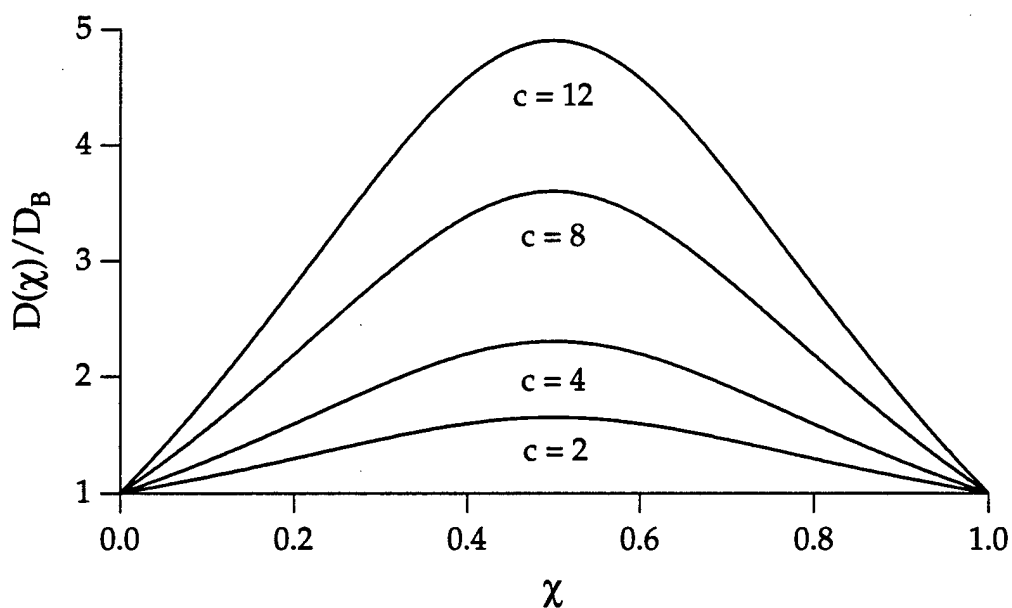
Figure 2.17 The thermodynamic term of the Quasi-Chemical Diffusion Coefficient is plotted for different values of the cation-cation coordination number, c, where the interaction energy term, ρ, is held constant at a value of -1.
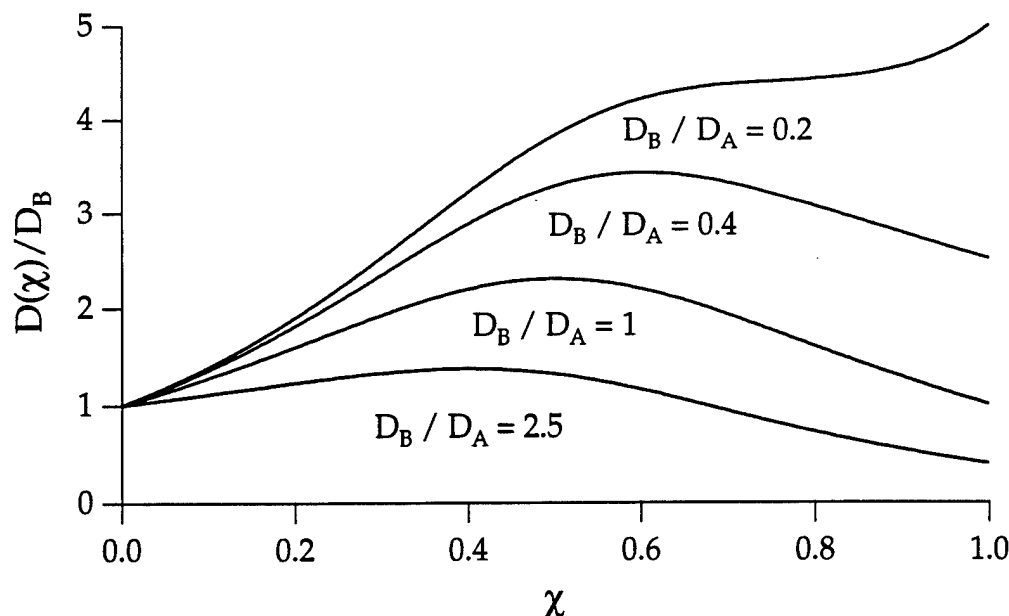
Figure 2.18 The Quasi-Chemical Diffusion Coefficient expression is plotted for different
values of the ratio D_B/D_A for $\rho = -1$ and $c = 4$.

2.3.6 _Modified Quasi-Chemical Diffusion Coefficient_

In the previous section, a new analytic expression for the concentration
dependence of the diffusion coefficient was derived that can be very useful
for fitting noisy Boltzmann-Matano calculations. For example, once the
four fitting coefficients are determined, then the expression can be placed
in a numerical routine to solve the diffusion equation for prediction of
concentration/index of refraction profiles. One main problem in this
procedure arises: in many glass systems the maximum value of the
diffusion coefficient is observed at values other than at $\chi=1/2$. The simple
quasi-chemical model cannot account for this behavior; the self-diffusion
coefficients are usually of similar magnitude in oxide glasses, and as a
result, the location of the maximum value of the diffusion coefficient is
not significantly shifted by the mobility term.

Good fits to experimental data can still be obtained, however, by
imposing a shift of the peak into the equation. Ideally, though, the final
form should still give the self-diffusion coefficients at $\chi=0$ and $\chi=1$, and

the simple mobility term should be recovered when $\varepsilon_{int} = 0$. One form that meets these requirements is called the Modified Quasi-Chemical (MQC) diffusion coefficient and is given by

$$D = \left[\frac{c}{2}\left(\frac{\chi\beta'(\chi=1)+(1-\chi)\beta'(\chi=0)}{\beta'}-1\right)+1\right]\frac{D_B}{1-\chi\alpha} \qquad (2.66)$$

where β' is a shifted version of β given by

$$\beta' = \sqrt{1-4(\chi-\chi_0)[1-(\chi-\chi_0)](1-e^{2\varepsilon_{int}/kT})} . \qquad (2.67)$$

This type of shift results in a maximum value in the $1/\beta'$ term at a concentration value of $\chi=\chi_0+1/2$. This effectively decreases the value of N_B in β' by $\chi_0(N_A+N_B)$ and increases N_A by the same amount. The numerator in the round brackets of Eq. (2.66) is simply a straight line, used for normalization to ensure that the endpoints at $\chi=0$ and $\chi=1$ are the self-diffusion coefficients. Thus, the new form now has five adjustable parameters, the four from Eq. (2.60) and χ_0.

It is noted that the theory behind the quasi-chemical diffusion coefficient does not predict this offset of the maximum from $\chi=1/2$ because the absolute number of sites has not been taken into account. Glasses with different total alkali and dopant concentrations have different transport rates, whereas the MQC model does not distinguish between a mobile cation-poor glass and a mobile cation-rich glass. In both cases, the theoretical solid has M cations for M to infinity. Furthermore, the quasi-chemical approximation allows for only one type of cation site, whereas real glasses may have multiple ones. For instance, in an aluminosilicate glass with an aluminum to alkali ratio that falls between 0 and 1, there is an alkali site associated with a non-bridging oxygen and a second type of site associated with an alumina oxyanion. The interaction energy here is modeled to be the same constant in this glass. If there is some preferential occupation of a type of site by one of the exchanging cations, the average interaction energy is then concentration dependent.

2.4 Solving the Diffusion Equation

2.4.1 Introduction

A model for concentration-dependent diffusion was developed in the previous sections. It uses Fickian diffusion theory and the diffusion equation to model the ion exchange manufacturing process and to incorporate the experimental parameters into the model. By solving the diffusion equation for a concentration profile, the results of a particular ion exchange experiment can be predicted. This process is complicated by the fact that the diffusion coefficient for typical ion exchange conditions becomes concentration-dependent; in general, the diffusion equation must be solved numerically. Therefore, the final step to completing a mathematical model for concentration-dependent diffusion is the development of a numerical routine which can solve the diffusion equation for a concentration-dependent diffusion coefficient.

In this section a numerical routine is discussed which calculates concentration profiles based on manufacturing parameters. Its accuracy is tested against known analytic solutions to the diffusion equation. It also incorporates the Modified Quasi-Chemical (MQC) Diffusion Coefficient expression to model the concentration-dependent diffusion coefficient. As a result, the numerical routine is useful for two reasons. First, the routine can be used to test the MQC model through the recovery of the initial index of refraction profile. Second, (if the diffusion coefficient model is accurate enough) it represents the final mathematical model of ion exchange required for the design-for-manufacture approach, and can then be used to predict future index of refraction profiles from experimental process parameters.

2.4.2 Numerical Routine

A finite difference routine to solve the diffusion equation for a set of general experimental conditions is presented. The program uses several standard routines developed by Numerical Algorithms Group (NAG) to solve the diffusion equation. The specific calling routine is written in Fortran and is given in appendix A. The two types of geometries

considered in this thesis are axial and radial, although the program will also solve the diffusion equation for a three-dimensional spherical geometry. The routine is currently set up to take in the coefficients of the MQC model for the diffusion coefficient, but if needed other representations for the concentration dependence of the interdiffusion coefficient are easily substituted. The calling routine was also designed to be easily linked to a lens design program for future optimization of the manufacturing parameters.

On input the program asks for the manufacturing parameters of the system: diffusion time, initial glass concentration, and salt concentration. It also requires knowledge of the concentration dependence of the diffusion coefficient (currently in the form of MQC coefficients). The manufacturing parameter of temperature is also included since the diffusion coefficient is temperature dependent. Finally, the index of refraction as a function of concentration must also be given to convert the concentration profile to an index of refraction profile (see Chapter 3 for further explanation). For added complexity, other experimental conditions can be easily included. For example, time-varying boundary conditions allow the inclusion of more complex experimental conditions such as finite salt baths and post-annealing of ion exchanged samples.

2.4.3 Error Analysis

The accuracy of the numerical routine is tested using two known analytic solutions for concentration-independent diffusion, one in an axial geometry and one in a radial geometry. The first test case is the one-dimensional diffusion for which the analytic solution is a complementary error function given by Eq. (2.9). Figure 2.19 (a) compares a theoretical solution (solid line) with a numerical solution (dashed line). Figure 2.19 (b) then shows the error between the two solutions. The second test case is a radial diffusion for which the analytic solution was the infinite sum of Bessel functions given by Eq. (2.17). Figure 2.20 (a) compares the theoretical solution with the numerical solution and Fig. 2.20 (b) shows the error between the two solutions. In both test cases, the maximum error in the solution is less than 0.1 percent.
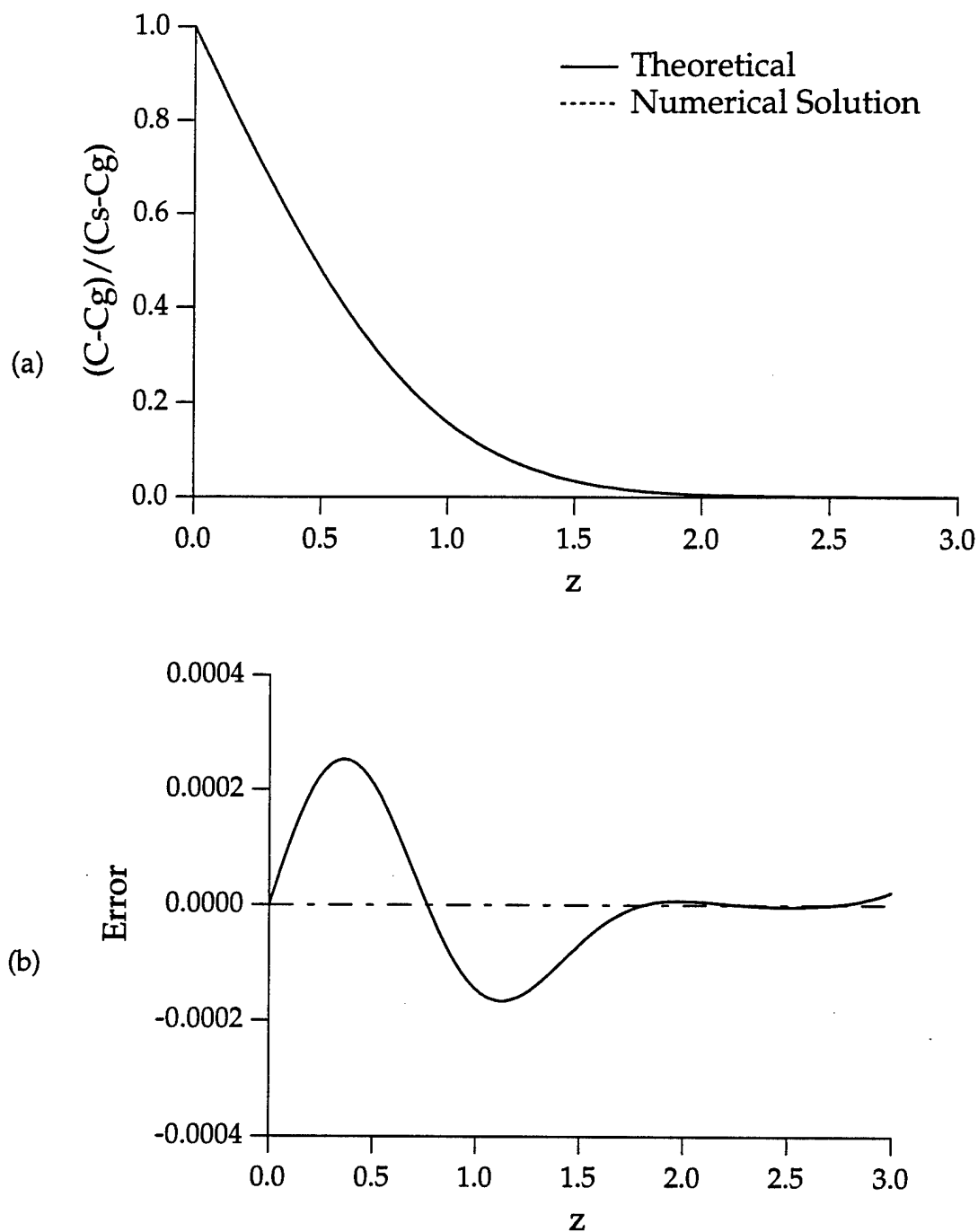
Figure 2.19 The accuracy of the numerical routine to solve the equation is illustrated where (a) shows both the theoretical concentration profile and the numerical solution for an axial gradient and (b) shows the difference between the two profiles.
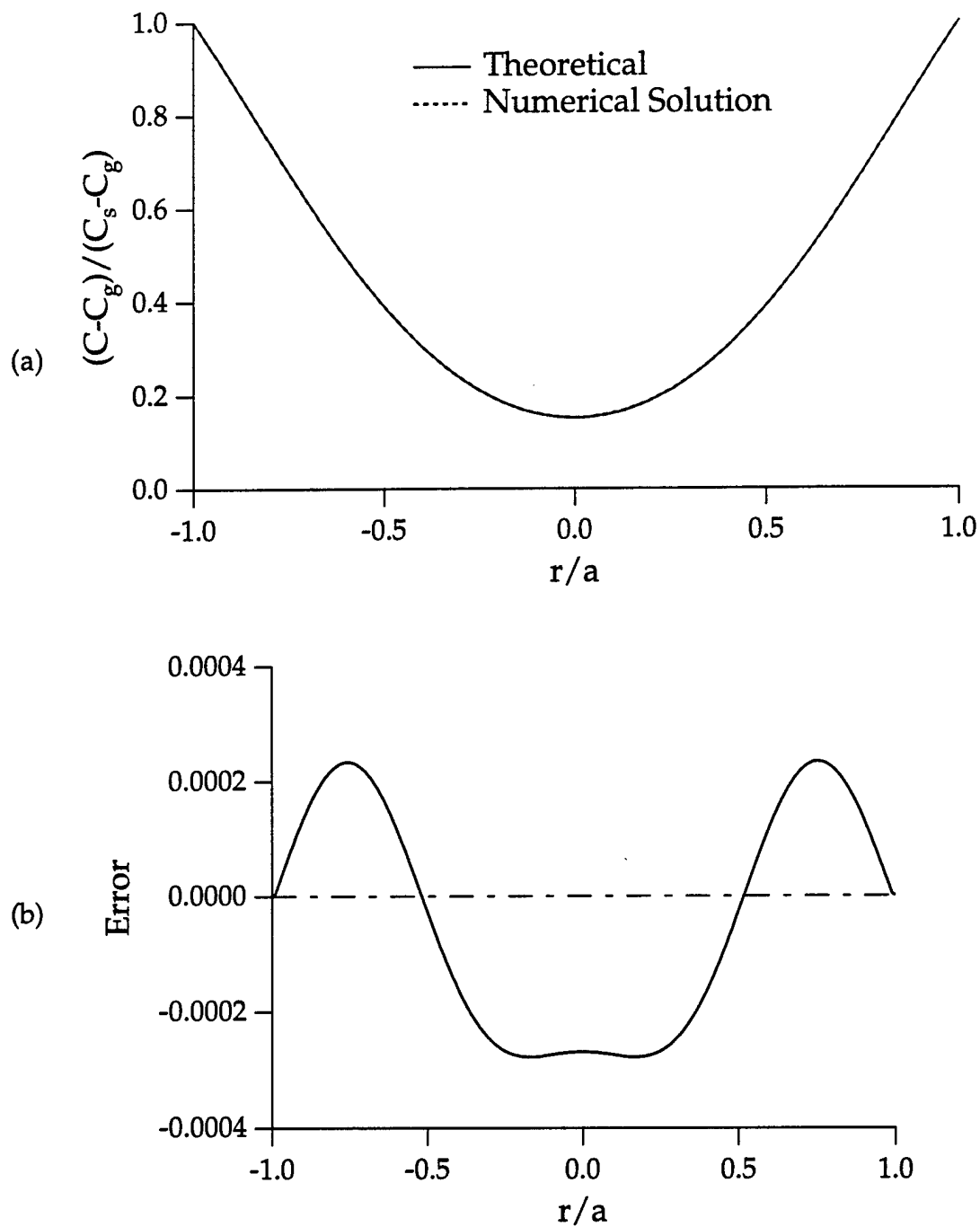
Figure 2.20 The accuracy of the numerical routine to solve the equation is illustrated where (a) shows both the theoretical concentration profile and the numerical solution for an radial gradient and (b) shows the difference between the two profiles.

2.4.4 Verification of the MQC Model

The numerical routine can also be used to test the new model for the concentration dependence of the diffusion coefficient. First, the experimental diffusion coefficient data shown in Fig. 2.13 can be fit (using least squares) to the MQC expression. The fitting coefficients are given in Table 2.1 and a plot of the experimental diffusion coefficient and its fit are shown in Fig. 2.21. Although it appears to fit the data, with the large amount of noise, it is difficult to tell if the model is truly an accurate representation for the concentration dependence of this diffusion coefficient. However, if the diffusion model can accurately recover the initial index of refraction profile by using the MQC expression for the concentration dependence of the diffusion coefficient, this indicates that the MQC model is a good representation for this diffusion coefficient.

Figure 2.22 (a) shows the result of using the MQC fit parameters (from Table 2.1) in the numerical routine to solve the diffusion equation and illustrates how accurately the initial concentration profile can be recovered. In particular, Fig. 2.22 (b) shows the error between the two solutions with a maximum error much less than one percent. Thus, the MQC diffusion coefficient appears to be a good model. A more detailed discussion of the errors involved in calculating the diffusion coefficient and the effect of the errors on the concentration profile is given in the Chapter 3.

Since the routine also accepts other types of concentration dependence for the diffusion coefficient, the diffusion coefficient given in Fig. 2.13 is also fit to the following gaussian form:

$$D(C) = D_0 + D_1 \exp\left(-((C - D_2)/D_3)^2\right), \tag{2.68}$$

where the D_i are the fitting coefficients. This fit is shown in Fig. 2.23 and the fit coefficients are listed in Table 2.2. Although this form also appears to give a good fit to the experimental data, as shown in Figs. 2.24 (a) and (b), the recovery of the initial index of refraction profile is not as accurate as the MQC model. In particular, the gaussian does not properly represent the diffusion coefficient near the low concentration region which can be

seen by the difference in fits in this area. Thus, in addition to being based
in physics with meaningful fit coefficients, the MQC diffusion coefficient
is also more accurate in recovering a known index of refraction profile. As
a result, it is all the more useful in predicting new experimental profiles.
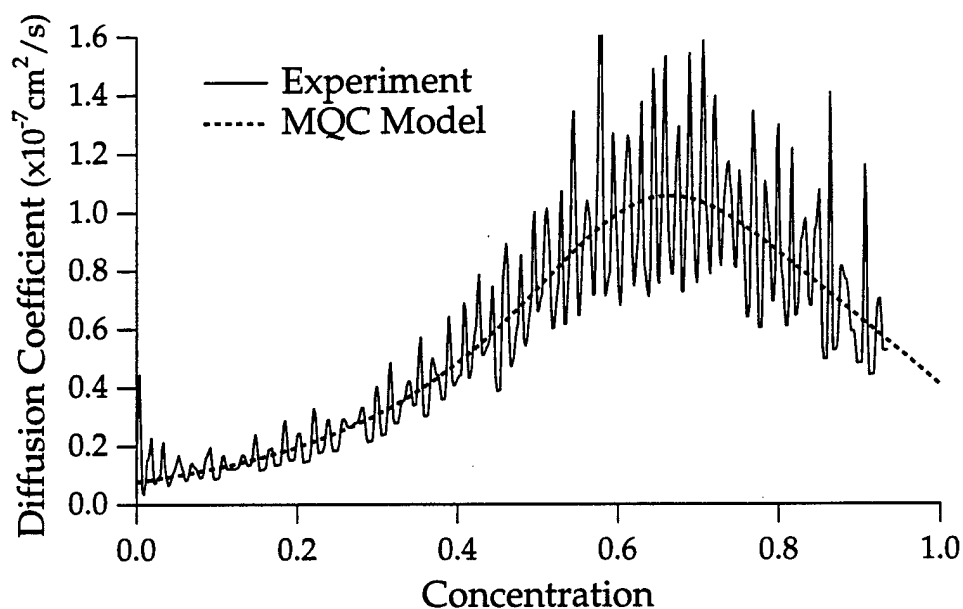
Figure 2.21 A typical example of a Modified Quasi-Chemical fit to an experimentally
calculated diffusion coefficient. The specific values of the fit parameters are listed in
Table 2.1.

D_B	α	ρ	χ_0	c
0.077	0.81	-1.855	0.131	8

Table 2.1 Modified Quasi-Chemical fitting parameters for the experimental diffusion
coefficient shown in Fig. 2.21.
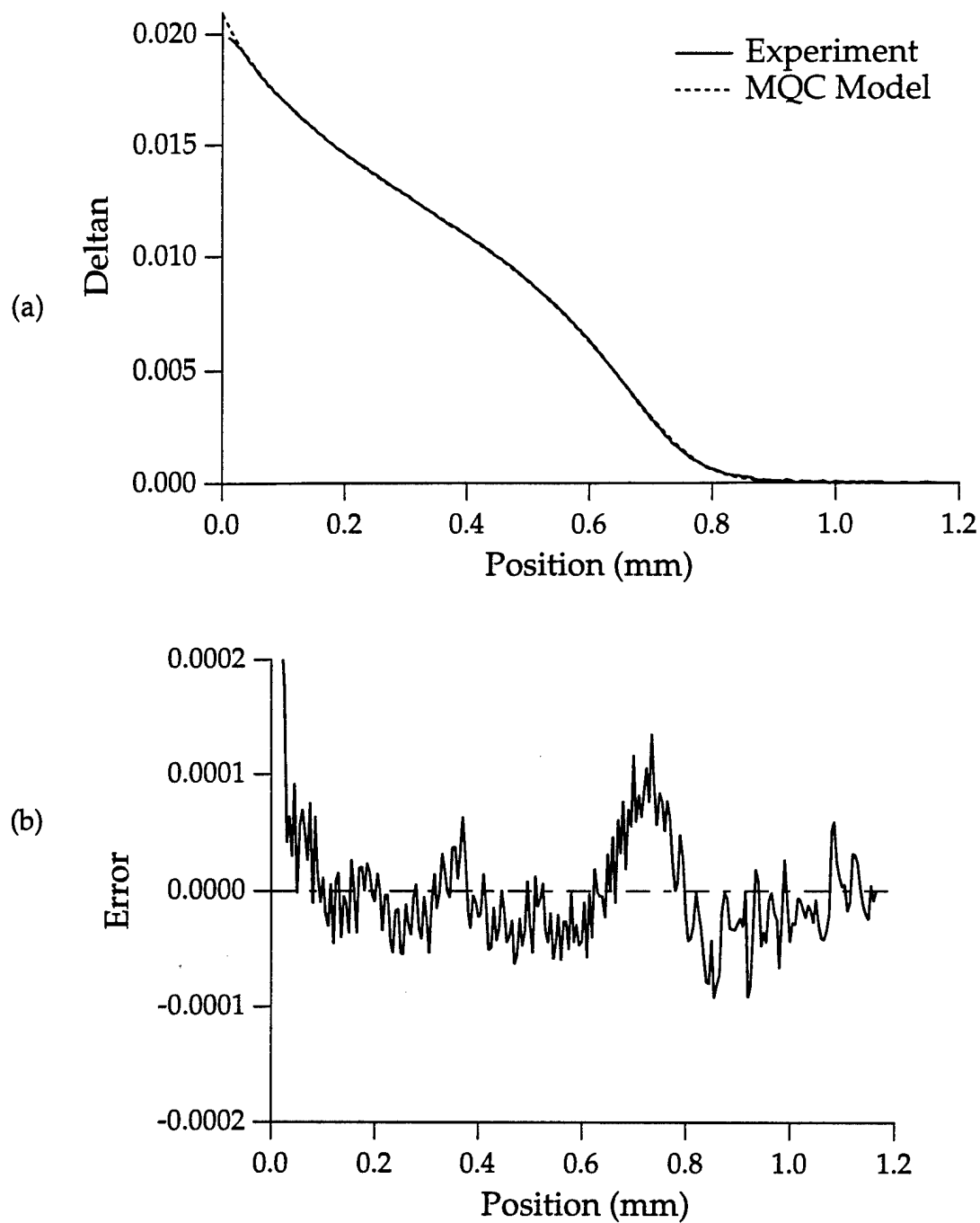
Figure 2.22 The accuracy of the MQC diffusion coefficient model is tested by comparing the original index of refraction profile to the numerical solution from the diffusion equation where (a) shows both the initial experimental profile and the numerical solution and (b) shows the difference between the two profiles.
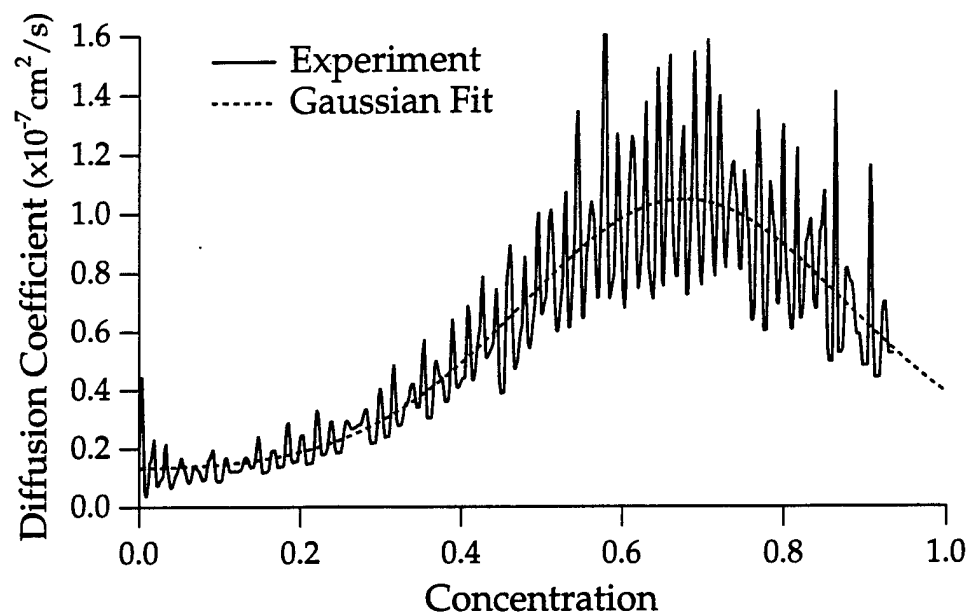
Figure 2.23 A gaussian fit to an experimentally calculated diffusion coefficient is shown
where the fit is defined by Eq. (2.68) and specific values of the fit parameters are listed
in Table 2.2.

D_1	D_2	D_3	D_4
0.1280	0.9165	0.6771	0.2875

Table 2.2 Gaussian fitting coefficients as defined by Eq. (2.68) for the fit to the
experimental diffusion coefficient shown in Fig. 2.23.
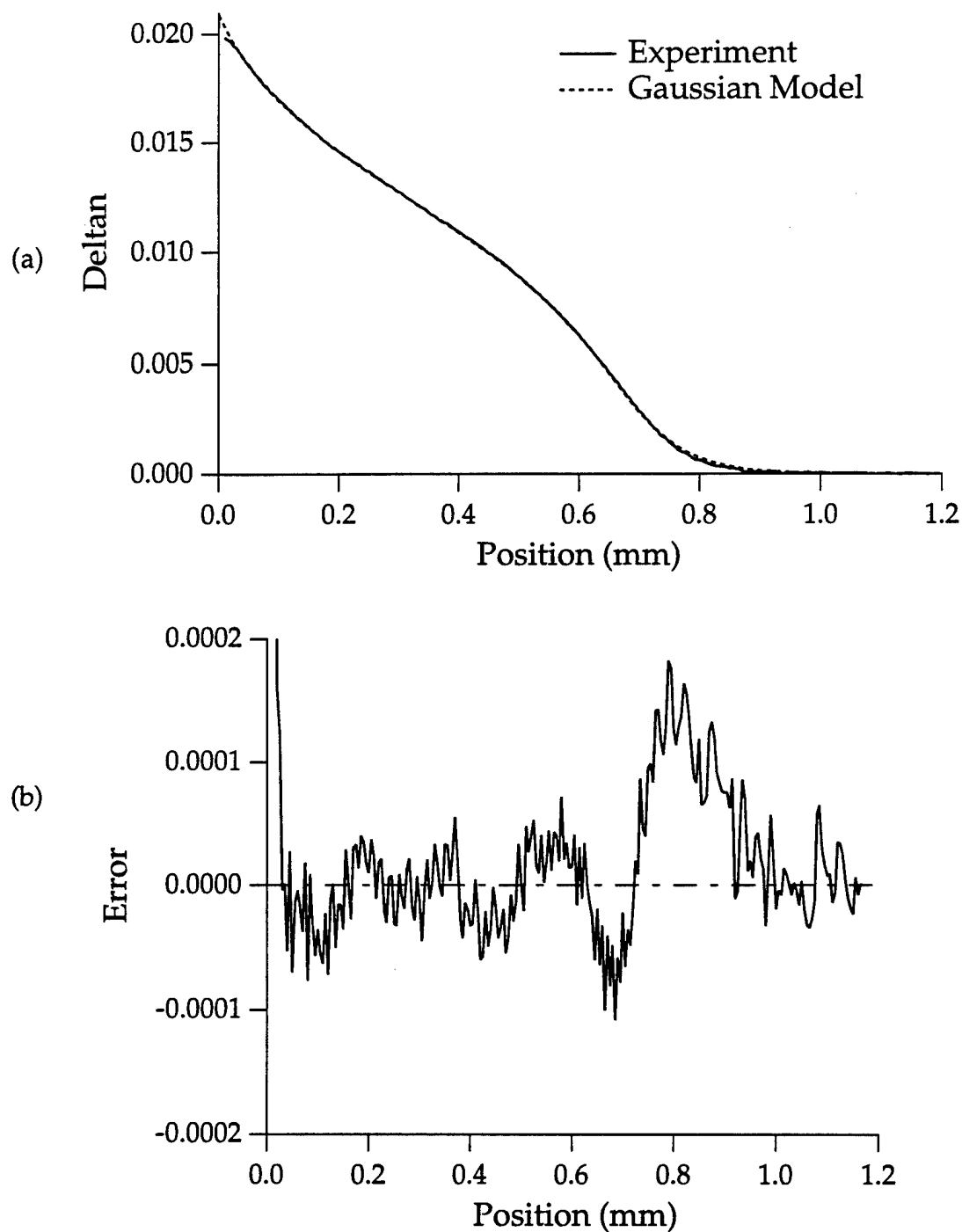
Figure 2.24 The accuracy of the gaussian fit to the experimental diffusion coefficient is tested by comparing the original index of refraction profile to the numerical solution from the diffusion equation where (a) shows both the initial experimental profile and the numerical solution and (b) shows the difference between the two profiles.

References

1. J. Crank, *The Mathematics of Diffusion*, second edition. Oxford University Press, New York (1975), ch. 1.

2. H. Fujita, "The exact pattern of a concentration-dependent diffusion in a semi-infinite medium, part I," J. Text. Res. **22**, 757-760 (1952).

3. R. H. Doremus, "Exchange and diffusion of ions in glass," J. Phys. Chem. **68**, 2212-2218 (1964).

4. G.H. Frischat and R. Kirchmeyer, "Relation between tracer diffusion and ion exchange in silicate glasses," J. Amer. Ceram. Soc. **56**, 552 (1973).

5. A.R. Cooper, "Diffusion processes in glass," in: *An Introduction to Glass Science*, ed. L.D. Pye, H.J. Stevens, and W.C. LaCourse, Plenum, New York (1972).

6. Reference 1, p. 2.

7. Reference 1, p. 212.

8. W. Jost, *Diffusion in Solids, Liquids, and Gases*, Academic Press, New York (1960) p. 145.

9. Reference 5.

10. Reference 4.

11. Reference 5.

12. R.H. Doremus, *Glass Science*, John Wiley and Sons, New York (1973), ch. 9.

13. Reference 3, p. 2212.

14. J. A. Marinsky, *Ion Exchange*, Marcel Dekker, Inc., New York, NY (1969), p. 9.

15. M. Garfinkel, "Ion exchange between glass and molten salts," J. Phys. Chem. **72**, 4175 (1968).

16. Kurt H. Stern, "Membrane potentials of fused silica in molten salts. A reevaluation," J. Phys. Chem. **74**, 1323-1329 (1970).

17. Reference 3.

18. Reference 12.

19. Reference 15.

20. Reference 16.

21. Moiseev, V. V., et al, "The thermodynamic characteristics of the ion exchange process in sodium silicate glasses," Fizika i Khimiya Stekla; for English translation see Soviet J. Phys. and Chem. **3**, 22 (1977).

22. G.L. McVay and D.E. Day, "Diffusion and internal friction in Na-Rb silicate glasses," J. Amer. Ceram. Soc. **53**, 508-513 (1970).

23. R.W. Laity, "Fused salt concentration cells with transference activity in the system silver nitrate-sodium nitrate," J. Amer. Chem. Soc. **79**, 1849-1851 (1850).

24. Reference 16.

25. R. Araujo, "Interdiffusion in a one-dimensional interacting system," J. Non-Cryst. Solids **152**, 70-74 (1993).

26. J.M. Inman, J.L. Bentley, and S.N. Houde-Walter, "Modeling ion-exchanged glass photonics: the modified quasi-chemical diffusion coefficient," J. of Non-Cryst. Solids **191**, 209-215 (1995).

27. T. L. Hill, *Statistical Mechanics*, McGraw-Hill, New York (1956), p.348.

28. S.N. Houde-Walter, et al., "Sodium and silver environments and ion-exchange processes in silicate and aluminosilicate glasses," J. Phys. Chem. **97**, 9330 (1993).

29. Reference 25.

30. Reference 21.

31. Reference 27.

32. Reference 27.

33. Reference 27.

Chapter III
Experimental Procedure

3.1 Introduction

A mathematical model for concentration-dependent diffusion is presented in Chapter 2. The model uses Fickian diffusion theory to calculate an index of refraction profile for a given set of experimental ion exchange parameters. However, the theoretical model requires prior knowledge of two quantities which, in most cases, must still be measured experimentally. First, the diffusion coefficient as a function of both concentration and temperature must be known to completely specify the diffusion equation. Second, the index of refraction as a function of concentration is needed to convert the concentration profile to an index of refraction profile. Each of these quantities depends on which glass composition and ion exchange pair is used in the experiment.

A wide variety of components can be added to a glass melt to change the optical, mechanical, chemical, and thermal properties of the glass. In most cases, small changes in glass composition (such as the addition of a single component) can cause large changes in the properties of the glass. As a result, a purely mathematical representation for either the index of refraction or the concentration dependence of the diffusion coefficient has

not been found that can be written solely as a function of glass composition and applied to any given glass and ion exchange pair. Therefore, these quantities must be determined experimentally for each particular glass composition. Empirical models can then be developed to quantify the experimental results and incorporate them into the diffusion model.

For example, Huggins developed a model to relate the density and the index of refraction of a glass to its composition. [1] In particular, he determined the values of the empirical constants of the model for many of the glass components used in silicate optical glasses. Similarly, a theoretical expression for the concentration dependence of the diffusion coefficient was developed in Chapter 2 that can be used as an empirical model for experimentally calculated diffusion coefficients. Although both of these models require initial experiments to determine the values of their empirical constants, once the constants are determined for a particular glass composition they do not need to be measured again. Furthermore, experiments in a series of glasses within a limited range of compositions can be used to develop an understanding of how the empirical constants change across that range. This could ultimately reduce the number of experiments required to define a diffusion model for each particular glass within this range of compositions.

An experimental procedure for determining both the diffusion coefficient and the index of refraction as a function of concentration for a particular glass composition is given in this chapter. For each step in the calculations an error analysis is given which includes a discussion of how the error affects the accuracy of the final diffusion model. The ultimate goal of the chapter is to determine an experimental procedure which characterizes a glass composition with the fewest experiments and the least error. This procedure is then used in Chapters 4 and 5 to develop empirical diffusion models for several different types of glasses.

3.2 Choosing a Glass Composition

Glass components are usually divided into three categories based on their oxygen bond strength: formers, intermediates, and modifiers (in order of decreasing bond strength). [2] Glass formers determine the basic molecular structure of a glass material and, as their name implies, can form glass by themselves. The most common glass former is SiO_2; others include B_2O_3 and P_2O_5. Although the intermediates can have a significant effect on the structure of the glass they cannot form glass alone. Examples of glass intermediates include Al_2O_3, TiO_2, La_2O_3, ZrO_2, and Nb_2O_5. They are usually added to a glass in small amounts to improve its optical, chemical, mechanical, and thermal properties. Glass modifiers are also used to changed the properties of the glass. For example, alkali oxides such as Na_2O, K_2O, and Li_2O are commonly used as fluxing agents in a glass melt to decrease its melting temperature.

The proper choice of glass components for a gradient-index glass requires a basic knowledge of glass science. [3,4] In particular, it is important to know the glass forming regions for the chosen components and the effect each component will have on both the optical properties of the glass and the ion exchange. For example, an extensive set of glass data (such as glass forming region, transition temperature, etc.) for many different types of homogeneous glasses (including binary silicate, binary non-silicate, and ternary silicate glass systems) has been compiled. [5] An excellent description of how to use this type of data to choose a set of glass components and develop a good gradient-index glass for ion exchange is given by Kindred. [6]

For most optical glasses, SiO_2 is chosen as the glass former because of its large glass forming regions with other components, low cost, high availability, and excellent optical properties. Although B_2O_3 is also used in many commercial homogeneous glass compositions, borate glasses tend to have relatively low ion exchange rates. [7] Other glass formers are sometimes used to obtain special glass properties, but are usually much more expensive. The modifiers which are added to the glass composition are usually limited to single valence oxides (such as Na_2O, K_2O, Ag_2O, and

Li$_2$O), since they are used as the source of ions for the ion exchange. Thus, the type and amount of modifier added to a glass composition plays a large part in determining the properties of the gradient. Finally, the intermediates are selected to obtain the desired optical and mechanical properties of the glass, but must be chosen carefully to ensure that they do not adversely affect the diffusion properties of the glass. For example, the addition of only a few percent Al$_2$O$_3$ to an alkali silicate can improve the hardness and durability of the glass but does not hinder the diffusion; for some compositions it can actually increase the ion exchange rate. [8]

Most of the glass compositions examined in this thesis were either developed by Kindred or are similar compositions based on the results of his work. The glasses usually have three to five components with SiO$_2$ or B$_2$O$_3$ as the glass former and Al$_2$O$_3$, TiO$_2$, and/or ZrO$_2$ as the intermediate components. The Li$^+$–Na$^+$ ion exchange pair is then examined through the addition of the single valence modifier oxides Na$_2$O and Li$_2$O. In particular, lithium for sodium exchange produces a positive index of refraction change in that the index of refraction of the material is increased after exchange. Negative index of refraction changes can be produced by the opposite exchange, sodium for lithium. In most glasses, Li$^+$–Na$^+$ exchange results in a relatively low index change and a low gradient dispersion, but this can be highly dependent on base glass composition. [9] Furthermore, this ion exchange pair is one of the few pairs which, in certain glass compositions, can produce an index of refraction gradient without creating a gradient in dispersion ($V_{grin} = \infty$) making it an interesting exchange to study for lens design.

3.3 Glass Melting

The base glass compositions needed to fabricate gradient-index materials are rarely available commercially and must be melted in the laboratory. For a thorough discussion of experimental glass melting techniques the reader is referred to Blair. [10] Kindred also gives a general description of the glass melting procedure and then modifies it for much smaller melt sizes to fabricate his gradient-index base glasses. [11] A

similar approach is taken to fabricate the homogeneous base glasses presented in this thesis and is described below.

The melting process can be divided into several stages: preparing and mixing the batch, pre-melting, melting, casting, and annealing. Once the composition is chosen, a set of batch chemicals is identified, and their proportions calculated. For example, fine powder, reagent grade oxides (such as SiO_2, B_2O_3, TiO_2, Al_2O_3) and carbonates (such as Li_2CO_3 and Na_2CO_3) are used as batch materials. The typical batch size ranges from 100 to 300 grams. Each chemical component is weighed out to an accuracy of ±0.01 grams. The components are then thoroughly ground and mixed in a mortar with a pestle for two to three minutes.

A 250 gram platinum crucible is then filled approximately two-thirds full with a portion of the mixed batch. The platinum is essential for good quality optical glass, as the molten glass usually attacks other types of crucibles (such as alumina clay pots) causing inhomogeneities in the melt. The platinum crucible is placed in a Lindberg electric resistance furnace which uses $MoSi_2$ heating coils and has maximum temperature of 1700 °C.

During the pre-melt stage the crucible is heated to a temperature between 900 °C and 1200 °C to allow the chemical reactions of the batch components to occur. For example, this step allows for dissociation of the carbonates according to

$$Na_2CO_3 \rightarrow Na_2O + CO_2 , \tag{3.1}$$

releasing CO_2 from the melt. Thus, the crucible was originally only partially filled to allow for the foaming and frothing of the melt as the gases are released. The remainder of the batch is usually added in half an hour increments until the entire batch is in the crucible and most of the carbon dioxide has been released.

The furnace is then turned up to a temperature at which the glass is sufficiently fluid to become homogeneous. The melt is held at this temperature for at least 4 to 8 hours to remove the remaining bubbles in the glass and allow the melt to homogenize. The glass is sometimes intermittently stirred with a platinum stir bar for improved homogeneity. The glass is then cooled to a temperature at which it is thick enough for

casting. (Note: the glass should readily flow from the crucible, but it should not be so thin that it overlaps itself during the pour since this creates inhomogeneities in the glass.) The glass is poured in a single, continuous stream into a room temperature steel mold. For some glasses, the mold can be heated to prevent any cracking of the glass while it is cooling in the mold. On the other hand, glasses which are prone to crystallize can be cast on water cooled molds and rapidly quenched.

Finally, when the glass is just cool enough to be rigid, it is lifted with a spatula and placed into an annealing furnace which has been preheated to a temperature between 450 °C and 650 °C. The glass is then allowed to cool slowly (over a period of approximately 24 hours) to room temperature. This last step is important since many of the properties of the glass, including the index of refraction, depend on the rate of cooling of the glass. Therefore, if the glass is cooled too quickly, the inside cools at a different rate than the outside, which creates stress and index of refraction inhomogeneity in the glass. The annealing step allows the glass to cool at a slow controlled rate to relieve the internal stresses caused by the differential cooling within the melt during the casting process and creates a uniform refractive index across the glass melt.

3.4 Index of Refraction/Dispersion

3.4.1 Introduction

At each position in a gradient-index material, the relationship between the index of refraction of the glass and the concentration of the diffusing ions at that position is required by the mathematical diffusion model for two reasons. First, it is needed to relate the concentration profile obtained from solving the diffusion equation to an index of refraction profile that can be used in optical design. Second, the experimental calculation of the diffusion coefficient using the Boltzmann-Matano method requires a measured concentration profile. For Ag^+–Na^+ exchange, concentration profiles can be measured directly from an ion exchanged sample using Energy Dispersive X-Ray Spectroscopy (EDX). [12] Unfortunately, for

Li^+–Na^+ exchange, the methods for the quantitative analysis of lithium concentration profiles are both difficult and costly.

Alternatively, an approach similar to Kindred's [13] can be used to determine the Li^+ concentration profile in an ion exchanged sample from the measurement of an index of refraction profile n(z), where z is the position in the sample. First, a series of homogeneous glasses must be melted with different concentrations of lithium ranging from zero to the maximum possible exchanged concentration. Therefore, each successive glass in the series has a different ratio of the two species involved in the ion exchange, but maintains equal mole fractions of the other constituents. Then, the index of refraction of each glass can be measured to determine an experimental relationship between refractive index and lithium concentration, or $n(C_{Li^+})$. Finally, the concentration profile can then be calculated indirectly according to

$$z(C_{Li^+}) = z(n(C_{Li^+})).$$
(3.2)

Furthermore, the same type of analysis can also be used to convert theoretical concentration profiles from the diffusion model to index of refraction profiles for lens design. Note that this technique assumes that the index of refraction of a glass is the same whether the lithium has been melted into the glass or diffused into the sample. This assumption was shown to be valid by Kindred for Li^+–Na^+ exchange in several glass systems similar to the ones studied in this thesis. [14]

3.4.2 Huggins, Sun, and Davis (HSD) Model

An accurate measurement of the experimental relationship between refractive index and lithium concentration, or $n(C_{Li^+})$ requires a large number of glass melts and a large amount of time. This can be reduced if a model for the index of refraction as a function of glass composition can be determined. For example, in 1940, Huggins used the Gladstone-Dale formula to relate the density [15] and the index of refraction [16] of silicate glasses to their compositions. He then used empirical data to calculate constants for nearly all the glass components used in silicate glasses. Later,

a more accurate dispersion relation was developed by Huggins, Sun, and Davis which improved the model. [17]

The index of refraction of a glass can be written as a function of the molar refractivity R and the molar volume V per gram atom of oxygen, according to

$$n_\lambda = 1 + \frac{R(\lambda)}{V} \ .$$

(3.3)

In his model, Huggins showed that both R and V can then be written as a weighted linear sum of each component oxide, M_mO_n, in the glass. For example, the volume, V, is given by a summation over all the oxides, M_mO_n, in the glass as

$$V = k + b_{Si} + c_{Si}N_{Si} + \sum_M c_M N_M$$

(3.4)

where

k is an annealing constant ranging from 0.001 to 0.05 which accounts for volume differences caused by changes in the annealing rate of the glass,

N_{Si} is the number of silicon atoms per oxygen atom in the glass,

N_M is the number of atoms of type M per oxygen atom in the glass,

and b_{Si}, c_{Si}, and c_M are volume constants. Similarly the refractivity is written as

$$R(\lambda) = \sum_M a_M(\lambda) N_M$$

(3.5)

where, again, the summation is over all the oxides in the glass, and a_M is the refraction constant for species M which varies with wavelength as

$$a_M(\lambda) = d_M \left[\frac{1}{\left(g_M - 1/\lambda^2 \right)} - 4.8 \times 10^{-5} \lambda^2 \right]$$

(3.6)

where d_M and g_M are refraction constants for each oxide component M.

Since the Huggins, Sun and Davis model (HSD) was developed for homogeneous glasses, Fantone [18] modified it to include gradient-index glasses to predict the refractive index of the material as a function of the dopant concentration. In addition, both Fantone and Ryan-Howard [19] updated and made corrections to the constants for better agreement with many of the modern optical glasses. Thus, once the empirical constants for each component in the glass are known, then the index of refraction, dispersion, and density of the homogeneous glass may be calculated, along with the maximum index change and gradient dispersion for a particular ion exchange pair. Therefore, for a specific glass composition, the HSD model can be used to determine the index of refraction as a function of the concentration of the diffusing species. Unfortunately, the published empirical constants do not apply to all possible glass compositions, and, as a result, the index of refraction as a function of concentration must still be measured experimentally for some glass compositions.

3.4.3   Measurement Procedure

A small sample is cut from each glass melt and polished flat to a $1/4\ \lambda$ on one side. The index of refraction of each piece is then measured on a Pulfrich refractometer (manufactured by Carl Zeiss, Jena, Germany) at the helium d line (587.6 nm), the mercury e and g lines (546.1 nm and 435.8 nm, respectively) and the HeNe laser line (632.8 nm). The index of refraction measurements at 632.8 nm are important since the index of refraction profiles are also measured at this wavelength. The measured refractive indices are also used to determine the dispersion of the glass,

$$V = \frac{n_d - 1}{n_F - n_C} ,$$ (3.7)

where F and C are hydrogen lines at 486.1 nm and 656.3 nm, respectively.

Since n_F and n_C could not be measured on the Pulfrich, they must be interpolated from the other measured index of refraction values. To

accomplish this, the wavelength dependence of the index of refraction can be expressed by the polynomial expansion

$$n(\omega) = n_0 + n_1\omega + n_2\omega^2 + ...$$ (3.8)

in the chromatic coordinate ω defined as

$$\omega = \frac{(\lambda - \lambda_0)}{1 + \alpha(\lambda - \lambda_0)}$$ (3.9)

for α = 2.5 and λ_0 = 0.574 µm. [20] This expansion is rapidly converging and can often be truncated at the second order. Therefore, the four measured indices can be plotted and fit to Eq. (3.8) using Eq. (3.9) to find the values of the constants n_0, n_1, and n_2. The indices n_F and n_C can then be interpolated from the fit for a calculation of the dispersion V.

3.4.4 Error Analysis

The refractometer is capable of measurements of refractive index to an accuracy of ±0.00001 for samples with exceptional homogeneity and high quality polished surfaces. Most of the samples in this thesis are limited by poor homogeneity and surface quality such that the index of refraction measurements are accurate to only ±0.0003. Some of the larger glass melts were more homogeneous and therefore the error in measuring the index of refraction was slightly better (±0.0001). The method for determining the index of refraction as a function of Li^+ concentration, or $n(C_{Li}^+)$, also assumes that the final melted glass composition is the same as that which was originally placed in the crucible. For this reason, the concentrations of some of the glasses were measured by Atomic Absorption Spectroscopy by Corning Engineering Laboratory Services, Corning Glass Works, Corning, New York. The measured component concentrations agreed with the initial concentrations to within ±0.1 percent.

3.5 Ion Exchange Experiments

3.5.1 Introduction

In a typical ion exchange experiment, a sample of glass (containing one type of single valent ion) is suspended in a molten salt bath (containing a

different type of single valent ion). The experiment is held at a set temperature for a specified period of time, during which an interdiffusion of the two ions occurs because of the concentration gradient across the glass/salt boundary. The glass is then removed from the molten salt and cooled to room temperature. The exchange of the ions between the glass and the salt bath produces a concentration gradient of both diffusing species in the glass sample. Since the refractive index of the glass is a function of concentration, the concentration profile in the exchanged sample results in a corresponding index of refraction profile.

For each glass composition, several ion exchange experiments are required to define and test an empirical diffusion model. First, an axial diffusion is needed to calculate the concentration dependence of the diffusion coefficient for that particular glass composition. Next, other experiments are used to test the diffusion model for different diffusion times and temperatures in both axial and radial geometries. The range of diffusion times that can be explored is usually limited by the sample size. For example, in a small axial sample, if the diffusion time is too long it can begin to diffuse through to other side. The range of temperatures is constrained by both the glass and the salt melt. For example, low diffusion temperatures are usually limited by the ability to find a salt composition which is molten at that temperature, while high diffusion temperatures are limited by the temperature at which the glass starts to deform.

3.5.2   Experimental Procedure

The two different sample geometries explored in this thesis are axial and radial. For axial diffusions, small samples, typically 10 x 15 x 15 mm, are cut from the homogeneous glass melt with a Buehler Isocut™ saw. A high density diamond blade is used such that the cut surfaces of the sample resemble fine ground glass surfaces. For radial diffusions, rods are core drilled from the glass melt and then hand ground to the desired diameter. Each glass sample is cleaned with acetone and wrapped in a "wire basket" (platinum wire for chloride salt melts and stainless steel wire for nitrate salt melts).

The sample basket is then suspended at the end of a long quartz tube by running a second wire along the inside of the tube and connecting it to the top of the basket. A hole the size of the diameter of the tube was drilled in the lid of a top loading furnace such that the quartz tube can be raised and lowered with a metal clamp on the top of the furnace. This set-up allows the sample to be easily placed into and out of a molten salt bath that is positioned directly below the hole in top of the furnace. The sample is always suspended far enough below the end of the quartz tube so that only the sample enters the molten salt bath and not the quartz tube.

The salt composition is weighed and mixed thoroughly. The salt is then placed in beakers ranging in size and type from 250 ml Pyrex™ beakers, used mainly for lithium chloride salt melts, to a 3000 ml stainless steel beaker used for sodium nitrate melts. (Note: the stainless steel beakers are reusable since the old salt baths can be removed from the beakers, while the Pyrex beakers crack and new beakers are required for each experiment.) The filled beaker of salt is then placed on the floor of the oven with the sample hanging directly over the salt bath.

The furnace is then heated to the diffusion temperature. During this time, the temperature of the salt bath is monitored until it stabilizes at the diffusion temperature. The glass sample is then lowered into the molten salt bath about 1 cm from the bottom of the bath and allowed to remain in the salt bath for the required diffusion time (ranging from six hours to seven days). Afterwards, the glass sample is raised out of the salt bath and the furnace turned down to room temperature.

The temperature cycle for a typical experiment is shown in Fig. 3.1. A 250 gram salt melt was heated to a temperature of 510 °C and after five hours it was allowed to cool to room temperature. The solid line in the figure gives the temperature of the furnace as read from the oven controller and the dashed line gives the actual temperature of the salt as measured from a thermocouple placed directly in the salt. A comparison of the two measurements shows that while it takes only one hour for the furnace thermocouple to read the diffusion temperature it takes at least four additional hours for the salt bath to reach the diffusion temperature and equilibrate. Figure 3.1 also shows that during the cooling cycle it takes
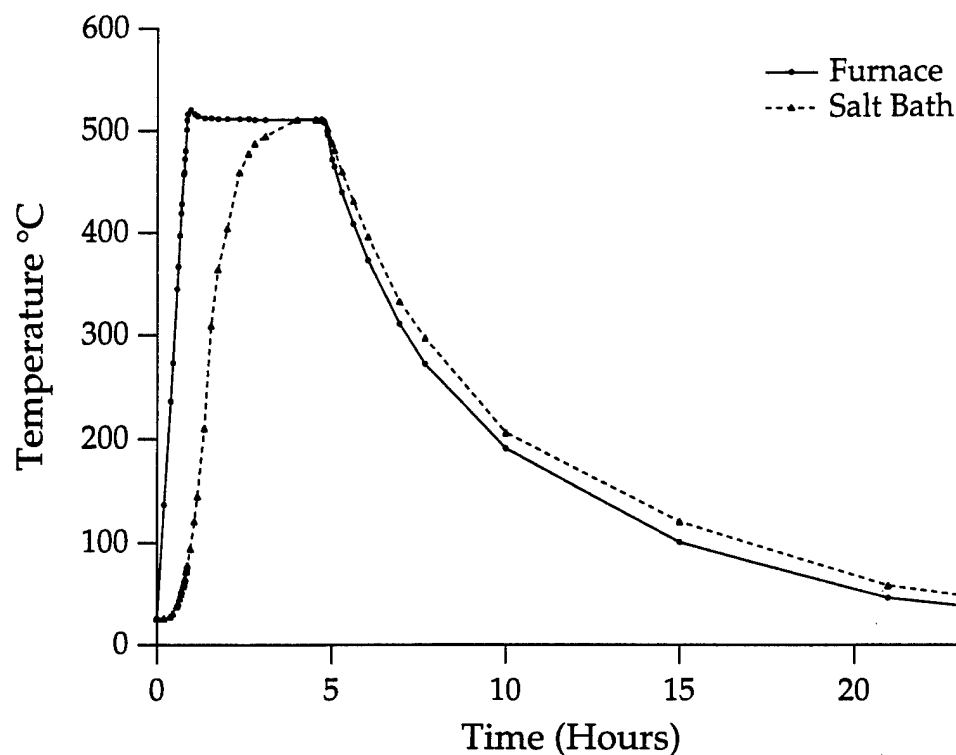
Figure 3.1 The temperature cycle for a typical experiment in which a 250 g salt melt was heated to a temperature of 510 °C and then allowed to cool to room temperature. The solid line shows the temperature of the furnace, while the dashed line shows the temperature of the salt melt.

approximately 16 hours for the furnace (and therefore the sample) to reach room temperature.

3.5.3   Error Analysis

The salt bath components are weighed to ± 0.01 grams. The diffusion temperature is measured to ± 1 °C using a K-type thermocouple. Although the diffusion time is known to ± 2 minutes, the extended cooling cycle (shown in Fig. 3.1) results in additional errors. First, any remaining salt on the faces of the sample during cooling results in an extra time period of diffusion for the sample. Second, the additional amount of time spent at an elevated temperature results in a post-annealing of the sample. The wire in which the sample is wrapped also has an effect on the diffusion near regions of glass where the wire touches the glass and special

care must be taken in determining the area from which to cut a sample for measurement.

3.6 Measurement of the Index of Refraction Profile

3.6.1 Introduction

The measurement of the index of refraction as a function of position in a gradient-index sample is important for characterizing the material for lens design. In this research, the measurements are also used to determine the concentration dependence of the diffusion coefficient and to compare theoretical diffusion model solutions against experimental index of refraction profiles. For each ion exchanged sample, the index of refraction profile was measured several different times in several different places on the sample using an automated AC harmonic phase shifting interferometer. [21] The configuration of the instrument is based on a single pass Mach-Zehnder interferometer and uses a 10 mW HeNe laser (λ=632.8 nm) as the illumination source.

During the measurement, the gradient-index sample is placed in one arm of the interferometer such that the direction of the gradient is perpendicular to the direction of propagation of the light. The other arm of the interferometer is the reference arm and the optical path difference between two arms is measured. A thin, flat, plane parallel sample is used so that the measured optical path difference is due entirely to the change in index of refraction across the sample. The index of refraction profile can then be determined from the optical path difference by

$$OPD = \Delta n(x, y)t = m(x, y)\lambda \tag{3.10}$$

where t is the thickness of the sample, λ is the wavelength of the light, and m(x,y) is the number of fringes or 2π phase changes across the sample. The interferometric technique of harmonic phase shifting adds a time dependence to the optical phase of the reference arm to improve the accuracy of the measurement. For a complete description of the principles behind this technique the reader is referred to Houk. [22]

3.6.2 Sample Preparation

To prepare a sample for measurement, the ion exchanged sample is first cleaned and waxed onto an aluminum block. Then a thin slice (typically 0.5-1.5 mm in thickness) is cut parallel to the direction of the gradient using the diamond saw. In particular, the samples could be cut parallel to within 0.5 milliradians, or 2λ over a typical 2 mm deep gradient. [23] The sample could then be polished flat on both sides or, as for most samples measured in this thesis, directly placed in an interferometric cell containing index matching fluid. The index of refraction of the index matching fluid is usually chosen to match the refractive index of the middle of the gradient profile. Although this technique adds more noise to the measurement of the profile because of the roughness of the surface, it is a much less expensive alternative to having over 100 samples polished flat and plane parallel.

3.6.3 Error analysis

There are several possible sources of error encountered in the measurement of an index of refraction profile. From Eq. (3.10), the error in the measured Δn can be written as

$$\delta(\Delta n) = \frac{m \ \delta\lambda}{t} + \frac{\delta m \ \lambda}{t} + \frac{m\lambda \ \delta t}{t^2} \ . \tag{3.11}$$

The first term is small for laser light sources. The interferometer has a peak-to-valley noise of roughly $\lambda/30$ and is capable of resolving approximately 100 fringes/mm in object space. (A more extensive description of the measurement error in the interferometer is given by Gardner. [24]) Therefore, the change in Δn due to a phase measurement error of $\lambda/30$ (for a HeNe laser and a typical sample thickness of 1 mm) is given by

$$\delta(\Delta n) = \frac{\delta m \ \lambda}{t} = \frac{(1/30) \ 0.6328\mu}{1000\mu} = 0.00002 \ . \tag{3.12}$$

(Note that the use of unpolished samples in index matching fluid increases this error and depends on how well the index of refraction of the

fluid is matched to the gradient-index sample.) The final term in Eq. (3.11) is an error due to an inaccurate thickness measurement. A digital micrometer is used to the measure thickness of the sample to an accuracy of ±1 μm. A typical gradient index sample with a $\Delta n = 0.025$ and a thickness of 1 mm results in approximately 40 fringes across the sample. Therefore the uncertainty in thickness contributes an error of

$$\delta(\Delta n) = \frac{m\lambda}{t^2} \delta t = \frac{(40 * 0.6328\mu)(2\mu)}{(1000\mu)^2} = 0.00005 \qquad (3.13)$$

to the index of refraction measurement.

There are additional errors in the measurement which can be attributed to sample preparation. For example, the thickness of an unpolished gradient sample can vary by as much as 10 μm across the depth of the gradient. This is especially true near the edges of the sample. A position measurement error can also be introduced if the faces of the sample slice are not cut parallel to the direction of the gradient and instead are cut an angle α relative to the direction of the gradient. The measured depth will be incorrect by a factor of cos(α) such that

$$z = z' \cos(\alpha) \qquad (3.14)$$

where z is the real position and z' is the measured position. However, this error is usually small since a five degree error produces only a 0.4 percent error in the position data and it is fairly easy to align the saw blade by eye to this accuracy. [25]

Two additional types of error in the measurement become important for the calculation of the concentration dependence of the diffusion coefficient. The first involves the determination of the exact edge position of the sample. During a measurement, the physical edge of the sample is usually ascertained by a large jump or discontinuity in the phase data relative to the background signal and can be determined to roughly ± 25 microns. The second error is in the removal of tilt fringes from the measurement. This becomes difficult due to extra noise in the measurement caused by the use of unpolished samples in index matching oil and the underlying inhomogeneity that exists in the glass sample

before ion exchange. For these reasons, the background fringes can only be "fluffed" to approximately 1/10 fringe per mm (here the term "fluffed" is used to indicate the complete removal of tilt fringes in the homogeneous region of the sample). Although most of the index of refraction profile measurements are made with the fringe pattern "fluffed" by eye, approximately 5-10 tilt fringes are purposely added to some of the measurements. For these measurements, the tilt in the profile is then removed in a graphing program. In some cases, both types of measurements were taken and later compared.

3.7 Concentration-Dependent Diffusion Coefficient

3.7.1 Introduction

The mathematical model for concentration-dependent diffusion requires that the diffusion coefficient as a function of both concentration and temperature be known to completely specify the diffusion equation. However, the concentration dependence of the diffusion coefficient is highly dependent on which glass composition and ion exchange pair is used in the experiment. Therefore, in general, the diffusion coefficient must be experimentally measured for each glass composition.

One method to determine the concentration dependence of the diffusion coefficient was described in detail in Chapter 2. This method uses a Boltzmann-Matano technique to calculate the diffusion coefficient from a concentration profile measured from a single diffusion experiment (with certain initial and boundary conditions). However, measurements of Li^+ concentration profiles are both difficult and costly. Therefore, as described in Section 3.4, the Li^+ concentration profile in an ion exchanged sample is interpolated from the measured index of refraction profile of that sample.

3.7.2 Error Analysis

The numerical errors associated with evaluation of the Boltzmann Matano relation were given in Chapter 2. Additional errors are now introduced into the calculation of the diffusion coefficient due to the

errors in the measurement of the index of refraction profile. For example, the determination of the exact edge position of the sample in the index of refraction profile measurement is important for the calculation of the diffusion coefficient. Figure 3.2 (a) shows two identical index of refraction profiles which have been shifted in position by 25 μm. The effect this has on the calculation of the diffusion coefficient is shown in Fig. 3.2 (b). Thus, a shift in the edge position of the profile of 25 μm increases the peak value of the calculated diffusion coefficient by ten percent.

A second important measurement error in the index of refraction profile measurement is the elimination of tilt fringes from the homogeneous region of the sample. Inhomogeneities in the base glass and noise in the measurement make it difficult to determine when the tilt in the interferometer is completely removed from the fringe pattern. Figure 3.3 (a) shows three identical index of refraction profiles except that a tilt error of 1/10 fringe per mm has been added to one and subtracted from the other. For a 1 mm thick gradient sample this equates to a change of 0.0005 in index of refraction over a 1 mm diffusion depth. The effect this has on the calculation of the diffusion coefficient is shown in Fig. 3.3 (b). Thus a positive tilt error increases the value of the peak of the diffusion coefficient and shifts it to the right, while a negative tilt error shifts the peak to the left. Both plots show that small errors in the removal of the tilt fringes can create a large error in the calculation of the diffusion coefficient, especially near high values of concentration.

Finally, thickness measurement errors and errors in the thickness across the sample cause errors in the index of refraction profile measurement and therefore errors in the calculation of the diffusion coefficient. Figure 3.4 (a) shows three identical index of refraction profiles, except that one has a nominal profile thickness of 1 mm, the second has a thickness error of +10 μm (from the nominal profile thickness of 1 mm) and the third has a thickness error of -10 μm. The effect this has on the calculation of the diffusion coefficient is shown in Fig. 3.4 (b). This shows that the effect of a typical thickness error on the error in the calculation of the diffusion coefficient is not as large as the effects of the previous two measurement errors.
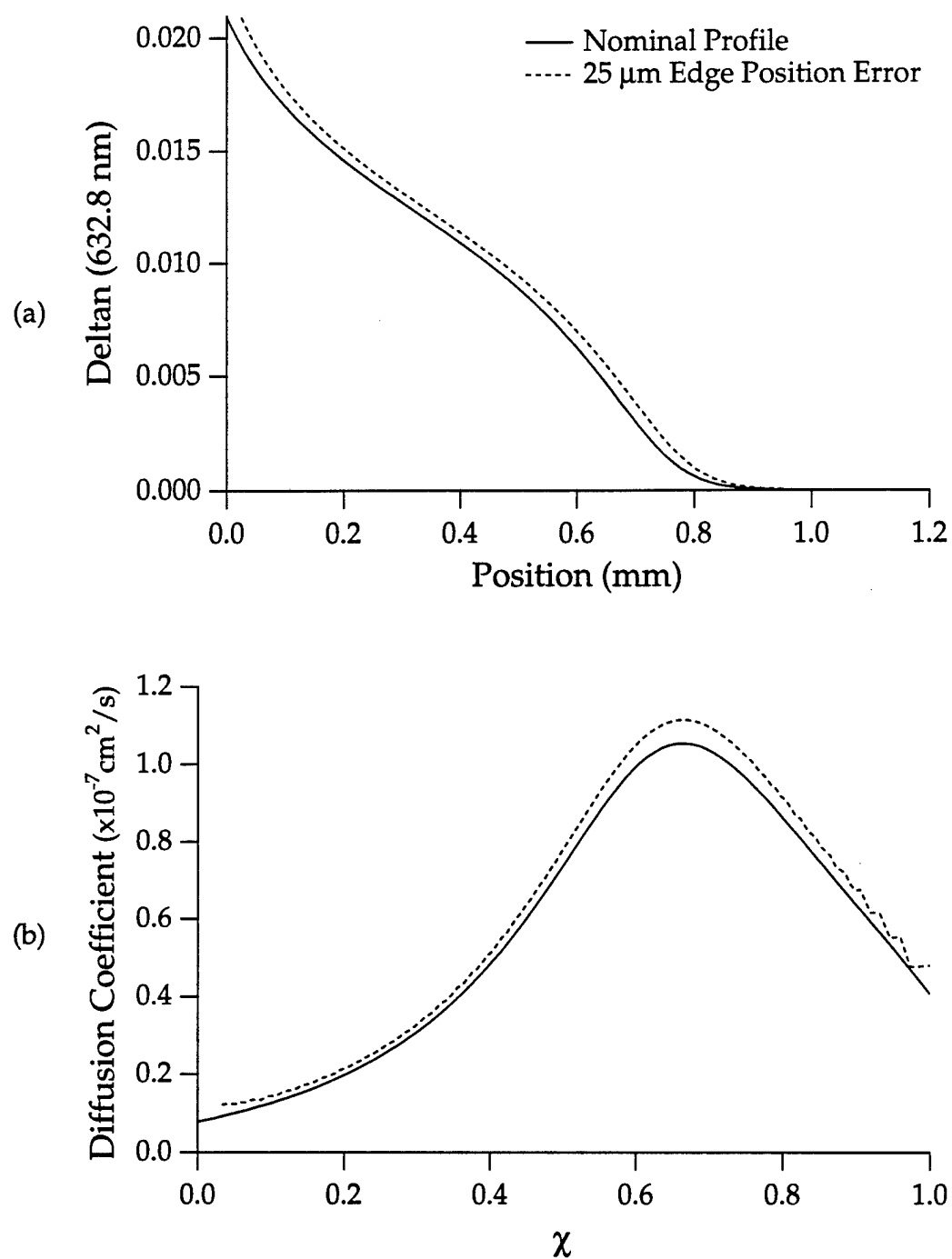
Figure 3.2 Effect of a 25 μm edge position measurement error on (a) the index of refraction profile and (b) the calculated diffusion coefficient.
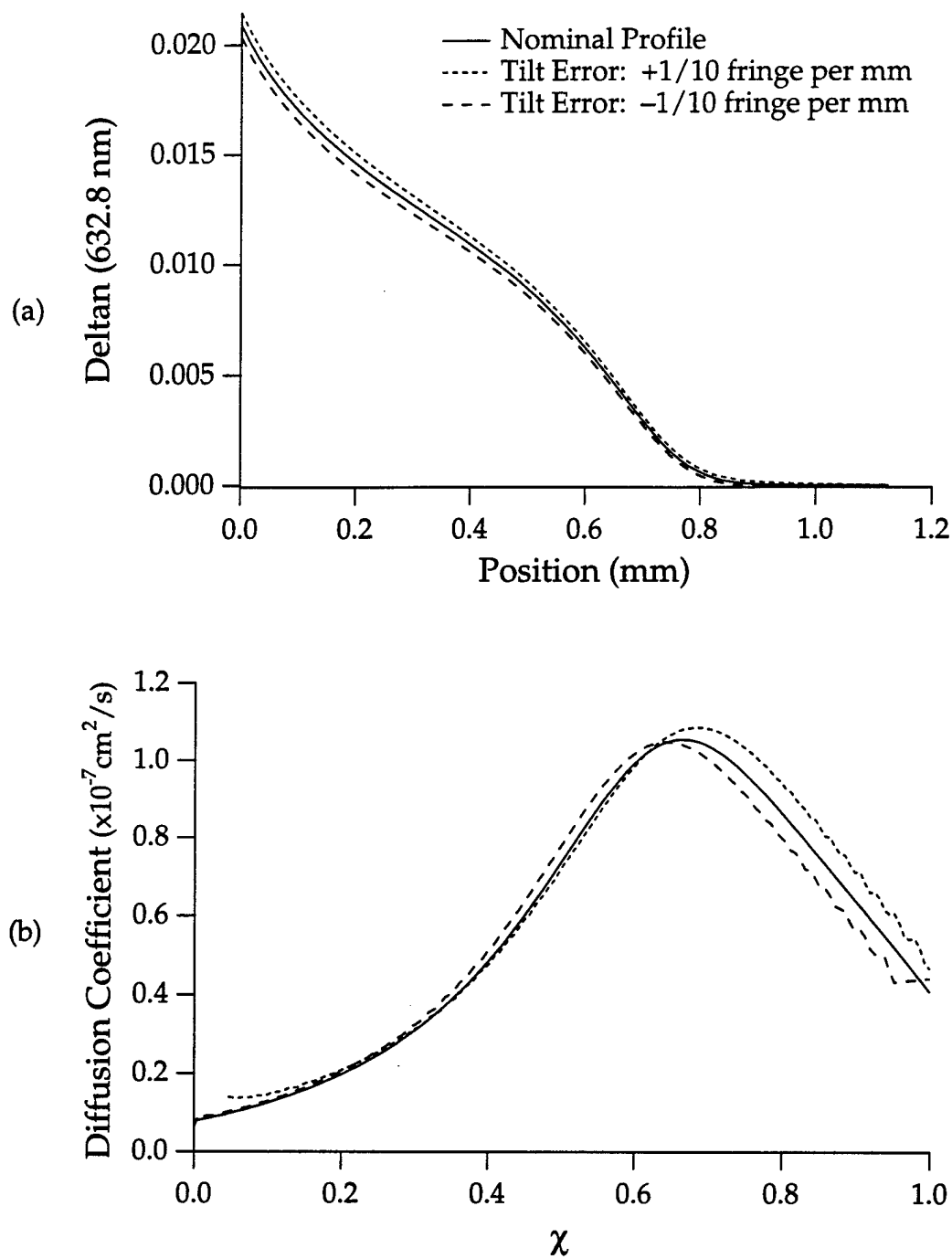
Figure 3.3 Effect of a tilt error of 1/10 of a fringe per mm on (a) the index of refraction profile and (b) the calculated diffusion coefficient.
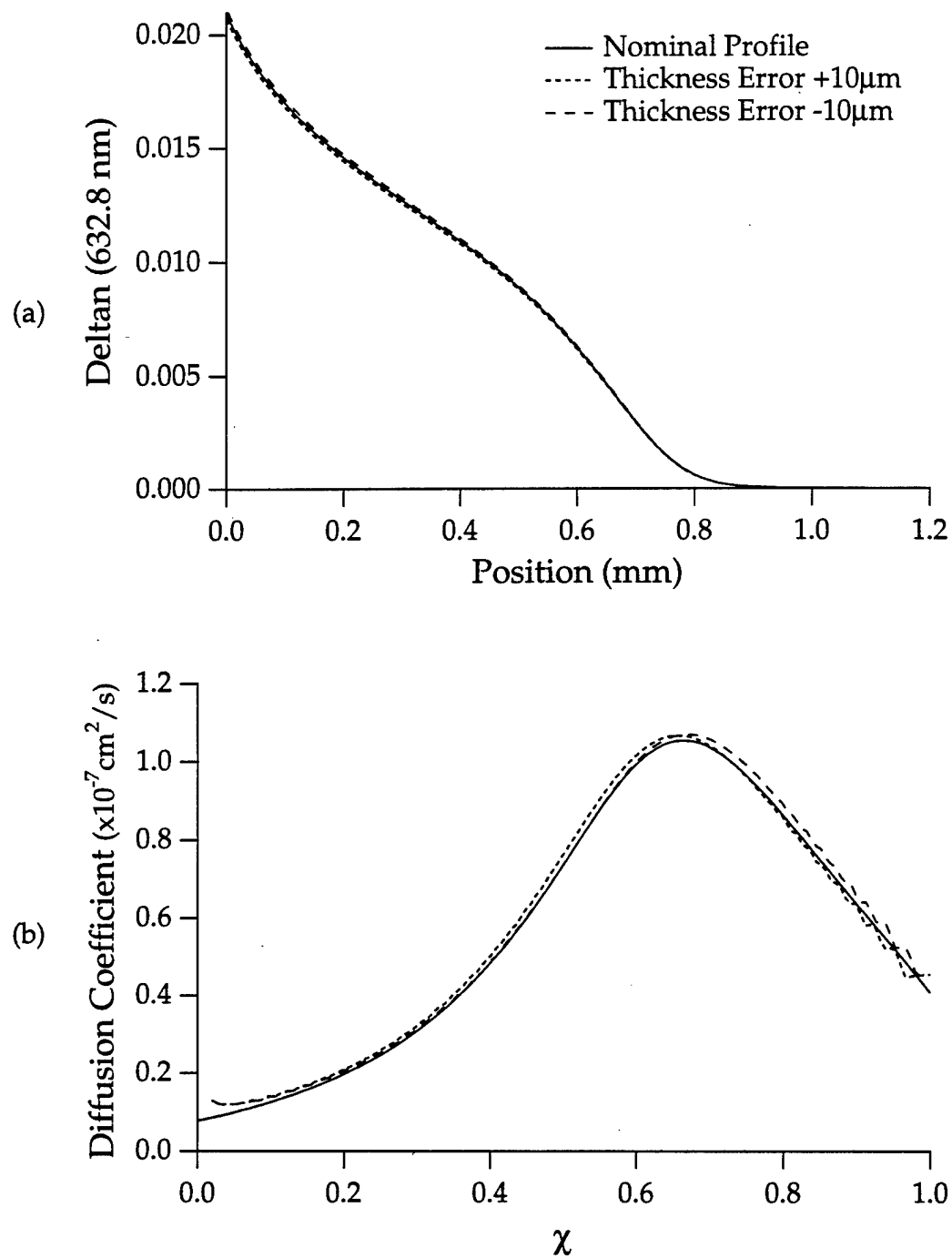
Figure 3.4 Effect of a 10 μm thickness error on (a) the index of refraction profile and (b) the calculated diffusion coefficient.

3.7.3   Modified Quasi-Chemical Diffusion Coefficient Model

The noise in the index of refraction profile measurement also creates problems for the calculation of the concentration-dependent diffusion coefficient. In particular, any noise in the profile is multiplied in the calculation of the differential in the Boltzmann-Matano relation. As a result, it appears as a much larger noise factor in the calculated diffusion coefficient. A typical example of this is demonstrated by the experimental diffusion coefficient shown in the Fig. 3.5 (a) which is calculated from the measured index of refraction profile shown in Fig. 3.5 (b).

The noise in the diffusion coefficient reveals the need for an accurate fitting function for the experimental data since the noise is too large to place the diffusion coefficient directly into the diffusion equation to calculate future experimental profiles. For this reason, an analytic expression for the concentration dependence of the diffusion coefficient was derived in chapter 2. The final result was termed the Modified Quasi-Chemical (MQC) Diffusion Coefficient and was written as a function of χ, the normalized concentration of the diffusion species, according to

$$D(\chi) = \left[\frac{c}{2} \left(\frac{\chi \beta'(\chi = 1) + (1 - \chi)\beta'(\chi = 0)}{\beta'} - 1 \right) + 1 \right] \frac{D_B}{1 - \chi \alpha} \qquad (3.15)$$

where β' was given by the expression

$$\beta' = \sqrt{1 - 4(\chi - \chi_0)[1 - (\chi - \chi_0)](1 - e^\rho)} \; . \qquad (3.16)$$

Furthermore, the parameters α and ρ were defined as

$$\alpha = 1 - \frac{D_B}{D_A} \quad \text{and} \quad \rho = -2\varepsilon_{int}/kT \; , \qquad (3.17)$$

respectively. Thus, the analytic expression has five adjustable parameters (D_B, α, ρ, χ_0, and c) for fitting to experimental calculations of the diffusion coefficient.

The noise in the diffusion coefficient also makes it difficult to determine the best curve fit to the experimental data using the MQC model. As a result, more than one set of fit coefficients can be used to

Model Number	D_B	α	ρ	χ_0	c
MQC Model 1	0.077	0.81	-1.855	0.131	8
MQC Model 2	0.059	0.83	-1.702	0.129	12

Table 3.1 MQC Model fitting coefficients for Figure 3.5 and the nominal fitting coefficients used in Figures 3.6-3.10.

recover the same initial index of refraction profile. For example, shown in Fig. 3.5 (a) are two MQC fits to an experimental diffusion coefficient. The first fit was generated by holding the coordination number c to a value of 8, while the remaining coefficients were allowed to vary. Similarly, the second fit was generated by holding the coordination number c to a value of 12. Both models appear to fit the diffusion coefficient to well within the noise of the calculation and they both can be used to recover (within experimental error) the initial index of refraction profile as shown in Fig. 3.5 (b). The specific variation in the values of the two sets of MQC coefficients is shown in Table 3.1.

Therefore, a series of figures (Fig. 3.6 to Fig 3.10) was generated to illustrate how changes in the fitting coefficients affect the index of refraction profile. In each figure, the value of one of the five coefficients is changed while the other four coefficients are held constant and a graph of both the MQC diffusion coefficients and the corresponding index of refraction profiles is shown. The nominal MQC coefficients are listed in Table 3.2. These values and the changes in these values used to generate the figures were chosen to be representative of the range in values obtained for some of the MQC diffusion coefficients given later in this thesis.

Figure 3.6 shows the effect of changing the value of the self diffusion coefficient, D_B, from 0.05 to 0.15. As expected, as the self diffusion coefficient is increased, the value of the diffusion coefficient increases, and therefore the depth of the profile also increases. Figure 3.7 shows the effect of changing the value of the mobility ratio, α, from -1.0 to 0.5. Since the value of the self diffusion coefficient D_B is held constant, this change represents a variation in the self diffusion coefficient D_A. In particular,

decreasing the mobility ratio, increases the value of the self diffusion coefficient D_A, and the depth of the profile is also increased. However, the change in the mobility ratio has the most effect on the diffusion coefficient for high lithium concentrations, while the change in self diffusion coefficient D_B, affects the diffusion coefficient at all concentrations.

Figure 3.8 shows the effect of changing the value of the interaction energy parameter, ρ, from -1.6 to -2.0. As shown, decreasing the value of ρ, increases the peak value of the diffusion coefficient, and effectively changes the shape of the index of refraction profile while maintaining its diffusion depth. However, relatively large changes in this parameter have only a small effect on the profile when compared to the other parameters. For example, Fig. 3.9 shows the effect of changing the value of the peak position shift, χ_0 from -0.2 to 0.2. This type of change has a large effect on the overall shape of the profile including the diffusion depth. Finally, Fig. 3.10 shows the effect of changing the value of the coordination number, c, from 4 to 12. As shown, increasing the coordination number c, increases the peak of the diffusion coefficient, and increases the depth of the profile.

In summary, the variations in the parameters can have similar effects on both the diffusion coefficient and the index of refraction profile. For example, both the interaction energy term, ρ, and the coordination number, c, can be used to change the peak value of the diffusion coefficient. As a result, more than one set of fit coefficients can be obtained because the noise in the diffusion coefficient makes it difficult to determine the best curve fit to the experimental data.

	D_B	α	ρ	χ_0	c
Variation #1	0.05	-1.0	-1.6	-0.2	4
MQC Nominal	0.10	0.0	-1.8	0.0	8
Variation #2	0.15	0.5	-2.0	0.2	12

Table 3.2 MQC Model nominal fitting coefficients and the variation in these parameters used to generate Figures 3.6-3.10.
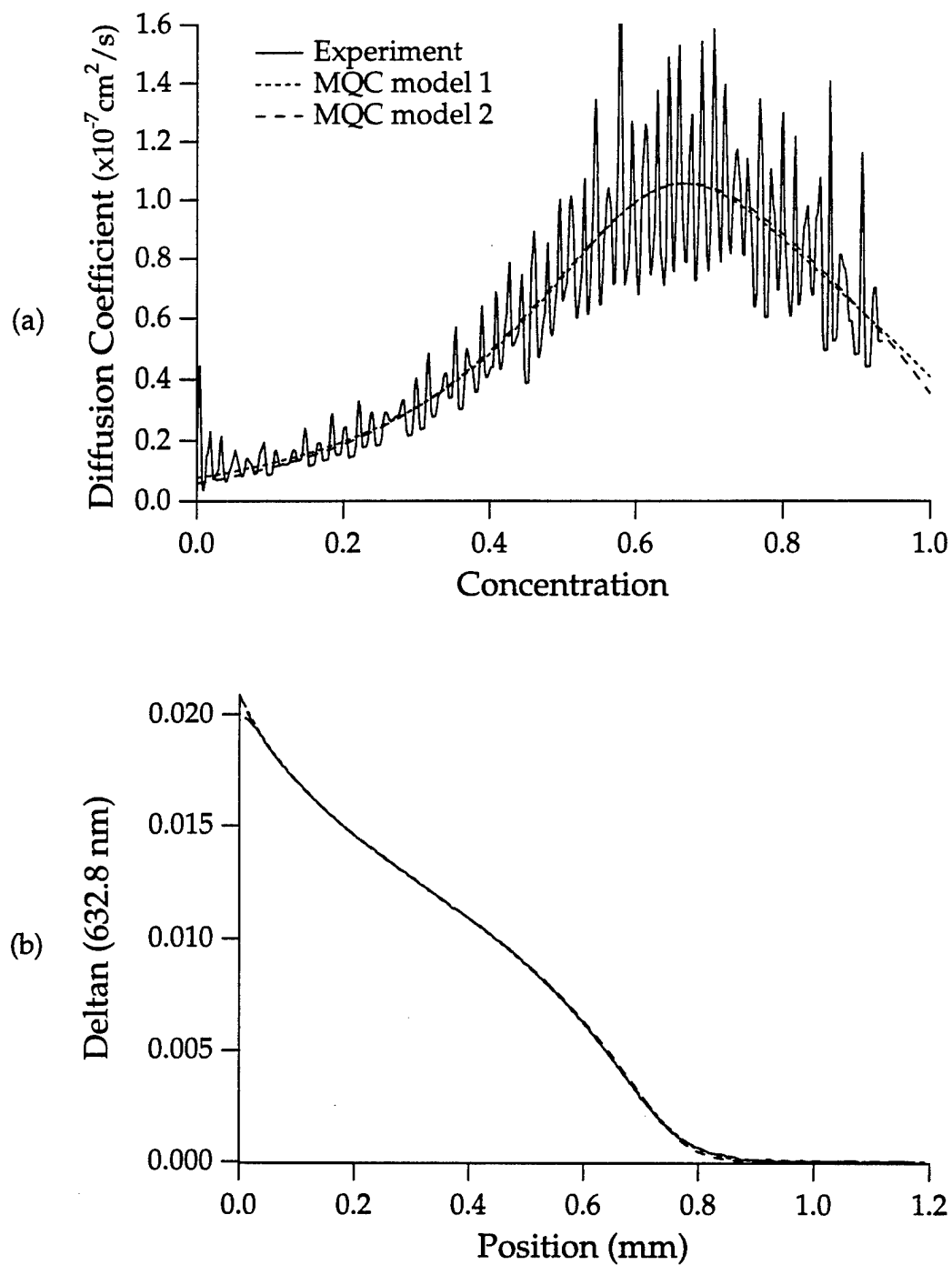
Figure 3.5 Variation in the MQC fitting coefficients for (a) two different curve fits to the experimental diffusion coefficient and (b) the recovery of the initial index of refraction profile for the two different fits.
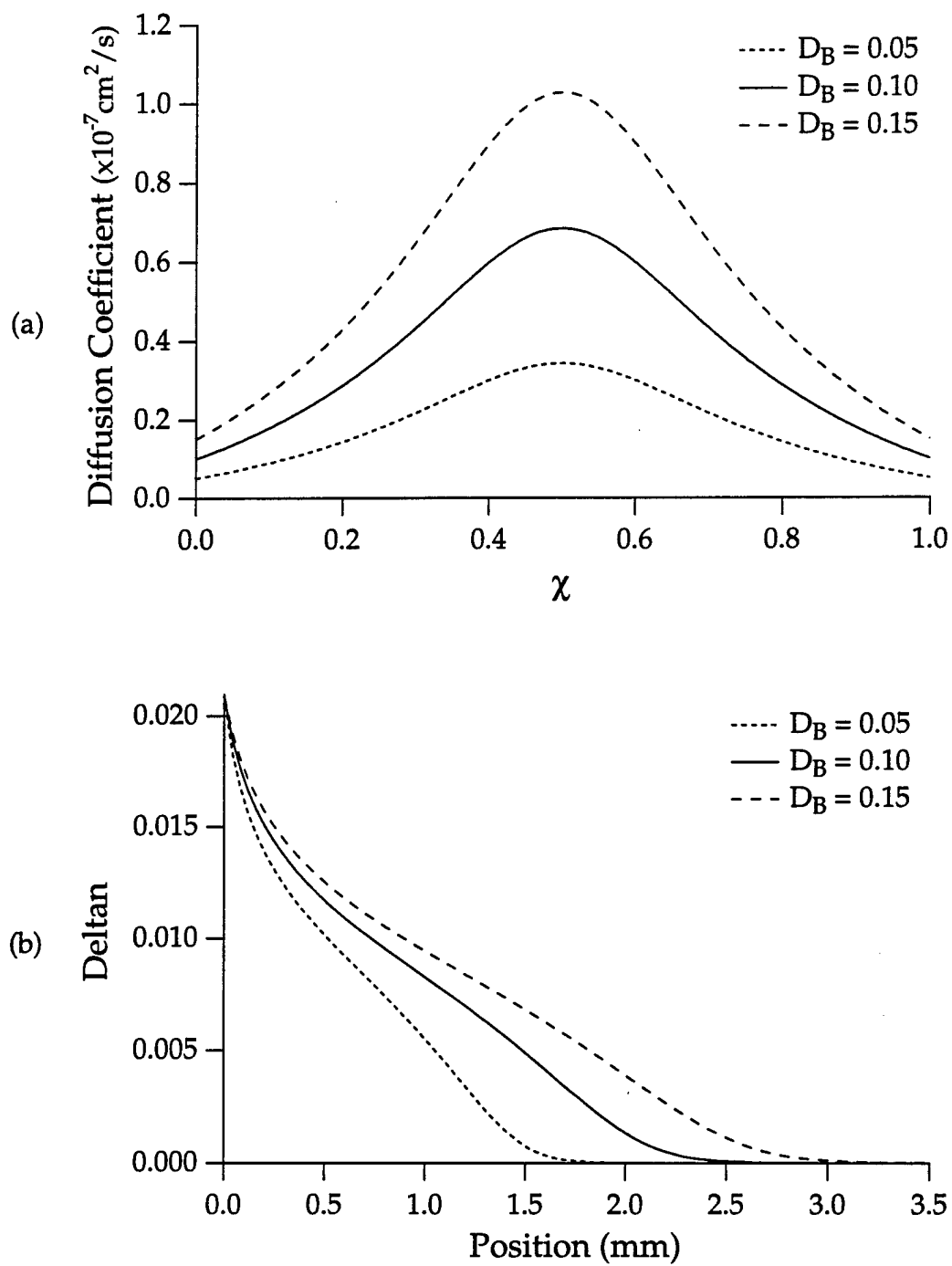
Figure 3.6 Effect of changing the value of the self diffusion coefficient, D_B, on (a) the Modified Quasi-Chemical Diffusion Coefficient and (b) the index of refraction profile.

(a)

(b)
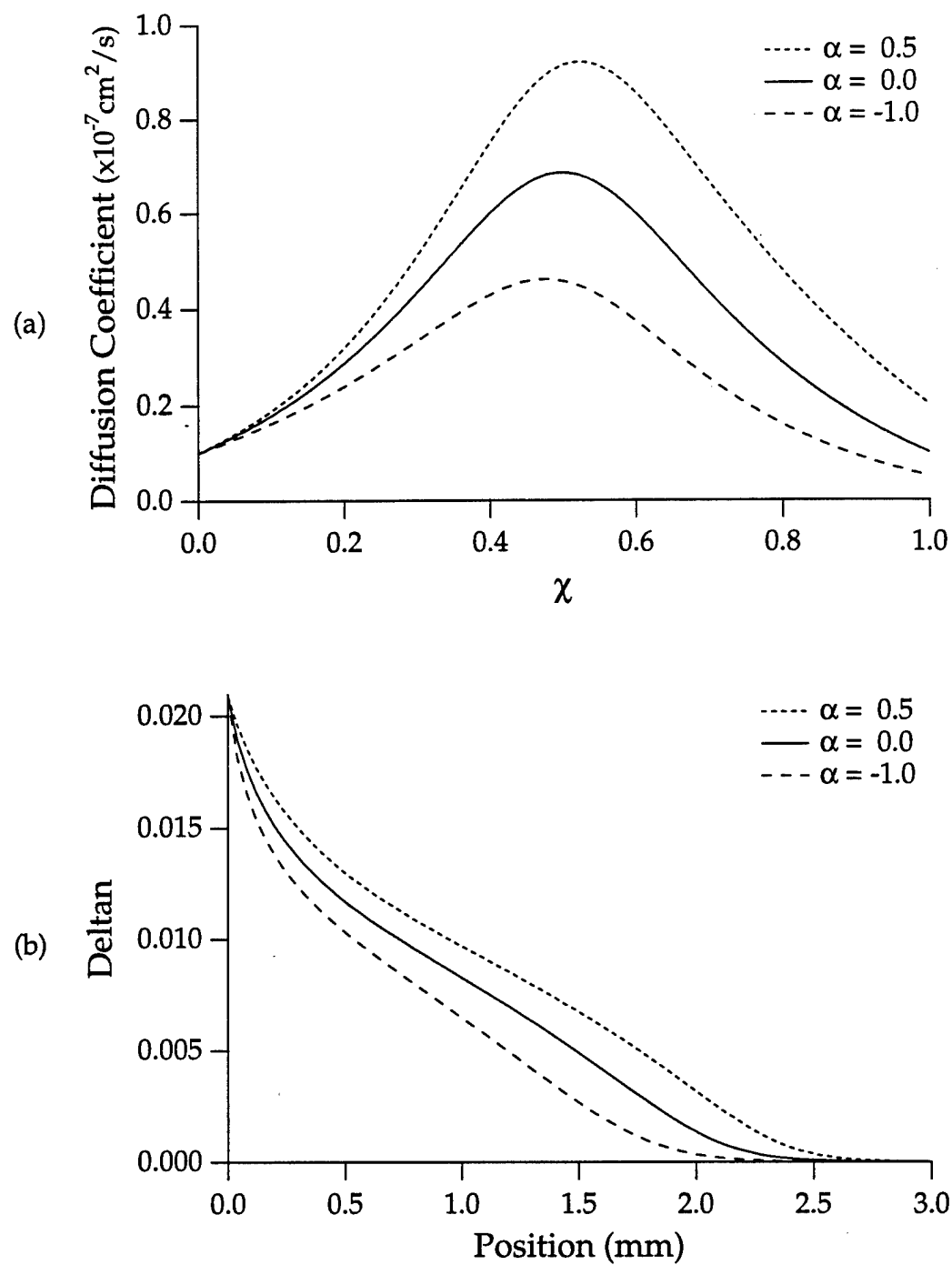
Figure 3.7 Effect of changing the value of the mobility ratio, α, on (a) the Modified Quasi-Chemical Diffusion Coefficient and (b) the index of refraction profile.
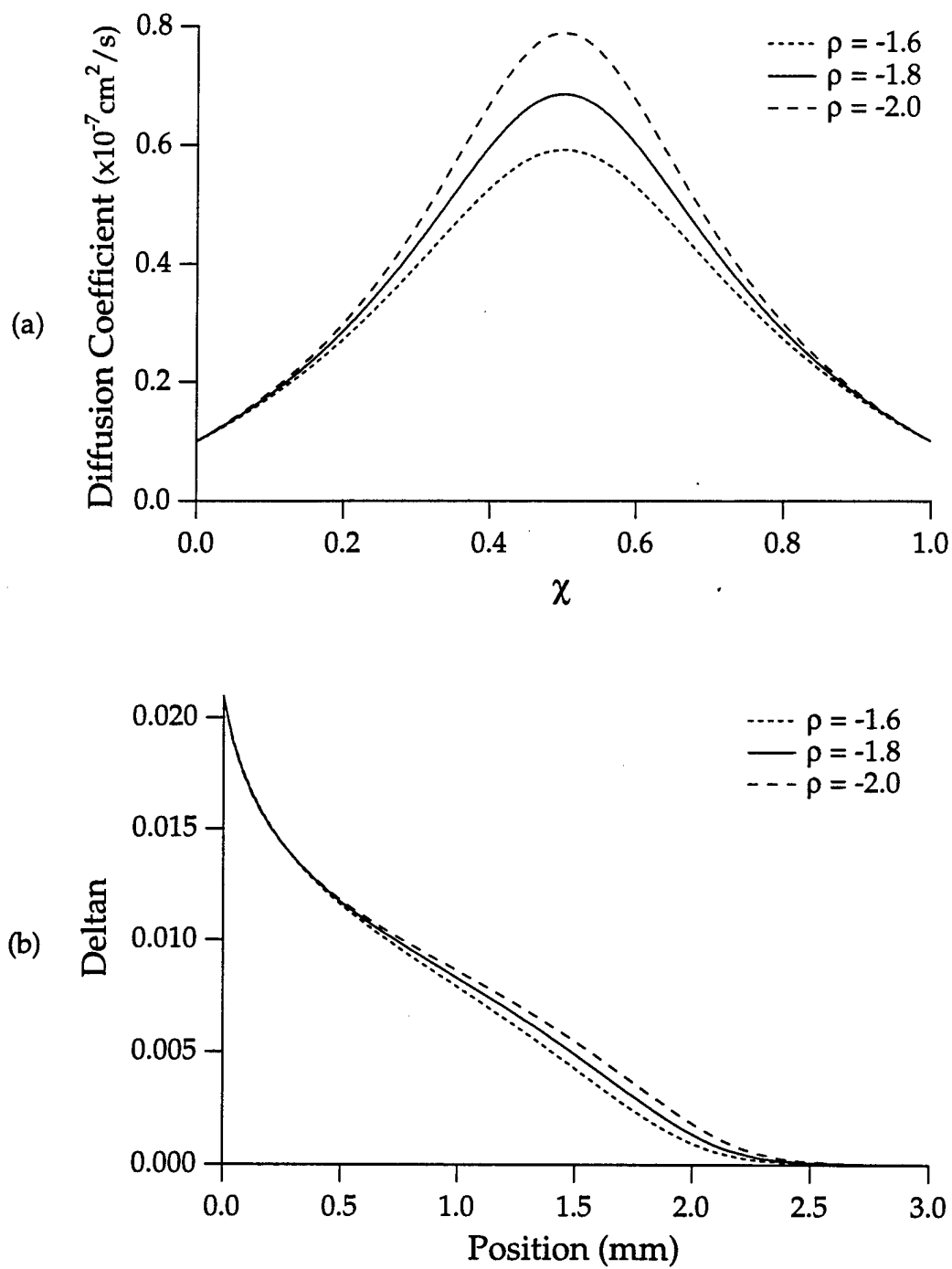
Figure 3.8 Effect of changing the value of the interaction energy parameter, ρ, on (a) the Modified Quasi-Chemical Diffusion Coefficient and (b) the index of refraction profile.
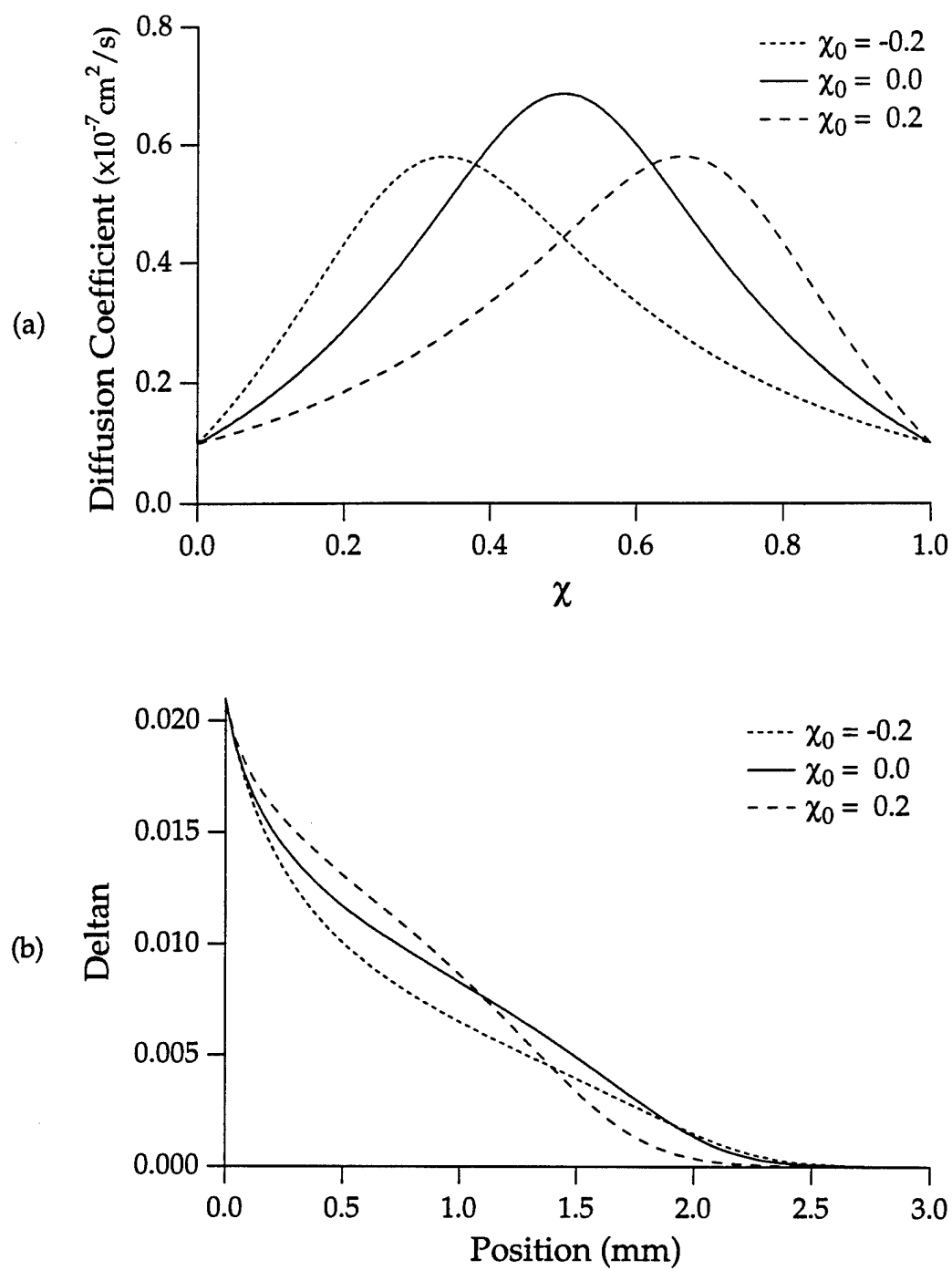
Figure 3.9 Effect of changing the value of the peak position shift, χ_0, on (a) the Modified Quasi-Chemical Diffusion Coefficient and (b) the index of refraction profile.
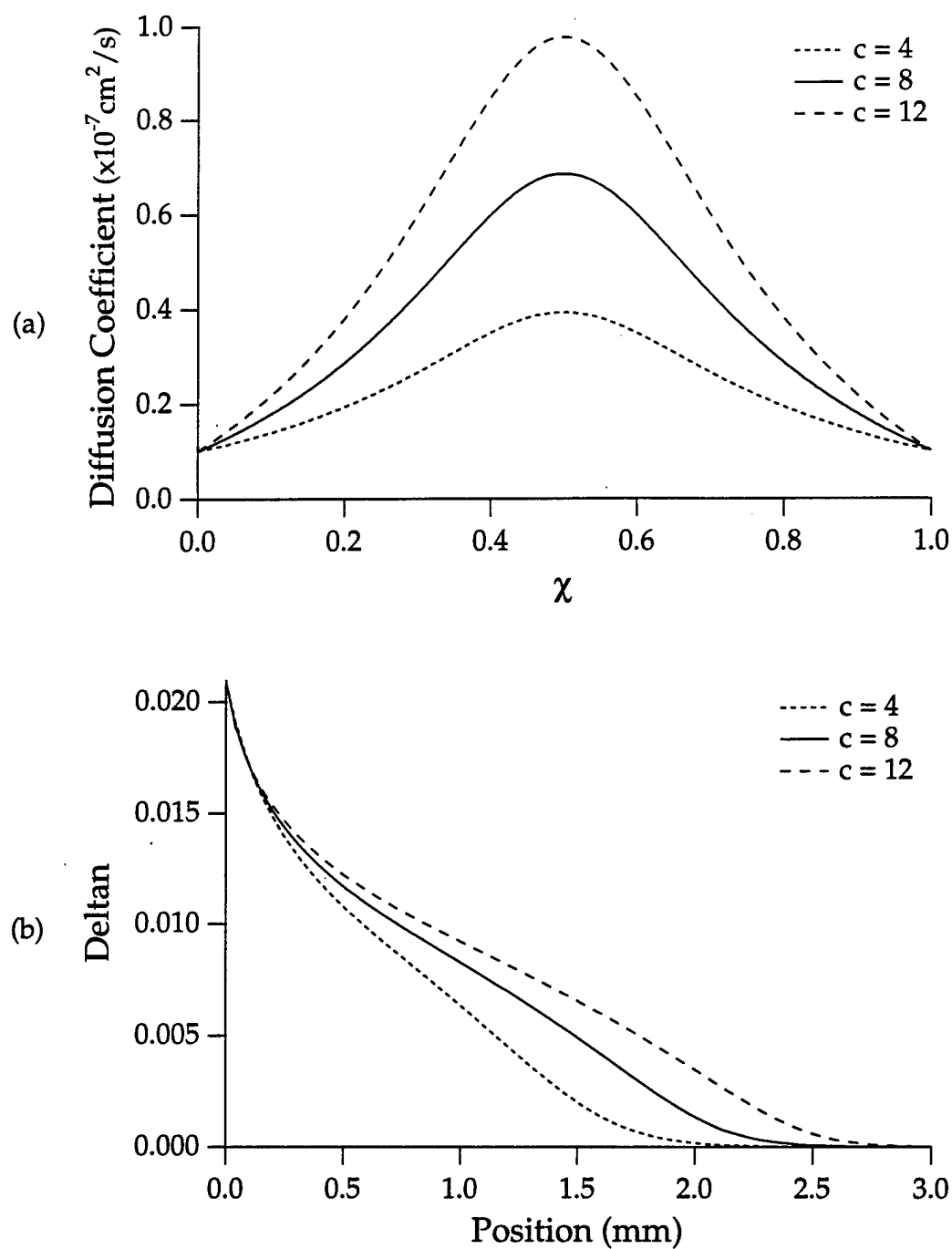
Figure 3.10 Effect of changing the value of the coordination number, c, on (a) the Modified
Quasi-Chemical Diffusion Coefficient and (b) the Index of Refraction Profile.

References

1. M. L. Huggins, "The index of refraction of silicate glasses as a function of composition," J. Opt. Soc. Am. **30**, 495 (1940).

2. W. D. Kingery, *Introduction to ceramics*, John Wiley and Sons, New York (1960), p. 148.

3. G. W. Morey, *Properties of glass*, Reinhold Publ., New York (1954).

4. D. R. Uhlman and N. J. Kreidl, eds., *Glass: science and technology, vols. 1-8*, Academic Press, New York (1983-1989).

5. O. V. Mazurin, et al., eds., *Handbook of glass data, part A, B, and C*, Elsevier, Amsterdam (1987).

6. D. S. Kindred, "Development of new gradient index glasses for optical imaging systems," Doctoral Dissertation, University of Rochester, Rochester, NY (1990), pp. 36-43.

7. G. H. Frischat, *Ionic Diffusion in Oxide Glasses*, Trans Tech Publications, Bay Village, OH (1975), p. 66-67.

8. Reference 7, p. 53.

9. D. P. Ryan-Howard, "Chromatic properties of gradient index glass," Doctoral Dissertation, University of Rochester, Rochester, NY (1983), pp. 212 and 263.

10. G. E. Blair, "Experimental glass melting techniques," in: *An Introduction to Glass Science*, ed. L.D. Pye, H.J. Stevens, and W.C. LaCourse, Plenum, New York (1972), pp. 329-341.

11. Reference 6, pp. 46-51.

12. K. F. J. Heinrich, et al., "Energy Dispersive X-Ray Spectroscopy," U.S. Department of Commerce, National Bureau of Standards, Special Publication 604, p. 97 (1981).

13. Reference 6, p. 62.

14. Reference 6, ch. 4.

15. M. L. Huggins, "The density of silicate glasses as a function of composition", J. Opt. Soc. Am. **30**, 420 (1940).

16. Reference 1.

17. M. L. Huggins, K. H. Sun, and D.O. Davis, "The dispersion of silicate glasses as a function of composition, II", J. Opt. Soc. Am. **32**, 635 (1942).

18. S. D. Fantone, "Design, engineering, and manufacturing aspects of gradient index optical components," Doctoral Dissertation, University of Rochester, Rochester, NY (1979).

19. Reference 9.

20. H. A. Buchdahl, *Optical Aberration Coefficients*, Dover, New York (1968), Sec. 87.

21. J. J. Miceli, "Infrared gradient index optics: materials, fabrication, and testing," Doctoral Dissertation, University of Rochester, Rochester, NY (1982).

22. M. T. Houk, "Fabrication and testing of index gradients in flouride materials," Doctoral Dissertation, University of Rochester, Rochester, NY (1990), chap. 5.4.

23. Reference 6, pp. 58-59.

24. L. R. Gardner, "Studies in gradient index polymer materials," Doctoral Dissertation, University of Rochester, Rochester, NY (1979), pp. 135-146.

25. Reference 6, p. 61.

Chapter IV
Alumina Silicate Glasses

4.1 Introduction/Background

Commercial optical glasses often contain components which can slow the diffusion and/or make the glass crack and devitrify in an ion exchange experiment. As a result, special glass compositions are needed to fabricate gradient-index lenses. For example, Bausch and Lomb and the University of Rochester developed one of the first glass compositions which was specifically designed for ion exchange. [1] The base glass (BL-2406) is a simple soda alumina silicate crown glass with a composition of

$$0.252 \ Na_2O + 0.044 \ Al_2O_3 + 0.704 \ SiO_2 \ . \tag{4.1}$$
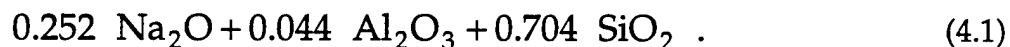
Investigations of Ag^+ for Na^+ exchange in this glass show that a relatively large total change in refractive index (≈ 0.10) and large gradient dispersion (≈ 18) can be obtained. [2,3] Furthermore, several gradient-index lenses (both axial and radial) have been fabricated in this glass using a silver for sodium exchange. [4,5,6]

A homogeneous crown glass which contains sodium has a slightly lower refractive index and higher dispersion than the corresponding homogeneous glass which contains lithium. Therefore, an exchange of Li^+ for Na^+ in the soda crown glass should give rise to a gradient material

with a positive change in refractive index and a negative gradient Abbe number. For example, Ryan-Howard showed that the BL-2406 glass could also be used in a Li^+ for Na^+ exchange to fabricate a gradient with a relatively low total change in index of refraction ($\Delta n = 0.016$) and a negative gradient dispersion ($V_{grin} = -113$). [7] The existence of negative V_{grin} numbers is important in optical design because it allows for color-corrected gradient-index systems which contain only positive elements. Fantone also showed that the Li^+ for Na^+ exchange pair is one of the few pairs for which a gradient dispersion of infinity can be realized. [8]

The success of Li^+ for Na^+ exchange in the BL-2406 glass led Kindred to investigate $Li^+ - Na^+$ exchange in some similar alumina silicate crown glasses within the composition range

$$xLi_2O + (0.25 - x)Na_2O + 0.05Al_2O_3 + 0.70SiO_2 \ , \tag{4.2}$$

where the initial amount of Li_2O in the base glass composition, x, was varied from 0.0 to 0.25. [9] The change in base glass composition permitted a large variation in the maximum index change of the gradient (the less sodium available for exchange, the smaller the corresponding refractive index change) while it also had a significant effect on the shape of the index of refraction profile. As a result, a variety of index of refraction profiles were obtained for Li^+ for Na^+ and Na^+ for Li^+ diffusions in the alkali alumina silicate glasses. Furthermore, most of the ion exchanged samples exhibited little or no cracking and devitrification.

In this chapter, a more extensive study of $Li^+ - Na^+$ exchange in alkali alumina silicate glasses is presented. The general glass composition range which is examined is given by

$$xLi_2O + (y - x)Na_2O + zAl_2O_3 + (1 - y - z)SiO_2 \tag{4.3}$$
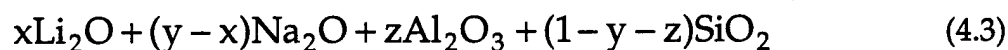
such that in the base glass, x is the initial amount of lithium, y is the total amount of alkali, and z is the amount of alumina. The glass forming region for this system is fairly large, but the values for x, y, and z are often limited by either the melting temperature or the chemical durability of the glass. In particular, the total alkali content in the glass, y, usually ranges from 0.20 to 0.30; below 20 percent the glass becomes difficult to melt and

also results in a lower total change in index of refraction. Above 30 percent the chemical durability of the glass becomes unfavorable. Furthermore, the alumina content must usually be kept below 10 percent, since it also increases the melting temperature of the glass and makes it difficult to get good glass homogeneity in large glass samples.

In this study, the general composition range given by Eq. (4.3) is divided into several separate glass subsystems, and then, an empirical diffusion model for $Li^+ - Na^+$ ion exchange is developed for the glass compositions within this subsystem. First, for a fixed alumina content and a fixed amount of total alkali, changes in x, the initial ratio of Li^+/Na^+ in the base glass are examined. This type of analysis is similar to Kindred's original analysis, and the results for two particular glass subsystems are presented in Sections 4.2 and 4.3. Second, changes in y, the total alkali content of the glass, and z, the alumina content of the glass, are explored in Section 4.4. In particular, the effect the change in the base glass composition has on the index of refraction and the concentration dependence of the diffusion coefficient (and therefore on the index of refraction profile) is investigated for each glass subsystem.

4.2 7% Alumina Silicate Glass System

4.2.1 Introduction

Kindred showed that changing the initial ratio of Li^+/Na^+ in the homogeneous base glass resulted in a wide variety of index of refraction profiles with different profile shapes and maximum changes in refractive index. Furthermore, the particular substitution of Li_2O for Na_2O in the base glass compositions of Eq. (4.2) maintained the same total alkali content in each of the glasses such that the general properties of the glasses (such as the melting temperature and the transition temperature) were similar. (For example, if a large portion of the Na_2O is replaced instead by either the alumina or the silica, the glass becomes very difficult to melt.) Then, since the properties of the glasses were similar, the results of the ion exchanges in the different glasses within this composition range could be compared for identical diffusion times and diffusion temperatures.

The first alkali alumina silicate glass subsystem which is examined in this chapter is written as

$$xLi_2O + (0.30 - x)Na_2O + 0.07Al_2O_3 + 0.63SiO_2 \ . \qquad (4.4)$$

Similar to Kindred's original glass system, each glass in this subsystem has the same total alkali (30 mole percent) and the same alumina content (7 mole percent), but the initial ratio of Li^+/Na^+ in the glass is different. First, several homogeneous glass compositions for different values of x, the ratio of Li^+/Na^+ initially in the glass, are melted. Second, the optical properties of these glasses are measured to determine the index of refraction as a function of concentration for the glass system. Third, several ion exchanges (both Li^+ for Na^+ and Na^+ for Li^+) in an axial geometry are used to calculate and examine the concentration dependence of the diffusion coefficient for the different glass compositions within this glass system. The temperature dependence of the diffusion coefficient is also examined for Li^+ for Na^+ exchange in one of the glasses for a limited temperature range. Then, once the empirical diffusion model for this glass system is determined, it is tested by comparing model solutions to experimental index of refraction profiles for other diffusion times and glass compositions within the system.

4.2.2 Glass Melting

Nine glass compositions were melted in this glass system and are listed in Table 4.1. Beginning at zero, the lithium concentration of each successive composition was increased (usually in five percent increments) up to the final glass composition which contains thirty percent lithium and no sodium. Several of the compositions were measured by flame spectroscopy at Corning Engineering Lab Services. The results of these measurements are also listed in Table 4.1 in parenthesis and show that the as melted compositions are accurate to ± 0.1%.

Each glass was melted in a 250 gram batch in a platinum crucible using the experimental procedure described in Chapter 3. Approximately 1/3 of the batch was premelted at 1100 °C for one hour. The rest of the batch material was added in half hour increments until the entire batch was in

Glass Name	Li$_2$O	Na$_2$O	Al$_2$O$_3$	SiO$_2$
JBGL-13	0.00	0.30 (0.2974)	0.07 (0.0708)	0.63 (0.6318)
JBGL-19	0.01	0.29	0.07	0.63
JBGL-20	0.03	0.27	0.07	0.63
JBGL-14	0.05	0.25	0.07	0.63
JBGL-15	0.10 (0.0982)	0.20 (0.2001)	0.07 (0.0730)	0.63 (0.6283)
JBGL-16	0.15	0.15	0.07	0.63
JBGL-17b	0.20 (0.1969)	0.10 (0.0999)	0.07 (0.0768)	0.63 (0.6264)
JBGL-18	0.25	0.05	0.07	0.63
JBGL-12	0.30 (0.2949)	0.00	0.07 (0.0724)	0.63 (0.6328)

Table 4.1 Compositions of the glasses melted in the system x Li$_2$O + (0.30-x) Na$_2$O + 0.07 Al$_2$O$_3$ + 0.63 SiO$_2$. The numbers in parenthesis are the compositions as measured by flame spectroscopy at Corning Engineering Lab Services.

the crucible. The glass was melted at 1575 °C for a time period which ranged from four to eight hours. Then, after being cooled in the crucible to a temperature of 1400 °C, the glass was poured into a cold steel mold. The glass was quickly placed into a preheated annealing furnace and allowed to cool slowly from a temperature of 550° C to room temperature. Note: even at 1575 °C the glass was still fairly thick which made it difficult to get good homogeneity for such a small batch size. Therefore, only about a quarter of the glass had a good homogeneous region that was usually four to six mm thick and near the top of the pour.

4.2.3 Index of Refraction Measurements

Small samples of each glass (1cm x 1cm x 0.5 cm) were polished flat on one side to $\lambda/4$. Then, for each sample, the index of refraction at four different wavelengths was measured using a Pulfrich refractometer to an accuracy of ±0.0003. Table 4.2 lists the results of these measurements. The glass with the largest lithium concentration has the largest index of refraction while the glass with the largest sodium concentration has the smallest index of refraction. Thus, a Li$^+$ for Na$^+$ exchange in the all soda glass (JBGL-13) should produce a gradient with a positive change in index

of refraction (the refractive index is increased at the edge of the sample) of approximately 0.03 at 632.8 nm.

The homogeneous dispersion of the glass was then calculated using the procedure described in Chapter 3, Section 3.4.3. First, equation (3.8) was used to fit the four index of refraction measurements as a function of wavelength. Then, the index of refraction values, n_F and n_C, were interpolated from the fit and the dispersion of the glass was calculated. Table 4.3 lists the coefficients of the fit, the indices of refraction, n_F and n_C, and finally the dispersion, V_d, for each glass. The glass with the largest lithium concentration has the smallest dispersion while the glass with the largest sodium concentration has the largest dispersion. Thus, a Li^+ for Na^+ exchange in the all soda glass (JBGL-13) should produce a material with a negative gradient dispersion (the refractive index change at the red wavelengths is larger than the refractive index change at the blue wavelengths). Note: the dispersion values for glasses JBGL-15 and JBGL-17b are somewhat suspect since the index of refraction, n_g, was not measured, and therefore, only three measured data points could be used to interpolate n_F and n_C for the calculation of the dispersion.

As discussed in Chapter 3, the index of refraction as a function of lithium concentration is necessary for the calculation of the concentration

Glass Name	x Li_2O	n_g	n_e	n_d	n_{HeNe}
JBGL-13	0.00	1.5195	1.5103	1.5081	1.5062
JBGL-19	0.01	1.5203	1.5112	1.5090	1.5071
JBGL-14	0.05	1.5243	1.5151	1.5129	1.5110
JBGL-15	0.10	*	1.5193	1.5172	1.5154
JBGL-16	0.15	1.5327	1.5238	1.5217	1.5198
JBGL-17b	0.20	*	1.5283	1.5263	1.5244
JBGL-18	0.25	1.5426	1.5336	1.5315	1.5296
JBGL-12	0.30	1.5486	1.5397	1.5377	1.5357

Table 4.2 The index of refraction of the homogeneous glass samples in the system x Li_2O + (0.30-x) Na_2O + 0.07 Al_2O_3 + 0.63 SiO_2 measured at four different wavelengths on a Pulfrich refractometer. * Not measured.

Glass Name	x Li$_2$O	n$_0$	n$_1$	n$_2$	n$_F$	n$_C$	V$_d$
JBGL-13	0.00	1.5088	-0.0510	-0.0009	1.5145	1.5053	55.13
JBGL-19	0.01	1.5097	-0.0510	-0.0034	1.5154	1.5062	55.30
JBGL-14	0.05	1.5136	-0.0510	-0.0009	1.5193	1.5101	55.65
JBGL-15	0.10	1.5178	-0.0484	0.0178	1.5235	1.5146	58.17
JBGL-16	0.15	1.5223	-0.0486	0.0020	1.5278	1.5190	59.20
JBGL-17b	0.20	1.5269	-0.0471	-0.0431	1.5317	1.5235	64.43
JBGL-18	0.25	1.5321	-0.0486	0.0045	1.5377	1.5288	60.23
JBGL-12	0.30	1.5383	-0.0461	0.0124	1.5437	1.5352	63.67

Table 4.3 The fit coefficients for Eq. (3.8), the interpolated values for n$_F$ and n$_C$, and the calculated dispersion V$_d$ for the homogeneous glasses in the system x Li$_2$O + (0.30-x) Na$_2$O + 0.07 Al$_2$O$_3$ + 0.63 SiO$_2$.

dependence of the diffusion coefficient for these glasses. It is also used by the diffusion model to convert concentration profile solutions to index of refraction profiles so that they can be compared with experimentally measured index of refraction profiles. Therefore, for this series of glass compositions, Fig. 4.1 shows a graph of the measured index of refraction (at 632.8 nm) as a function of normalized lithium concentration, χ, where

$$\chi = \frac{x}{0.30} \, ,$$

(4.5)

and x is the initial mole percent of lithium in the glass. A third order polynomial curve fit to the data given by

$$n(\chi) = 1.5062 + 0.03076\chi - 0.01277\chi^2 + 0.01155\chi^3$$

(4.6)

is also shown. Figure 4.2 then compares the measured index of refraction values to the predicted values from the Huggins, Sun, Davis model. The model values were calculated using the original empirical constants from Huggins, Sun, and Davis [10] and an annealing constant of k = -0.125, and agree with the measured values to within 0.1% except for the glasses with either very low or very high lithium concentrations.
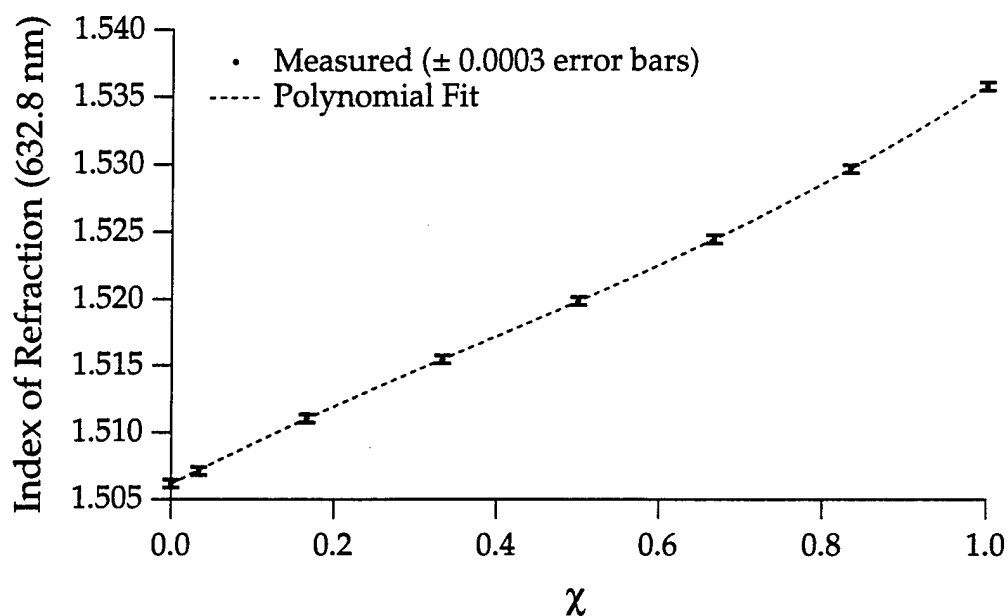
Figure 4.1 Index of refraction as a function of normalized lithium concentration, χ, for glasses in the system x Li_2O + (0.30-x) Na_2O + 0.07 Al_2O_3 + 0.63 SiO_2. Both the measured data points and a third order polynomial fit to the data are shown.
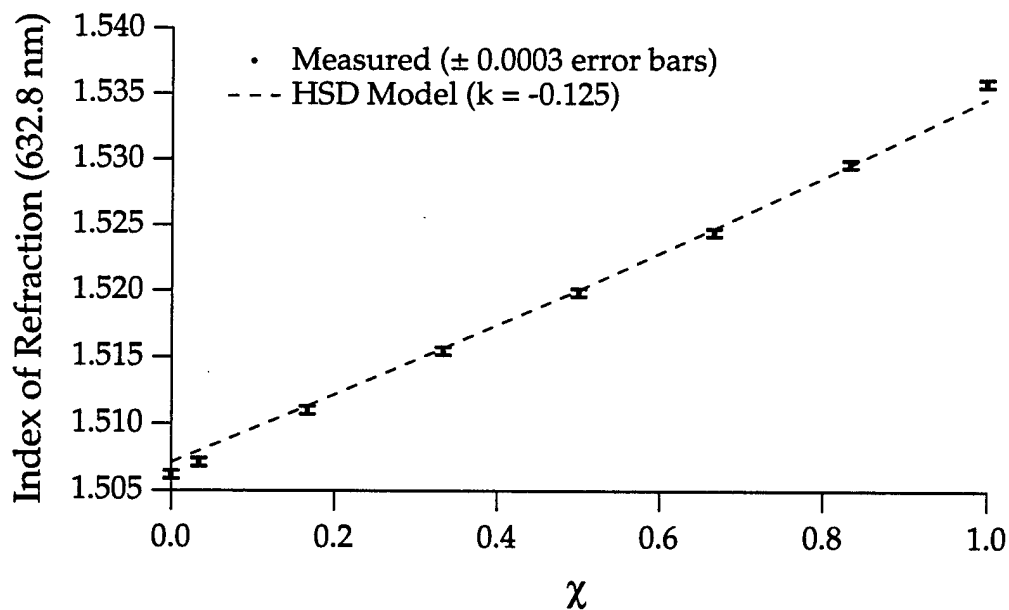
Figure 4.2 Index of refraction as a function of normalized lithium concentration, χ, for glasses in the system x Li_2O + (0.30-x) Na_2O + 0.07 Al_2O_3 + 0.63 SiO_2. Both the measured data points and the predicted values from the HSD model are shown.

4.2.4 Li+ for Na+ Diffusions

Axial gradients were fabricated in several of the glass compositions from the 7% alumina silicate glass system using Li^+ for Na^+ exchange. For each diffusion, a small sample of the glass, approximately 8 x 10 x 10 mm, was wrapped in platinum wire basket and suspended in a molten salt bath. Molten LiCl can be used as the source of the Li^+ ions, but the melting temperature of pure LiCl is 605 °C and at this temperature the glass samples would no longer hold their shape and begin to deform as discussed below.

Measurements of the anneal and strain temperatures for several of the glasses were conducted by Corning Engineering Lab Services and are listed in Table 4.4. The anneal point is defined as the temperature at which the viscosity of the glass is $10^{13.4}$ poises, while the strain point is defined as the temperature at which the viscosity of the glass is 4×10^{14} poises. The transformation temperature of the glass T_g corresponds to a viscosity of from 10^{13} to 10^{14} poises depending on the definition and method of measurement. Therefore, the measurements of the anneal and strain temperatures can be used to determine an approximate value for the transition temperatures for these glasses.

However, $CaCl_2$ can be added to the LiCl salt bath to form a eutectic [11] and reduce the melting temperature of the salt bath without having any adverse effects on the diffusion. [12] For each experiment, 250 grams of the mixture 0.40 LiCL + 0.60 $CaCl_2$, by weight, was placed in 250 ml Pyrex

Glass Name	x Li_2O	Anneal Temperature	Strain Temperature
JBGL-13	0.00	494 °C	457 °C
JBGL-15	0.10	439 °C	407 °C
JBGL-16	0.15	439 °C	407 °C
JBGL-17b	0.20	441 °C	409 °C
JBGL-12	0.30	472 °C	439 °C

Table 4.4 Anneal and strain temperatures for glasses in the system x Li_2O + (0.30-x) Na_2O + 0.07 Al_2O_3 + 0.63 SiO_2 measured at Corning Engineering Lab Services.

beaker. A diffusion temperature of 510 °C was used for all the experiments and is slightly higher than the melting temperature of this mixture which is 496 °C.

In particular, two series of axial diffusions were examined, one for an 18 hour diffusion time and the other for a 48 hour diffusion time. Each experiment in the series started with a homogeneous glass composition which had a different value of x, the initial amount of lithium in the glass. The experimental data for the series of 18 hour diffusions is listed in Table 4.5 and the measured index of refraction profiles are shown in Fig. 4.3. Similarly, the experimental data for the series of 48 hour diffusions is listed in Table 4.6 and the measured index of refraction profiles are shown in Fig. 4.4. Both figures show the wide variety of index of refraction profiles that can be obtained by changing the initial lithium concentration in the base glass, x, from 0.0 to 0.25. A comparison between the two series of diffusions shows that increasing the diffusion time increases the depth of the diffusion but the overall shape of the profile is maintained for each particular glass composition. Note: several of the 48 hour diffusions appear to have diffused all the way through because of the small sample size and the large diffusion depth.

4.2.5 Na+ for Li+ Diffusions

Axial gradients were also fabricated in several of the glass compositions from the 7% alumina silicate glass system using Na+ for Li+ exchange. For each diffusion a small sample of the glass, approximately 8 x 10 x 10 mm, was wrapped in stainless steel wire basket and suspended in a molten salt bath. Molten $NaNO_3$ was used as the source of Na+ ions, and a diffusion temperature of 510 °C was chosen for comparison with the Li+ for Na+ diffusions. The published decomposition temperature of $NaNO_3$ is 380 °C, [13] but Kindred showed that this salt composition could be used for diffusion temperatures up to 550° C. [14]

First, a series of six diffusions was examined in which glass samples were placed in 250 grams of molten $NaNO_3$ in 250 ml Pyrex™ beakers for 48 hours. Each experiment in the series started with a homogeneous glass composition which had a different value of x, the initial amount of

lithium in the glass. The experimental data is listed in Table 4.7. All of the samples with initial lithium concentrations greater than 0.15 cracked, and the amount of cracking in the sample increased as the initial lithium concentration (and therefore the amount of sodium being exchanged) was increased. Thus, it was difficult to find a place to measure the index of refraction profile for several of these samples.

Figure 4.5 shows the measured index of refraction profiles for the series of 48 hour diffusions, and, again, demonstrates that a wide variety of index of refraction profiles can be obtained by changing the initial lithium concentration in the base glass, x, from 0.05 to 0.30. However, unlike the Li^+ for Na^+ exchanges, the total index of refraction change is lower than expected for each of the experiments which indicates that none of the diffusions experienced complete exchange. This result is not unexpected, since Haun, et al. demonstrated that this type of glass shows an extreme preference for Li^+ over Na^+. [15] Note: several of the 48 hour diffusions also appear to have diffused all the way through because of the small sample size and large diffusion depth.

A second experiment was conducted in one of the glasses, JBGL 14, for a diffusion time of 24 hours. In this experiment, the salt bath was increased in size to 1000 grams, and placed in a 1000 ml Pyrex™ beaker. Figure 4.6 compares the measured index of refraction profiles for the two different experiments in this glass composition. At first, it appears that as the diffusion time is increased, the total Δn is decreased indicating that the salt bath is being "poisoned" in time. But, since the total Δn is also decreased as the amount of salt used in the experiment is decreased, it is hard to compare the two experiments. These effects are investigated further in Section 4.4.5 in a similar glass composition in which a large number of experiments could be examined since a large batch of glass was melted.

4.2.6 *Temperature Dependence*

The effect of changing the diffusion temperature on the Li^+ for Na^+ exchange was examined in one particular glass composition, JBGL-13, over a limited temperature range. In this study, axial gradients at three separate temperatures (500 °C, 510 °C, and 520 °C) were fabricated in this glass

composition for two different diffusion times (24 and 48 hours). This particular temperature range was chosen since the $LiCl/CaCl_2$ salt mixture does not melt lower than 500 °C, while the glass itself begins to deform and devitrify for diffusion temperatures much higher than 520 °C. The data for the series of temperature diffusions is listed in Table 4.8 and the measured index of refraction profiles are shown in Fig. 4.3. As expected, an increase in the diffusion temperature of the experiment, for the same diffusion time, increases the depth of the diffusion, but the overall shape of the profile is maintained.
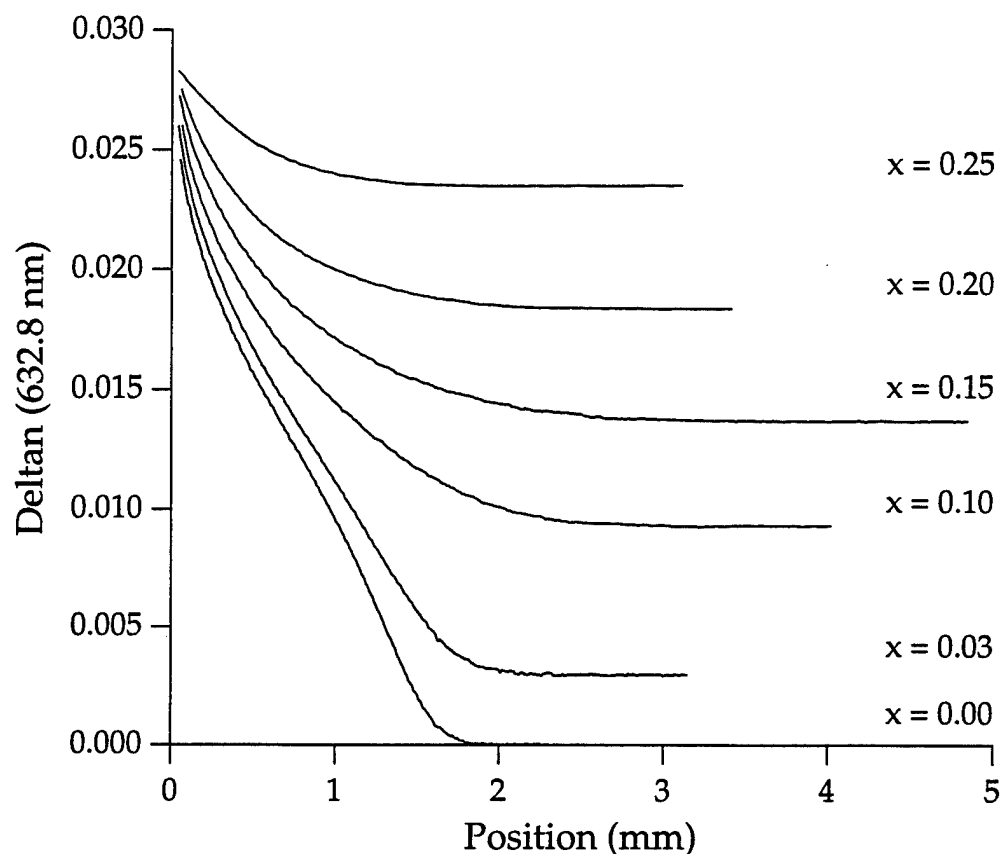
Figure 4.3 Measured index of refraction profiles for 18 hour Li$^+$ for Na$^+$ diffusions in glasses in the system x Li$_2$O + (0.30-x) Na$_2$O + 0.07 Al$_2$O$_3$ + 0.63 SiO$_2$ for various values of x, the initial lithium concentration in the glass. The experimental data is listed in Table 4.5.

Exp. #	Glass Name	x Li$_2$O	Temperature (°C)	Time (hours)
JLB-34	JBGL-13	0.0	510	18
JLB-39	JBGL-20	0.03	510	18
JLB-37	JBGL-15	0.10	510	18
JLB-35	JBGL-16	0.15	510	18
JLB-36	JBGL-17b	0.20	510	18
JLB-38	JBGL-18	0.25	510	18

Table 4.5 Experimental data for the 18 hour Li$^+$ for Na$^+$ diffusions in the glasses of the system x Li$_2$O + (0.30-x) Na$_2$O + 0.07 Al$_2$O$_3$ + 0.63 SiO$_2$ for various values of x, the initial lithium concentration in the glass. The measured index of refraction profiles are shown in Fig. 4.3.
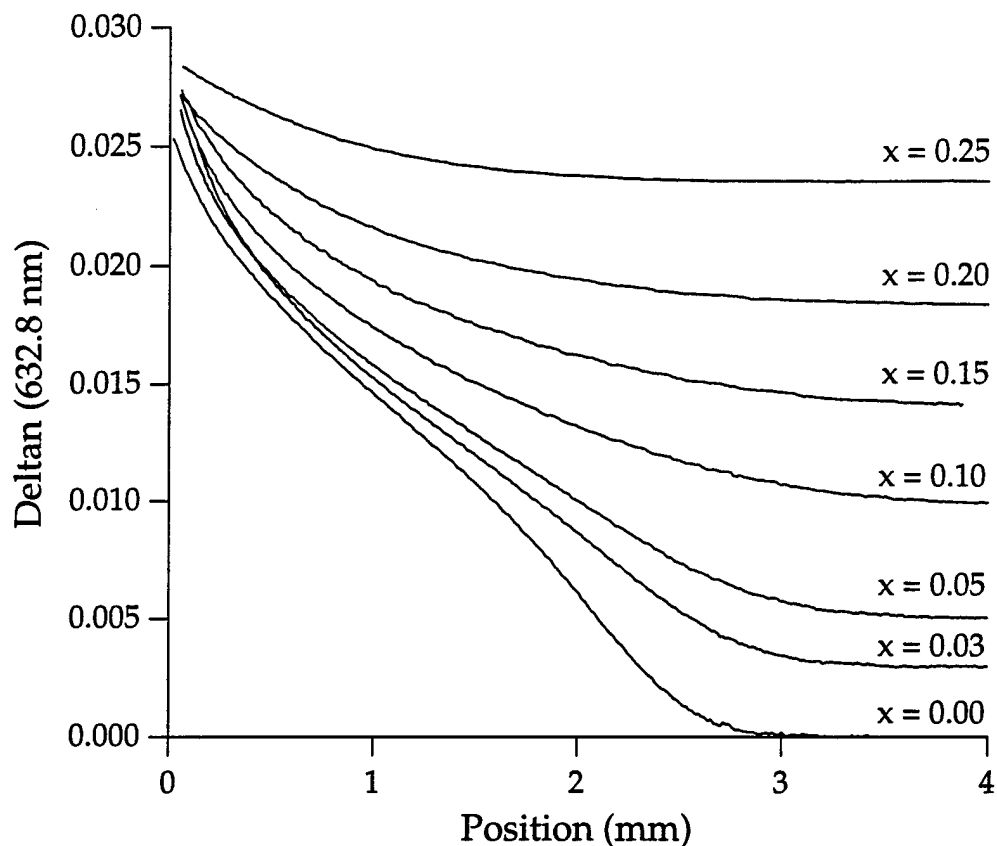
Figure 4.4 Measured index of refraction profiles for 48 hour Li^+ for Na^+ diffusions in glasses in the system x Li_2O + (0.30-x) Na_2O + 0.07 Al_2O_3 + 0.63 SiO_2 for various values of x, the initial lithium concentration in the glass. The experimental data is listed in Table 4.6.

Exp. #	Glass Name	x Li_2O	Temperature (°C)	Time (hours)
JLB-28	JBGL-13	0.0	510	48
JLB-29	JBGL-20	0.03	510	48
JLB-13	JBGL-14	0.05	510	48
JLB-14	JBGL-15	0.10	510	48
JLB-15	JBGL-16	0.15	510	48
JLB-20	JBGL-17b	0.20	510	48
JLB-21	JBGL-18	0.25	510	48

Table 4.6 Experimental data for the 48 hour Li^+ for Na^+ diffusions in the glasses of the system x Li_2O + (0.30-x) Na_2O + 0.07 Al_2O_3 + 0.63 SiO_2 for various values of x, the initial lithium concentration in the glass. The measured index of refraction profiles are shown in Fig. 4.4.
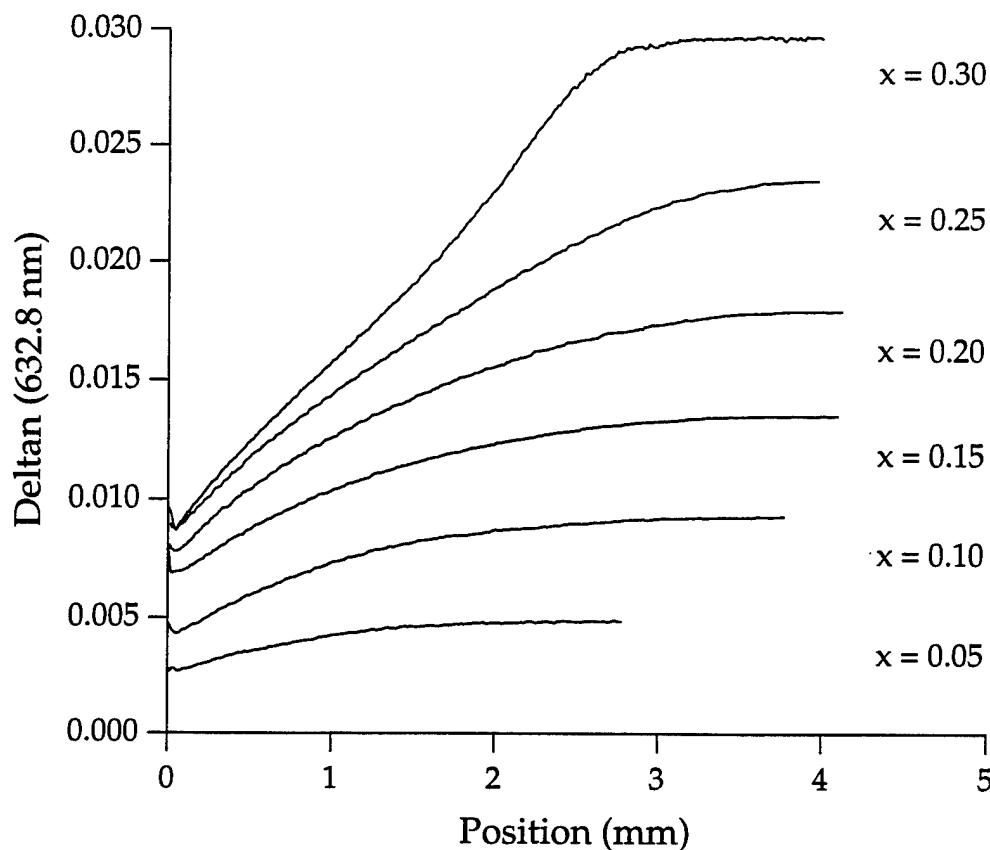
Figure 4.5 Measured index of refraction profiles for 48 hour Na$^+$ for Li$^+$ diffusions in glasses in the system x Li$_2$O + (0.30-x) Na$_2$O + 0.07 Al$_2$O$_3$ + 0.63 SiO$_2$ for various values of x, the initial lithium concentration in the glass. The experimental data is listed in Table 4.7.

Exp. #	Glass Name	x Li$_2$O	Temperature (°C)	Time (hours)
JLB-25	JBGL-14	0.05	510	24
JLB-16	JBGL-14	0.05	510	48
JLB-17	JBGL-15	0.10	510	48
JLB-18	JBGL-16	0.15	510	48
JLB-23	JBGL-17b	0.20	510	48
JLB-24	JBGL-18	0.25	510	48
JLB-22	JBGL-12	0.30	510	48

Table 4.7 Experimental data for the 48 hour Na$^+$ for Li$^+$ diffusions in the glasses of the system x Li$_2$O + (0.30-x) Na$_2$O + 0.07 Al$_2$O$_3$ + 0.63 SiO$_2$ for various values of x, the initial lithium concentration in the glass. The measured index of refraction profiles are shown in Fig. 4.5 and Fig 4.6.
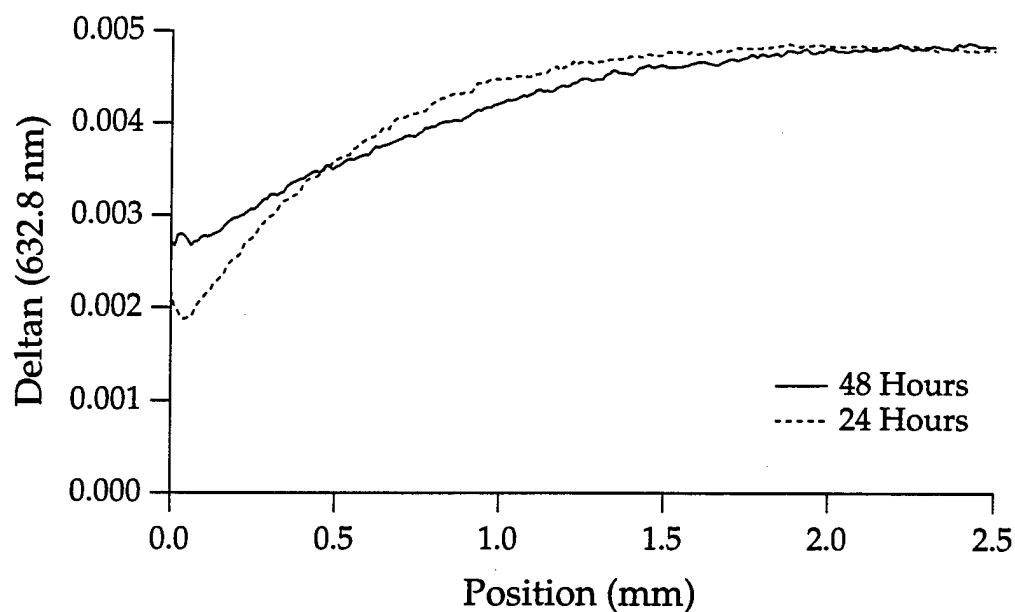
Figure 4.6 Measured index of refraction profiles for a 48 hour and a 24 hour Na^+ for Li^+ diffusion in the glass composition given by 0.05 Li_2O + 0.25 Na_2O + 0.07 Al_2O_3 + 0.63 SiO_2. The experimental data is listed in Table 4.7.
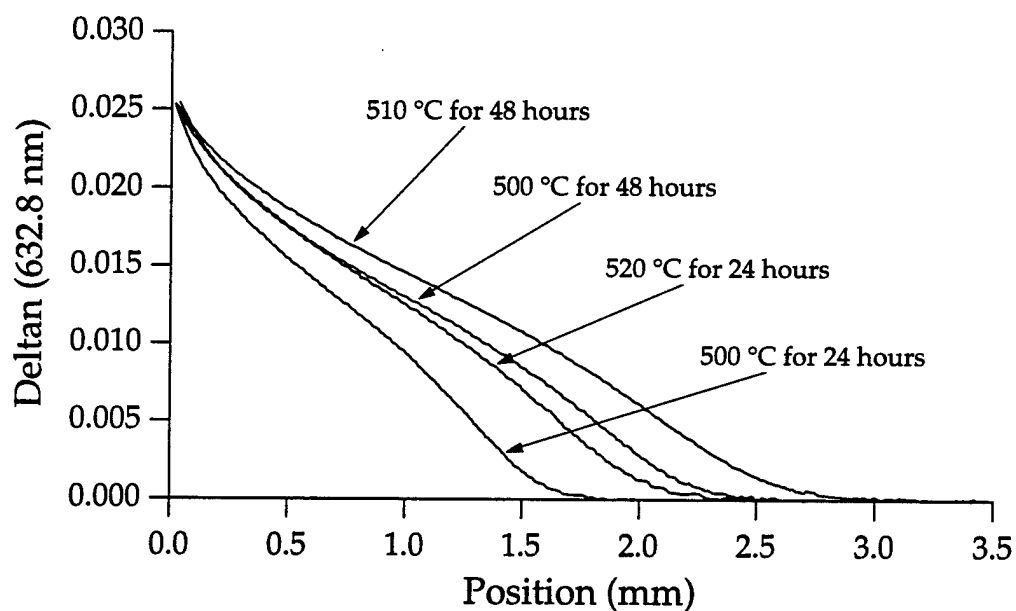
Figure 4.7 Measured index of refraction profiles for Li^+ for Na^+ diffusions at three different temperatures in the glass composition given by 0.30 Na_2O + 0.07 Al_2O_3 + 0.63 SiO_2. The experimental data is listed in Table 4.8.

Exp. #	Glass Name	x Li$_2$O	Temperature	Time
JLB-31	JBGL-13	0.0	520	24
JLB-28	JBGL-13	0.0	510	48
JLB-33	JBGL-13	0.0	500	24
JLB-32	JBGL-13	0.0	500	48

Table 4.8 Experimental data for Li$^+$ for Na$^+$ diffusions at three different temperatures in the glass composition given by 0.30 Na$_2$O + 0.07 Al$_2$O$_3$ + 0.63 SiO$_2$. The measured index of refraction profiles are shown in Fig. 4.7.

4.2.7 Calculation of the Diffusion Coefficient and Comparison of the Model Solutions with Experiment

In this section, the concentration dependence and the temperature dependence of the diffusion coefficient are examined for both Li$^+$ for Na$^+$ and Na$^+$ for Li$^+$ exchange in glass compositions from the 7% alumina silicate glass system. An experimental index of refraction profile (from the set of measured profiles in Sections 4.2.5 and 4.2.5) is first converted to a concentration profile using Eq. (4.6). Then, the Boltzmann-Matano technique is used to calculate the concentration dependent diffusion coefficient for that particular glass composition. This calculation is then curve fit to the Modified Quasi-Chemical (MQC) expression. (A more detailed description of this procedure was given in Chapters 2 and 3.)

The accuracy of the MQC fit is tested by numerically solving the diffusion equation to see if the MQC fit parameters can be used to recover the original index of refraction profile. Then, the diffusion model is used to calculate the index of refraction profiles for other diffusion times in that particular glass composition, and, in some cases, for other glass compositions within the system. In each case, the model solution is compared with the measured index of refraction profile, and if it does not agree to within the experimental error, the differences are explained.

4.2.7.1 Concentration Dependence

Each glass in the 7% alumina silicate glass subsystem has the same total alkali and the same alumina content, and only the initial ratio of Li$^+$/Na$^+$

in the glass is different. This particular change in composition was chosen for two reasons. First, it is the change in composition that is needed to determine the concentration dependence of the index of refraction from a series of homogeneous glass melts (as discussed in Section 4.2.3). Second, an exchange of Li^+ for Na^+ in a glass which contains no initial amount of Li^+ should produce a concentration gradient which encompasses the entire glass composition range. As a result, it is expected that the calculation of the diffusion coefficient from this single experiment would be useful for predicting the index of refraction profiles of diffusions in the other glasses across the entire glass composition range for both Li^+ for Na^+ and Na^+ for Li^+ exchange. This would greatly reduce the number of experiments required to define a diffusion model for such a wide variety of index of refraction profiles, since, in general, the concentration dependence of the diffusion coefficient must be determined experimentally for each particular glass composition.

In experiment JLB-28, an axial gradient is fabricated in a glass which initially contains no Li^+ ($x = 0.0$) using Li^+ for Na^+ exchange. The measured index of refraction profile for this experiment is shown in Fig. 4.4. This index of refraction profile was then converted to a concentration profile and used to calculate the diffusion coefficient. The result is shown in Fig. 4.8, where the diffusion coefficient is plotted as a function of normalized lithium concentration, χ. As expected, the calculation is very noisy, and is therefore fit to the Modified Quasi-Chemical Diffusion Coefficient expression. The MQC curve fit is shown as a dashed line in Fig. 4.8, and the fitting parameters for the MQC expression are listed in Table 4.9.

Exp. #	x Li$_2$O	D_B	α	ρ	χ_0	c
JLB-28	0.0	0.1236	0.4416	-1.3362	0.0912	11.87
JLB-39	0.03	0.1236	0.3000	-1.5035	0.0674	10.87
JLB-22	0.30	0.1236	0.0094	-1.6571	0.0600	11.28

Table 4.9 MQC fit parameters for the concentration dependent diffusion coefficients for glass compositions in the glass system x Li$_2$O + (0.30-x) Na$_2$O + 0.07 Al$_2$O$_3$ + 0.63 SiO$_2$.

The accuracy of the MQC fit is tested by using the MQC fit parameters to numerically solve the diffusion equation and recover the original index of refraction profile. The results are shown in Fig. 4.9. The experimental profile is shown as a solid line while two theoretical solutions are shown as dashed lines. The first theoretical profile (labeled as full exchange) was generated from the diffusion model with the assumption that a complete exchange of Na^+ for Li^+ occurred at the edge of the sample. As shown in the figure, the initial index of refraction profile cannot be recovered from the MQC fit parameters to within the experimental error under this assumption. However, if partial exchange (for $\chi_{max} = 0.9$) is assumed, a second solution is obtained (labeled as partial exchange in Fig. 4.9) which easily matches the experimental profile to well within the experimental error. In this particular glass composition, the concept of partial exchange is easy to justify from the measurements of the index of refraction profile since they often have a wide variety of Δn's (ranging from 0.19 to 0.27) depending on where the measurement is taken on the sample.

The x=0.0 diffusion coefficient was then used to generate theoretical index of refraction profiles for the other diffusions in this glass composition series. For example, both the theoretical solution and the experimental index of refraction profile for experiment JLB-39 (base glass composition of x=0.03) are shown in Fig. 4.10. As shown in the figure, the theoretical index of refraction profile generated with the x=0.0 diffusion coefficient does not match the experimental index of refraction profile to within the experimental error. Therefore, the index of refraction profile for x=0.03 glass was converted to a concentration profile and used to calculate the diffusion coefficient for this particular glass composition.

Figure 4.11 shows the diffusion coefficient and the MQC curve fits for both the x=0.03 glass composition and the x=0.0 glass composition. The specific fitting parameters for the x=0.03 glass are also listed in Table 4.9. As shown in the figure, there is fairly large difference between the x=0.0 diffusion coefficient and the x=0.03 diffusion coefficient for lithium concentrations greater than $\chi = 0.5$. The accuracy of the MQC fit to the x=0.03 diffusion coefficient is tested by using the MQC fit parameters to numerically solve the diffusion equation and recover the original index of

refraction profile. The result is also shown in Fig. 4.10 and easily recovers the initial index of refraction profile to within the experimental error.

Unlike the x=0.0 diffusion coefficient, the x=0.03 diffusion coefficient could be used to predict the experimental index of refraction profiles for Li^+ for Na^+ exchange in several other glass compositions within this composition range. For example, in Fig. 4.12, a series of experimental index of refraction profiles for 18 hour diffusions in different base glass compositions (from x=0.03 to x=0.25) are shown as solid lines, while the theoretical solutions generated with the x=0.03 diffusion coefficient are shown as dashed lines. Thus, the experiment and the model agree to within the experimental error for base glass compositions up to at least x=0.15. Figure 4.13 shows that the same is true for a second longer diffusion time of 48 hours, although a few of the samples may have begun to diffuse all the way through.

The x=0.03 diffusion coefficient was also used to generate theoretical index of refraction profiles for the Na^+ for Li^+ diffusions and these profiles are shown in Fig. 4.14 in comparison with the actual experimental profiles. Again, this diffusion coefficient works very well for the glass compositions from x=0.05 to x=0.15, but does not work for the other three compositions. Note: since full exchange did not occur for any of the samples, when the model profiles were generated this was taken into account by holding the boundary condition at the edge of the sample at the required value instead of keeping it at zero. For example, two diffusions in the same glass composition but for different diffusion times and salt bath size were shown earlier (in Fig. 4.6) to have different total Δn's. A comparison of the model solutions for these two profiles is shown in Fig. 4.15 where the solution for the 24 hour diffusion was generated by holding the maximum salt concentration at 0.05 while for the 48 hour diffusion the concentration was held at 0.09. As shown, this type of analysis works very well in predicting the profile.

The diffusion coefficient for the remainder of the glasses in this series was calculated from the measured index of refraction profile for experiment JLB-22 (a Na^+ for Li^+ diffusion in an x=0.30 base glass). Figure 4.16 shows the calculated diffusion coefficient and the MQC curve

fit for this glass composition along with the MQC curve fits for the x=0.03 glass composition and the x=0.0 glass composition. The specific fitting parameters for the x=0.30 glass are also listed in Table 4.9. Figure 4.17 shows the recovered index of refraction profile for both full and partial exchange in this glass. Figure 4.18 then shows the model solutions generated with this diffusion coefficient for the lithium for sodium exchanges in the x=0.20 and x=0.25 glasses for both the 18 and the 48 hour diffusions while Fig. 4.19 shows the same, but for sodium for lithium exchange.

In summary, only three different MQC diffusion coefficients were required to model Li^+ for Na^+ exchange and Na^+ for Li^+ exchange across the range of glass compositions in this system. In particular, each diffusion coefficient could be applied to a subset of compositions in the system and applied for any diffusion time. Thus, an empirical diffusion model for the alumina silicate glasses in this series has been developed for a diffusion temperature of 510° C.

4.2.7.2 Temperature Dependence

Diffusion coefficients are also highly temperature dependent. For a concentration-independent diffusion coefficient this dependence is often described in restricted temperature ranges by an Arrhenius-type equation

$$D(T) = D_0 e^{(-Q/RT)} \tag{4.7}$$

where T is the temperature, R is the gas constant, and Q and D0 must be determined from the experimental data. The experimental data is often plotted on a semi-log plot and then fitted to the equation

$$\ln(D(T)) = \ln(D_0) - \frac{Q}{RT} . \tag{4.8}$$

In some glasses an abrupt change in the slope of the fit occurs near the transition temperature of the glass. [16]

The effect of changing the diffusion temperature on the diffusion coefficient for Li^+ for Na^+ exchange is examined in one particular glass composition, JBGL-13, over a limited temperature range from 500 °C to 520 °C. The measured index of refraction profiles which are used to

calculate the diffusion coefficients were shown in Fig. 4.3. First, the diffusion coefficient for the 520 °C diffusion is calculated and is shown in Fig. 4.20. As expected, an increase in the diffusion temperature of the experiment, increases the value of the diffusion coefficient, but the overall shape of the concentration dependence is similar. Also shown in the figure are the MQC fits for both 510° C and 520 °C and the MQC fitting parameters are listed in Table 4.10. Similarly, Fig. 4.21 shows the calculated diffusion coefficient for 500 °C and its MQC fit, and the fitting parameters are listed in Table 4.10. Each of the fits can be used to recover the initial index of refraction profile to within experimental error as shown by Fig. 4.22.

The MQC fit parameters were then examined to determine how they change across this temperature range. First, as the temperature of the diffusion is increased, there is a definite increase in the self diffusion coefficient value, D_B, while the ratio of self diffusion coefficients, α, remains constant to within experimental error. Shown in Fig. 4.23 is a plot of the natural logarithm of D_B as a function of $1000/T$ where T is temperature. These values were then fit to Eq. (4.8) and the result is

$$\ln(D_B) = 18.8 - 10.7 * \frac{1000}{T} .$$

(4.9)

The temperature dependence of the MQC diffusion coefficient model is also found in the interaction energy term, ρ, where

$$\rho = -\frac{2\varepsilon_{int}}{kT} .$$

(4.10)

However, as discussed in Chapter 3, because of the amount of noise in the diffusion coefficient calculation, a range of MQC fits to the same diffusion coefficient can often be obtained that will recover the initial index of refraction profile to within experimental error. Therefore, the changes in the remaining coefficients are within the experimental error of the fit and a temperature dependence of these coefficients is difficult to determine. In addition, a more detailed study of the temperature dependence of the diffusion coefficient for alumina silicate glasses is given in Section 4.3.7.2 for two similar glass compositions.

Exp. #	Temp.	D_B	α	ρ	χ_0	c
JLB-32	500 °C	0.0725	0.4544	-1.3648	0.0413	14.47
JLB-28	510 °C	0.1236	0.4416	-1.3362	0.0912	11.87
JLB-31	520 °C	0.1648	0.4400	-1.2210	0.0938	11.99

Table 4.10 MQC fitting coefficients for the temperature dependence of the diffusion coefficient in the glass $0.30\ Na_2O + 0.07\ Al_2O_3 + 0.63\ SiO_2$.
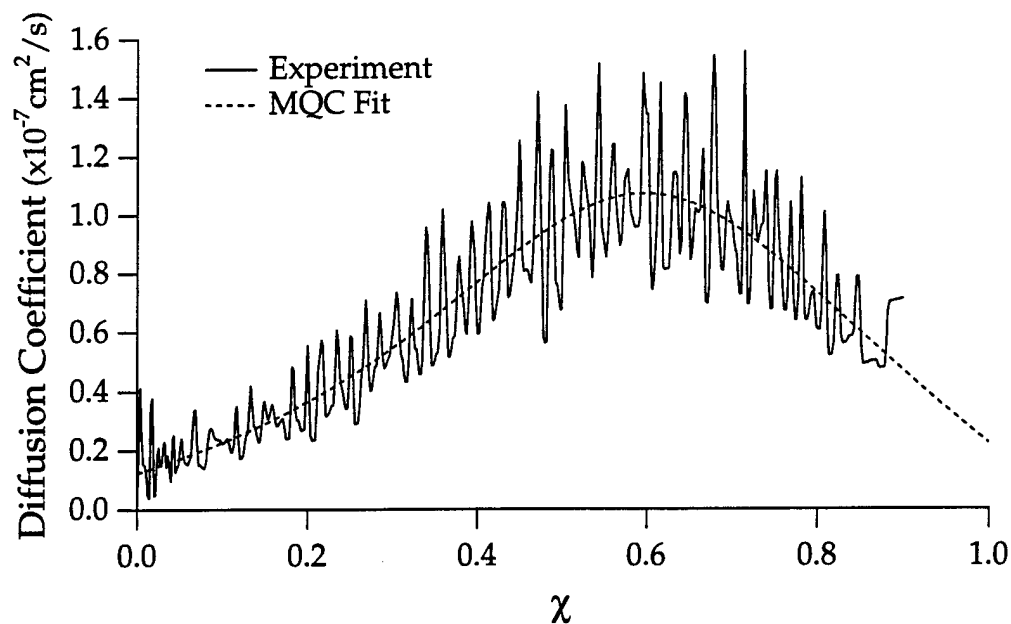
Figure 4.8 Calculated diffusion coefficient from experiment JLB-28 and the curve fit to the Modified Quasi-Chemical Diffusion Coefficient expression. The fit parameters are listed in Table 4.9.
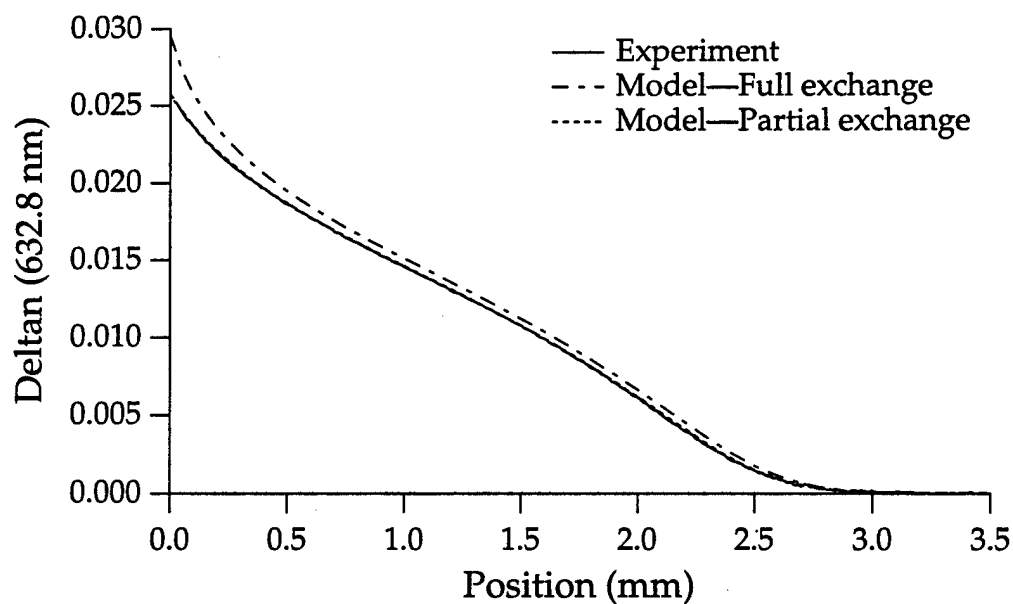
Figure 4.9 Experimental index of refraction profile for experiment JLB-28 and two model solutions: one for complete exchange, and the second for partial exchange.
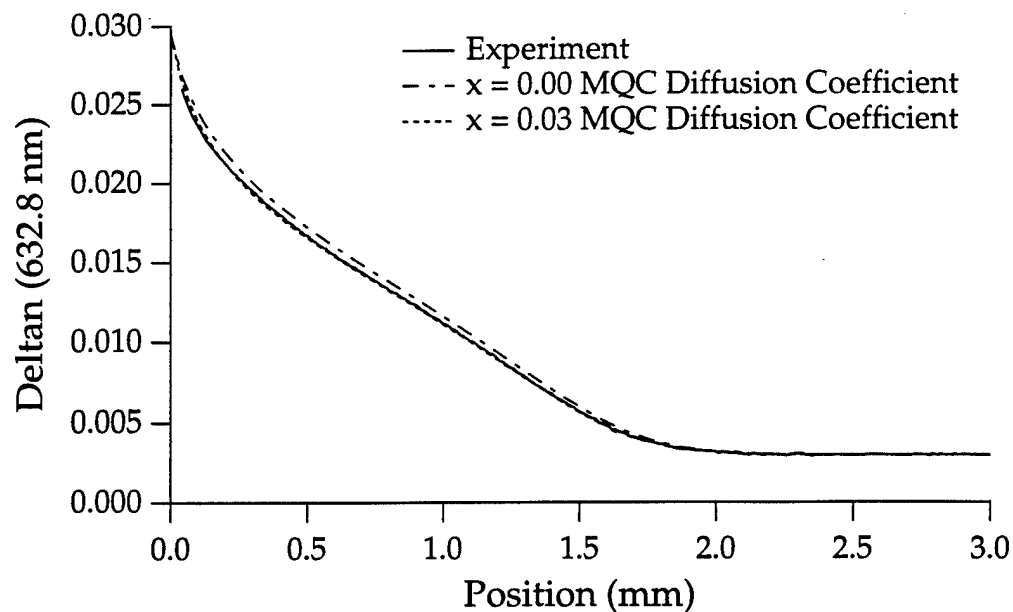
Figure 4.10 Experimental index of refraction profile for experiment JLB-39 and two model
solutions: one generated with the x = 0.0 MQC diffusion coefficient and the other
generated with the x = 0.03 MQC diffusion coefficient.
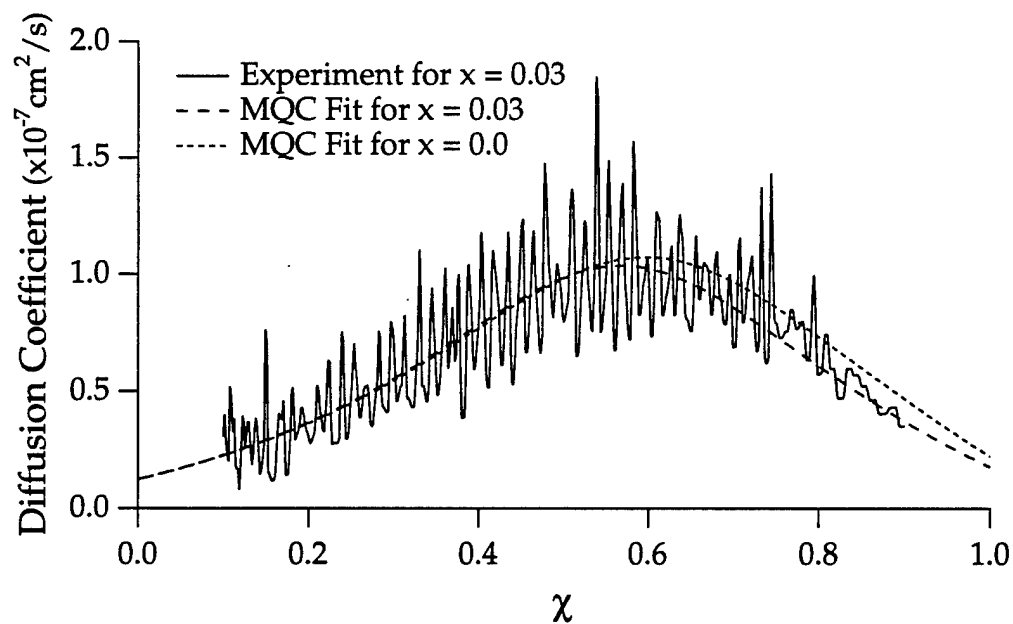
Figure 4.11 Calculated diffusion coefficient from experiment JLB-39 and the curve fit to the
MQC Diffusion Coefficient expression. The fit parameters are listed in Table 4.9. The
MQC Diffusion Coefficient for the x = 0.0 glass is also shown.
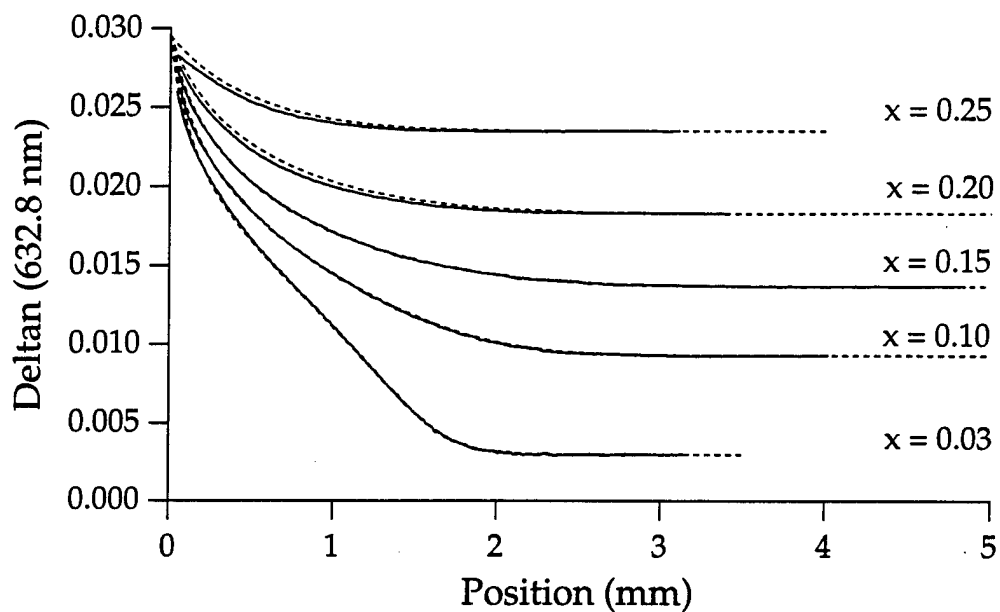
Figure 4.12 Experimental index of refraction profiles for 18 hour Li$^+$ for Na$^+$ diffusions in glasses in the system x Li$_2$O + (0.30-x) Na$_2$O + 0.07 Al$_2$O$_3$ + 0.63 SiO$_2$ and the model solutions generated with the x = 0.03 MQC diffusion coefficient.
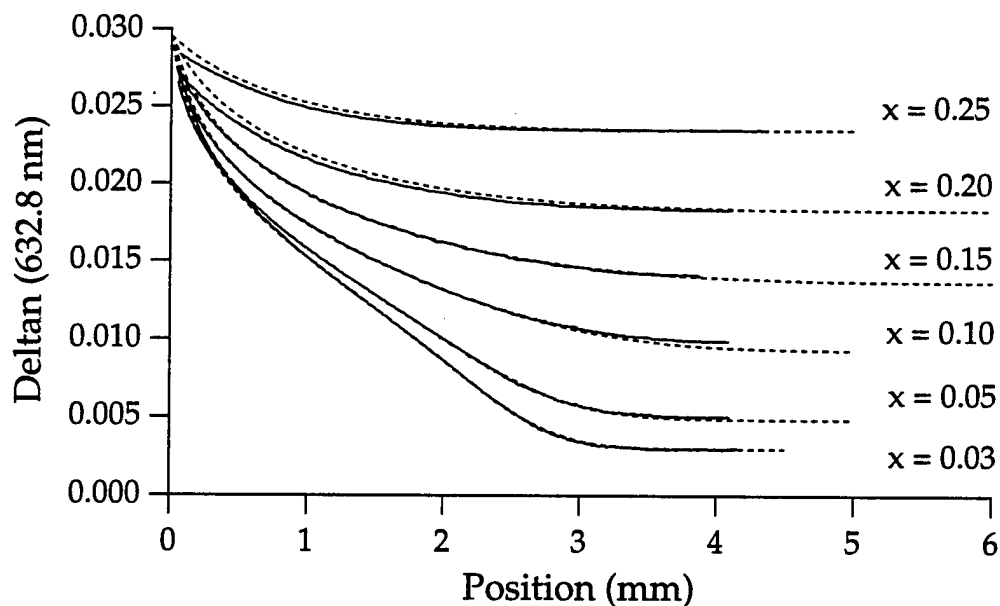
Figure 4.13 Experimental index of refraction profiles for 48 hour Li$^+$ for Na$^+$ diffusions in glasses in the system x Li$_2$O + (0.30-x) Na$_2$O + 0.07 Al$_2$O$_3$ + 0.63 SiO$_2$ and the model solutions generated with the x = 0.03 MQC diffusion coefficient.
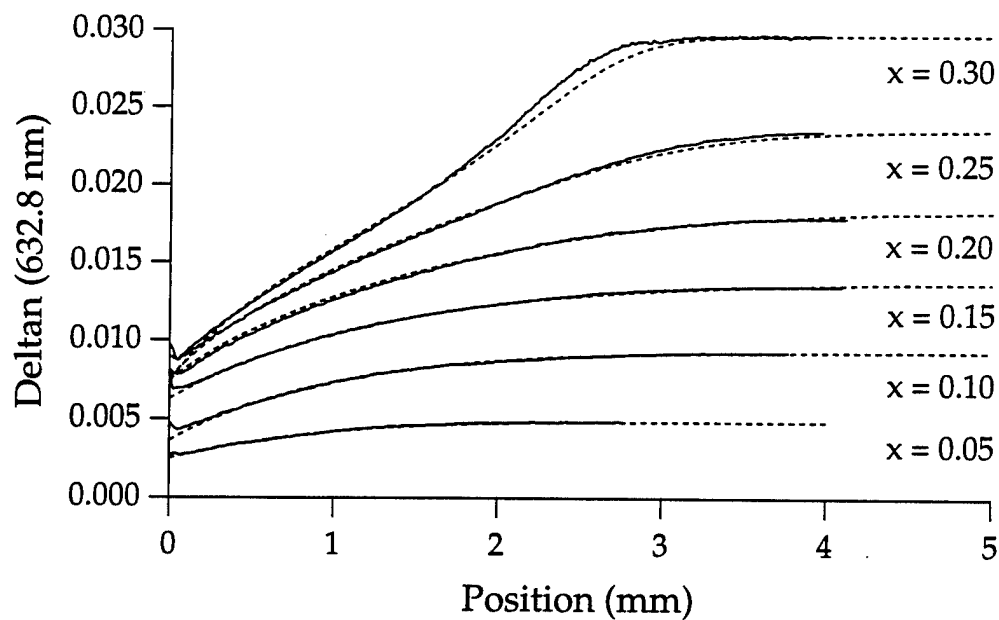
Figure 4.14 Experimental index of refraction profiles for 48 hour Na$^+$ for Li$^+$ diffusions in glasses in the system x Li$_2$O + (0.30-x) Na$_2$O + 0.07 Al$_2$O$_3$ + 0.63 SiO$_2$ and the model solutions generated with the x = 0.03 MQC diffusion coefficient.
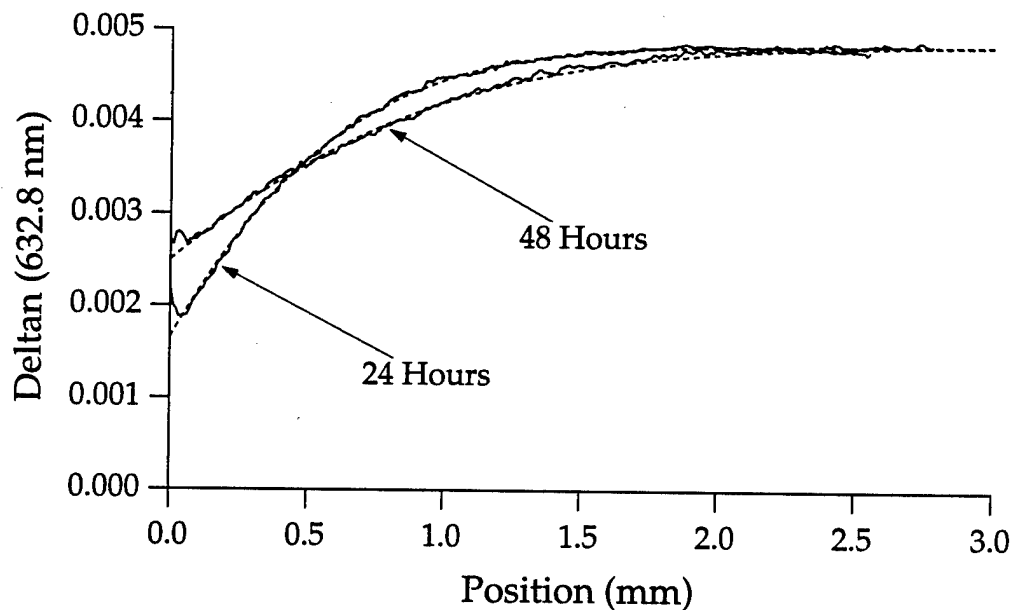
Figure 4.15 Experimental index of refraction of profiles for a 48 hour and a 24 hour Na$^+$ for Li$^+$ diffusion in the glass composition given by 0.05 Li$_2$O + 0.25 Na$_2$O + 0.07 Al$_2$O$_3$ + 0.63 SiO$_2$ and the model solutions generated with the x = 0.03 MQC diffusion coefficient.
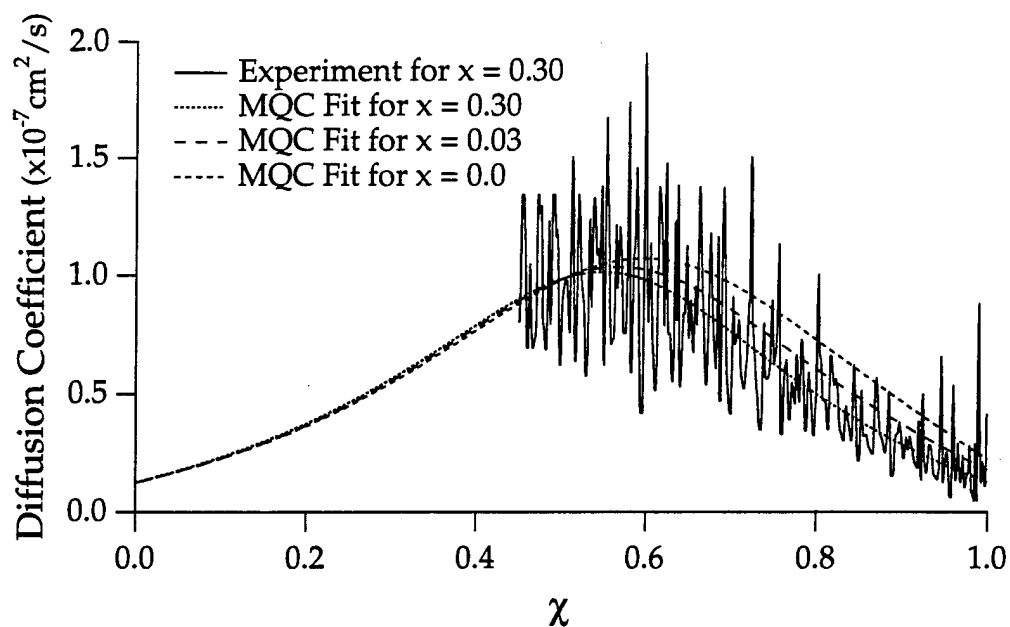
Figure 4.16 Calculated diffusion coefficient from experiment JLB-22 and the curve fit to the MQC Diffusion Coefficient expression. The fit parameters are listed in Table 4.9. The MQC Diffusion Coefficient for the x = 0.0 and x = 0.03 glasses are also shown.
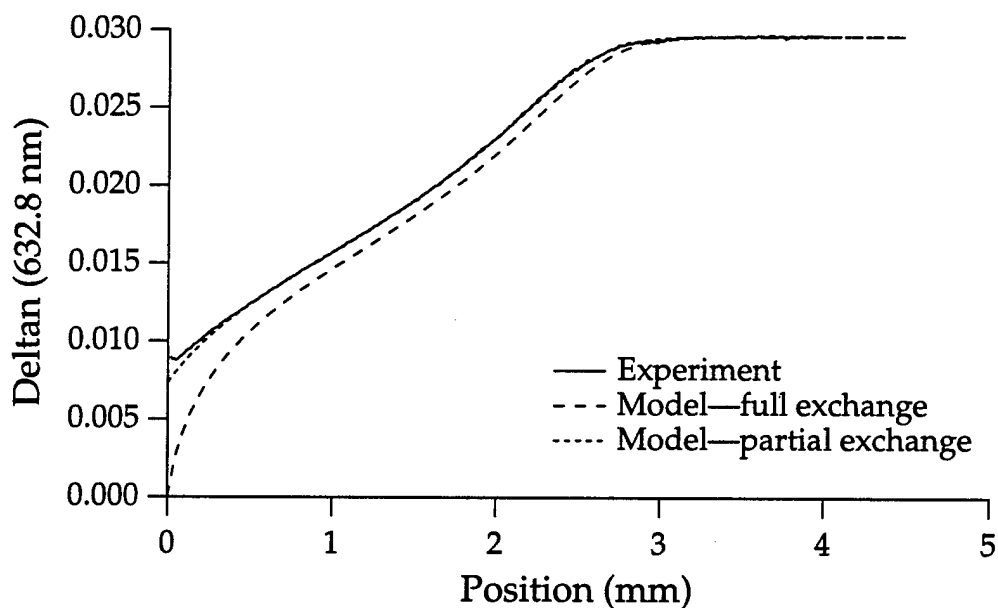
Figure 4.17 Experimental index of refraction profile for experiment JLB-22 and two model solutions: one for complete exchange, and the second for partial exchange.
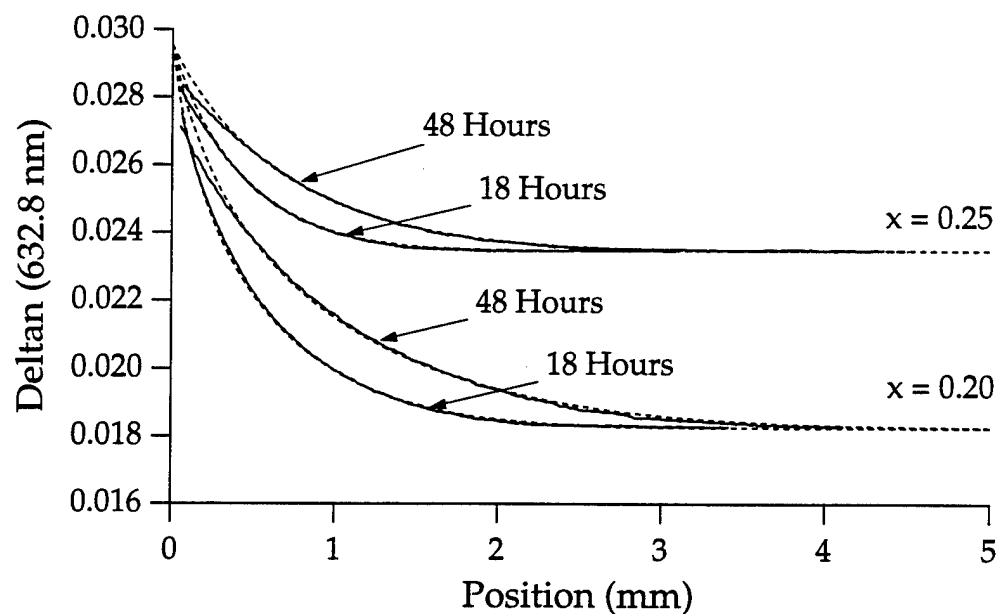
Figure 4.18 Experimental index of refraction profiles for 18 and 48 hour Li$^+$ for Na$^+$ diffusions in glasses in the system x Li$_2$O + (0.30-x) Na$_2$O + 0.07 Al$_2$O$_3$ + 0.63 SiO$_2$ and the model solutions generated with the x = 0.30 MQC diffusion coefficient.
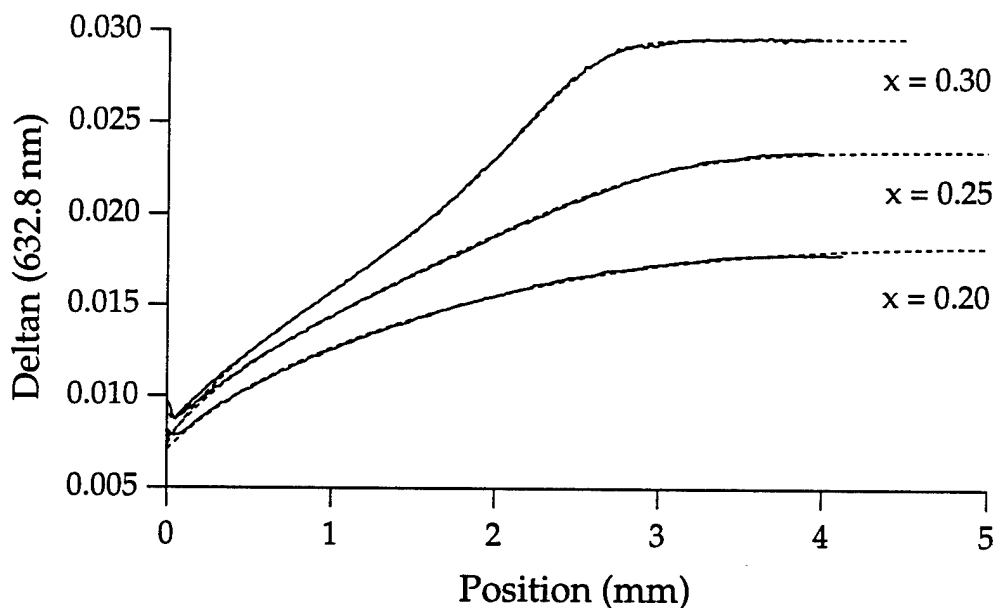
Figure 4.19 Experimental index of refraction profiles for 48 hour Na$^+$ for Li$^+$ diffusions in glasses in the system x Li$_2$O + (0.30-x) Na$_2$O + 0.07 Al$_2$O$_3$ + 0.63 SiO$_2$ and the model solutions generated with the x = 0.30 MQC diffusion coefficient.
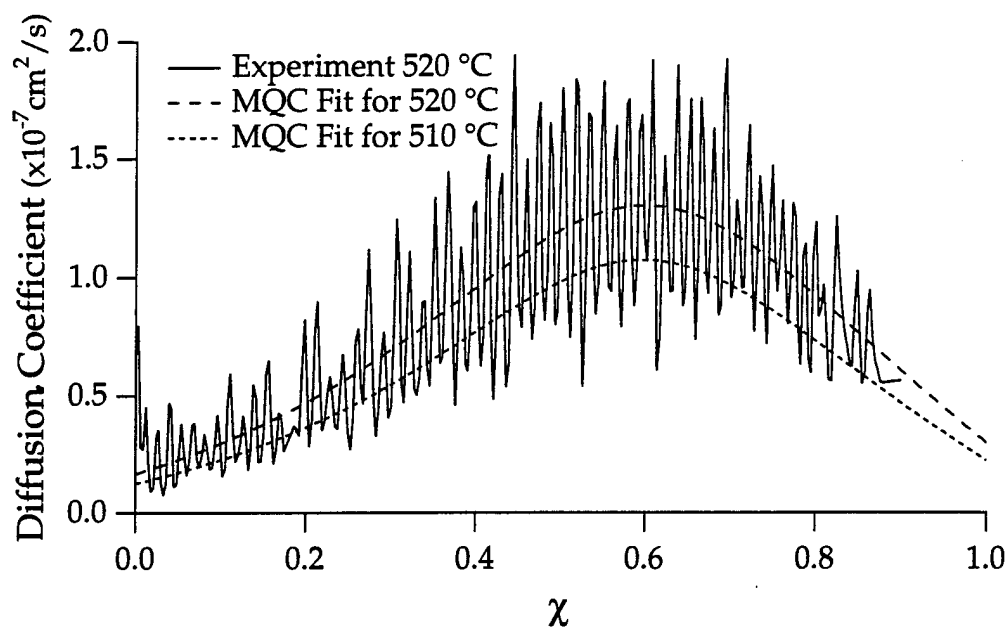
Figure 4.20 Calculated diffusion coefficient from experiment JLB-31 and the curve fit to the MQC Diffusion Coefficient expression. The fit parameters are listed in Table 4.10. The MQC Diffusion Coefficient for experiment JLB-28 is also shown.
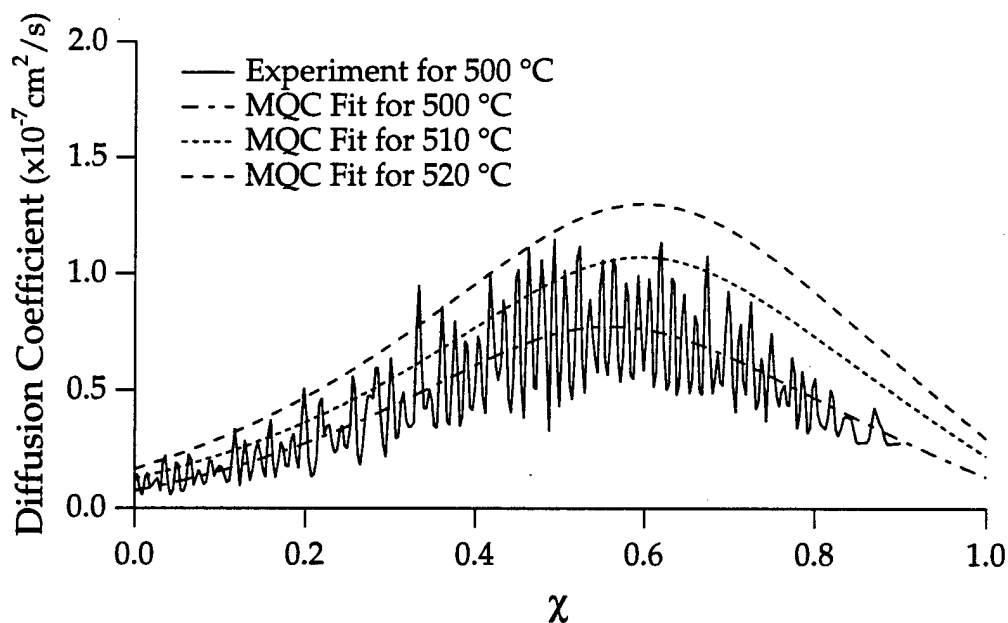
Figure 4.21 Calculated diffusion coefficient from experiment JLB-32 and the curve fit to the MQC Diffusion Coefficient expression. The fit parameters are listed in Table 4.10. The MQC Diffusion Coefficient for experiments JLB-28 and JLB-31 are also shown.
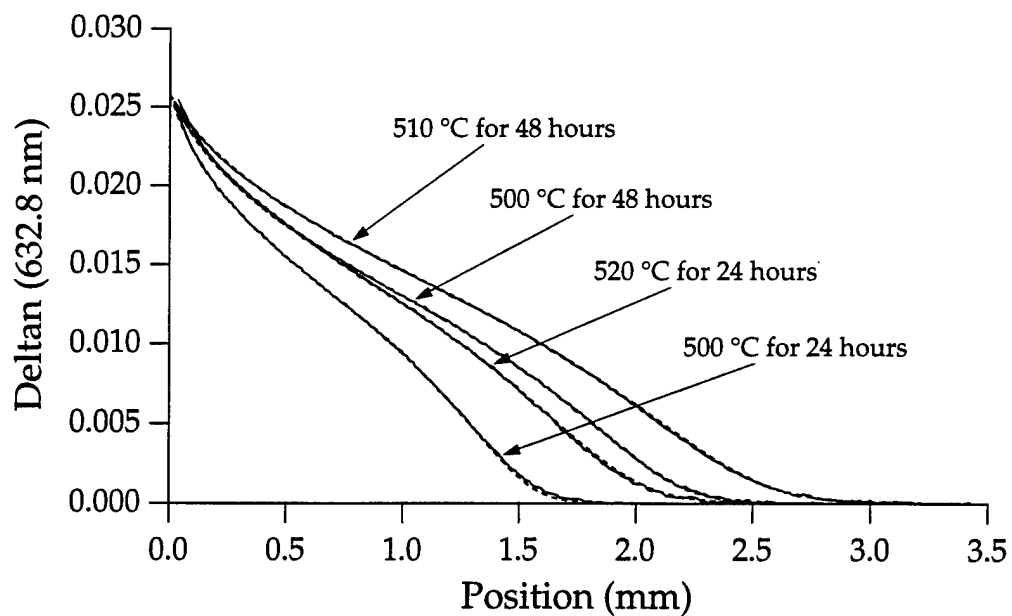
Figure 4.22 Measured index of refraction profiles and model solutions for Li^+ for Na^+ diffusions at three different temperatures in the glass composition given by 0.30 Na_2O + 0.07 Al_2O_3 + 0.63 SiO_2.
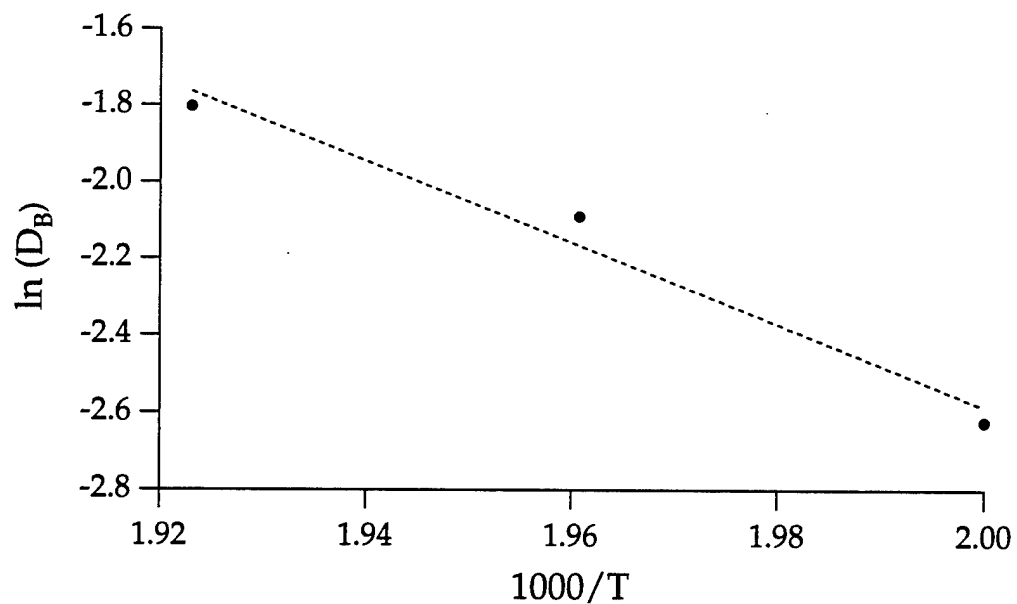
Figure 4.23 Natural logarithm of the MQC self-diffusion coefficient parameter, D_B plotted as a function of 1000/T where T is temperature.

4.3 5% Alumina Silicate Glass System

4.3.1 Introduction

The second alkali alumina silicate glass subsystem which is examined in this chapter is given by the composition formula

$$xLi_2O + (0.25 - x)Na_2O + 0.05Al_2O_3 + 0.70SiO_2 \qquad (4.11)$$

where x, the initial amount of lithium in the base glass, is varied from 0.00 to 0.25. This glass system is similar in composition to 7% alumina silicate glass system and was specifically chosen to verify the results of the previous study of the change in the ratio of Li^+/Na^+ in the base glass and the variation of the concentration dependence of the diffusion coefficient.

In addition, large glass melts were made for a few of the glass compositions in this composition range for several reasons. First, the improved homogeneity of the glasses reduces the error in measuring the index of refraction of the base glass and in determining the homogeneous region in grin profile. Second, the large amount of glass allows for a more extensive examination of the unusual properties of the system including the incomplete exchange results for Na+ for Li+ diffusions and the temperature dependence of the diffusion coefficient. Furthermore, radials can be core drilled from the glass melt to determine if the diffusion model is valid for a radial geometry since all of the previous diffusions in earlier section were done for only an axial geometry.

4.3.2 Glass Melting

Nine glass compositions were melted in this glass system and are listed in Table 4.11. Beginning at zero, the lithium concentration of each successive composition was increased (usually in five percent increments) up to the final glass composition which contains twenty-five percent lithium and no sodium. Several of the compositions were measured by flame spectroscopy at Corning Engineering Lab Services. The results of these measurements are also listed in Table 4.11 in parenthesis and show that the as melted compositions are accurate to ± 0.5%.

Four of the glass compositions (JBGL-5, 6, and 27, and DKGL-118) were melted in 250 gram batches in a platinum crucible using the experimental

procedure described in Section 4.2.2. The remaining five glasses (RH-1A0017, 1A0018, 3A2116, 3A2117, and 3A2119) were melted in a much larger size melt, approximately 10# of glass. The glass was melted at 1500 °C for a longer period of time of 24 hours. Then, after being cooled in the crucible to a temperature of 1400 °C, the glass was poured into a heated steel mold. The glass was quickly placed into a preheated annealing furnace and allowed to cool slowly from a temperature of 500° C to room temperature over a long period of time of 48 hours. The homogeneity of the large glass melts was much better and as a result many samples (both axial and radial) could be obtained from the melt.

4.3.3 Index of Refraction measurements

Small samples of several of the glasses (1cm x 1cm x 0.5 cm) were polished flat on one side to $\lambda/4$. Then, for each sample, the index of refraction at six different wavelengths was measured using a Pulfrich refractometer to an accuracy of ± 0.0001. Table 4.12 lists the results of these measurements. Similar to the index of refraction measurements for the 7% alumina silicate glass system, the glass with the largest lithium concentration has the largest index of refraction while the glass with the

Glass Name	Li_2O	Na_2O	Al_2O_3	SiO_2
RH-1A0018	0.0	0.25 (0.2464)	0.05 (0.0507)	0.70 (0.703)
JBGL-6	0.0125	0.2375	0.05	0.70
JBGL-5	0.0375	0.2125	0.05	0.70
RH-3A2119	0.075 (0.0771)	0.175 (0.1642)	0.05 (0.0506)	0.70 (0.7081)
RH-3A2116	0.10 (0.0996)	0.15 (0.1439)	0.05 (0.0504)	0.70 (0.7060)
RH-1A0017	0.125 (0.1175)	0.125 (0.1320)	0.05 (0.0492)	0.70 (0.7014)
RH-3A2117	0.15 (0.1451)	0.10 (0.0989)	0.05 (0.0492)	0.70 (0.7069)
JBGL-27	0.21	0.04	0.05	0.70
DKGL-118	0.25 (0.245)	0.0	0.05 (0.051)	0.70 (0.704)

Table 4.11 Compositions of the glasses melted in the system x Li_2O + (0.25-x) Na_2O + 0.05 Al_2O_3 + 0.70 SiO_2. The numbers in parenthesis are the compositions as measured by flame spectroscopy at Corning Engineering Lab Services.

largest sodium concentration has the smallest index of refraction. Thus, a Li$^+$ for Na$^+$ exchange in the all soda glass (RH-1A0018) should produce a gradient with a positive change in index of refraction of approximately 0.021 at 632.8 nm. Thus, a comparison with the previous glass system shows that the decrease in alumina content (from 0.07 to 0.05) and the decrease in total alkali (from 0.30 to 0.25) changes the base index of refraction of the glasses by a relatively small amount (1.5062 to 1.5006) but has a significant effect on the total change in refractive index of the gradient (0.03 to 0.021).

The homogeneous dispersion of the glass was then calculated using the procedure described in Chapter 3, Section 3.4.3. First, equation (3.8) was used to fit the six index of refraction measurements as a function of wavelength. Then, the index of refraction values, n$_F$ and n$_C$, were interpolated from the fit and the dispersion of the glass was calculated. Table 4.13 lists the coefficients of the fit, the indices of refraction, n$_F$ and n$_C$, and finally the dispersion, V$_d$, for each glass. Similar to the dispersion measurements for the 7% alumina silicate glass system, the dispersion of the glass appears to increase with the lithium concentration in the glass although not as much as in the previous glass system. Thus, a Li$^+$ for Na$^+$ exchange in the all soda glass (RH-1A0018) should produce a material with a negative gradient dispersion but it should have a very low dispersion because of the relatively small differences in homogeneous dispersion

Glass Name	x Li$_2$O	n$_g$	n$_{F'}$	n$_e$	n$_d$	n$_{HeNe}$	n$_{C'}$
RH-1A0018	0.0	1.5128	1.5087	1.5044	1.5024	1.5006	1.5002
RH-3A2119	0.075	1.5185	1.5207	1.5103	1.5083	1.5066	1.5062
RH-3A2116	0.10	1.5205	1.5165	1.5123	1.5103	1.5085	1.5081
RH-1A0017	0.125	1.5224	1.5185	1.5142	1.5122	1.5105	1.5050
RH-3A2117	0.15	1.5240	1.5201	1.5159	1.5139	1.5122	1.5118
DKGL-118	0.25	*	*	*	*	1.5221	*

Table 4.12 Index of refraction of homogeneous glass samples in the glass system x Li$_2$O + (0.25-x) Na$_2$O + 0.05 Al$_2$O$_3$ + 0.70 SiO$_2$ measured at six different wavelengths on a Pulfrich refractometer. *Not measured

Glass Name	x Li$_2$O	n$_0$	n$_1$	n$_2$	nF	nC	V$_d$
RH-1A0018	0.0	1.5030	-0.0470	-0.0028	1.5083	1.4998	59.32
RH-3A2119	0.075	1.5089	-0.0459	-0.0020	1.5141	1.5058	61.42
RH-3A2116	0.10	1.5109	-0.0452	-0.0007	1.5160	1.5079	62.52
RH-1A0017	0.125	1.5129	-0.0462	-0.0038	1.5180	1.5097	61.59
RH-3A2117	0.15	1.5145	-0.0457	-0.0034	1.5196	1.5114	62.36

Table 4.13 The fit coefficients for Eq. (3.8), the interpolated values for nF and nC , and the calculated dispersion V$_d$ for the homogeneous glasses in the system x Li$_2$O + (0.25-x) Na$_2$O + 0.05 Al$_2$O$_3$ + 0.70 SiO$_2$.

across the composition range. A gradient made by Kindred in this same glass composition (DSK-90) [17] was measured by Saxer and Moore [18] and the dispersion is approximately -100.

As discussed in Chapter 3, the index of refraction as a function of lithium concentration is necessary for the calculation of the concentration dependence of the diffusion coefficient for these glasses. It is also used by the diffusion model to convert concentration profile solutions to index of refraction profiles so that they can be compared with experimentally measured index of refraction profiles. Therefore, for this series of glass compositions, Fig. 4.24 shows a graph of the measured index of refraction (at 632.8 nm) as a function of normalized lithium concentration, χ, and a third order polynomial curve fit to the data given by

$$n(\chi) = 1.5006 + 0.01875\chi + 0.0002688\chi^2 + 0.001892\chi^3 . \quad (4.12)$$

Figure 4.25 then compares the measured index of refraction values to the predicted values from the Huggins, Sun, Davis model. The model values were calculated using the original empirical constants from Huggins, Sun, and Davis and an annealing constant of k = -0.024, and agree very well with the measured values to within 0.1%.
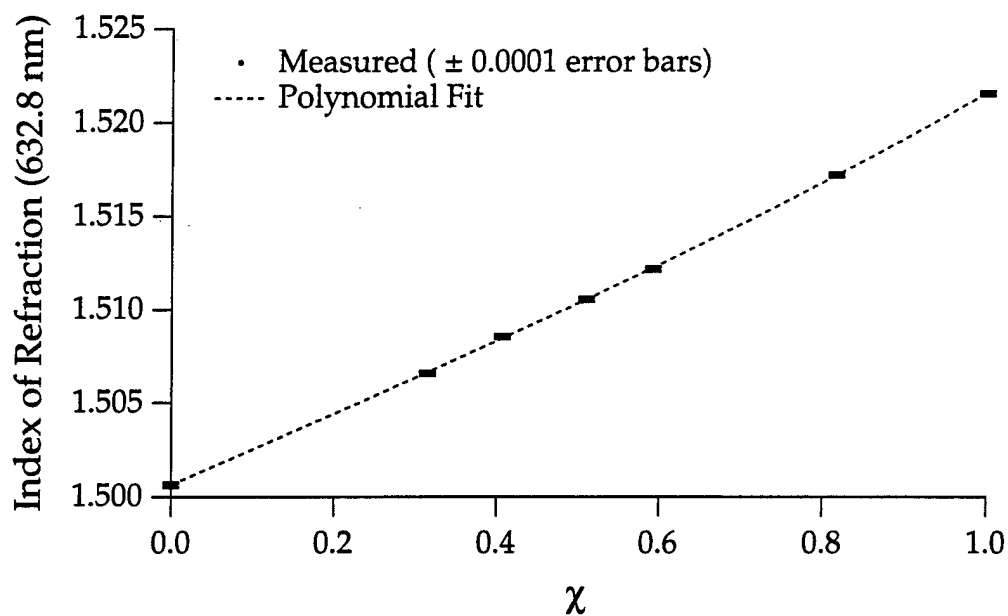
Figure 4.24 Index of refraction plotted as function of normalized lithium concentration, χ, for glasses in the system x Li_2O + (0.25-x) Na_2O + 0.05 Al_2O_3 + 0.70 SiO_2. Both the measured data points and a third order polynomial fit to the data are shown.
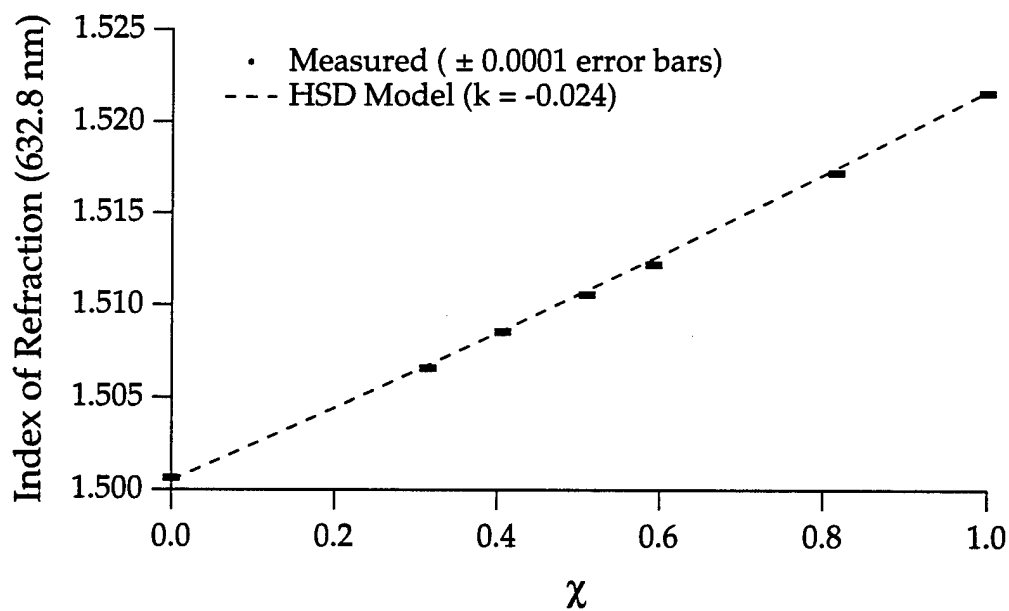
Figure 4.25 Index of refraction plotted as function of normalized lithium concentration, χ, for glasses in the system x Li_2O + (0.25-x) Na_2O + 0.05 Al_2O_3 + 0.70 SiO_2. Both the measured data points and the predicted values from the HSD model are shown.

4.3.4 Li+ for Na+ Diffusions

Axial and radial gradients were fabricated in several of the glass compositions from the 5% alumina silicate glass system using Li^+ for Na^+ exchange. For each diffusion, the glass sample was placed in platinum wire basket and suspended in a molten salt. The salt bath consisted of 250 grams of the mixture 0.40 LiCL + 0.60 $CaCl_2$, by weight, and was placed in 250 ml Pyrex™ beaker. A diffusion temperature of 510 °C was used for all of the experiments.

In particular, two series of axial diffusions were examined, one for a 6 hour diffusion time and the other for a 20 hour diffusion time. Each experiment in the series started with a homogeneous glass composition which had a different value of x, the initial amount of lithium in the glass. The experimental data for the series of 6 hour diffusions is listed in Table 4.14 and the measured index of refraction profiles are shown in Fig. 4.26. Similarly, the experimental data for the series of 20 hour diffusions is listed in Table 4.15 and the measured index of refraction profiles are shown in Fig. 4.27. Both figures show the wide variety of index of refraction profiles that can be obtained by changing the initial lithium concentration in the base glass, x. A comparison between the two series of diffusions shows that increasing the diffusion time increases the depth of the diffusion but the overall shape of the profile is maintained for each particular glass composition. These results are also very similar to the results from the 7% alumina silicate glass system.

Several three millimeter diameter radial gradients were also fabricated in three of the glass compositions of this composition range and the experimental data for these diffusions is listed in Table 4.16. Figure 4.28 shows the measured index of refraction profiles for two radial diffusions in the glass RH-3A2119 for different diffusion times. The figure shows that increasing the diffusion time from 6 to 20 hours can change the shape of the profile dramatically and also decreases the Δn of the gradient since after a certain diffusion time it begins to diffuse all the way through the material. Figure 4.29 shows the measured index of refraction profiles for two radial diffusions in the glass RH-3A2116 for two different diffusion

times, 6 and 18 hours. Again, increasing the diffusion time for a radial gradient can have a dramatic effect on the profile. This is unlike the axial gradients in which the diffusion depth is increased but the overall shape of the profile remains constant for the same glass composition. The change in glass composition for the same diffusion time is illustrated by Fig. 4.30, which shows 6 hour diffusions in three different glass compositions.

4.3.5 Na+ for Li+ Diffusions

Axial gradients were also fabricated in several of the glass compositions from the 5% alumina silicate glass system using Na^+ for Li^+ exchange. For each diffusion the glass sample was placed in stainless steel wire basket and suspended in a molten $NaNO_3$ salt bath at a diffusion temperature of 510 °C (for comparison with the Li^+ for Na^+ diffusions).

First, a series of three diffusions was examined in which glass samples were placed in 1000 grams of molten $NaNO_3$ in 1000 ml stainless steel beakers. Each experiment in the series started with a homogeneous glass composition which had a different value of x, the initial amount of lithium in the glass. The experimental data is listed in Table 4.17. Figure 4.31 shows the measured index of refraction profiles for the series. However, unlike the Li^+ for Na^+ exchanges, the total index of refraction change is lower than expected for each of the experiments which indicates that none of the diffusions experienced complete exchange. This result was also seen in the 7% alumina silicate glass system and is investigated further in the next series of experiments.

A second series of experiments was conducted in one of the glass compositions, RH-1A00017, in which the size of the sample, the size of the salt bath, and the length of the diffusion were varied in an organized fashion. The experimental data for this series of diffusions is also listed in Table 4.17. First, Fig. 4.32 compares the measured index of refraction profiles from experiments JLB-81 and JLB-84 in which the same size sample (2.3 grams) and the same size salt bath (250 grams) were used in the experiment, however the diffusion time was increased from 10 to 22 hours. Although neither diffusion achieves complete exchange they both

appear to have the same the total Δn. In addition, a scaled version of the 10 hour diffusion to 22 hours (scaled by the square root of time for Fickian diffusion) shown as a dashed line in Fig. 4.32 agrees very well with the measured 22 hour diffusion index of refraction profile.

The results of these two diffusions indicate that the boundary condition is constant in time for a set sample size and salt bath size at least for this limited range of diffusion times. Therefore a larger range of diffusion times was explored in the next set of experiments, JLB-87 through JLB-89. The sample size was increased to 8.2 grams and the size of the salt bath increased to 1000 grams, and a range of diffusion times from 15 hours to 92 hours was explored. Figure 4.33 shows the measured index of refraction profiles for these experiments. Again, they appear to have the same total change in refractive index and a scaled version of the 15 hour diffusion overlaps the 92 hour diffusion to within the experimental error of the measurement.

To examine the effect of the sample size/salt bath size two more sets of experiments were performed. First, a change in the salt bath size for a 2.3 gram sample from 100 grams to 250 grams is examined in experiments JLB-92, JLB-100, and JLB-84. The measured index of refraction profiles for these experiments are shown in Fig. 4.34. It appears that the total Δn increases as the salt bath size is increases, however, it is difficult to completely compare these diffusions since they were done for different diffusion times. However, Fig. 4.35 shows two experiments, JLB-90 and JLB-87, which used vary different salt bath sizes (250 grams to 1000 grams) for similar sample sizes (8 grams) and similar diffusion times. The increase in Δn as the salt bath size is increased is very apparent in these two measurements.

The results of this section indicate that time-dependent boundary conditions in the diffusion model are not needed, but a more appropriate model would have the user input the sample size and the salt bath size where an appropriate study has been done which developed a function for the maximum value of the boundary condition based on something like the salt to glass mass ratio.

4.3.6   Temperature Dependence

The effect of changing the diffusion temperature on the Li$^+$ for Na$^+$ exchange was examined in two of the glass compositions in this series, RH-1A0017 and RH-1A0018. In this study, axial gradients at five different temperatures from 500 °C to 520 °C in five degree increments were fabricated in each of the two glasses.

The data for the series of temperature diffusions in the RH-1A0018 listed in Table 4.18 and the measured index of refraction profiles are shown in Fig. 4.36. Note: because of the different diffusion times used in the experiments, the index of refraction profiles were all scaled to a diffusion time of 20 hours to highlight the effect of temperature on the profile since increasing the diffusion time has a similar effect as increasing the diffusion temperature. As expected, an increase in the diffusion temperature of the experiment, for the same diffusion time, increases the depth of the diffusion, but the overall shape of the profile is maintained.

The data for the series of temperature diffusions in the RH-1A0017 glass is listed in Table 4.19 and the measured index of refraction profiles are shown in Fig. 4.37. Note: because of the different diffusion times used in the experiments, the index of refraction profiles were all scaled to a diffusion time of 20 hours to highlight the effect of temperature on the profile.
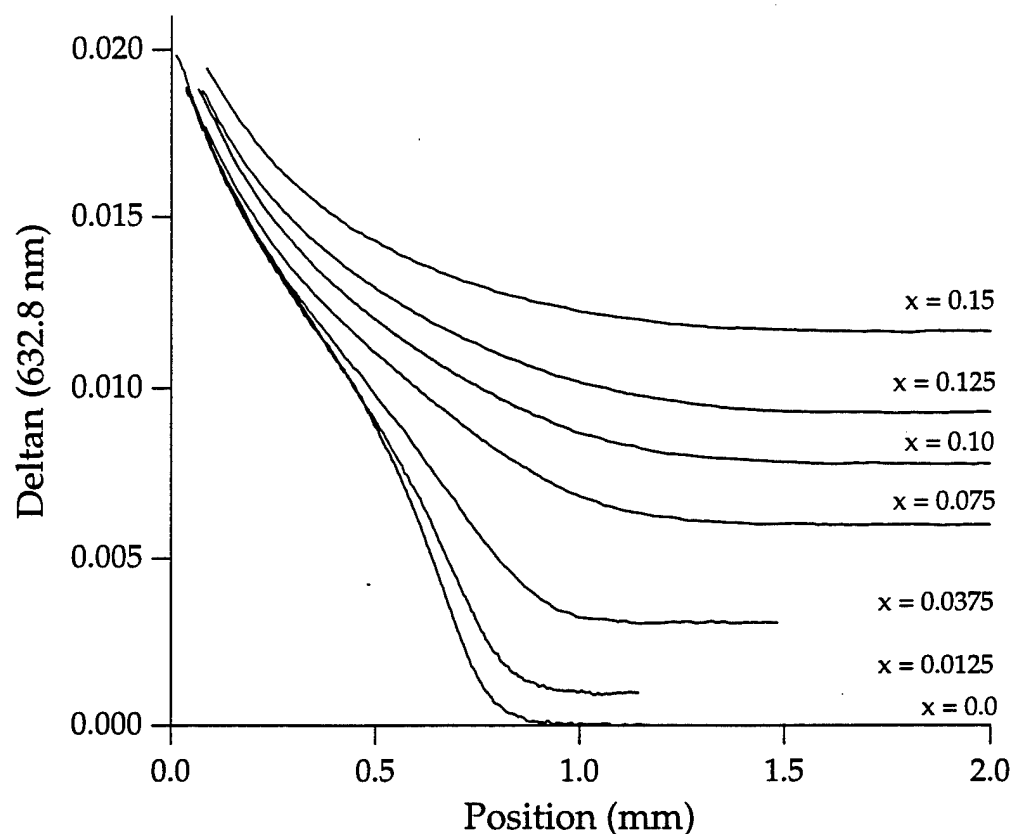
Figure 4.26 Measured index of refraction profiles for 6 hour Li$^+$ for Na$^+$ diffusions in glasses in the system x Li$_2$O + (0.25-x) Na$_2$O + 0.05 Al$_2$O$_3$ + 0.70 SiO$_2$ for various values of x, the initial lithium concentration in the glass. The experimental data is listed in Table 4.14.

Exp. #	Glass Name	x Li$_2$O	Temperature (°C)	Time (hours)
JLB-53	1A0018	0.0	510	6
JLB-99	JBGL-6	0.0125	510	6
JLB-98	JBGL-5	0.0375	510	6
JLB-51	3A2119	0.075	510	6
JLB-54	3A2116	0.10	510	6
JLB-52	1A0017	0.125	510	6
JLB-55	3A2117	0.15	510	6

Table 4.14 Experimental data for the 6 hour Li$^+$ for Na$^+$ diffusions in the glasses of the system x Li$_2$O + (0.25-x) Na$_2$O + 0.05 Al$_2$O$_3$ + 0.70 SiO$_2$ for various values of x, the initial lithium concentration in the glass. The measured index of refraction profiles are shown in Fig. 4.26.
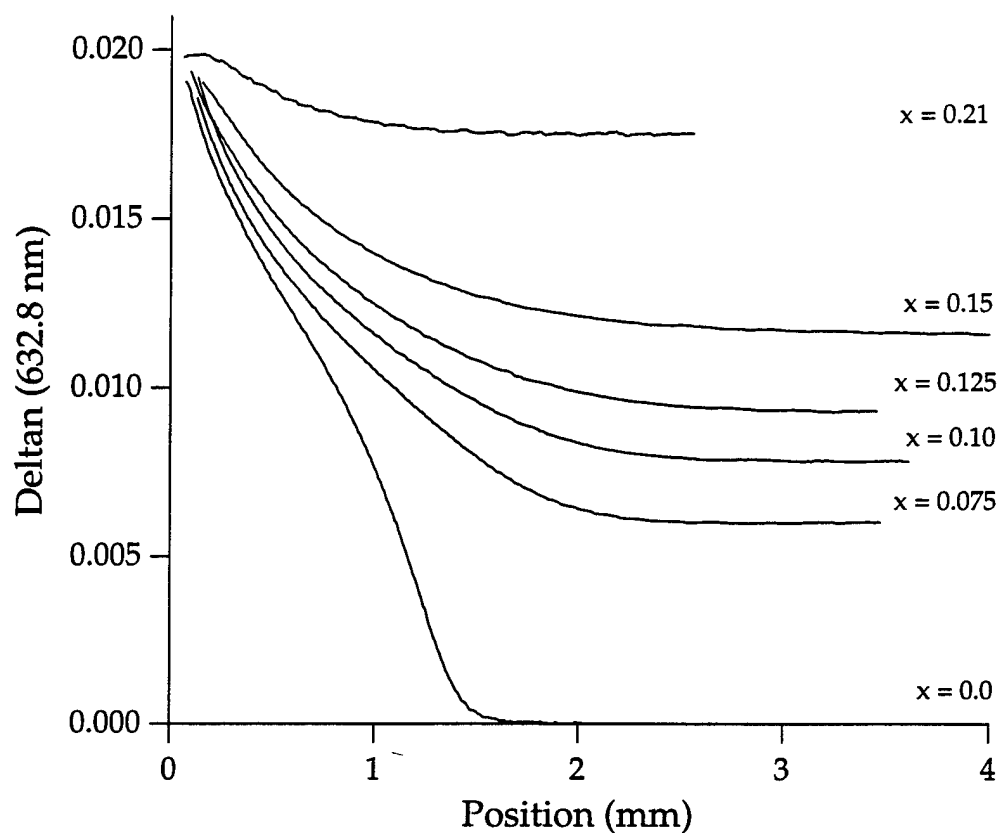
Figure 4.27 Measured index of refraction profiles for 20 hour Li^+ for Na^+ diffusions in glasses in the system x Li_2O + (0.25-x) Na_2O + 0.05 Al_2O_3 + 0.70 SiO_2 for various values of x, the initial lithium concentration in the glass. The experimental data is listed in Table 4.15.

Exp. #	Glass Name	x Li_2O	Temperature (°C)	Time (hours)
JLB-57	1A0018	0.0	510	20
JLB-45	3A2119	0.075	510	20
JLB-43	3A2116	0.10	510	20
JLB-46	1A0017	0.125	510	20
JLB-44	3A2117	0.15	510	20
JLB-94	JBGL-27	0.21	510	17

Table 4.15 Experimental data for the 20 hour Li^+ for Na^+ diffusions in the glasses of the system x Li_2O + (0.25-x) Na_2O + 0.05 Al_2O_3 + 0.70 SiO_2 for various values of x, the initial lithium concentration in the glass. The measured index of refraction profiles are shown in Fig. 4.27.

Figure 4.28 Measured index of refraction profiles for Li^+ for Na^+ radial diffusions in the glass composition 0.075 Li_2O + 0.175 Na_2O + 0.05 Al_2O_3 + 0.70 SiO_2. The experimental data is listed in Table 4.16.

Exp. #	Glass Name	x Li_2O	Temperature (°C)	Time (hours)
JLB-56	3A2119	0.075	510	6
JLB-59	3A2119	0.075	510	20
JLB-40	3A2116	0.10	510	6
JLB-48	3A2116	0.10	510	18
JLB-41	3A2117	0.15	510	6

Table 4.16 Experimental data for the Li^+ for Na^+ radial diffusions in the glasses of the system x Li_2O + (0.25-x) Na_2O + 0.05 Al_2O_3 + 0.70 SiO_2 for various values of x, the initial lithium concentration in the glass. The measured index of refraction profiles are shown in Fig. 4.28, Fig. 4.29, and Fig. 4.30.
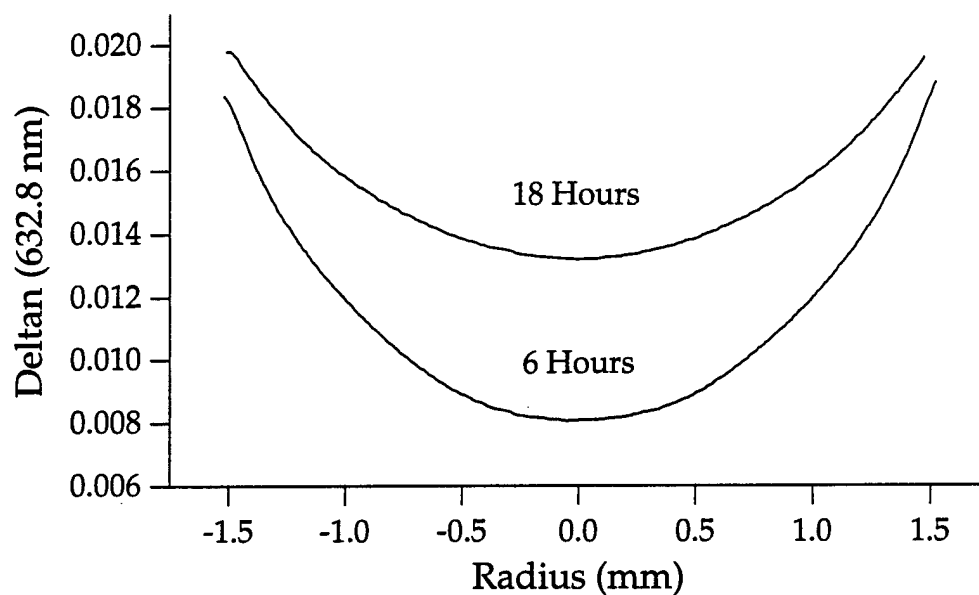
Figure 4.29 Measured index of refraction profiles for Li$^+$ for Na$^+$ radial diffusions in the glass composition 0.10 Li$_2$O + 0.15 Na$_2$O + 0.05 Al$_2$O$_3$ + 0.70 SiO$_2$. The experimental data is listed in Table 4.16.

Figure 4.30 Measured index of refraction profiles for 6 hour Li$^+$ for Na$^+$ radial diffusions in glasses in the system x Li$_2$O + (0.25-x) Na$_2$O + 0.05 Al$_2$O$_3$ + 0.70 SiO$_2$ for various values of x, the initial lithium concentration in the glass. The experimental data is listed in Table 4.16.

Figure 4.31 Measured index of refraction profiles for Na^+ for Li^+ diffusions in the system $x\ Li_2O + (0.25-x)\ Na_2O + 0.05\ Al_2O_3 + 0.70\ SiO_2$ for various values of x, the initial lithium concentration in the glass. The experimental data is listed in Table 4.17.

Exp. #	Glass	x Li₂O	Temp (°C)	Time (hours)	Sample (grams)	Salt (grams)
JLB-93	3A2119	0.075	510	6	2.5	1000
JLB-95	3A2116	0.10	510	8	2.5	1000
JLB-97	3A2117	0.15	510	15	3.25	1000
JLB-81	1A0017	0.125	510	22	2.3	250
JLB-84	1A0017	0.125	510	10	2.3	250
JLB-92	1A0017	0.125	510	4.5	2.3	100
JLB-100	1A0017	0.125	510	6	2.4	200
JLB-87	1A0017	0.125	510	92	8.4	1000
JLB-88	1A0017	0.125	510	48	8.1	1000
JLB-89	1A0017	0.125	510	15	8.2	1000
JLB-90	1A0017	0.125	510	96	7.7	250

Table 4.17 Experimental data for the Na^+ for Li^+ diffusions in the glasses of the system $x\ Li_2O + (0.25-x)\ Na_2O + 0.05\ Al_2O_3 + 0.70\ SiO_2$ for various values of x, the initial lithium concentration in the glass. The measured index of refraction profiles are shown in Fig. 4.31 through Fig 4.35.

Figure 4.32 Measured index of refraction profiles for Na$^+$ for Li$^+$ diffusions in 250 grams of salt in the glass composition 0.125 Li$_2$O + 0.125 Na$_2$O + 0.05 Al$_2$O$_3$ + 0.70 SiO$_2$ for two different diffusion times. The experimental data is listed in Table 4.17.
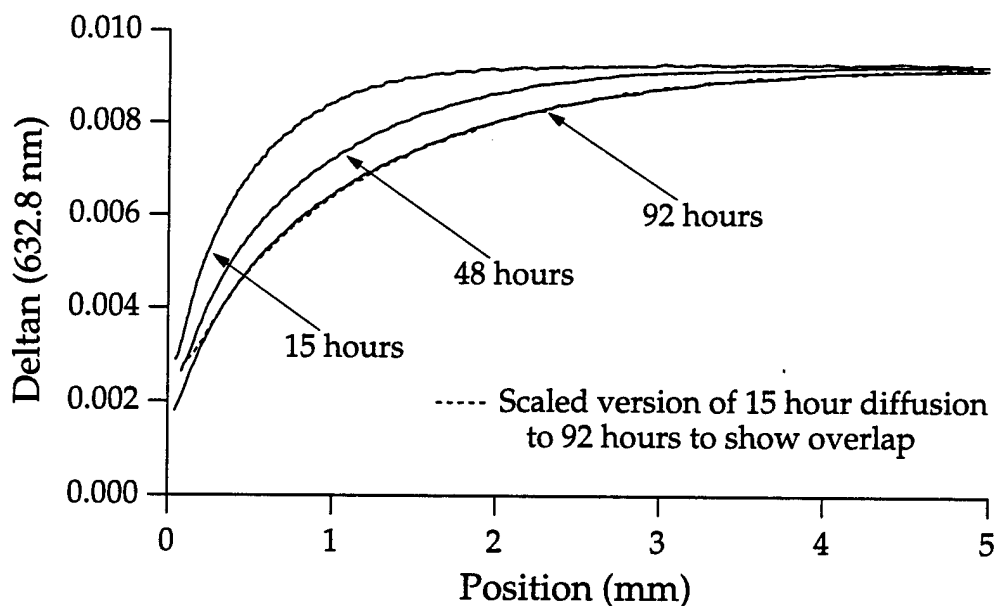
Figure 4.33 Measured index of refraction profiles for Na$^+$ for Li$^+$ diffusions in 1000 grams of salt in the glass composition 0.125 Li$_2$O + 0.125 Na$_2$O + 0.05 Al$_2$O$_3$ + 0.70 SiO$_2$ for several different diffusion times. The experimental data is listed in Table 4.17.
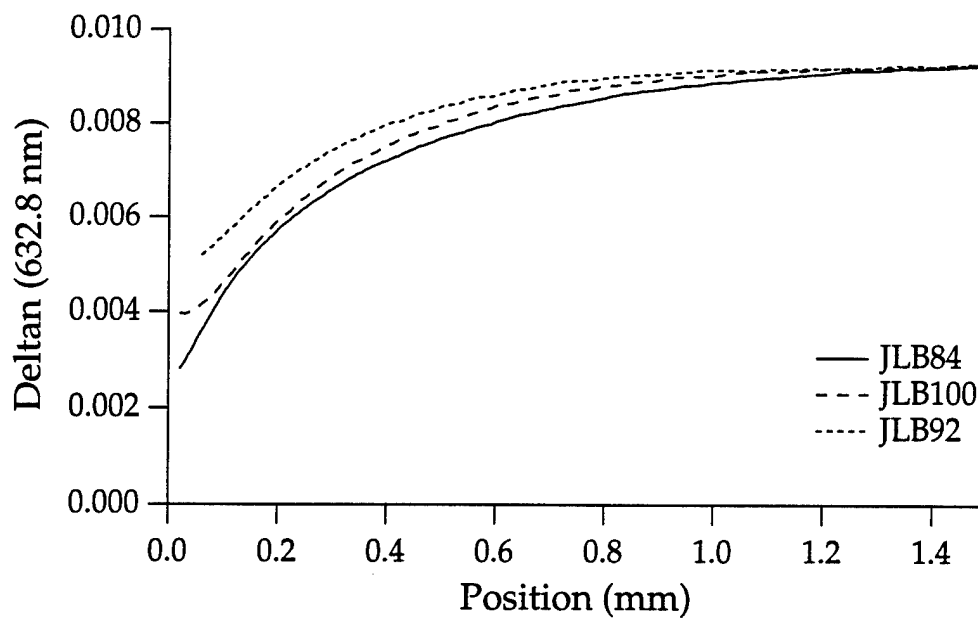
Figure 4.34 Measured index of refraction profiles for Na^+ for Li^+ diffusions in the glass composition 0.125 Li_2O + 0.125 Na_2O + 0.05 Al_2O_3 + 0.70 SiO_2 for different salt bath sizes. The experimental data is listed in Table 4.17.
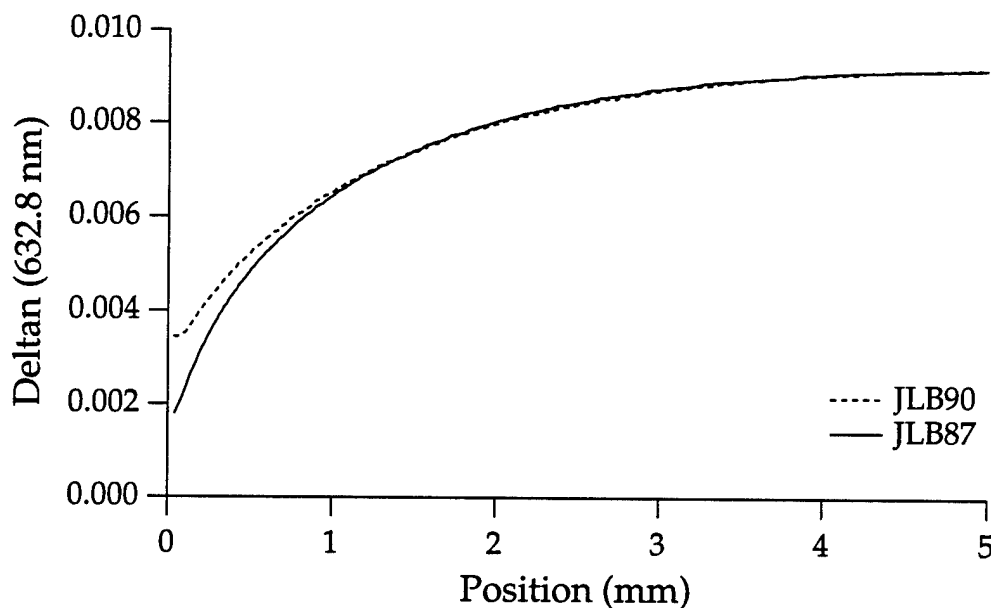
Figure 4.35 Measured index of refraction profiles for Na^+ for Li^+ diffusions in the glass composition 0.125 Li_2O + 0.125 Na_2O + 0.05 Al_2O_3 + 0.70 SiO_2 for different salt bath sizes. The experimental data is listed in Table 4.17.
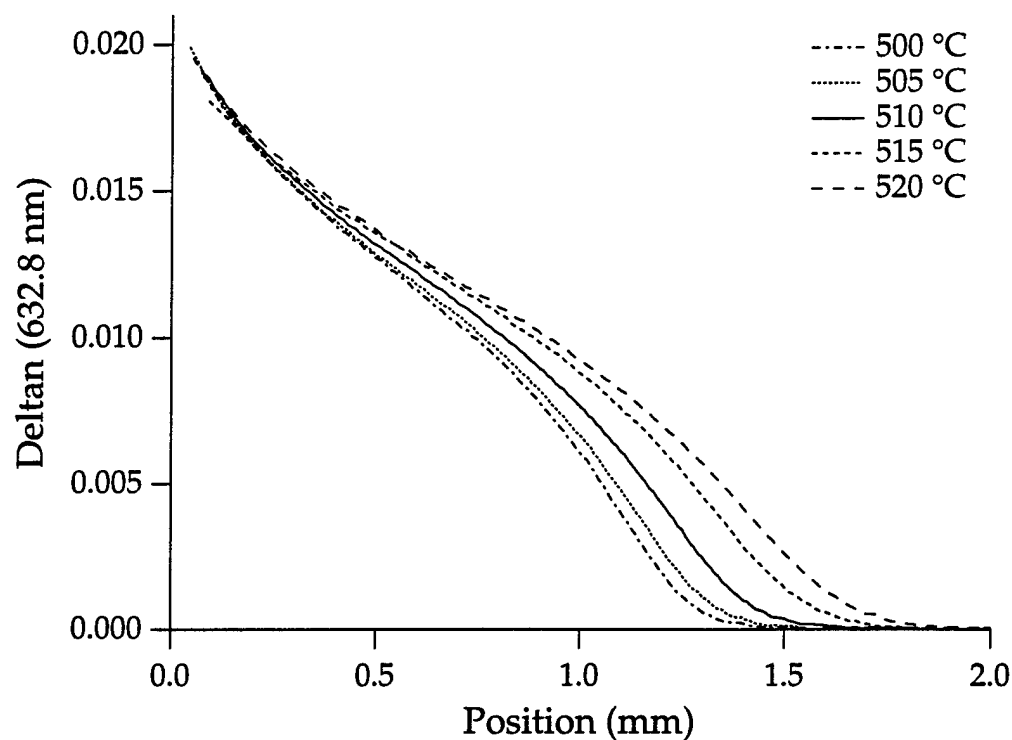
Figure 4.36 Measured index of refraction profiles for Li^+ for Na^+ diffusions at five different temperatures in the glass composition given by 0.25 Na_2O + 0.05 Al_2O_3 + 0.70 SiO_2. The experimental data is listed in Table 4.18. Note: the measured profiles are scaled to a common diffusion time of 20 hours for comparison.

Exp. #	Glass Name	x Li_2O	Temperature (°C)	Time (hours)
JLB-62	1A0018	0.0	500	24
JLB-64	1A0018	0.0	505	22
JLB-57	1A0018	0.0	510	20
JLB-68	1A0018	0.0	515	18
JLB-71	1A0018	0.0	520	14

Table 4.18 Experimental data for Li^+ for Na^+ diffusions at five different temperatures in the glass composition given by 0.25 Na_2O + 0.05 Al_2O_3 + 0.70 SiO_2. The measured index of refraction profiles are shown in Fig. 4.36.
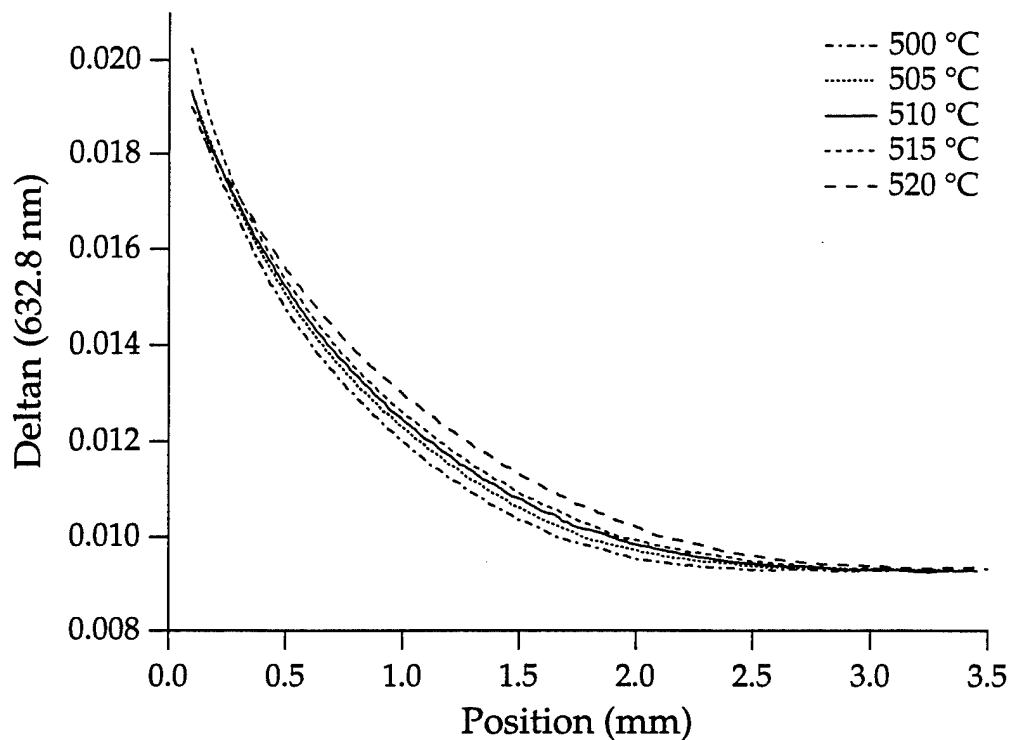
Figure 4.37 Measured index of refraction profiles for Li^+ for Na^+ diffusions at five different temperatures in the glass composition given by 0.125 Li_2O + 0.125 Na_2O + 0.05 Al_2O_3 + 0.70 SiO_2. The experimental data is listed in Table 4.19. Note: the measured profiles are scaled to a common diffusion time of 20 hours for comparison.

Exp. #	Glass Name	x Li₂O	Temperature (°C)	Time (hours)
JLB-61	1A0017	0.125	500	24
JLB-63	1A0017	0.125	505	22
JLB-46	1A0017	0.125	510	20
JLB-69	1A0017	0.125	515	18
JLB-70	1A0017	0.125	520	14

Table 4.19 Experimental data for Li^+ for Na^+ diffusions at five different temperatures in the glass composition given by 0.125 Li_2O + 0.125 Na_2O + 0.05 Al_2O_3 + 0.70 SiO_2. The measured index of refraction profiles are shown in Fig. 4.37.

4.3.7 Calculation of Diffusion Coefficient and Comparison of Model with Experiment

4.3.7.1 Concentration Dependence

Similar to the 7% alumina glass system, the diffusion coefficient was calculated from the measured index of refraction profile for several different glass compositions in this series. The experimental data was then fitted to the MQC model. The MQC fits which can recover the initial index of refraction profile to within experimental error are shown in Fig. 4.38. In particular, a diffusion coefficient was calculated for an x=0.0, x=0.0125, x=0.03, and an x=0.125 glass and the fitting coefficients are listed in Table 4.20. The same trend is seen that was discovered in the first alumina silicate system. Furthermore, a comparison of these coefficients to the MQC parameters for the 7% alumina silicate system shows that the coordination number drops from 11 to 8 which might be explained by the drop in total alkali content in the glass between the two systems.

The four diffusion coefficients were then used to calculate theoretical diffusion profiles for the remaining experiments in this glass system. These are shown in Fig. 4.39 for the 6 hour diffusions and Fig. 4.40 for the 20 hour diffusions. The x=0.0, x=0.0125, and x=0.03 diffusion coefficient was first used for diffusions in its own glass composition, and then, similar to the 7% alumina silicate glasses, the x=0.125 diffusion coefficient can be used to model any of the glass compositions from x=0.075 to x=0.15, but cannot be used for the x=0.21 glass and appears to be too large, similar to the results in the 7% alumina silicate glass system.

Exp. #	x Li_2O	D_B	α	ρ	χ_0	c
JLB-53	0.0	0.0770	0.8100	-1.8550	0.1310	8.00
JLB-99	0.01	0.0770	0.8050	-1.7252	0.1041	8.47
JLB-98	0.03	0.0770	0.7909	-1.8299	0.0820	7.54
JLB-46	0.125	0.0770	0.7839	-1.8072	0.0730	7.18

Table 4.20 MQC fit parameters for the concentration dependent diffusion coefficients for glass compositions in the glass system x Li_2O + (0.25-x) Na_2O + 0.05 Al_2O_3 + 0.70 SiO_2.

The model can also be applied to the radial diffusions with good results using the x=.125 MQC diffusion coefficient. As shown in Fig. 4.41, the model solutions and the experiment agree very well for the two diffusions in glass composition x=0.075. This is also true for the glass composition of x=0.10 as shown in Fig. 4.42 and for 6 hour diffusions in the three different glass compositions as shown in Fig. 4.43. Finally, the model using the x=.125 MQC diffusion coefficient can also be used to predict Na^+ for Li^+ exchange as shown in Fig. 4.44 in three different glass compositions.

4.3.7.2   Temperature Dependence

The effect of changing the diffusion temperature on the diffusion coefficient for Li^+ for Na^+ exchange was examined in two of the glass compositions in this series, RH-1A0017 and RH-1A0018. In particular, five different temperatures from 500 °C to 520 °C in five degree increments were examined. The measured index of refraction profiles which were used to calculate the diffusion coefficients are shown in Fig. 4.36 and Fig. 4.37. The MQC fits for the diffusion coefficients are shown in Fig. 4.46 and Fig. 4.47. (Each of the fits were used to recover the initial index of refraction profile to within experimental error.) As expected, an increase in the diffusion temperature of the experiment, increases the value of the diffusion coefficient, but the overall shape of the concentration dependence is similar. The MQC fitting parameters for each of these diffusion coefficients are listed in Table 4.21.

The MQC fit parameters were then examined to determine how they change across this temperature range. Similar to the study of the 7% alumina silicate glass system, as the temperature of the diffusion is increased, there is a definite increase in the self diffusion coefficient value, D_B, while the other coefficients remain constant to within the experimental error. Shown in Fig. 4.47 is a plot of the natural logarithm of D_B as a function of 1000/T where T is temperature. These values were then fit to Eq. (4.8). The result is also shown in the figure and given by

$$\ln(D_B) = 9.1 - 5.9 * \frac{1000}{T} \ . \tag{4.13}$$
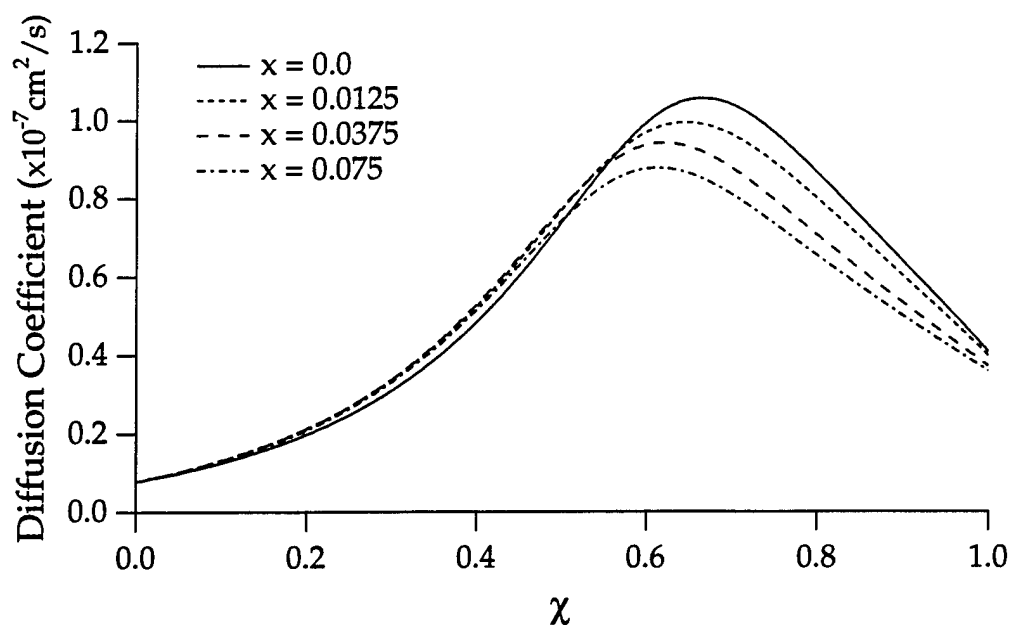
Figure 4.38 MQC diffusion coefficients for glass compositions in the glass system x Li_2O + (0.25-x) Na_2O + 0.05 Al_2O_3 + 0.70 SiO_2. The fit parameters are listed in Table 4.20.
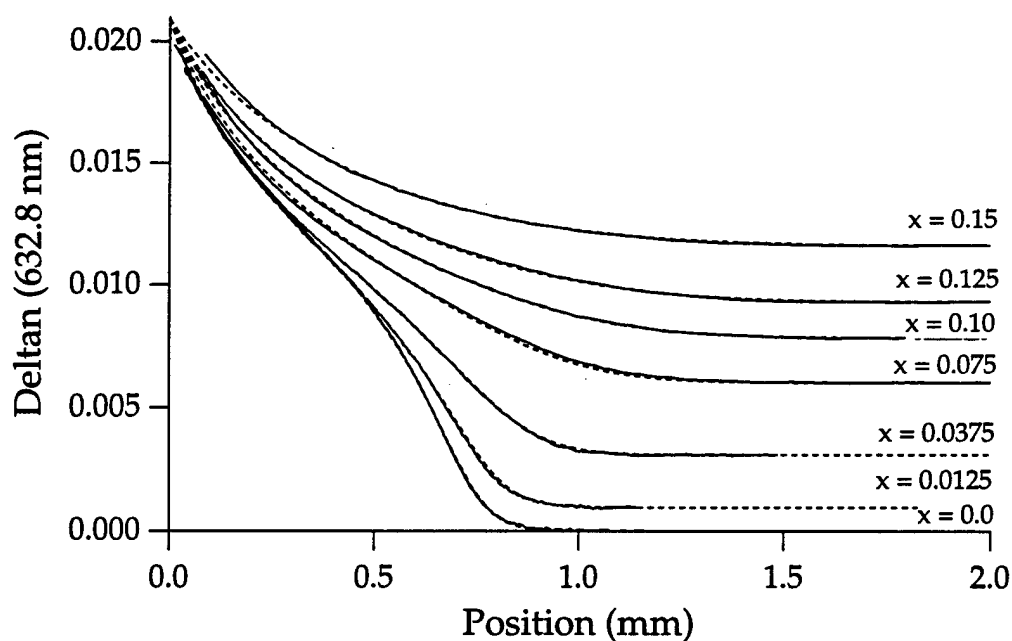
Figure 4.39 Experimental index of refraction profiles for 6 hour Li^+ for Na^+ diffusions in glasses in the system x Li_2O + (0.25-x) Na_2O + 0.05 Al_2O_3 + 0.70 SiO_2 and the model solutions generated with the MQC diffusion coefficients shown in Fig. 4.38.
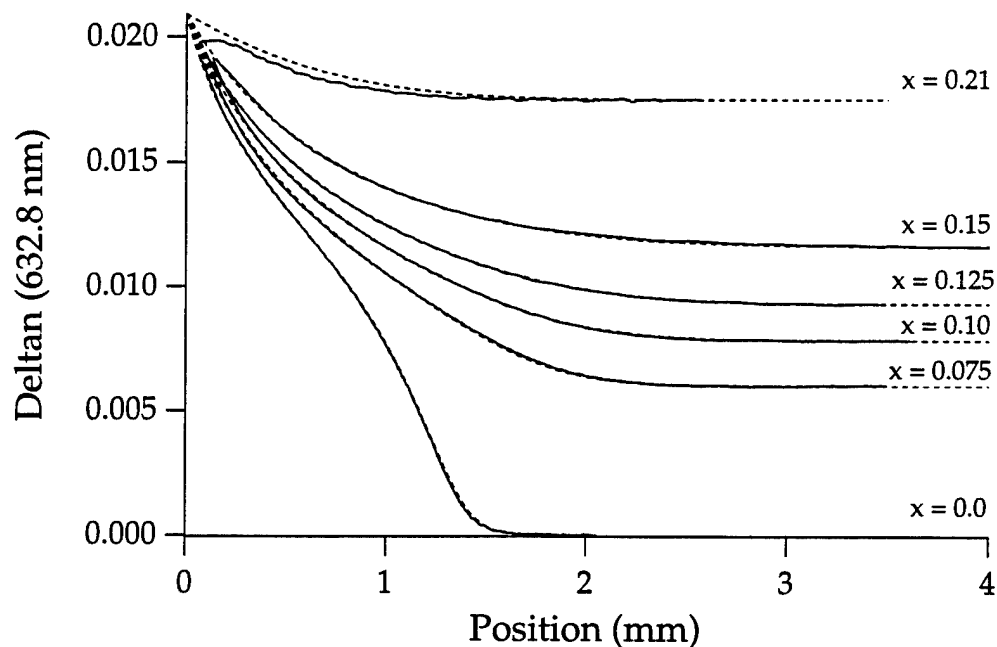
Figure 4.40 Experimental index of refraction profiles for 20 hour Li^+ for Na^+ diffusions in glasses in the system x Li_2O + (0.25-x) Na_2O + 0.05 Al_2O_3 + 0.70 SiO_2 and the model solutions generated with the MQC diffusion coefficients shown in Fig. 4.38.
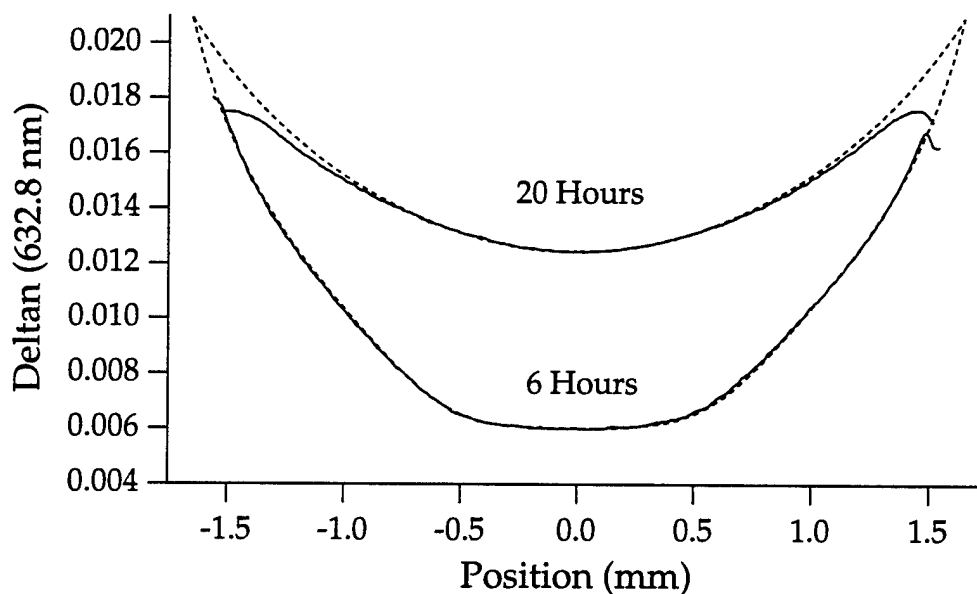
Figure 4.41 Experimental index of refraction profiles for Li^+ for Na^+ radial diffusions in the glass composition 0.075 Li_2O + 0.175 Na_2O + 0.05 Al_2O_3 + 0.70 SiO_2 and the model solutions generated with the x = 0.125 MQC diffusion coefficient.
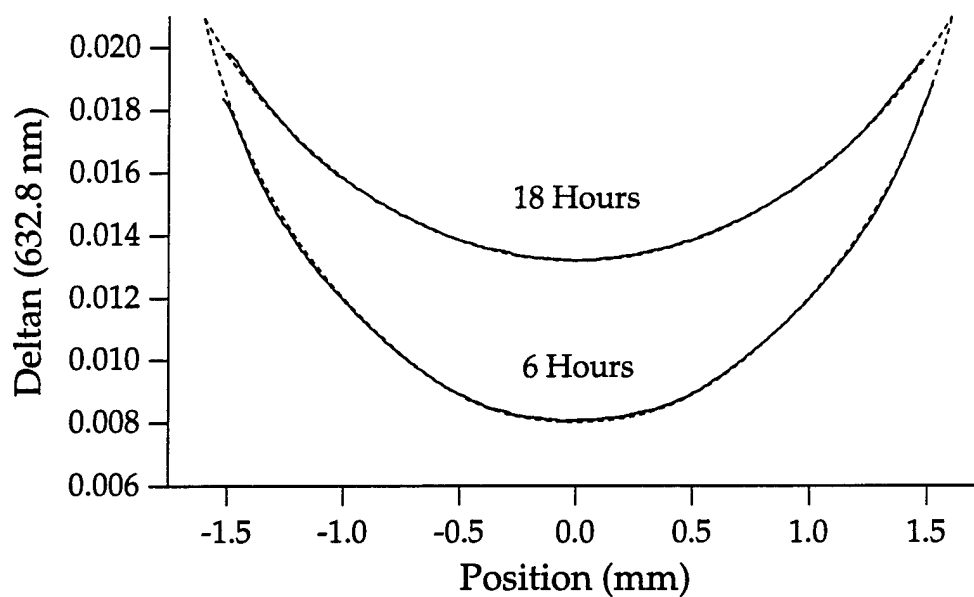
Figure 4.42 Experimental index of refraction profiles for Li$^+$ for Na$^+$ radial diffusions in the glass composition 0.10 Li$_2$O + 0.15 Na$_2$O + 0.05 Al$_2$O$_3$ + 0.70 SiO$_2$ and the model solutions generated with the x = 0.125 MQC diffusion coefficient.
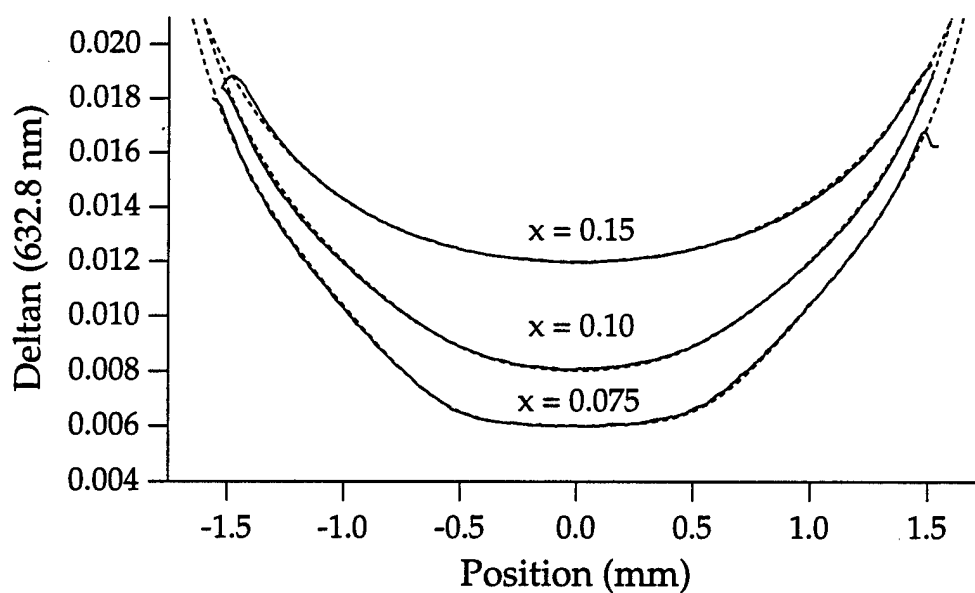
Figure 4.43 Experimental index of refraction profiles for 6 hour Li$^+$ for Na$^+$ radial diffusions in glasses in the system x Li$_2$O + (0.25-x) Na$_2$O + 0.05 Al$_2$O$_3$ + 0.70 SiO$_2$ and the model solutions generated with the x = 0.125 MQC diffusion coefficient.
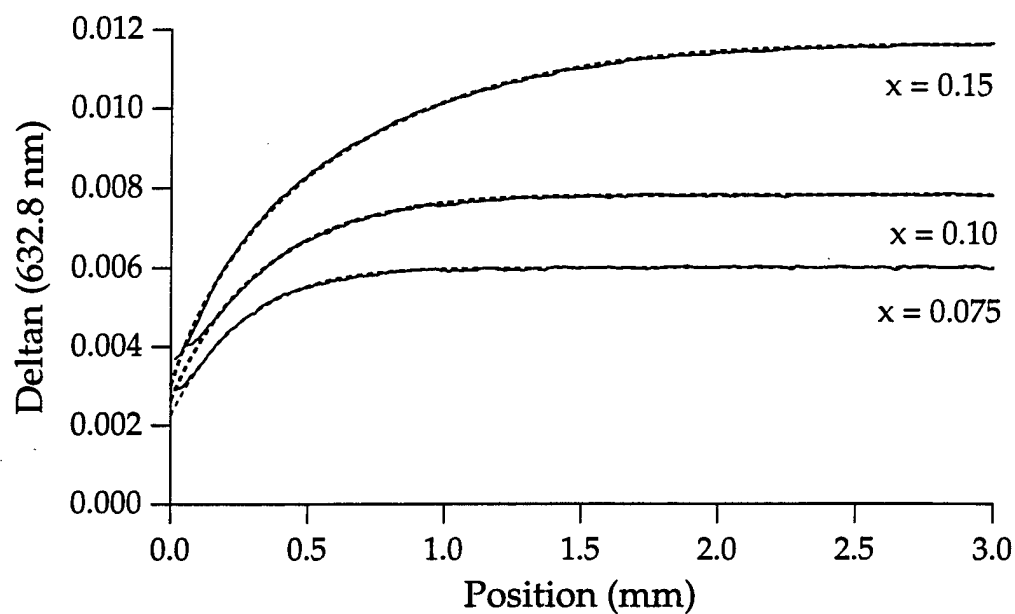
Figure 4.44 Experimental index of refraction profiles for Na^+ for Li^+ diffusions in the system x Li_2O + (0.25-x) Na_2O + 0.05 Al_2O_3 + 0.70 SiO_2 and the model solutions generated with the x = 0.125 MQC diffusion coefficient.

Exp. #	Temp	D_B	α	ρ	χ_0	c
JLB-62	500	0.0610	0.8368	-1.8517	0.1242	7.8
JLB-64	505	0.0690	0.8225	-1.8784	0.1270	7.4
JLB-57	510	0.0770	0.8100	-1.8550	0.1310	8.0
JLB-68	515	0.0857	0.7970	-1.8428	0.1294	9.0
JLB-71	520	0.0970	0.7883	-1.7740	0.1180	9.3
JLB-61	500	0.0610	0.7950	-1.8035	0.0833	7
JLB-63	505	0.0690	0.7900	-1.8049	0.0725	7
JLB-46	510	0.0770	0.7839	-1.8072	0.0730	7.2
JLB-69	515	0.0857	0.7800	-1.8224	0.0721	7
JLB-70	520	0.0970	0.7700	-1.8959	0.0750	7

Table 4.21 MQC fitting coefficients for the temperature dependence of the diffusion coefficient in the glass compositions 0.25 Na_2O + 0.05 Al_2O_3 + 0.70 SiO_2 and 0.125 Li_2O + 0.125 Na_2O + 0.05 Al_2O_3 + 0.70 SiO_2.
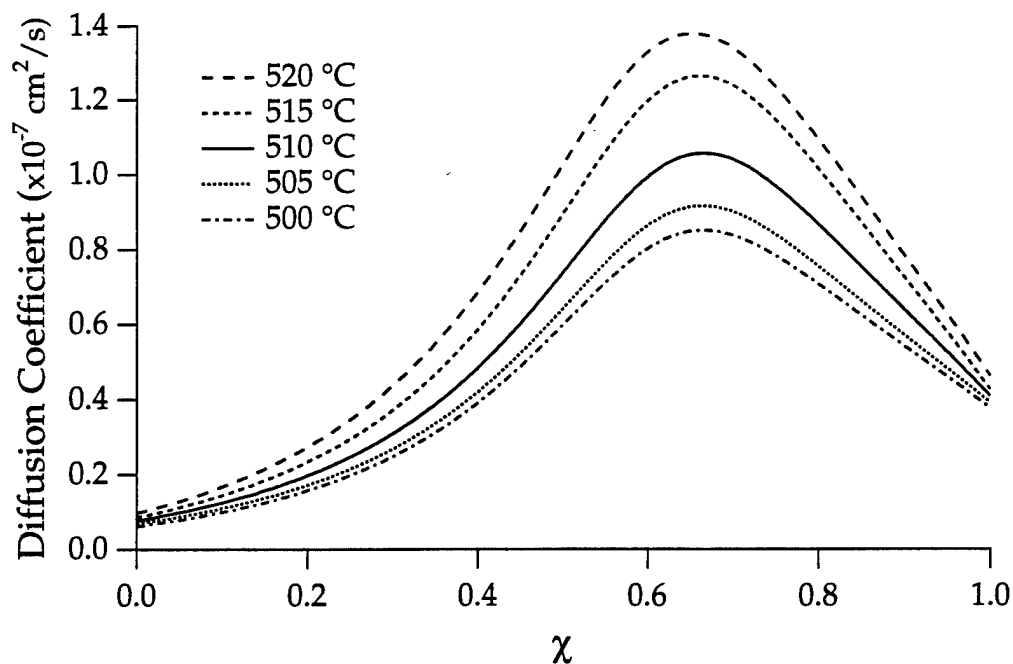
Figure 4.45 MQC diffusion coefficients for glass composition 0.25 Na_2O + 0.05 Al_2O_3
+ 0.70 SiO_2 at five different temperatures. The fit parameters are listed in Table 4.21.
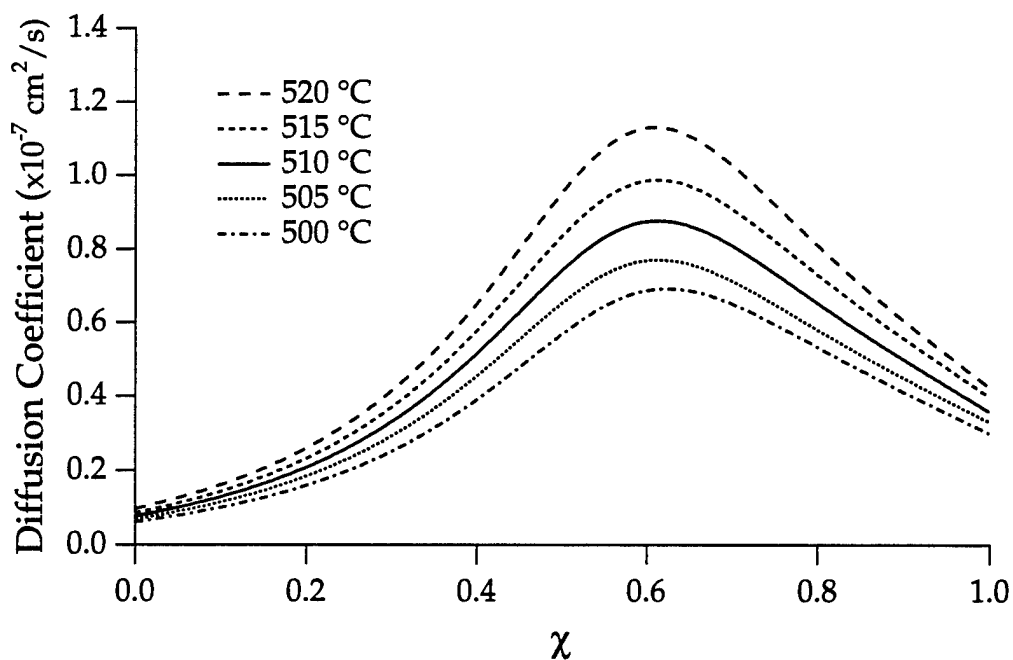
Figure 4.46 MQC diffusion coefficients for glass composition 0.125 Li_2O + 0.125 Na_2O
+ 0.05 Al_2O_3 + 0.70 SiO_2 at five different temperatures. The fit parameters are listed
in Table 4.21.
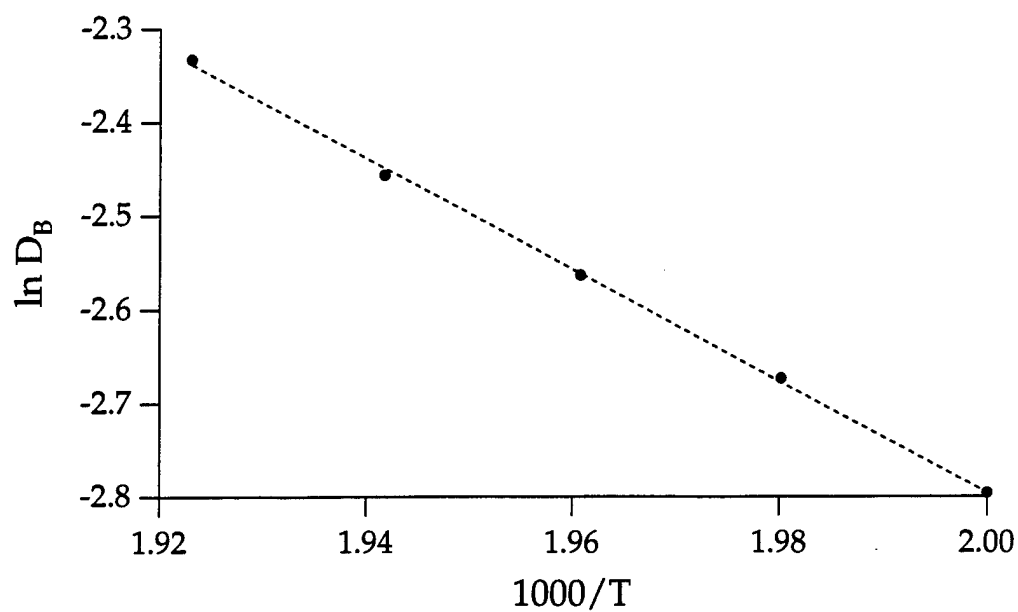
Figure 4.47 Natural logarithm of the MQC self-diffusion coefficient parameter, D_B plotted as a function of 1000/T where T is temperature.

4.4 Alumina and Alkali Dependence

4.4.1 Introduction

In the previous two sections, the change in the ratio of Li^+/Na^+ in the base glass composition and its effect on the index of refraction profile and diffusion coefficient was investigated for two different glass systems which both had a fixed total alkali content and a fixed alumina content. However, it is also interesting to examine how changes in the alkali and the alumina content of the glass affect these properties for several reasons. First, a change in the base glass composition allows a variation in the base glass optical properties such as index of refraction and dispersion and also in the gradient properties such as the Δn. For example, an increase in the alkali content of a the glass increases the index of refraction of the glass and also increases the maximum refractive index change for the gradient. Second, changes in the base glass composition can also increase the diffusion rates in the glass. [19] Finally, the effect this particular change in glass composition has on the concentration dependence of the diffusion coefficient and therefore on the shape of the index of refraction profile can be examined.

Therefore, the third alkali alumina silicate glass subsystem which is examined in this chapter is written as

$$yNa_2O + zAl_2O_3 + (1-y-z)SiO_2 \qquad (4.14)$$

such that y is the total alkali content of the glass and z is the alumina content of the glass. An initial Li_2O concentration of zero was chosen to simplify the glass system, since changing the ratio of Li^+/Na^+ in the base glass was investigated in detail in the previous two sections. In addition, a Li^+ for Na^+ diffusion in an axial geometry is used to calculate and examine the concentration dependence of the diffusion coefficient for the different glass compositions within this glass system. Thus, a complete diffusion coefficient (from $\chi = 0$ to 1) can be obtained in these glasses and then compared to each other.

4.4.2 Glass Melting

Two series of glass compositions were melted in this glass system in which the alumina content of the glass was varied from 3 to 10 percent. The first study used 25 percent sodium, or y = 0.25, while the second study used 30 percent sodium, or y = 0.30. The glass compositions are listed in Table 4.22. Note: since the concentration dependence of the diffusion coefficient changes as the ratio of Li^+/Na^+ in the base glass is varied, (as evidenced by the results of the previous two sections) two additional glass compositions are included in the second study which both have a ratio of one half for the alkali, but have a different alumina content. These glass compositions are also listed in Table 4.22.

Each glass was melted in a 250 gram batch in a platinum crucible using the experimental procedure described in Chapter 3. Approximately 1/3 of the batch was premelted at 1100 °C for one hour. The rest of the batch material was added in half hour increments until the entire batch was in the crucible. The glass was melted at 1575 °C for a time period which

Glass Name	Li_2O	Na_2O	Al_2O_3	SiO_2
JBGL-24	0.0	0.25	0.03	0.72
RH-1A0018	0.0	0.25 (0.2464)	0.05 (0.0507)	0.70 (0.703)
JBGL-25	0.0	0.25	0.07	0.68
JBGL-26	0.0	0.25	0.10	0.65
JBGL-22	0.0	0.30	0.03	0.67
JBGL-21	0.0	0.30	0.05	0.65
JBGL-28	0.15	0.15	0.05	0.65
JBGL-13	0.00	0.30 (0.2974)	0.07 (0.0708)	0.63 (0.6318)
JBGL-16	0.15	0.15	0.07	0.63
JBGL-23	0.0	0.30	0.10	0.60

Table 4.22 Compositions of the glasses melted in the system x Li_2O + (y-x) Na_2O + z Al_2O_3 + (1-y-z) SiO_2.

ranged from four to eight hours. Then, after being cooled in the crucible to a temperature of 1400 °C, the glass was poured into a cold steel mold. The glass was quickly placed into a preheated annealing furnace and allowed to cool slowly from a temperature of 550° C to room temperature. Note: even at 1575 °C the glass was still fairly thick which made it difficult to get good homogeneity for such a small batch size. Therefore, only about a quarter of the glass had a good homogeneous region that was usually four to six mm thick and near the top of the pour. Note: the glass homogeneity of the 10 percent alumina and 25 percent alkali glass was exceptionally bad and after several attempts nothing could be obtained that could be used in an ion exchange experiment.

4.4.3 Index of Refraction Measurements

As discussed in Chapter 3, the index of refraction as a function of lithium concentration is necessary for the calculation of the concentration dependence of the diffusion coefficient for these glasses. It is also used by the diffusion model to convert concentration profile solutions to index of refraction profiles so that they can be compared with experimentally measured index of refraction profiles. A large number of glass melts is required to accurately measure this function for each of the glass compositions melted in this glass system. Therefore, because of the earlier success of Huggins, Sun, Davis model to predict the index of refraction as a function of lithium concentration, it was used to calculate the index of refraction values. In particular, the original empirical constants from Huggins, Sun, and Davis were used for an annealing constant of k=0.0.

Thus, for each glass composition, the index of refraction for different Li^+ concentrations starting at zero and increasing in five percent increments up to the maximum value of exchange was calculated with the model. This data was then fit to a second order polynomial given by

$$n(\chi) = N_0 + N_1\chi + N_2\chi^2 \tag{4.15}$$

and the fitting coefficients for this function for each particular glass composition are listed in Table 4.23. This polynomial is then used later in this chapter to convert the measured index of refraction profile to a

Glass Name	y Na_2O	z Al_2O_3	N_0	N_1	N_2
JBGL-24	0.25	0.03	1.49959	0.01958	0.00218
RH-1A0018	0.25	0.05	1.49995	0.02006	0.00106
JBGL-25	0.25	0.07	1.49977	0.01912	0.00206
JBGL-22	0.30	0.03	1.50322	0.02406	0.00336
JBGL-21	0.30	0.05	1.50299	0.02372	0.00326
JBGL-13	0.30	0.07	1.50277	0.02339	0.00316
JBGL-23	0.30	0.10	1.50049	0.02262	0.00296

Table 4.23 The fit coefficients for Eq. (4.15) for the second order polynomial fit to the index of refraction versus concentration as calculated from the HSD model for the glass compositions in the system y Na_2O + z Al_2O_3 + (1-y-z) SiO_2.

concentration profile for the calculation of the concentration dependence of the diffusion coefficient for this glass composition.

4.4.4 Li+ for Na+ Diffusions

An axial gradient was fabricated in each of the glass compositions listed in Table 4.22 using Li^+ for Na^+ exchange. For each diffusion, a small sample of the glass, approximately 8 x 10 x 10 mm, was placed in platinum wire basket and suspended in a molten salt. The salt bath consisted of 250 grams of the mixture 0.40 LiCL + 0.60 $CaCl_2$, by weight, and was placed in 250 ml Pyrex™ beaker. A diffusion temperature of 510 °C was chosen based on the results of the previous two sections.

First, two series of axial diffusions were examined, one for the twenty five percent alkali glasses and the other for the thirty percent alkali glasses. Each experiment in the series started with a homogeneous glass composition which had a different value of z, the initial amount of alumina in the glass. The experimental data for the series of y = 0.25 diffusions is listed in Table 4.24 and the measured index of refraction profiles are shown in Fig. 4.48. Similarly, the experimental data for the series of y = 0.30 diffusions is listed in Table 4.25 and the measured index of refraction profiles are shown in Fig. 4.49. Both figures show that

increasing the alumina content of the glass decreases the depth of the diffusion but the overall shape of the profile is maintained for each particular glass composition. Note: because the diffusions were done at different diffusion times they were scaled to the same diffusion time; 20 hours for Fig. 4.48 and 16 hours for Fig. 4.49.

Since the concentration dependence of the diffusion coefficient changes as the ratio of Li^+/Na^+ in the base glass is varied, (as evidenced by the results of the previous two sections) diffusion in two additional glass compositions were also measured which both have a ratio of one half for the alkali, but have a different alumina content. The experimental data for the study is listed in Table 4.26 and the measured index of refraction profiles are shown in Fig. 4.50. Again the two diffusions were done at different diffusion times so they were scaled to the same diffusion time of 18 hours. As expected, the figure shows that as the alumina content of the glass decreases the depth of the diffusion but the overall shape of the profile is maintained for each particular glass composition.

A second thing that can be seen from the three figures is that while changing the alumina content of the glass (over this range of compositions) has a relatively small effect on the maximum change in refractive index for the same alkali content, while changing the alkali content of the glass makes a large difference. This result is not unexpected; as the amount of ions available for exchange is increased so is the refractive index change. Figures 4.51 and 4.52 show this result clearly for an alumina content of 3 and 7 percent respectively. Again, the diffusion times were scaled so that the figures also show that the diffusion depth is increased as the alkali content is increased for the same diffusion time and diffusion temperature.
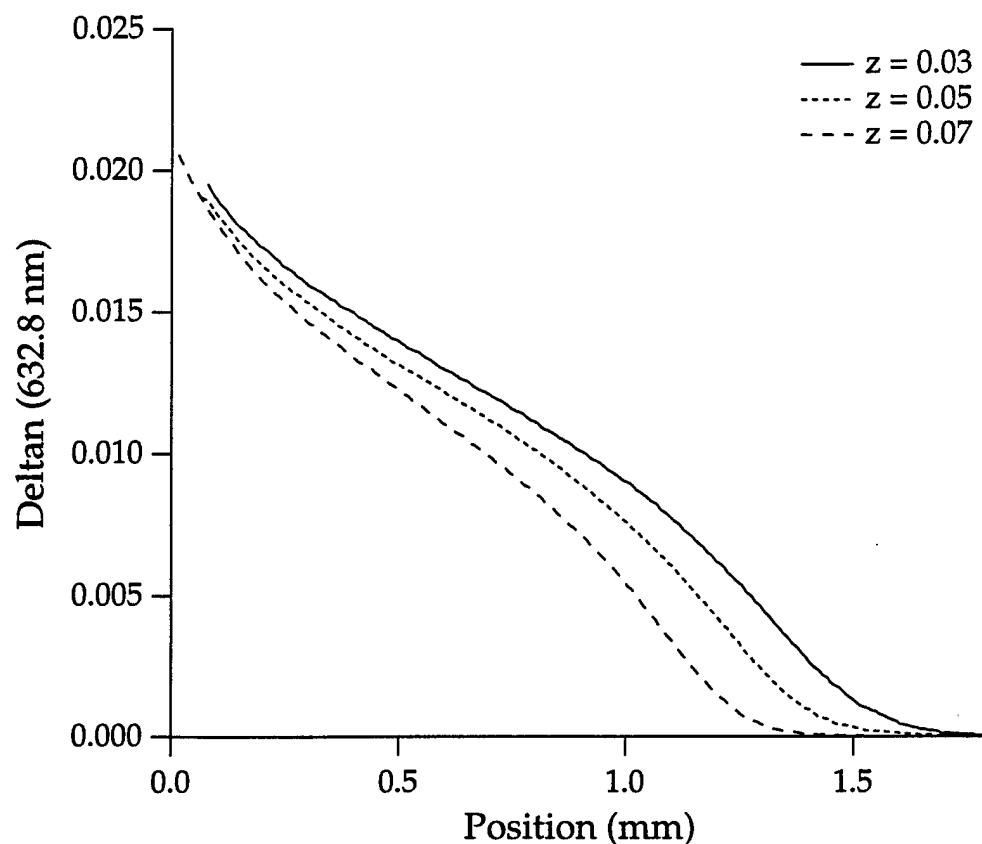
Figure 4.48 Measured index of refraction profiles for 20 hour Li$^+$ for Na$^+$ diffusions in glasses in the system 0.25 Na$_2$O + z Al$_2$O$_3$ + (0.75 - z) SiO$_2$ for various values of z, the alumina concentration in the glass. The experimental data is listed in Table 4.24. Note: the measurement for experiment JLB-83 has been scaled in position from 18 hours to 20 hours for comparison.

Exp. #	Glass Name	z Al$_2$O$_3$	Temperature	Time
JLB-83	JBGL-24	0.03	510	18
JLB-57	1A0018	0.05	510	20
JLB-82	JBGL-25	0.07	510	20

Table 4.24 Experimental data for Li$^+$ for Na$^+$ diffusions in glasses in the system 0.25 Na$_2$O + z Al$_2$O$_3$ + (0.75 - z) SiO$_2$ for various values of z, the alumina concentration in the glass. The measured index of refraction profiles are shown in Fig. 4.48.
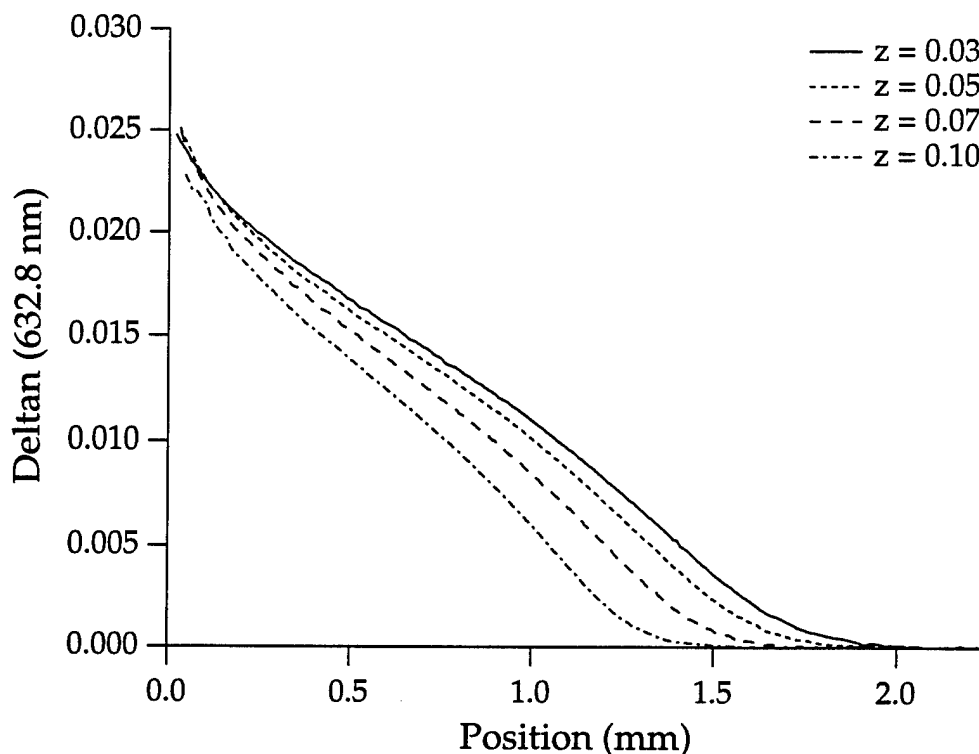
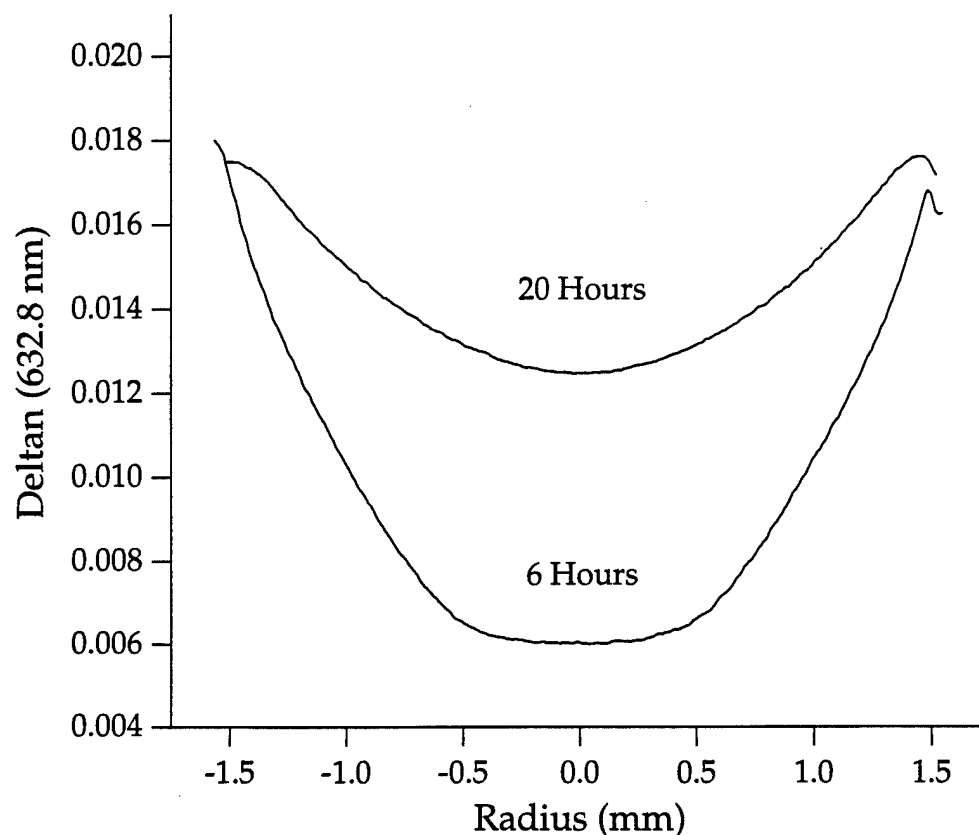**Figure 4.49** Measured index of refraction profiles for 16 hour Li$^+$ for Na$^+$ diffusions in glasses in the system 0.30 Na$_2$O + z Al$_2$O$_3$ + (0.70 - z) SiO$_2$ for various values of z, the alumina concentration in the glass. The experimental data is listed in Table 4.25. Note: the measurement for experiment JLB-28 has been scaled in position from 48 hours to 16 hours and the measurement for experiment JLB-80 has been scaled in position from 20 hours to 16 hours for comparison.

Exp. #	Glass Name	z Al$_2$O$_3$	Temperature (°C)	Time (hours)
JLB-79	JBGL-22	0.03	510	16
JLB-77	JBGL-21	0.05	510	16
JLB-28	JBGL-13	0.07	510	48
JLB-80	JBGL-23	0.10	510	20

Table 4.25 Experimental data for Li$^+$ for Na$^+$ diffusions in glasses in the system 0.30 Na$_2$O + z Al$_2$O$_3$ + (0.70 - z) SiO$_2$ for various values of z, the alumina concentration in the glass. The measured index of refraction profiles are shown in Fig. 4.49.
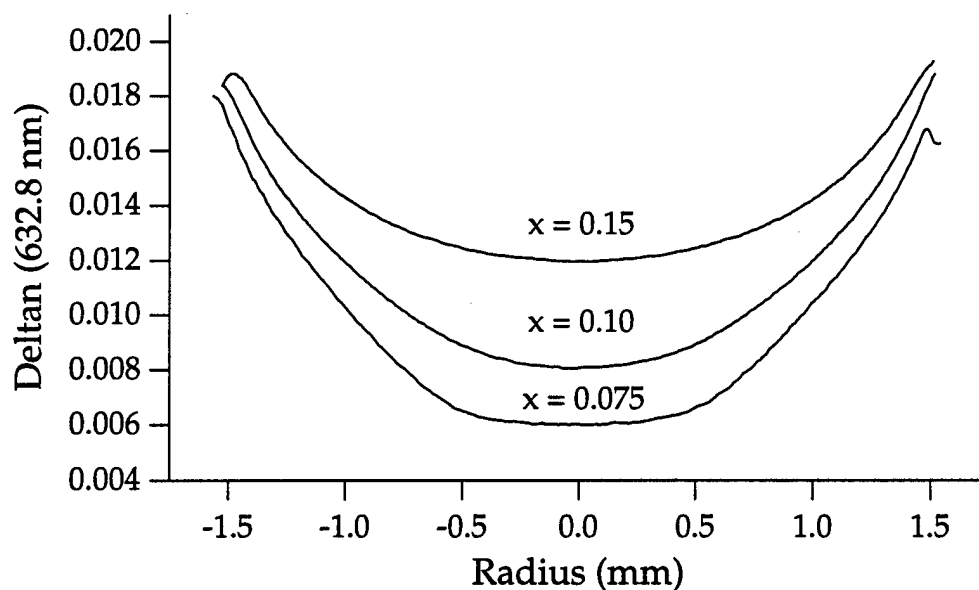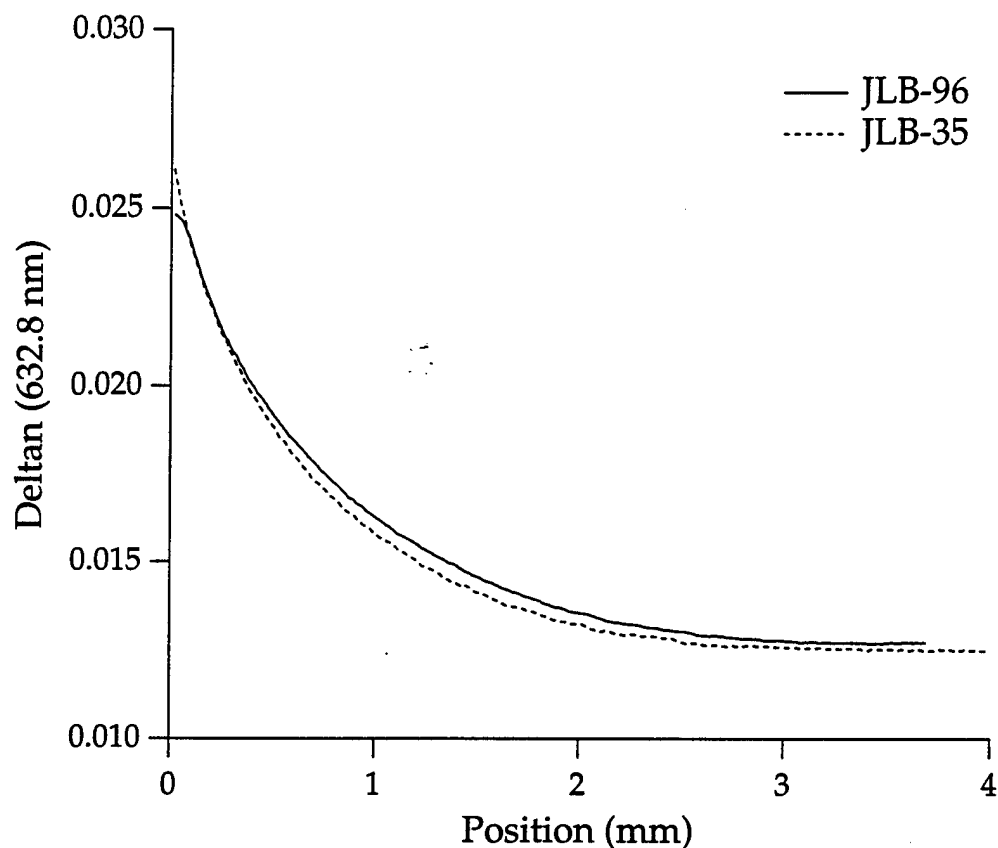
Figure 4.50 Measured index of refraction profiles for 18 hour Li^+ for Na^+ diffusions in glasses in the system $0.15 \, Li_2O + 0.15 \, Na_2O + z \, Al_2O_3 + (0.70 - z) \, SiO_2$ for two values of z, the initial lithium concentration 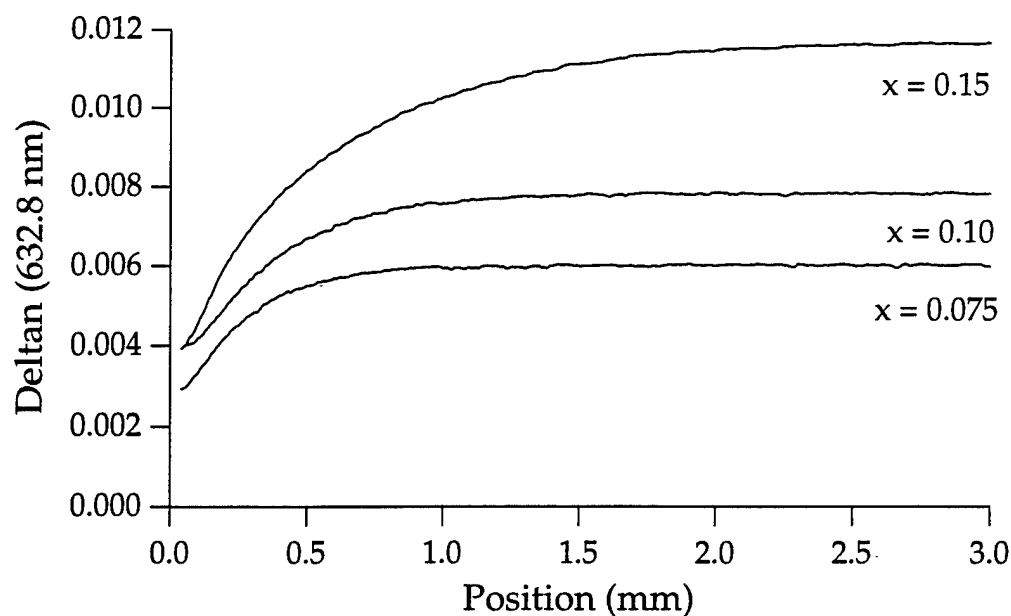in the glass. The experimental data is listed in Table 4.26. Note: the measurement for experiment JLB-96 has been scaled in position from 6 hours to 18 hours

Exp. #	Glass Name	z Al_2O_3	Temperature (°C)	Time (hours)
JLB-96	JBGL-28	0.05	510	6
JLB-35	JBGL-16	0.07	510	18

Table 4.26 Experimental data for Li^+ for Na^+ diffusions in glasses in the system $0.30 \, Na_2O + z \, Al_2O_3 + (0.70 - z) \, SiO_2$ for various values of z, the alumina concentration in the glass. The measured index of refraction profiles are shown in Fig. 4.50.

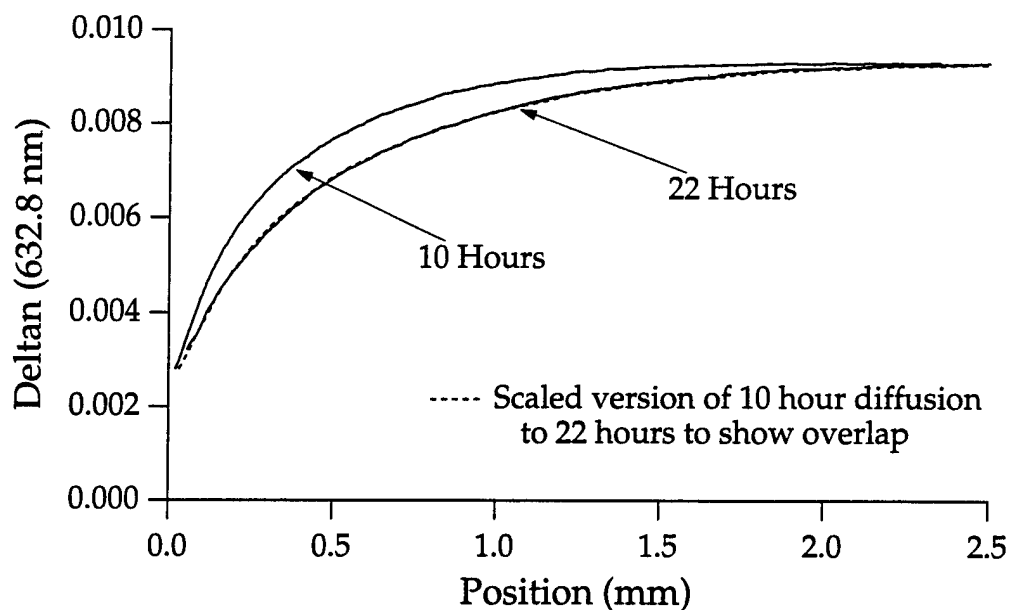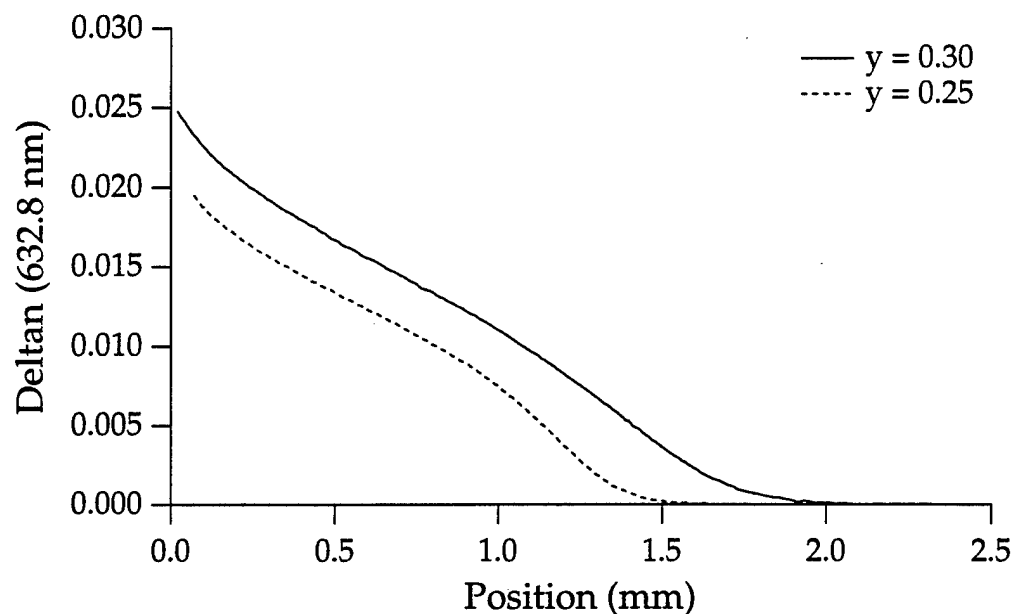Figure 4.51 Measured index of refraction profiles for Li$^+$ for Na$^+$ diffusions in glasses in the system y Na$_2$O + 0.03 Al$_2$O$_3$ + (0.97 - y) SiO$_2$ for two values of y, the sodium concentration in the glass. Note: the measurement for experiment JLB-83 has been scaled from 18 to 16 hours for comparison.
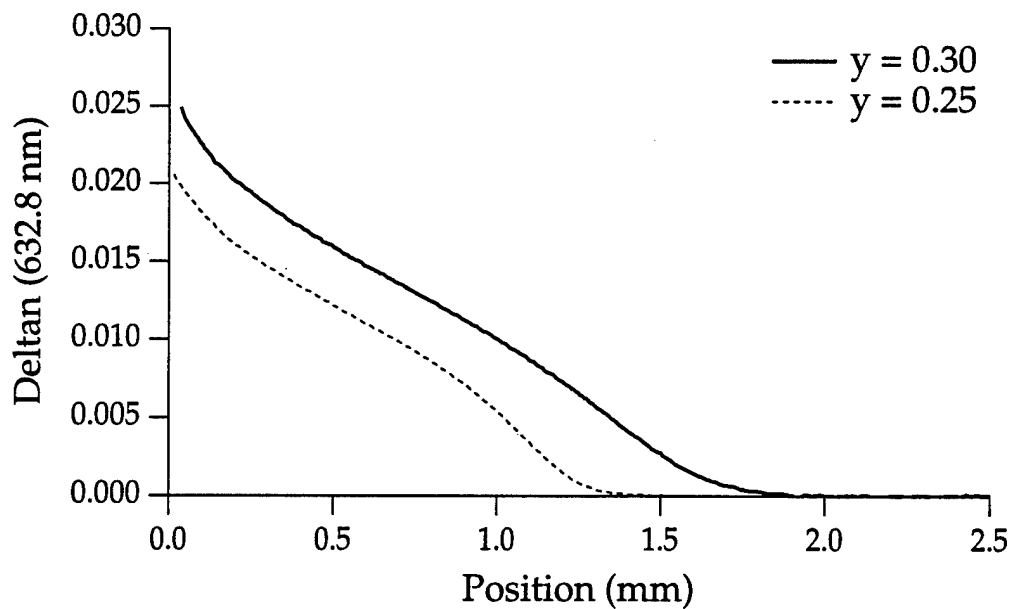
Figure 4.52 Measured index of refraction profiles for 16 hour Li$^+$ for Na$^+$ diffusions in glasses in the system y Na$_2$O + 0.07 Al$_2$O$_3$ + (0.93 - y) SiO$_2$ for two values of y, the sodium concentration in the glass. Note: the measurement for experiment JLB-28 has been scaled from 48 to 20 hours for comparison.

4.4.5 Calculation of the Concentration Dependence of the Diffusion Coefficient

Similar to the previous two alumina silicate glass systems, the diffusion coefficient was calculated from the measured index of refraction profiles for several different glass compositions in this series. The experimental data was then fitted to the MQC model. The MQC fits which can recover the initial index of refraction profile to within experimental error are shown in Figs. 4.53 and 4.54. The fitting coefficients are then listed in Table 4.27.

The MQC fit parameters were then examined to determine how they changed with alumina concentration in both the 25 percent alkali and the 30 percent alkali systems. First, as the alumina concentration is increased, there is a definite decrease in the self diffusion coefficient value D_B for both systems. Second, the mobility ratio α increases with increasing alumina. Third, the interaction energy term ρ decreases with increasing alumina content. Finally, there is a shift in the peak of the diffusion coefficient as a function of alumina concentration, while the coordination number remains constant to within the experimental error. However, a comparison of the coordination number between the two systems shows an increase with an increase in total alkali in the glass.

Exp. #	z Al_2O_3	D_B	α	ρ	χ_0	c
JLB-83	0.03	0.085	0.7082	-1.7588	0.1255	10.7
JLB-57	0.05	0.0707	0.7235	-1.8230	0.1050	9.7
JLB-82	0.07	0.0512	0.7674	-1.6940	0.0825	10.7
JLB-79	0.03	0.1752	0.3311	-1.5919	0.1407	11.64
JLB-77	0.05	0.1430	0.3714	-1.6273	0.1216	11.7
JLB-28	0.07	0.1100	0.4500	-1.4625	0.1005	12.9
JLB-80	0.10	0.0834	0.5167	-1.4492	0.0945	12.4

Table 4.27 MQC fit parameters for the concentration dependent diffusion coefficients for glass compositions in the glass system y Na_2O + z Al_2O_3 + (1-y-z) SiO_2.
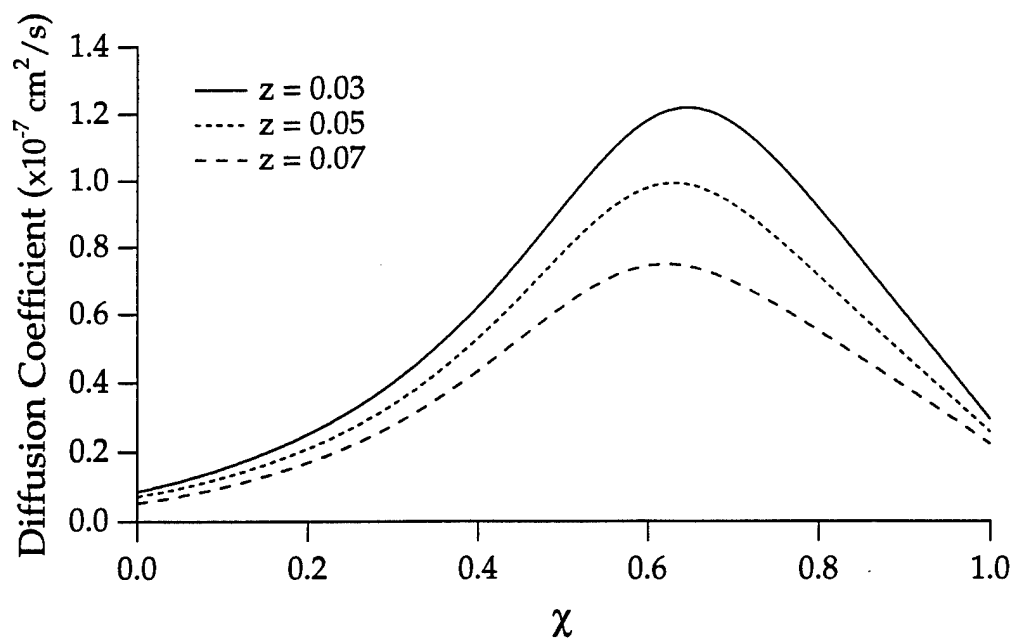
Figure 4.53 MQC diffusion coefficients for glass compositions in the system 0.25 Na$_2$O + z Al$_2$O$_3$ + (0.75 - z) SiO$_2$ for various values of z, the alumina concentration in the glass. The fit parameters are listed in Table 4.28.
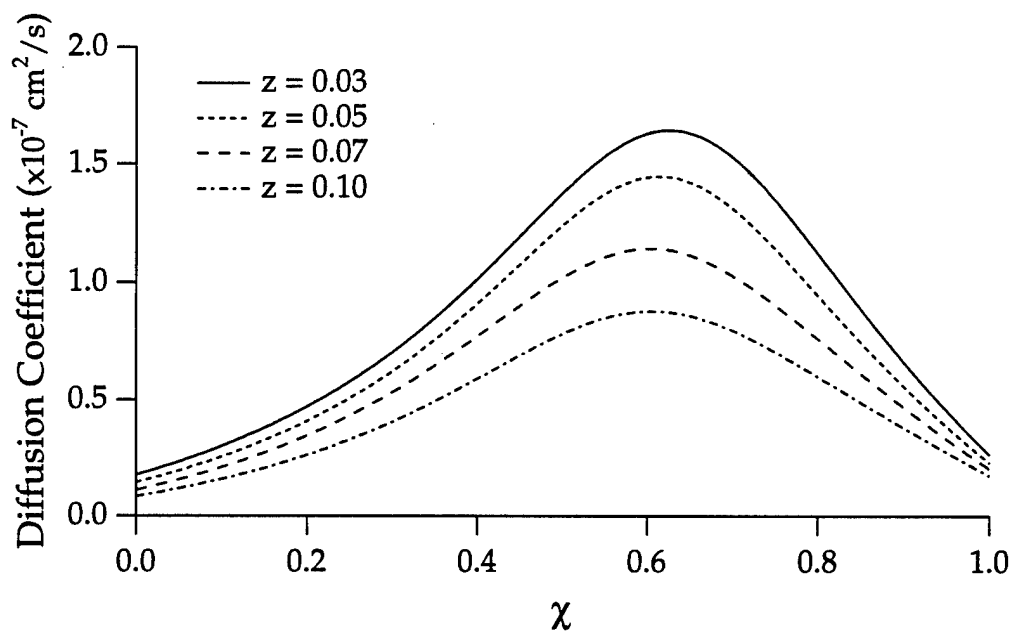
Figure 4.54 MQC diffusion coefficients for glass compositions in the system 0.30 Na$_2$O + z Al$_2$O$_3$ + (0.70 - z) SiO$_2$ for various values of z, the alumina concentration in the glass. The fit parameters are listed in Table 4.28.

References

1. J. R. Hensler, "Multi-focal lens with index gradient," U. S. Patent 3,542,535 (November, 1970).

2. S. N. Houde-Walter, "Gradient index profile control by ion exchange in glass," Doctoral Dissertation, University of Rochester, Rochester, NY (1987).

3. J. E. Samuels, "Influence of the molten salt bath on ion exchange in glass and the gradient-index profile," M.S. Thesis, University of Rochester, Rochester, NY (1989).

4. D. T. Moore, "Gradient index optics: aspects of design, testing and tolerancing," Doctoral Dissertation, University of Rochester, Rochester, NY (1974).

5. D. S. Kindred and D. T. Moore, "Design, fabrication, and testing of a gradient-index binocular objective," App. Opt. **27**, 492-495 (1988).

6. J. B. Caldwell, D. S. Kindred, and D. T. Moore, "Large diameter radial gradient index glass," Paper ThD3-1, Seventh topical meeting on gradient index imaging systems, Reno, Nevada (1987).

7. D. P. Ryan, "Chromatic properties of index of refraction gradients in glass," Doctoral Dissertation, University of Rochester, Rochester, NY (1983).

8. S.D. Fantone, "Design, engineering, and manufacturing aspects of gradient index optical components," Doctoral Dissertation, University of Rochester, Rochester, NY (1979).

9. D. S. Kindred, "Development of new gradient index glasses for optical imaging systems," Doctoral Dissertation, University of Rochester, Rochester, NY (1990), pp. 96-111.

10. The index of refraction values were calculated using an Excel macro written by Chris Saxer at the University of Rochester which contains a complete compilation of the empirical constants determined for this model to date.

11. Levin, et. al., Phase Diagrams for Ceramists, Am. Ceram. Soc., Columbus, OH (1964).

12. Reference 9, p. 77.

13. Handbook of Physics and Chemistry, (CRC Press, Boca Raton, FL, 1981).

14. Reference 9, p. 90.

15. N. Haun et al., "Index profile control using Li+ for Na+ exchange in aluminosilicate glasses," Appl. Opt. **29**, 4056 (1990).

16. R. H. Doremus, Glass Science (Wiley, New York, 1973), ch. 9.

17. Reference 9, p.103.

18. C. E. Saxer and D.T. Moore, "Measurement of the chromatic properties of gradient index glasses: method and results, " paper #G16 in the Technical Digest of the 2nd Microoptics Conference and the 8th Topical Meeting on Gradient Index Optical Imaging Systems, July 24-26, 1989, Tokyo, Japan, p. 200.

19. G. H. Frischat, *Ion exchange in glass*. Trans Tech Publications, Bay Village, OH (1975), p. 53.

Chapter V
Application of the Diffusion Model
to Other Types of Glass

5.1 Introduction

In the last chapter, empirical diffusion models were developed for a wide variety of alumina silicate glass compositions. These models were shown to be very successful in the prediction of the index of refraction profile for $Li^+ - Na^+$ ion exchange for several different diffusion times and temperatures in both an axial and a radial geometry. Furthermore, a general procedure for the development and evaluation of an empirical diffusion model using a series of ion exchange experiments was established. Unfortunately, the alumina silicate glass compositions have very similar base glass optical properties (such as index of refraction and dispersion). If a designer is restricted to using only this type of glass in the design, then the extra degree of freedom gained from the index of refraction gradient is eliminated.

This chapter examines the application of the diffusion model to other types of base glasses to see if the same development procedure can be applied to them. First, a change in glass former is investigated in a series of alumina borate glasses. The optical properties of these glasses are

similar to the alumina silicate glasses, but the change in glass former from silica to boron results in much different diffusion properties including the shape of the index of refraction profile. Second, the type of intermediate used in the glass can be changed, although many of the available intermediates have adverse effects on the diffusion. Kindred showed that the addition of a small amount of TiO_2 to a glass composition can dramatically change the properties of the base glass (in particular, TiO_2 increases the index of refraction and the dispersion of the glass) and yet does not adversely affect the diffusion. [1] Therefore, a titanium silicate glass composition is examined in the second part of this chapter.

Finally, only simple glass compositions (with three to four components) have been studied so far, even though many of the compositions for homogeneous glasses have as many as 10 components (usually with two to three major components and then small amounts of many other components). The extra components are added to the glass composition to give it special optical and mechanical properties. Since similar techniques can be applied to the development of gradient-index base glasses, the final glass composition explored in this chapter is a more complicated system. In particular, it contains a glass former, a modifier, and three different intermediates to see if the model will in fact be applicable to much more complicated glass compositions.

5.2 Alumina Borate Glasses

5.2.1 Introduction

Small amounts of boron are often added to homogeneous glass compositions and used as a fluxing agent to lower the melting temperature of the glass to improve its homogeneity. As a result, many of the commercial glasses found in a glass catalog contain boron. This makes it useful to study the effect that boron has on the index of refraction profile and to determine if these glasses can be modeled using the diffusion theory presented in this thesis.

Borate gradient-index glasses have not been studied in depth in the past because boron tends to slow the diffusion and produce ion exchange

rates which are an order of magnitude lower than in silicate glasses. [2] As a result, many of the previous gradient index glasses have been silicates or borosilicates with only very small amounts of boron. However, a glass composition using boron as the glass former was first proposed and investigated by Kindred and Sun for use as a gradient-index material. [3]

A similar borate glass system is investigated for ion exchange in the first part of this chapter. The specific range of glass compositions is

$$xLi_2O + (0.30 - x)Na_2O + 0.10Al_2O_3 + 0.60B_2O_3 \qquad (5.1)$$

where x, the initial lithium concentration in the base glass, varies from 0.0 to 0.30. Therefore, similar to the alumina silicate glasses, a total alkali content of thirty percent is maintained in this series of glasses by substituting Li_2O for Na_2O in the base glass composition. The alumina was then added to the glass composition to improve the chemical durability of the glass. Note: much more alumina can be added to the borate glasses than can be added to the silicate glasses, since, in general, borate glasses melt at much lower temperatures than silicate glasses.

First, several homogeneous glass compositions for different values of x, the ratio of Li^+/Na^+ initially in the glass, are melted. Second, the optical properties of these glasses are measured to determine the index of refraction as a function of concentration for the glass system. Third, several ion exchanges (both Li^+ for Na^+ and Na^+ for Li^+) in an axial geometry are used to calculate and examine the concentration dependence of the diffusion coefficient for the different glass compositions within this glass system at a single diffusion temperature. Then, once the empirical diffusion model for this glass system is determined, it is tested by comparing model solutions to experimental index of refraction profiles for other diffusion times and glass compositions within the system.

5.2.2 Glass Melting

Seven glass compositions were melted in this glass system and are listed in Table 5.1. Beginning at zero, the lithium concentration of each successive composition was increased in five percent increments up to the final glass composition which contains thirty percent lithium and no

Glass Name	Li_2O	Na_2O	Al_2O_3	B_2O_3
JRGL-1	0.00	0.30 (0.3074)	0.10 (0.0977)	0.60 (0.5949)
JRGL-15	0.05	0.25	0.10	0.60
JRGL-3	0.10 (0.1083)	0.20 (0.1951)	0.10 (0.1003)	0.60 (0.5962)
JRGL-6	0.15	0.15	0.10	0.60
JRGL-16	0.20 (0.1980)	0.10 (0.1076)	0.10 (0.1012)	0.60 (0.5932)
JRGL-17	0.25	0.05	0.10	0.60
JRGL-2	0.30 (0.2895)	0.00	0.10 (0.1012)	0.60 (0.6093)

Table 5.1 Compositions of the glasses melted in the system x Li_2O + (0.30-x) Na_2O + 0.10 Al_2O_3 + 0.60 B_2O_3. The numbers in parenthesis are the compositions as measured by flame spectroscopy at Corning Engineering Lab Services.

sodium. Several of the compositions were measured by flame spectroscopy at Corning Engineering Lab Services. The results of these measurements are also listed in Table 5.1 in parenthesis and show that the as melted compositions are accurate to ± 0.1%.

Each glass was melted in a 250 gram batch in a platinum crucible using the experimental procedure described in Chapter 3. The batch was first premelted at a temperature of 800 °C. Several problems were encountered during the premelt stage of these glasses. As the batch was first heated, it had a tendency to foam and froth, and then bubble over the side of crucible. In addition, a hard layer was often formed at the top of the crucible (trapping the CO_2 underneath) such that only small amounts of the batch could be added to the crucible at one time. Note: to eliminate these problems, a substitution of the chemicals $LiAlO_3$ and $Na_2B_4O_7$ for lithium carbonate and sodium carbonate in the batch material was tried. Although the use of these chemicals reduced the foaming of the melt, it is suspected that the exact composition of these chemicals is unknown, since the final compositions of the melted glasses were inaccurate.

The glass was melted at 950 °C for a time period which ranged from four to six hours. Then, after being cooled in the crucible to a temperature of 750 °C, the glass was poured into a cold steel mold. The glass was quickly placed into a preheated annealing furnace and allowed to cool

slowly from a temperature of 450° C to room temperature. The glasses were fairly thin even at the pouring temperature, and it was difficult to pour a thick sample without having the glass overlap itself during the pour. Therefore, it was difficult to get good homogeneity and only about a quarter of the glass had a good homogeneous region that was usually two to four millimeters thick, near the top of the pour.

5.2.3 Index of Refraction measurements

Small samples of each glass (1cm x 1cm x 0.5 cm) were polished flat on one side to $\lambda/4$. Then, the index of refraction of the sample at three different wavelengths was measured using a Pulfrich refractometer to an accuracy of ±0.0003. Table 5.2 lists the results of these measurements. Similar to the alumina silicate glasses, the glass with the largest lithium concentration has the largest index of refraction while the glass with the largest sodium concentration has the smallest index of refraction. Thus, a Li^+ for Na^+ exchange in the all soda glass (JRGL-1) should produce a gradient with a positive change in index of refraction (the refractive index is increased at the edge of the sample) of approximately 0.037 at 632.8 nm.

The homogeneous dispersion of four of the glass samples was then calculated using the procedure described in Chapter 3, Section 3.4.3. First, equation (3.8) was used to fit the index of refraction measurements as a

Glass Name	x Li$_2$O	n_e	n_d	n_{HeNe}
JRGL-1	0.00	1.5097	1.5077	1.5059
JRGL-15	0.05	*	*	1.5131
JRGL-3	0.10	1.5226	1.5206	1.5188
JRGL-6	0.15	1.5279	1.5259	1.5240
JRGL-16	0.20	*	*	1.5307
JRGL-17	0.25	*	*	1.5382
JRGL-2	0.30	1.5465	1.5444	1.5426

Table 5.2 Index of refraction of homogeneous glass samples in the glass system x Li$_2$O + (0.30-x) Na$_2$O + 0.10 Al$_2$O$_3$ + 0.60 B$_2$O$_3$ measured at three different wavelengths on a Pulfrich refractometer. * Not measured.

Glass Name	x Li$_2$O	n$_0$	n$_1$	n$_2$	n$_F$	n$_C$	V$_d$
JRGL-1	0.00	1.5083	-0.0467	-0.0047	1.5135	1.5051	60.4
JRGL-3	0.10	1.5212	-0.0472	-0.0087	1.5264	1.5179	61.5
JRGL-6	0.15	1.5265	-0.0470	-0.0115	1.5316	1.5232	62.5
JRGL-2	0.30	1.5451	-0.0481	-0.0102	1.5503	1.5417	63.1

Table 5.3 The fit coefficients for Eq. (3.8), the interpolated values for n$_F$ and n$_C$, and the calculated dispersion V$_d$ for the homogeneous glasses in the system x Li$_2$O + (0.30-x) Na$_2$O + 0.10 Al$_2$O$_3$ + 0.60 B$_2$O$_3$.

function of wavelength. Then, the index of refraction values, n$_F$ and n$_C$, were interpolated from the fit and the dispersion of the glass was calculated. Table 5.3 lists the coefficients of the fit, the indices of refraction, n$_F$ and n$_C$, and finally the dispersion, V$_d$, for each glass. The glass with the largest lithium concentration has the smallest dispersion while the glass with the largest sodium concentration has the largest dispersion. Thus, a Li$^+$ for Na$^+$ exchange in the all soda glass (JRGL-1) should produce a material with a negative gradient dispersion (the refractive index change at the red wavelengths is larger than the refractive index change at the blue wavelengths). In addition, a comparison of the optical properties of the base glasses in this glass system with the alumina silicates glasses from Chapter 4 shows a large similarity between the two types of glass.

As discussed in Chapter 3, the index of refraction as a function of lithium concentration is necessary for the calculation of the concentration dependence of the diffusion coefficient for these glasses. It is also used by the diffusion model to convert concentration profile solutions to index of refraction profiles so that they can be compared with experimentally measured index of refraction profiles. Therefore, for this series of glass compositions, Fig. 5.1 shows a graph of the measured index of refraction (at 632.8 nm) as a function of normalized lithium concentration, χ, where

$$\chi = \frac{x}{0.30} ,$$

(5.2)
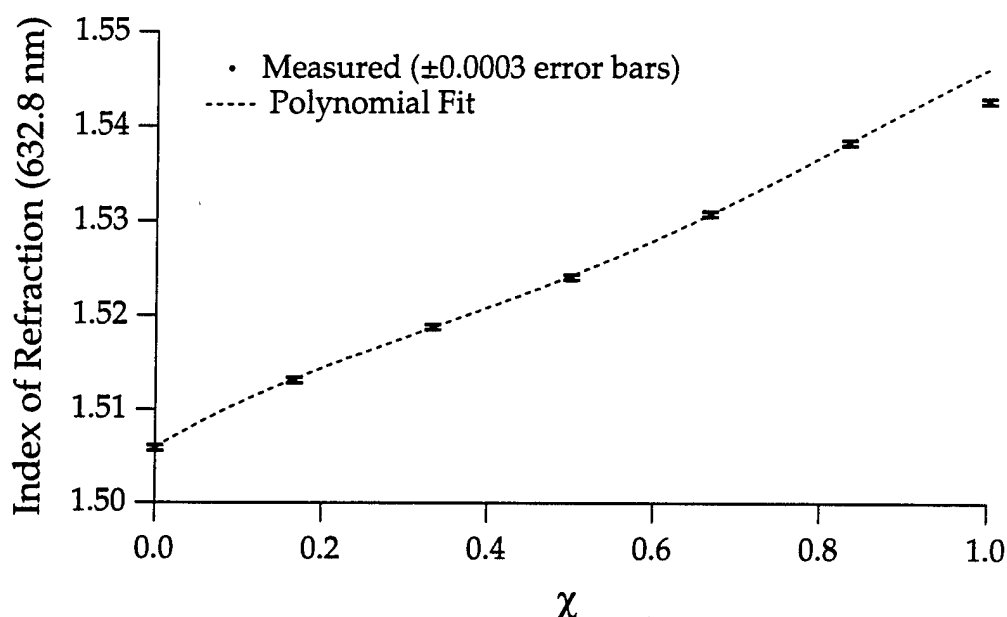
Figure 5.1 Index of refraction as a function of normalized lithium concentration, χ, for glasses in the system x Li_2O + (0.30-x) Na_2O + 0.10 Al_2O_3 + 0.60 B_2O_3. Both the measured data points and a fourth order polynomial fit to the data are shown.

and x is the initial mole percent of lithium in the glass. A fourth order polynomial curve fit to the data given by

$$n(\chi) = 1.5059 + 0.0545\chi - 0.0819\chi^2 + 0.117\chi^3 - 0.0494\chi^4 \quad (5.3)$$

is also shown. Note: the index of refraction measurement for the x = 0.30 glass was not used in the curve fit; the value appears to be too low and is most likely a result of the fact that the actual measured total alkali in this glass is much lower (29% as compared to 30%) than the other glass compositions as shown by Table 5.1.

5.2.4 Li+ for Na+ Diffusions

Axial gradients were fabricated in several of the glass compositions from the alumina borate glass system using Li^+ for Na^+ exchange. For each diffusion, a small sample of the glass, approximately 8 x 10 x 10 mm, was wrapped in platinum wire basket and suspended in a molten salt bath. A diffusion temperature of 460 °C was chosen based on the available salt melts and the measurements of the anneal and strain temperatures for the glasses which are listed in Table 5.4. A comparison with the alumina

silicate glasses shows that these temperatures are lower by approximately twenty to fifty degrees. This suggests that the borate diffusions should be done at a temperature lower than 510 °C, but since the lowest melting temperature of the $LiCl/CaCl_2$ salt mixture is 496 °C, this salt could not be used for a diffusion temperature of 460 °C.

A single experiment was performed (JLR22) using a $LiCl/CaCl_2$ salt bath at a diffusion temperature of 510 °C, but as expected, the sample deformed and divitrified during the experiment. In a second experiment (JLR26) $LiNO_3$ was used at a lower diffusion temperature of 460 °C, but the sample also divitrified throughout the entire gradient region. However, KCl can also be added to a LiCl salt bath to form a eutectic, but at an even lower temperature than the $LiCl/CaCl_2$ mixture. [4] The initial ion exchange experiments with this salt bath showed good results for a diffusion temperature of 460 °C. In particular, 250 grams of the mixture 0.40 LiCl + 0.60 KCl (in mole percent), was placed in 250 ml Pyrex™ beaker. Note: potassium is also a single valent ion and can potentially exchange with the sodium causing problems during the diffusion. Fortunately, potassium is a large ion and its diffusion rates are much smaller than for lithium such that if it is entering the glass it is only over micron depths.

In particular, two series of axial diffusions were examined in these glasses, one for an 120 hour diffusion time and the other for a 216 hour diffusion time. Each experiment in the series started with a homogeneous glass composition which had a different value of x, the initial amount of lithium in the glass. The experimental data for the series of 120 hour

Glass Name	x Li_2O	Anneal Temperature	Strain Temperature
JRGL-01	0.00	445 °C	420 °C
JRGL-03	0.10	418 °C	395 °C
JRGL-06	0.15	418 °C	395 °C
JRGL-16	0.20	424 °C	401 °C
JRGL-02	0.30	450 °C	427 °C

Table 5.4 Anneal and strain temperatures for glasses in the system x Li_2O + (0.30-x) Na_2O + 0.10 Al_2O_3 + 0.60 B_2O_3 measured at Corning Engineering Lab Services.

diffusions is listed in Table 5.5 and the measured index of refraction profiles are shown in Fig. 5.2. Similarly, the experimental data for the series of 216 hour diffusions is listed in Table 5.6 and the measured index of refraction profiles are shown in Fig. 5.3. Both figures show the wide variety of index of refraction profiles that can be obtained by changing the initial lithium concentration in the base glass, x, from 0.0 to 0.25.

A comparison between the two series of diffusions shows that increasing the diffusion time increases the depth of the diffusion but the overall shape of the profile is maintained for each particular glass composition. It also shows that for the 216 hours diffusion a large region of divitrification was present on the surface of the sample as evidenced by the inability to measure the index of refraction profile in this region. For example, divitrified layers up to 0.5 mm thick were present in some of the samples. In addition, large inclusions are often found at the edge of the samples for the longer diffusion periods. It is speculated that this is caused by the longer diffusion time which gives the potassium an opportunity to diffuse further into the edge of the glass. Therefore, if this type of glass/salt is to be used for manufacturing gradient-index lenses, additional glass components are needed to optimize the glass composition for ion exchange to eliminate these problems.

The optical properties of the homogeneous alumina silicate glasses and the homogeneous alumina borate glasses are very similar, but a comparison of the index of refraction profiles for the borate glasses to a similar series of Li^+ for Na^+ diffusions in an alumina silicate glass system shows some marked differences. First, as expected, the diffusion rates for the borate glasses appear to be at least an order of magnitude slower than in alumina silicate glasses; in some cases, the diffusion time for the borate glasses which is required to reach the same diffusion depth as in the alumina silicate glasses is almost ten times longer. Second, although the maximum change in refractive index is similar for the glass compositions with the same lithium concentration in the base glass, x, there is a noticeable difference in the shape of the index of refraction profile, especially for the glasses which contain no initial lithium. Finally, the shape of the borate index of refraction profiles are closer to complementary

error functions than the alumina silicate index of refraction profiles. Therefore, it is expected that the concentration dependence of the diffusion coefficient for the alumina borate glasses will be less than that of the alumina silicate glasses.

5.2.5 Na+ for Li+ Diffusions

Axial gradients were also fabricated in several of the borate glass compositions using Na^+ for Li^+ exchange. For each diffusion a small sample of the glass, approximately 8 x 10 x 10 mm, was placed in stainless steel wire basket and suspended in a molten $NaNO_3$. A diffusion temperature of 460 °C was chosen for comparison with the Li^+ for Na^+ diffusions. In particular, six glass samples were placed into the same salt bath (3000 grams of molten $NaNO_3$ in a 3000 ml Pyrex™ beaker) for 216 hours. Each glass sample started with a homogeneous glass composition which had a different value of x, the initial amount of lithium in the glass. The data for these experiments is listed in Table 5.7.

Similar to the alumina silicate glasses, all of the samples with initial lithium concentrations greater than 0.15 cracked and began to form small inclusions at the edge of the samples. In addition, the amount of cracking in the sample increased as the initial lithium concentration (and therefore the amount of sodium being exchanged) was increased making it difficult to find a place to measure the index of refraction profile for two of these samples (JLR40 and JLR41). Figure 5.4 shows the measured index of refraction profiles for the 216 hour diffusions, and, again, demonstrates that a wide variety of index of refraction profiles can be obtained by changing the initial lithium concentration in the base glass.

However, unlike the Na^+ for Li^+ exchanges in the alumina silicate glass system, it appears that the Na^+ for Li^+ diffusions in the borate glasses do experience complete exchange. Furthermore, a second experiment in the x = 0.15 glass, JLR20, was also performed using a much smaller salt bath (250 grams of $NaNO_3$ in a 250 ml Pyrex™ beaker) for a diffusion time of 96 hours. The measured index of refraction profile for this experiment is also shown in Fig. 5.4 and it also appears to have experienced complete exchange.
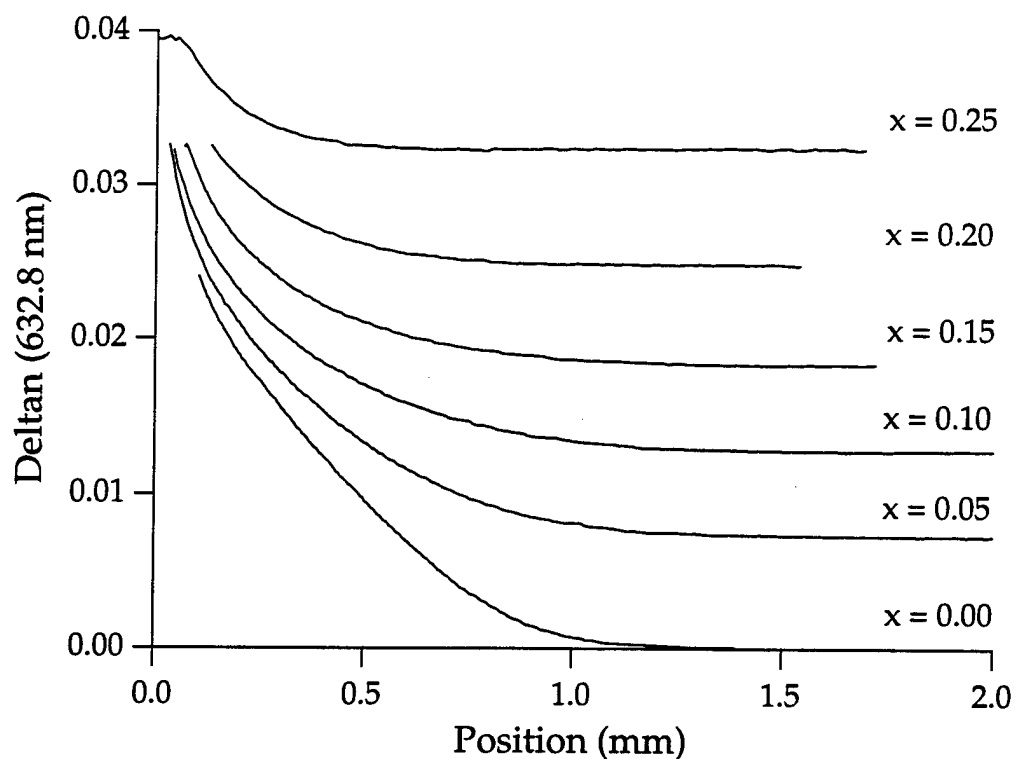
Figure 5.2 Measured index of refraction profiles for 120 hour Li⁺ for Na⁺ diffusions in glasses in the system x Li_2O + (0.30-x) Na_2O + 0.10 Al_2O_3 + 0.60 B_2O_3 for various values of x, the initial lithium concentration in the glass. The experimental data is listed in Table 5.5.

Exp. #	Glass Name	x Li_2O	Temperature (°C)	Time (hours)
JLR-6	JRGL-1	0.0	460	120
JLR-27	JRGL-15	0.05	460	120
JLR-3	JRGL-3	0.10	460	120
JLR-5	JRGL-6	0.15	460	120
JLR-28	JRGL-16	0.20	460	120
JLR-29	JRGL-17	0.25	460	120

Table 5.5 Experimental data for the 120 hour Li⁺ for Na⁺ diffusions in the glasses of the system x Li_2O + (0.30-x) Na_2O + 0.10 Al_2O_3 + 0.60 B_2O_3 for various values of x, the initial lithium concentration in the glass. The measured index of refraction profiles are shown in Fig. 5.2.
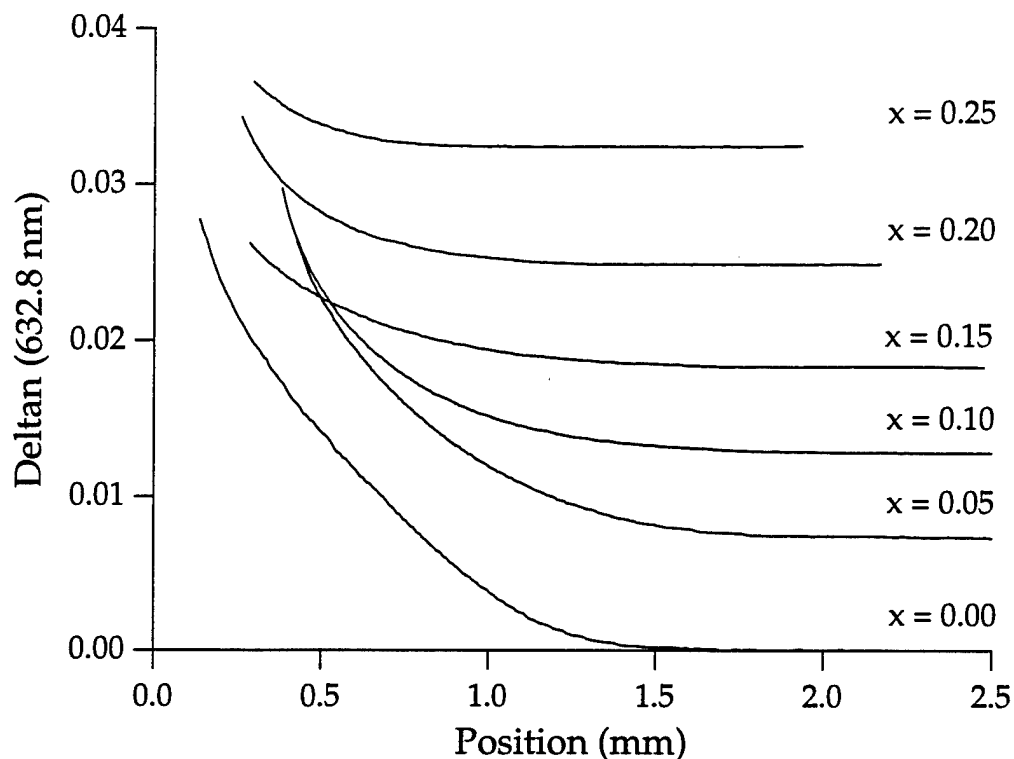
Figure 5.3 Measured index of refraction profiles for 216 hour Li^+ for Na^+ diffusions in glasses in the system x Li_2O + (0.30-x) Na_2O + 0.10 Al_2O_3 + 0.60 B_2O_3 for various values of x, the initial lithium concentration in the glass. The experimental data is listed in Table 5.6.

Exp. #	Glass Name	x Li_2O	Temperature (°C)	Time (hours)
JLR-30	JRGL-1	0.0	460	216
JLR-31	JRGL-15	0.05	460	216
JLR-32	JRGL-3	0.10	460	216
JLR-33	JRGL-6	0.15	460	216
JLR-34	JRGL-16	0.20	460	216
JLR-35	JRGL-17	0.25	460	216

Table 5.6 Experimental data for the 216 hour Li^+ for Na^+ diffusions in the glasses of the system x Li_2O + (0.30-x) Na_2O + 0.10 Al_2O_3 + 0.60 B_2O_3 for various values of x, the initial lithium concentration in the glass. The measured index of refraction profiles are shown in Fig. 5.3.
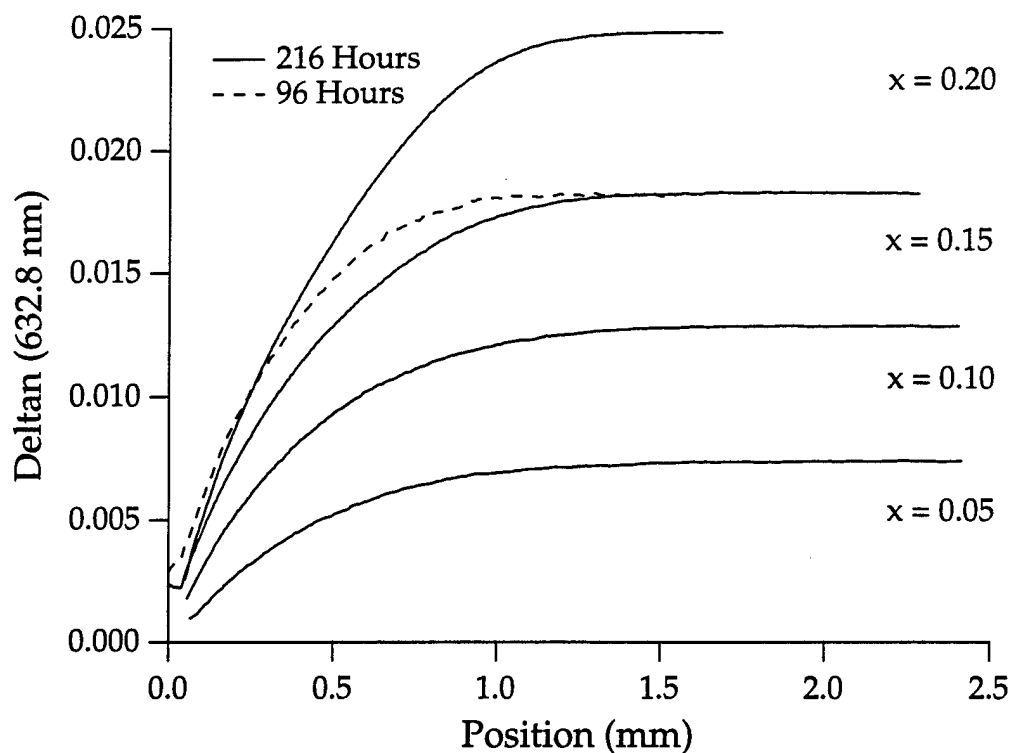
Figure 5.4 Measured index of refraction profiles for Na^+ for Li^+ diffusions in glasses in the
system x Li_2O + (0.30-x) Na_2O + 0.10 Al_2O_3 + 0.60 B_2O_3 for various values of x, the
initial lithium concentration in the glass. The experimental data is listed in Table 5.7.

Exp. #	Glass Name	x Li_2O	Temperature (°C)	Time (hours)
JLR-36	JRGL-15	0.05	460	216
JLR-37	JRGL-3	0.10	460	216
JLR-20	JRGL-6	0.15	460	96
JLR-38	JRGL-6	0.15	460	216
JLR-39	JRGL-16	0.20	460	216
JLR-40	JRGL-17	0.25	460	216
JLR-41	JRGL-2	0.30	460	216

Table 5.7 Experimental data for Na^+ for Li^+ diffusions in glasses in the system x Li_2O +
(0.30-x) Na_2O + 0.10 Al_2O_3 + 0.60 B_2O_3 for various values of x, the initial lithium
concentration in the glass. The measured index of refraction profiles are shown in
Fig. 5.4.

5.2.6   Calculation of Diffusion Coefficient and Comparison of Model Solutions with Experiment

In this section, the concentration dependence of the diffusion coefficient is examined at one temperature for both Li^+ for Na^+ and Na^+ for Li^+ exchange in glass compositions from the alumina borate glass system. An experimental index of refraction profile (from the set of measured profiles in Sections 5.2.4 and 5.2.5) is first converted to a concentration profile using Eq. (5.3). Then, the Boltzmann-Matano technique is used to calculate the concentration dependent diffusion coefficient for that particular glass composition. This calculation is then fitted to the Modified Quasi-Chemical (MQC) expression. (A more detailed description of this procedure was given in Chapters 2 and 3.)

The accuracy of the MQC fit is tested by numerically solving the diffusion equation to see if the MQC fit parameters can be used to recover the original index of refraction profile. Then, the diffusion model is used to calculate the index of refraction profiles for a second diffusion time in that particular glass composition, and, in some cases, for other glass compositions within the system. In each case, the model solution is compared with the measured index of refraction profile, and if it does not agree to within the experimental error, the differences are explained.

Each glass in the alumina borate glass system has the same total alkali and the same alumina content, and only the initial ratio of Li^+/Na^+ in the glass is different. This particular change in composition was chosen for two reasons. First, it is the change in composition that is needed to determine the concentration dependence of the index of refraction from a series of homogeneous glass melts. Second, an exchange of Li^+ for Na^+ in a glass which contains no initial amount of Li^+ should produce a concentration gradient which encompasses the entire glass composition range. As a result, it is expected that the calculation of the diffusion coefficient from this single experiment would be useful for predicting the index of refraction profiles of diffusions in the other glasses across the entire glass composition range for both Li^+ for Na^+ and Na^+ for Li^+ exchange. This would greatly reduce the number of experiments required

to define a diffusion model for such a wide variety of index of refraction profiles, since, in general, the concentration dependence of the diffusion coefficient must be determined experimentally for each particular glass composition.

In experiment JLR-06, an axial gradient is fabricated in a glass which initially contains no Li^+ (x = 0.0) using Li^+ for Na^+ exchange. The measured index of refraction profile for this experiment is shown in Fig. 5.2. This index of refraction profile was then converted to a concentration profile and used to calculate the diffusion coefficient. The result is shown in Fig. 5.5, where the diffusion coefficient is plotted as a function of normalized lithium concentration, χ. As expected, the calculation is very noisy, and is therefore fit to the Modified Quasi-Chemical Diffusion Coefficient expression. The MQC curve fit is shown as a dashed line in Fig. 5.5, and the fitting parameters for the MQC expression are listed in Table 5.8.

A comparison of the concentration dependence of the diffusion coefficient for the alumina borate glass to the diffusion coefficient for an alumina silicate glass shows some marked differences. First, the diffusion rate for the borate glass is at least an order of magnitude slower than for an alumina silicate glass. In addition, the self-diffusion coefficient for lithium in a borate glass is much lower than the self-diffusion coefficient for sodium. This is unlike the alumina silicate glasses where either the two self-diffusion coefficients are similar in value (7% alumina silicates) or the self-diffusion coefficient for lithium is larger than the self-diffusion coefficient for sodium (5% alumina silicates). Second, the concentration dependence of the diffusion coefficient for the alumina borate glasses is less than that of the alumina silicate glasses. This is demonstrated by the

Exp. #	x Li_2O	D_B	α	ρ	χ_0	c
JLR-06	0.00	0.01881	-3.9897	-1.7879	0.01838	4.99
JLR-39	0.20	0.01713	-4.1566	-1.1601	0.03601	5.04

Table 5.8 MQC fit parameters for the concentration dependent diffusion coefficients for glass compositions in the glass system x Li_2O + (0.30-x) Na_2O + 0.10 Al_2O_3 + 0.60 B_2O_3.

fact the both the interaction energy term and the coordination number is smaller for the borate glasses and most of the concentration dependence appears to be caused by the relatively large difference between the self diffusion coefficients.

The accuracy of the MQC fit is then tested by using the MQC fit parameters to numerically solve the diffusion equation and recover the original index of refraction profile. The results are shown in Fig. 5.6. The experimental profile is shown as a solid line while the theoretical solution is shown as a dashed line. As shown in the figure, the initial index of refraction profile can be recovered from the MQC fit parameters to within the experimental error. These results also demonstrate how useful the MQC model is for fitting experimentally calculated diffusion coefficients. As shown in Fig. 5.5 not only is the data extremely noisy, but it is missing the data for lithium concentrations greater than $\chi = 0.65$ since the edge of the gradient sample was divitrified and the index of refraction profile could not be measured in this region. Therefore the MQC model can be used to extrapolate the unknown values of the diffusion coefficient with very good results.

The x=0.0 diffusion coefficient was then used to generate theoretical index of refraction profiles for the Li^+ for Na^+ diffusions in the other glass composition of this series. The theoretical solutions and the experimental index of refraction profiles for the 120 hour diffusions are shown in Fig. 5.6. Thus, unlike the alumina silicate glasses, a single diffusion coefficient can be used to recover the initial index of refraction profile to within the experimental error for any glass composition in this series. It is speculated that there could be two reasons for this. First, the general properties of the glass compositions in the borate series are more similar as shown by the measurements of the anneal and strain temperatures for both series of compositions. For example, in the alumina silicate glass system, the anneal temperature varied by as much as 50 °C across the series while in the borate glass system, the anneal temperature variation was much smaller and at a maximum of 30 °C. Second, the overall concentration dependence is smaller for the borate glasses such that

changes in the base glass composition may not have as much of an effect on the concentration dependence of the diffusion coefficient.

The x=0.0 diffusion coefficient was also used to generate theoretical index of refraction profiles for the 216 hour diffusions, and both the theoretical solutions and the experimental index of refraction profiles are shown in Fig. 5.7. However, the theoretical index of refraction profiles for this diffusion time do not match the experimental index of refraction profiles to within the experimental error. A large region of divitrification was present on the surface of the sample which for some samples was as large as 0.5 mm thick. It is believed that in this area the potassium from the mixed salt bath may also be exchanging with the sodium. This then causes the glass to devitry which essentially creates a moving boundary as the diffusion time increases such that for the relatively long diffusion times for these experiments simple Fickian diffusion theory no longer applies.

The x=0.0 diffusion coefficient was then used to generate theoretical index of refraction profiles for the 216 hour Na$^+$ for Li$^+$ diffusions. The theoretical index of refraction profiles for this diffusion time did not match the experimental index of refraction profiles to within the experimental error. For example, Fig. 5.8 shows the theoretical solution (dashed line) and the experimental index of refraction profile (solid line) for experiment JLR-39 in a glass composition for which x = 0.20. However, as shown by Fig. 5.9, the experiment and the theory do agree to within experimental error for the 96 hour diffusion (JLR-20 in a glass composition for which x = 0.15), while the 216 hour diffusion in this same glass composition cannot be predicted. After further examination, it was noticed that the actual temperature of the salt bath was never measured, and it was only allowed to melt for 2 hours before the sample were dropped in. It was later determined that for this amount of salt at this low of a diffusion temperature it would take the salt bath at least 12 hours to reach temperature and equilibrate.

Thus, the 216 hour diffusion samples experienced a change in temperature as the diffusion progressed, but since they were all placed in the same salt bath at the same time they should have experienced a

similar change in temperature. Therefore, a diffusion coefficient for this series of experiments was calculated from the measured index of refraction profile for experiment JLR-39. Figure 5.10 shows the calculated diffusion coefficient and the MQC curve fit for this experiment along with the MQC curve fit for the x=0.0 glass composition. The specific fitting parameters for the two curve fits are listed in Table 5.8. As expected, the diffusion coefficient for JLR-39 is lower than that of JLR-06 as shown by the figure.

The accuracy of the MQC fit to the JLR-39 diffusion coefficient is then tested by using the MQC fit parameters to numerically solve the diffusion equation and recover the original index of refraction profile. The results are shown in Fig. 5.11. The experimental profile is shown as a solid line while the theoretical solution is shown as a dashed line. Thus, the initial index of refraction profile can be recovered from the MQC fit parameters to within the experimental error. It can then be used to predict the index of refraction profiles for the remaining set of three experiments which are also shown in Fig. 5.11.
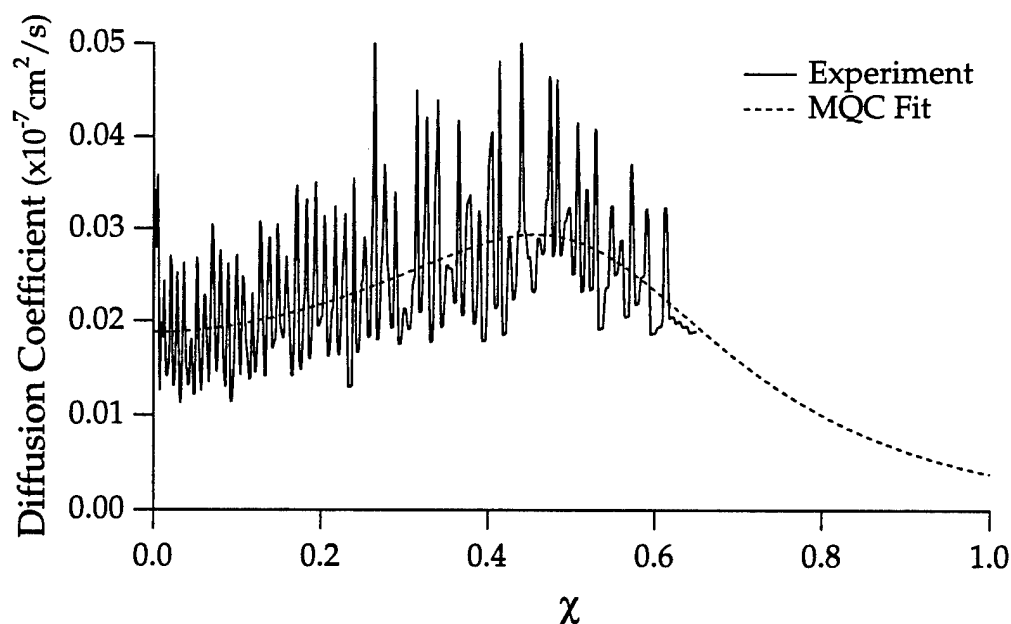
Figure 5.5 Calculated diffusion coefficient from experiment JLR 06 and the curve fit to the Modified Quasi-Chemical Diffusion Coefficient expression. The fit parameters are listed in Table 5.8.
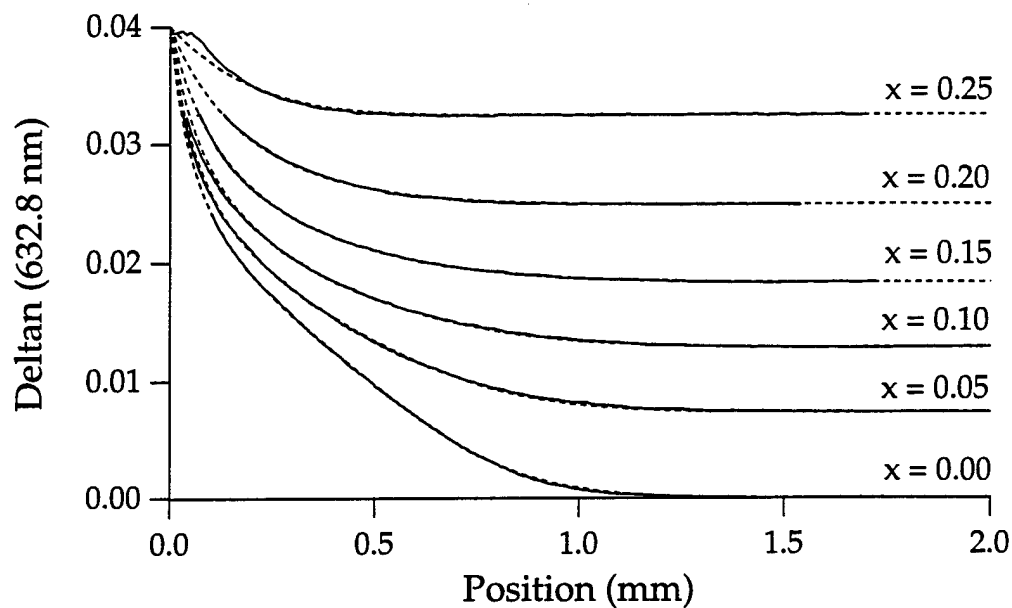
Figure 5.6 Experimental index of refraction profiles for 120 hour Li^+ for Na^+ diffusions in glasses in the system x Li_2O + (0.30-x) Na_2O + 0.10 Al_2O_3 + 0.60 B_2O_3 and the model solutions generated with the x = 0.0 MQC diffusion coefficient.
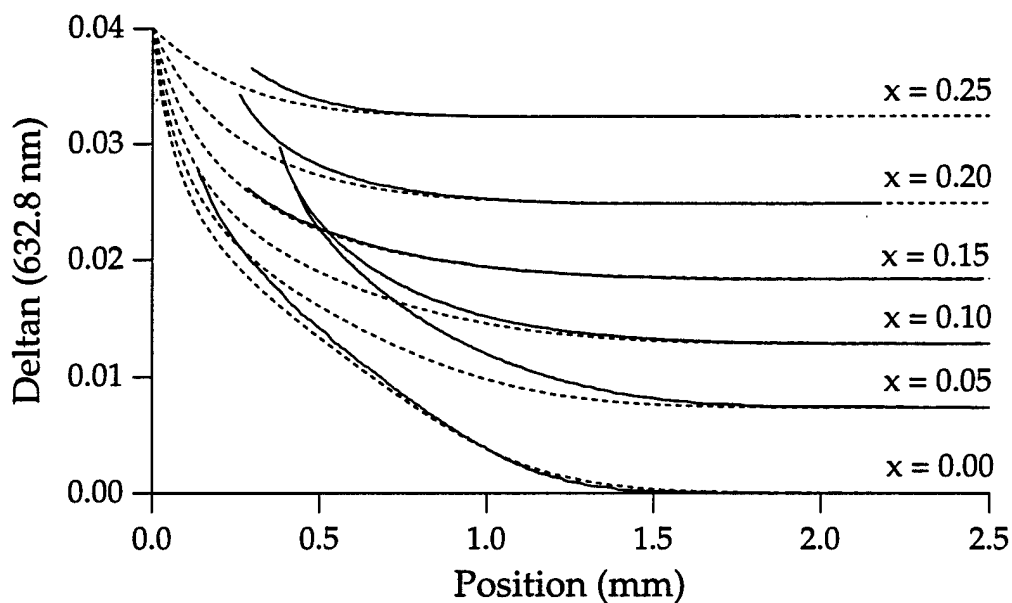
Figure 5.7 Experimental index of refraction profiles for 216 hour Li^+ for Na^+ diffusions in glasses in the system x Li_2O + (0.30-x) Na_2O + 0.10 Al_2O_3 + 0.60 B_2O_3 and the model solutions generated with the x = 0.0 MQC diffusion coefficient.
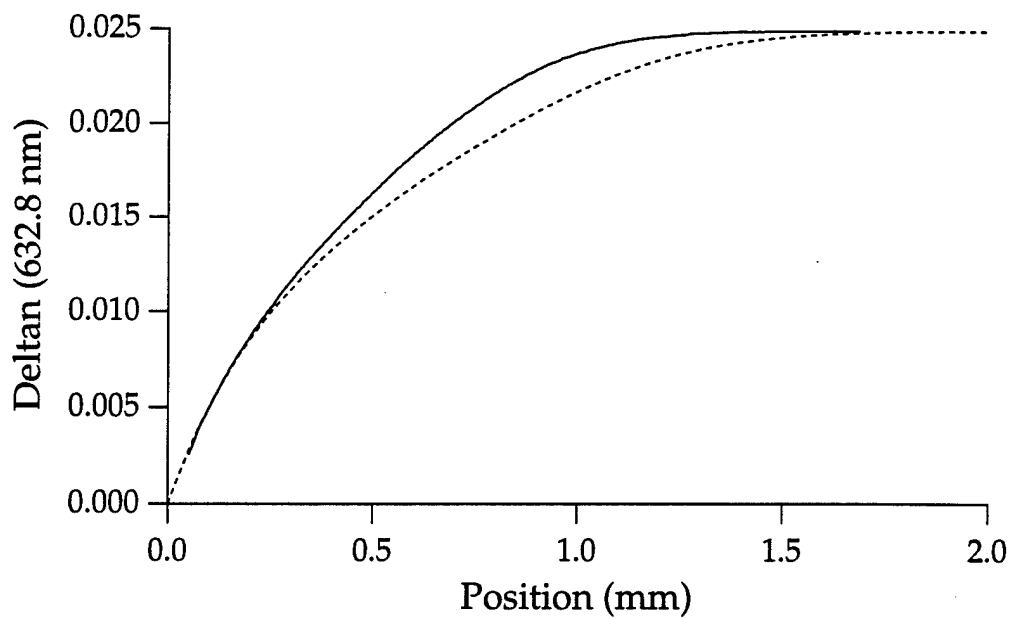
Figure 5.8 Experimental index of refraction profile for Na$^+$ for Li$^+$ in glass composition 0.20 Li$_2$O + 0.10 Na$_2$O + 0.10 Al$_2$O$_3$ + 0.60 B$_2$O$_3$ and the model solution generated with the x = 0.0 MQC diffusion coefficient.
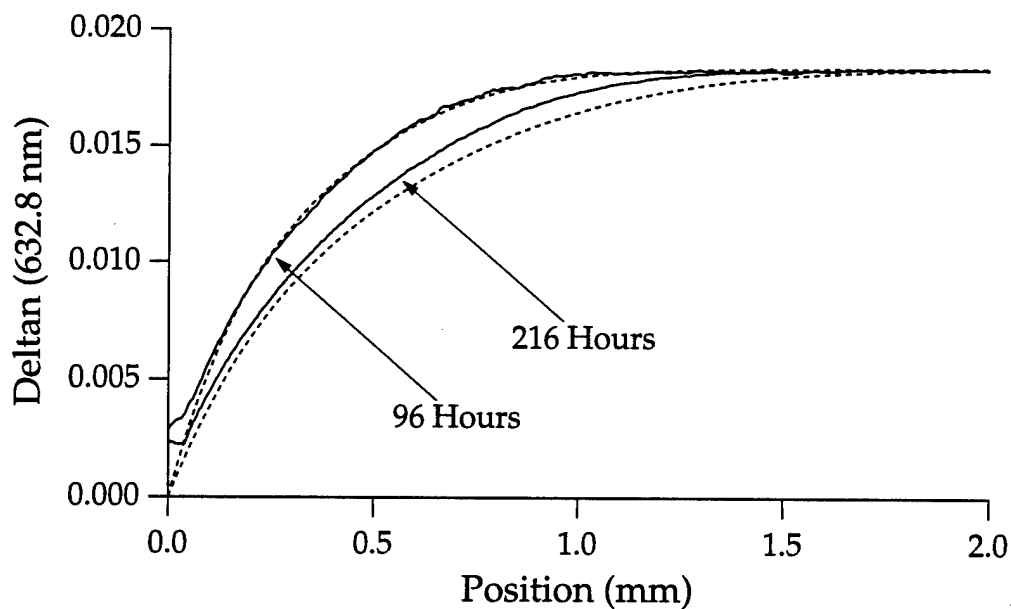
Figure 5.9 Experimental index of refraction profiles for Na$^+$ for Li$^+$ diffusions in glass composition 0.15 Li$_2$O + 0.15 Na$_2$O + 0.10 Al$_2$O$_3$ + 0.60 B$_2$O$_3$ and the model solution generated with the x = 0.0 MQC diffusion coefficient.

Figure 5.10 Calculated diffusion coefficient from experiment JLR-39 and the curve fit to the Modified Quasi-Chemical Diffusion Coefficient expression. The fit parameters are listed in Table 5.8. The MQC Diffusion Coefficient for JLR-06 is also shown.

Figure 5.11 Experimental index of refraction profiles for 216 hour Na^+ for Li^+ diffusions in glasses in the system x Li_2O + (0.30-x) Na_2O + 0.10 Al_2O_3 + 0.60 B_2O_3 and the model solutions generated with the x = 0.20 MQC diffusion coefficient.

5.3 Titania Silicate Glasses

5.3.1 Introduction

Both the alumina silicate glasses and the alumina borate glasses are crown glasses with a relatively low index of refraction and low dispersion. In order to fabricate a gradient-index flint glass, a different type of intermediate must be added to the glass composition to increase the index of refraction and dispersion of the host glass. Commercially, the two most common flint glasses are lead silicates and titania silicates. Lead glasses have very low ionic conductivity, [5] but titania, on the other hand, has only a small effect on the ion exchange rate of the glass. [6]

Kindred investigated $Li^+ - Na^+$ exchange in a series of titania silicate glasses given by

$$xLi_2O + (0.25 - x)Na_2O + yTiO_2 + (0.75 - y)SiO2 \ . \tag{5.4}$$
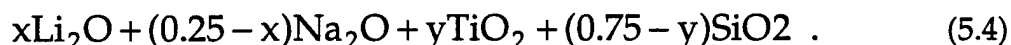
where x, the initial amount of lithium in the base glass was varied from 0.0 to 0.25, and y, the initial amount of titania in the base glass was varied from 0.05 to 0.20. In particular, he showed that for x = 0.0, the index of refraction of the base glass increased linearly with TiO_2 concentration (from 1.498 for y=0.0 to 1.637 for y=0.20) and the Abbe number of the glass decreased (60 to 33). Thus a relatively large range of base glass optical properties can be explored by adding relatively small amounts of titania to the glass composition. Furthermore, a wide variety of index of refraction profiles can be obtained in these glass compositions which have fast ion exchange rates and little or no divitrification. Therefore, the applicability of the diffusion model to titania silicate glasses is investigated in this section.

5.3.2 Glass Melting

Several attempts at melting titania silicate glasses in 250 gram batches were made, but the resulting glasses were very inhomogeneous. As a result, two particular titania silicate glass compositions were selected and then melted in a large, four kilogram, batch size. [7] These compositions are listed in Table 5.9. Each glass has the same initial amount of sodium

Glass Name	Na$_2$O	TiO$_2$	Al$_2$O$_3$	ZrO$_2$	SiO$_2$
RH-1A0068	0.25	0.15	0.00	0.00	0.60
RH-1A0069	0.25	0.10	0.02	0.03	0.60

Table 5.9 Titania silicate glass compositions melted in 10# size melt.

and the same percentage of silica, but the intermediate composition was varied. In particular, RH-1A0068 has fifteen percent titania while RH-1A0069 has ten percent of titania and an additional five percent total of alumina and zirconia. Thus, a simple titania silicate glass is examined and then a more complicated glass composition is also examined.

Each glass was melted in a large platinum crucible at 1450 °C for 20 hours and was continuously stirred with a platinum stir bar during this time period. (The batch material was first added in 9 steps at 20 minute intervals also at 1450 °C.) An additional four grams of arsenic was added to the melt to reduce the number of bubbles. Then, the glass was cooled in the crucible to a temperature of 1100 °C and cast into a warm steel mold. The glass was then placed into a preheated annealing furnace at a temperature of 565° C. After two hours, it was allowed to cool slowly, at a rate of 3 °C per hour, to a temperature of 425 °C, and then at 75 °C per hour, to room temperature.

5.3.3   Index of Refraction measurements

Small samples of each glass (1cm x 1cm x 0.5 cm) were polished flat on one side to $\lambda/4$. Then, the index of refraction of the sample at four different wavelengths was measured using a Pulfrich refractometer to an accuracy of ±0.0001. Table 5.10 lists the results of these measurements. First, in comparison to the alumina silicate glasses and the alumina borates these compositions have a much higher index of refraction which was expected. Second, the addition of the alumina and the zirconia to the glass composition in substitution for the titania lowered the refractive index of the glass by approximately 0.02.

The homogeneous dispersion of the titania silicate glasses was then calculated using the procedure described in Chapter 3, Section 3.4.3. First,

Glass Name	n_g	n_e	n_d	n_{HeNe}
RH-1A0068	1.6217	1.6053	1.6016	1.5980
RH-1A0069	1.6019	1.5877	1.5844	1.5816

Table 5.10 The index of refraction of the homogeneous titania glass samples measured at four different wavelengths on a Pulfrich refractometer.

equation (3.8) was used to fit the index of refraction measurements as a function of wavelength. Then, the index of refraction values, n_F and n_C, were interpolated from the fit and the dispersion of the glass was calculated. Table 5.11 lists the coefficients of the fit, the indices of refraction, n_F and n_C, and finally the dispersion, V_d, for each glass. Thus, a comparison of the optical properties of these base glasses with the alumina silicates glasses examined in Chapter 4 and the alumina borate glasses examined in the first part of this chapter shows that these glass compositions are much more dispersive. Furthermore, the addition of the alumina and the zirconia to the glass composition (in substitution of the titania) has also decreased the dispersion of the glass.

As discussed in Chapter 3, the index of refraction as a function of lithium concentration is necessary for the calculation of the concentration dependence of the diffusion coefficient for these glasses. It is also used by the diffusion model to convert concentration profile solutions to index of refraction profiles so that they can be compared with experimentally measured index of refraction profiles. However, a large number of glass melts is required to accurately measure this function for each of these glass compositions which has not yet been completed. [8]

Glass Name	n_0	n_1	n_2	n_F	n_C	V_d
RH-1A0068	1.6027	-0.0855	0.0175	1.6126	1.5970	38.57
RH-1A0069	1.5854	-0.0764	0.0053	1.5941	1.5802	42.17

Table 5.11 The fit coefficients for Eq. (3.8), the interpolated values for n_F and n_C, and the calculated dispersion V_d for the homogeneous titania silicate glasses.
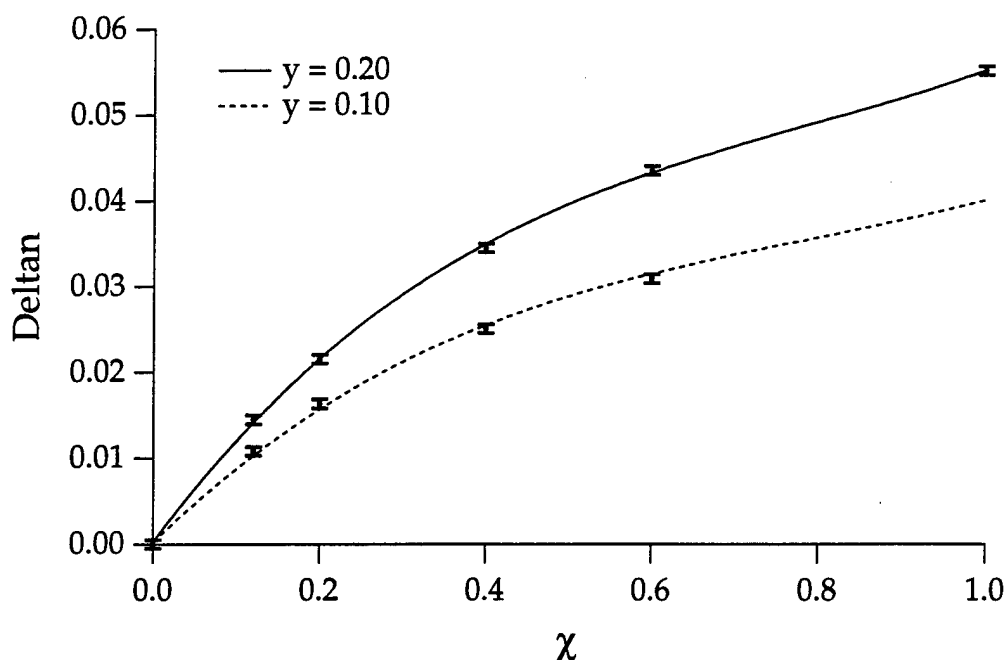
Figure 5.12 Index of refraction as a function of normalized lithium concentration, χ, for two different titania silicate glass systems. Both the measured data points and a third order polynomial fit to the data are shown.

Kindred, however, did the required study for two very similar series of titania glasses in the general glass system given by Eq. (5.4), one for a set titania concentrations of y = 0.10 and the other for y = 0.20. Figure 5.12 shows the measured change in index of refraction as a function of normalized lithium concentration, χ, where

$$\chi = \frac{x}{0.25} ,$$
(5.5)

and x is the initial mole percent of lithium in the glass, for both the series of twenty percent titania glasses and the series of ten percent titania glasses. A third order polynomial curve fit to the measured twenty percent titania index of refraction as a function of concentrations data, given by

$$\Delta n(\chi) = 0.1305\chi - 0.1314\chi^2 + 0.05576\chi^3 ,$$
(5.6)

is also shown as a solid line in the figure. In addition, a second curve is shown as a dashed line which appears to fit the ten percent titania

measured data fairly well. This particular curve was generated by scaling the polynomial given by Eq. (5.6) to the appropriate maximum Δn for the ten percent titania glasses.

Therefore, in the analysis of the two titania glasses examined in this chapter, Eq. (5.6) is scaled to the maximum change in refractive index for these glasses and then used to convert the index of refraction profile to a concentration profile for the calculation of the diffusion coefficient. Although, this may not be entirely accurate, especially for the more complicate glass composition, it was a good place to start until the required data can be measured. Furthermore, in this section, only the temperature dependence of the diffusion coefficient is examined in these two glass compositions such that the exact index as a function of concentration is not needed.

5.3.4   Li+ for Na+ Diffusions

The effect of changing the diffusion temperature on Li+ for Na+ exchange was examined in the two titania silicate glass compositions, RH-1A0068 and RH-1A0069. In this study, axial gradients were fabricated in each glass for a wide range of temperatures. For each diffusion, a sample of the glass, approximately 15 x 15 x 15 mm, was placed in platinum wire basket and suspended in 250 grams of a 0.40 LiCL + 0.60 CaCl$_2$ mixture, by weight, that was placed in a 250 ml Pyrex™ beaker. In particular, each glass had a range of temperatures over which the sample did not deform and experienced only small amounts of devitrification.

First, a series of diffusions were performed in RH-1A0068 for a temperature range of 540 °C to 570 °C. The experimental data is listed in Table 5.12 and the measured index of refraction profiles are shown in Figs. 5.13 and 5.15. Note: because of the different diffusion times used in the experiments, the index of refraction profiles were all scaled to a diffusion time of 52 hours to highlight the effect of temperature on the profile since increasing the diffusion time has a similar effect as increasing the diffusion temperature. As shown by the figure, increasing the temperature of the diffusion 30 °C has increased the diffusion depth by almost two millimeters for this diffusion time. A relatively large

divitrification region (approximately 250 microns) is present in most of these sample as evidenced by the fact that the index of refraction profile could not be measured in this region. Furthermore, an additional diffusion at 520 °C showed extreme divitrification and cracking of the sample, while the glass begins to deform at temperatures much higher than 570 °C.

Next, a series of diffusions were performed in RH-1A0069 for an even larger temperature range, from 540 °C to 590 °C. The experimental data is listed in Table 5.13 and the measured index of refraction profiles are shown in Fig. 5.14. Note: because of the different diffusion times used in the experiments, the index of refraction profiles were all scaled to a diffusion time of 61 hours to highlight the effect of temperature on the profile. Thus, increasing the temperature of the diffusion 50 °C has almost doubled the diffusion depth for this particular diffusion time. Very little divitrification is present in most of these sample, although the amount of divitrification increased (from 10 microns to 150 microns) as the temperature of the diffusion was decreased (from 590 °C to 540 °C).

Thus, the addition of the alumina and zirconia to the glass composition has had several important effects on the diffusion. Figure 5.16 compares the index of refraction profiles for a diffusion in each glass composition for 61 hours at a temperature of 560 °C. First, the divitrification of the sample has been essentially eliminated, without having an adverse effect on the diffusion rate since the diffusion depth is approximately the same for both samples. Second, the overall shape of two profiles is somewhat different and, in particular, the total change in refractive index is lower for the glass composition which contains alumina.
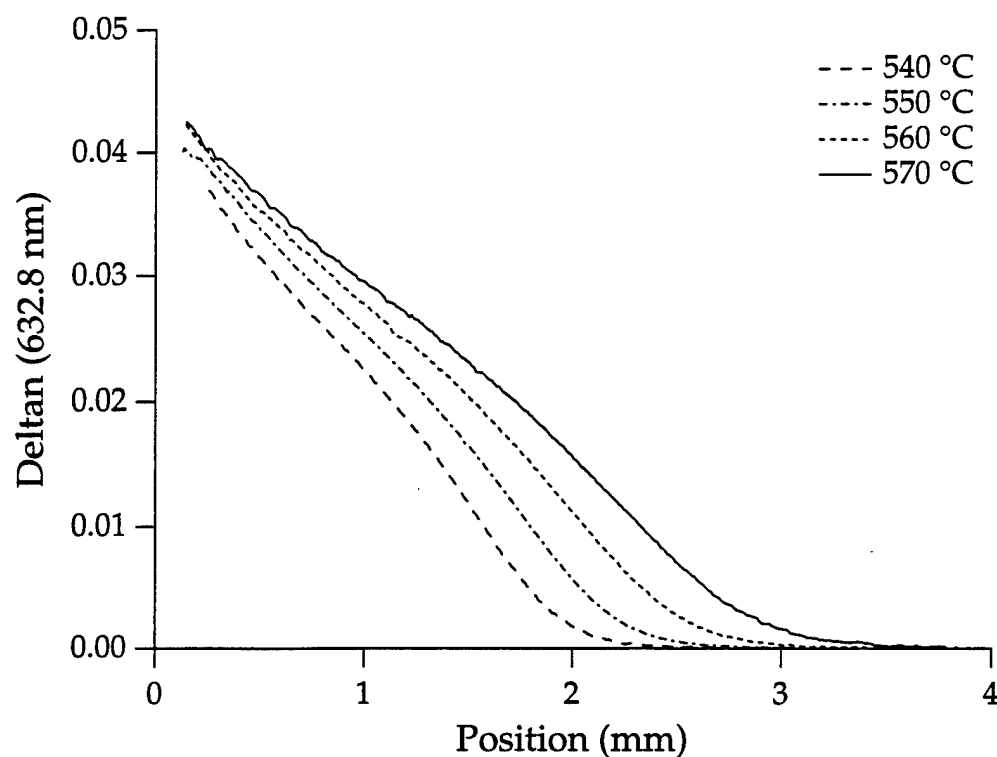
Figure 5.13 Measured index of refraction profiles for Li^+ for Na^+ diffusions at four different temperatures in RH-1A0068. The experimental data is listed in Table 5.12. Note: the measured profiles are scaled to a common diffusion time of 52 hours for comparison.

Exp. #	Glass Name	x Li$_2$O	Temperature (°C)	Time (hours)
JLB-112	RH-1A0068	0.0	540	95
JLB-102	RH-1A0068	0.0	550	72
JLB-114	RH-1A0068	0.0	560	61
JLB-108	RH-1A0068	0.0	570	45
JLB-110	RH-1A0068	0.0	570	52

Table 5.12 Experimental data for Li^+ for Na^+ diffusions at four different temperatures in RH-1A0068. The measured index of refraction profiles are shown in Fig. 5.13.
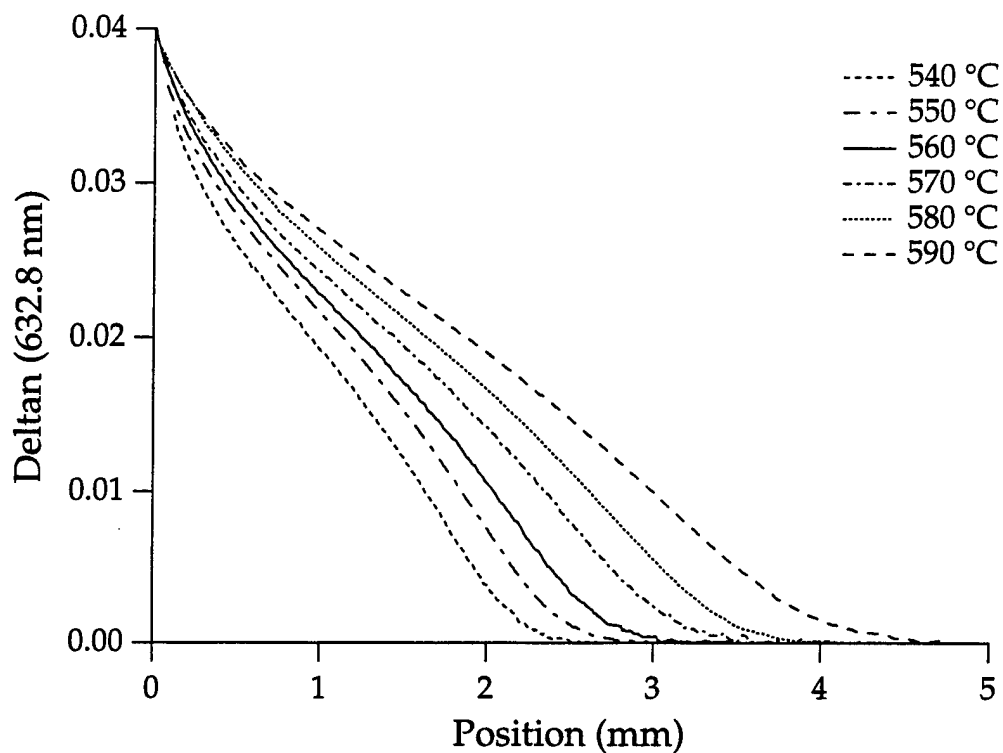
Figure 5.14 Measured index of refraction profiles for Li$^+$ for Na$^+$ diffusions at six different temperatures in RH-1A0069. The experimental data is listed in Table 5.13. Note: the measured profiles are scaled to a common diffusion time of 61 hours for comparison.

Exp. #	Glass Name	x Li$_2$O	Temperature (°C)	Time (hours)
JLB-113	RH-1A0069	0.0	540	95
JLB-103	RH-1A0069	0.0	550	72
JLB-115	RH-1A0069	0.0	560	61
JLB-109	RH-1A0069	0.0	570	45
JLB-116	RH-1A0069	0.0	580	42
JLB-117	RH-1A0069	0.0	590	37

Table 5.13 Experimental data for Li$^+$ for Na$^+$ diffusions at six different temperatures in RH-1A0069. The measured index of refraction profiles are shown in Fig. 5.14.
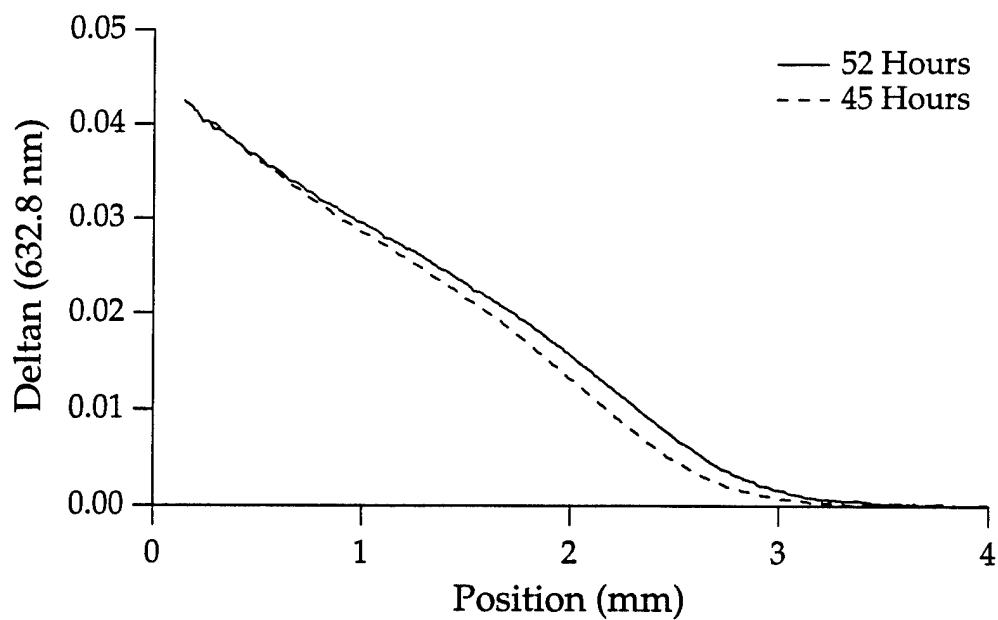
Figure 5.15 Measured index of refraction profiles for Li$^+$ for Na$^+$ diffusions for two different diffusion times in RH-1A0069. The experimental data is listed in Table 5.12.
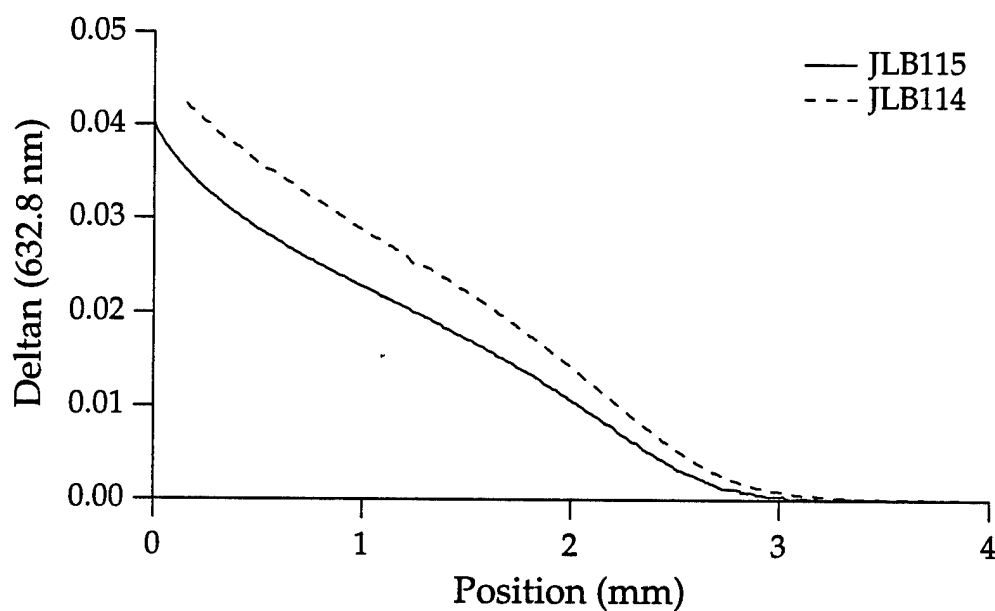
Figure 5.16 Measured index of refraction profiles for 61 hour Li$^+$ for Na$^+$ diffusions at 560 °C in glasses RH-1A0068 and RH-1A0069. The experimental data is listed in Tables 5.12 and 5.13.

5.3.5 Calculation of Diffusion Coefficient and Comparison of Model Solutions with Experiment

5.3.5.1 Concentration Dependence

In this section, the concentration dependence of the diffusion coefficient is examined at one temperature (560 °C) for Li^+ for Na^+ exchange in the two titania silicate glass compositions. An experimental index of refraction profile (from the set of measured profiles in Section 5.3.4) is first converted to a concentration profile using a scaled version of Eq. (5.4). Then, the Boltzmann-Matano technique is used to calculate the concentration dependent diffusion coefficient for that particular glass composition. This calculation is then fitted to the Modified Quasi-Chemical (MQC) expression. The accuracy of the MQC fit is also tested by numerically solving the diffusion equation to see if the MQC parameters can be used to recover the original index of refraction profile to within the experimental error.

Figure 5.17 shows the diffusion coefficient, plotted as a function of normalized lithium concentration, χ, for glass RH-1A0068, which was calculated from experiment JLB-114. Table 5.14 lists the MQC parameters for the MQC fit that is shown as a dashed line in the figure. Similarly, Figure 5.18 shows the diffusion coefficient, plotted as a function of normalized lithium concentration, χ, for glass RH-1A0069, which was calculated from experiment JLB-115. Table 5.14 also lists the MQC parameters for this MQC fit which is shown as a dashed line in the figure.

A comparison of the concentration dependence of the diffusion coefficient for these two glass compositions is shown in Fig. 5.19. (The recovery of the initial index of refraction profile to within experimental

Exp. #	D_B	α	ρ	χ_0	c
JLB-114	0.1486	0.0646	-2.0216	-0.2269	4.4
JLB-115	0.1412	-0.4796	-2.2760	-0.2281	4.7

Table 5.14 MQC fit parameters for the concentration dependent diffusion coefficients for the titania silicate glass compositions.

error for these two MQC fits is shown in Fig. 5.20.) The curves are very similar for low lithium concentrations and then begin to differ as the lithium concentration is increased. This can be seen in the MQC fitting parameters which are all very similar, except for the ratio of self diffusion coefficients such that the self diffusion coefficient for lithium is much higher in the strictly titania glass composition.

4.3.7.2 Temperature Dependence

Next, the effect of changing the diffusion temperature on the diffusion coefficient for Li^+ for Na^+ exchange was examined in the two titania glass compositions, RH-1A0068 and RH-1A0069. First, the diffusion coefficients were calculated from the measured index of refraction profiles for the series of temperature diffusions in each glass composition. The experimental data was then fit to the MQC model. The MQC fits which can recover the initial index of refraction profile to within experimental error for the glass RH-1A0068 are shown in Fig. 5.21. Similarly, the MQC fits which can recover the initial index of refraction profile to within experimental error for the glass RH-1A0069 are shown in Fig. 5.21. As expected, an increase in the diffusion temperature of the experiment, increases the value of the diffusion coefficient, but the overall shape of the concentration dependence is similar. The MQC fitting parameters for each of these diffusion coefficients are listed in Table 5.15.

Exp. #	Temp	D_B	α	ρ	χ_0	c
JLB-112	540	0.0936	-0.4004	-2.2913	-0.2159	4.2
JLB-102	550	0.1155	-0.0462	-2.0947	-0.2248	4.3
JLB-114	560	0.1486	0.0646	-2.0216	-0.2269	4.4
JLB-110	570	0.2183	0.0049	-2.0577	-0.2118	3.5
JLB-113	540	0.0937	-1.5533	-2.3724	-0.2215	6.0
JLB-103	550	0.1026	-0.8243	-2.0553	-0.2156	7.1
JLB-115	560	0.1412	-0.4796	-2.2760	-0.2281	4.7
JLB-109	570	0.1895	-0.6023	-2.2136	-0.2215	4.9
JLB-116	580	0.2284	-0.1798	-2.2890	-0.2311	4.1
JLB-117	590	0.3166	-0.4797	-2.0340	-0.2208	5.0

Table 5.15 MQC fitting coefficients for the temperature dependence of the diffusion coefficient in the glass compositions RH-1A0068 and RH-1A0069.
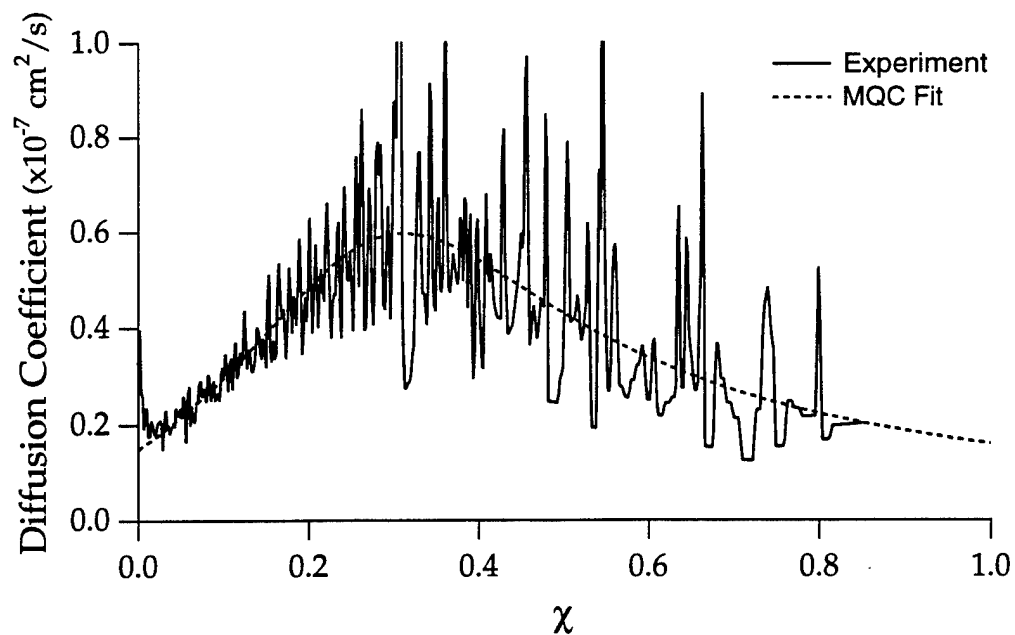
Figure 5.17 Calculated diffusion coefficient from experiment JLB-114 and the curve fit to
the Modified Quasi-Chemical Diffusion Coefficient expression. The fit parameters
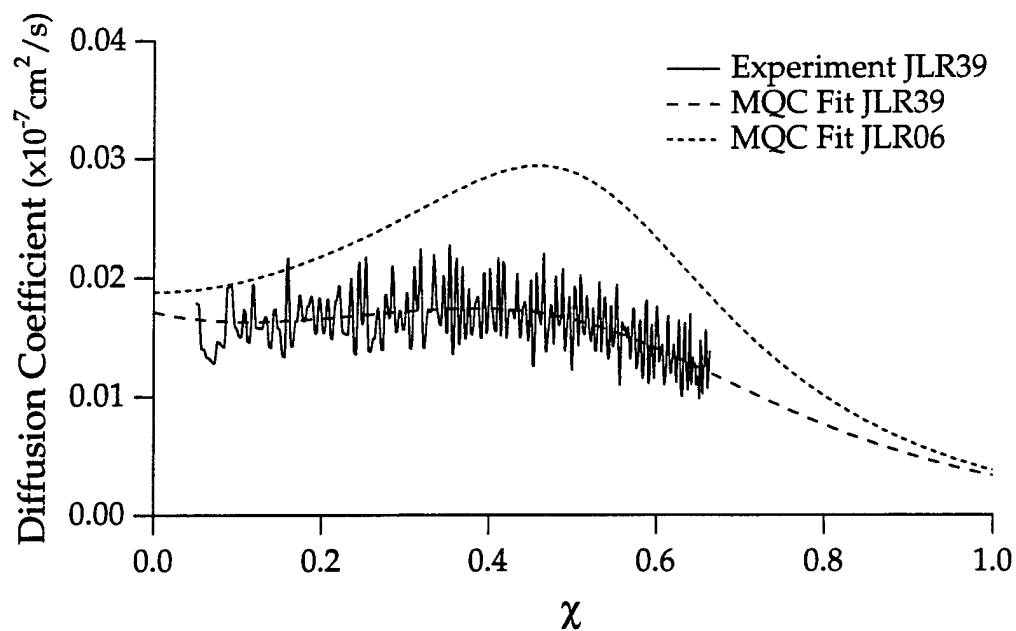are listed in Table 5.14.
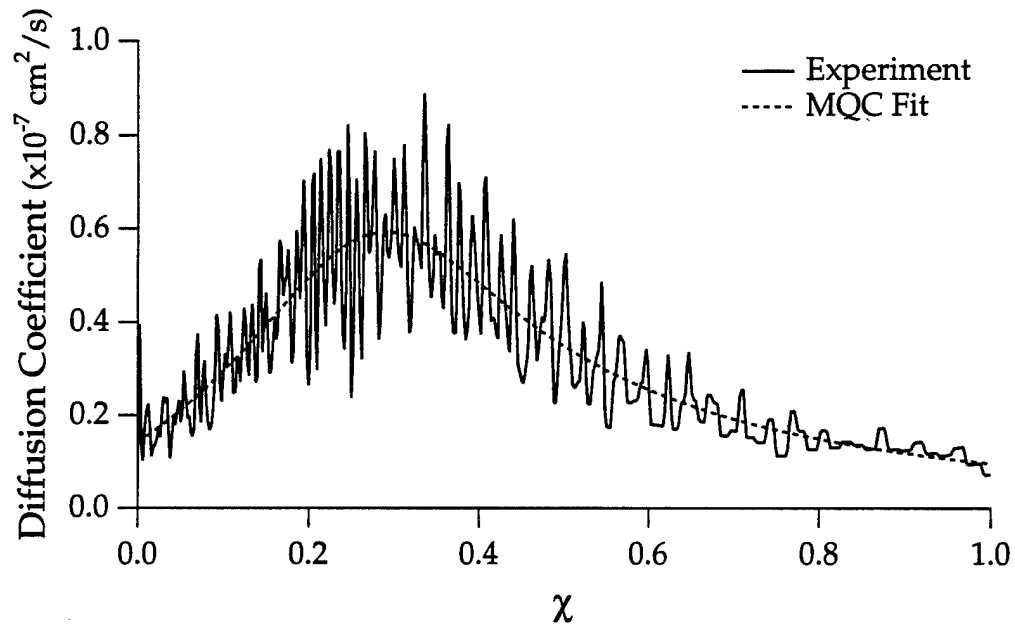
Figure 5.18 Calculated diffusion coefficient from experiment JLB-115 and the curve fit to
the Modified Quasi-Chemical Diffusion Coefficient expression. The fit parameters
are listed in Table 5.14.
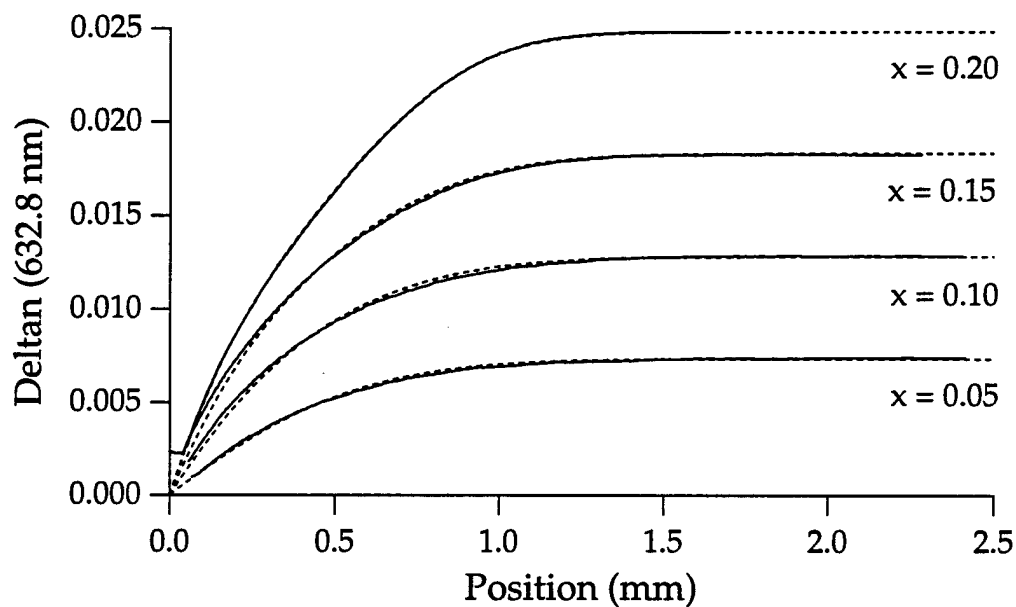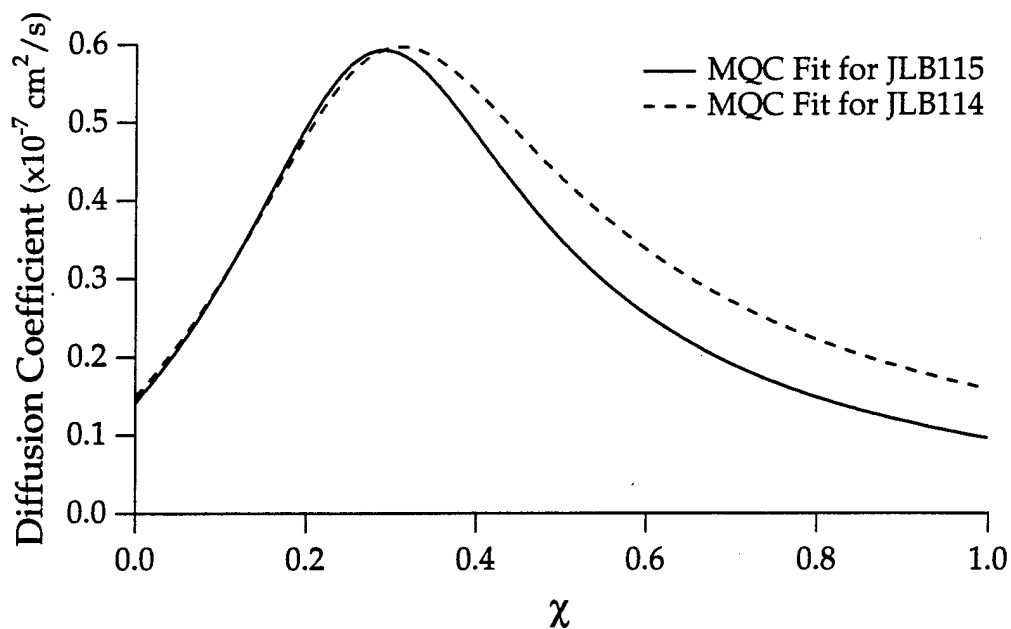
Figure 5.19 MQC diffusion coefficients for the two titania silicate glass compositions. The fit parameters are listed in Table 5.14.
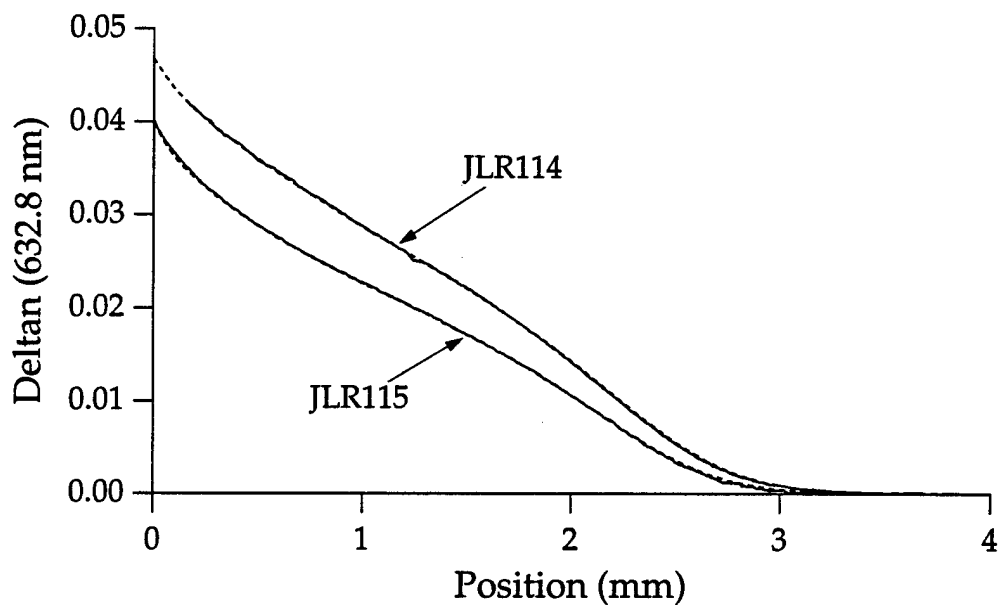
Figure 5.20 Experimental index of refraction profiles for JLB-114 and JLB-115 and the model solutions generated with the MQC diffusion coefficient.
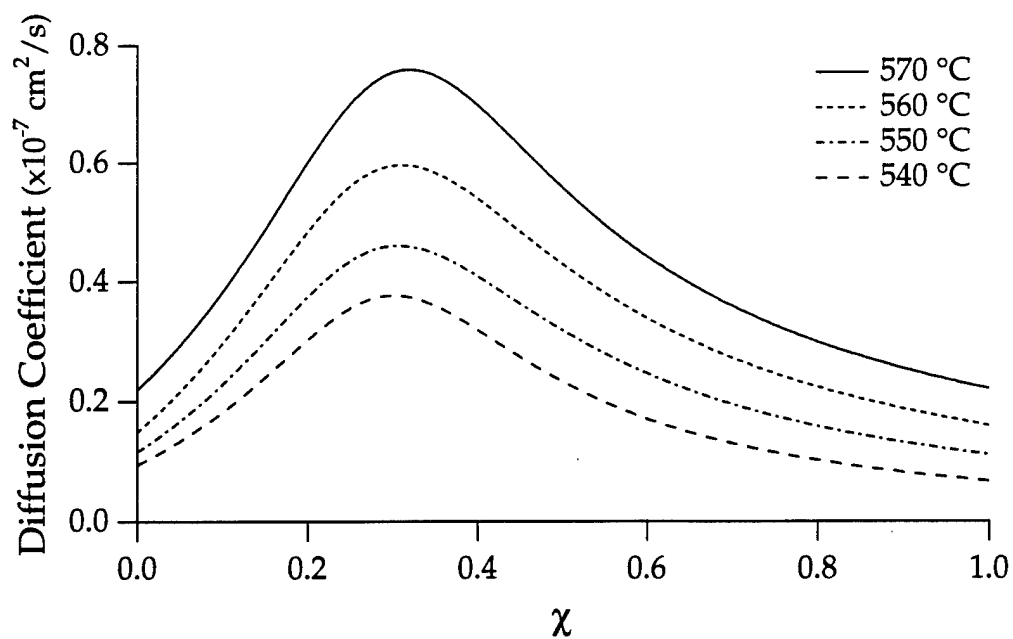
Figure 5.21 MQC diffusion coefficients for glass composition RH-1A0068 for four different temperatures. The fit parameters are listed in Table 5.15.
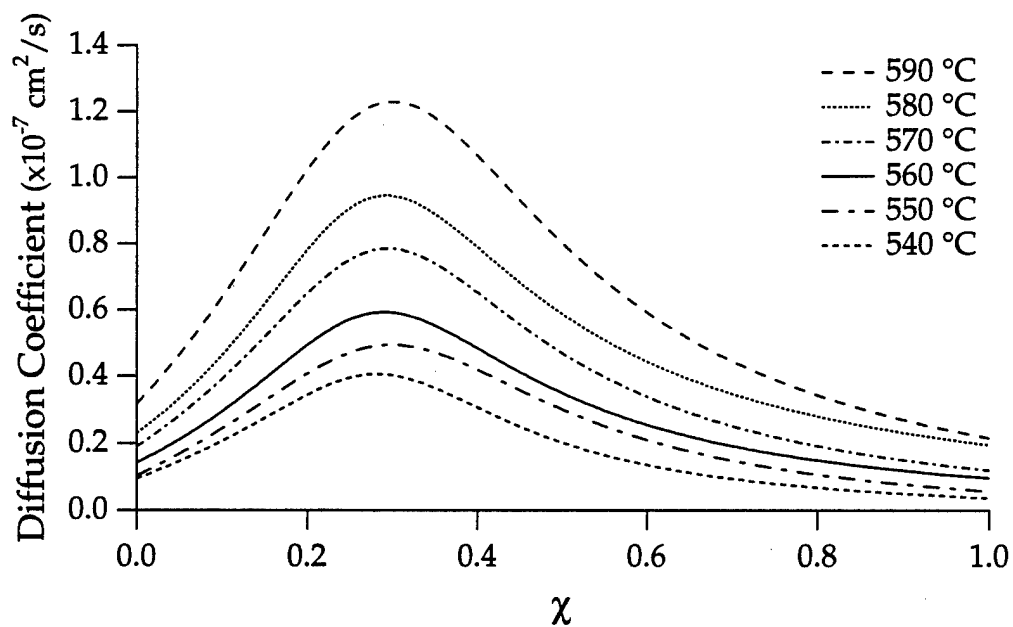
Figure 5.22 MQC diffusion coefficients for glass composition RH-1A0069 for six different temperatures. The fit parameters are listed in Table 5.15.

References

1. D. S. Kindred, "Development of new gradient index glasses for optical imaging systems," Doctoral Dissertation, University of Rochester, Rochester, NY (1990).

2. G. H. Frischat, *Ionic Diffusion in Oxide Glasses*, Trans Tech Publications, Bay Village, OH (1975), p. 66-67.

3. Private communications with Dr. Douglas Kindred at University of Rochester, Rochester, NY.

4. Levin, et. al., Phase Diagrams for Ceramists, Am. Ceram. Soc., Columbus, OH (1964).

5. R. H. Doremus, *Glass Science* (Wiley, New York, 1973), p. 162.

6. Reference 2, p. 80.

7. Melted by J. R. Hensler.

8. This is currently being examined by Curtis Harkrider at the University of Rochester.

Chapter VI
Lens Design

6.1 Introduction

The research presented in the previous chapters of this dissertation shows that significant progress has been made in the development of a gradient-index manufacturing model for ion exchange in a variety of different glass materials. The final objective of this thesis is to investigate the model in an optical context. The diffusion model must be linked with a lens design program such that experimental parameters (such as time or temperature) can be optimized directly during the lens design process. This allows a designer to specify the appropriate experimental conditions required to produce the index profile shape that yields optimal optical performance. Furthermore, this approach guarantees that the gradient-index lenses designed with the diffusion model can be manufactured using current technology.

The first issue that needs to be addressed is how to link the diffusion model with the lens design software and what experimental parameters are to be varied during the design process. In general, the parameters that should be chosen are those which can be readily changed in the laboratory in a continuous manner. Preliminary research by Hoppe showed the

feasibility of optimizing on diffusion parameters, but his method was limited to an axial geometry, and experimentally he considered only one glass/salt pair. [1] Haun successfully investigated the radial geometry in a sol-gel material, but his model used a concentration-independent diffusion coefficient. [2]

In the first part of this chapter, the diffusion model is linked to the lens design program, CodeV™. [3] By coupling the model with CodeV's design algorithms, a designer has access to a range of glass compositions, diffusion temperatures, and diffusion times within a particular glass/salt system. This allows the user to optimize an index of refraction profile for its Δn, depth, and shape in terms of manufacturing process parameters. Therefore, a designer can choose a particular glass composition and then explore a range of profiles without spending time developing something that cannot be manufactured.

In the second part of this chapter, several lens designs using the diffusion model are presented. These are an axial gradient singlet, a radial gradient focusing rod, and gradient-index compact disc objective. For each lens system, the old method (using the index polynomial coefficients) and the new method (using manufacturing parameters) of design and optimization are compared. These examples demonstrate that the new diffusion model can be used for the design of a variety of optical systems utilizing both axial and radial gradients while guaranteeing that the designs can be manufactured using current ion exchange technology. Furthermore, the new diffusion model allows for studies on the tolerances of the various diffusion parameters such as time and temperature. Typically, studies of gradient tolerances have utilized the polynomial index of refraction coefficients and have been hard to relate to laboratory parameters. Thus, the new method gives manufacturers information about the tolerances on the process parameters required to fabricate the specific optical systems.

6.2 Linking the Model with CodeV

The diffusion model can be linked with CodeV's algorithms through a user-defined subroutine (called "usergrn") which takes in the coordinates of a particular ray (x, y, and z) and then returns the index of refraction at that point in the lens. The manufacturing parameters for a system are passed to the subroutine through a set of twenty coefficients. Then, the diffusion equation is solved and the solution is sent to an array of 250 points. The subroutine uses a linear interpolation between the two closest ray positions in the array to determine the index of refraction at a specific ray position. Furthermore, if a diffusion parameter (such as diffusion time) is changed in the lens design program, the subroutine re-solves the diffusion equation and the new solution is stored in the array. (In the ideal land of infinite computing power, a routine can be written which solves the diffusion equation at each specific ray point and eliminates the need for linear interpolation.)

The user-defined subroutine used in the following lens designs is listed in Appendix A and is based on the diffusion model that was developed in the previous chapters. The specific details of how to link the usergrn subroutine with CodeV can be found in the reference manuals. The specific parameters that must be defined by the subroutine are also listed in Appendix A. The subroutine is then accessed in CodeV through a private catalog entry which specifies a user-defined gradient by entering the values for the set of coefficients (C0-C20). The relation between these coefficients and the fabrication parameters is also listed in Appendix A.

6.3 Axial Gradient Singlet

6.3.1 Background

A homogeneous singlet with a relatively large aperture and small field of view is dominated by spherical aberration. In the past, aspheres, diffractive elements, and gradient-index lenses have been used to improve the optical performance of this type of lens. For example, placing a linear

axial gradient in a homogeneous singlet can correct the third order spherical aberration of the lens.

In this section, a homogeneous singlet is compared to an axial gradient to illustrate the effect of the gradient on spherical aberration. In particular, three different designs are examined for the following system specifications:

- 25 mm focal length,
- f#/ 2.5,
- half field of view of 1°,
- 4.0 mm thick lens, and
- the stop at the first surface.

First, a homogeneous singlet is designed, and then two axial gradient singlets are designed. The first gradient design uses the index polynomial coefficients to specify the gradient profile, while the second design uses the diffusion model for a titania silicate glass composition that was investigated in Chapter 5 to specify the gradient material. The index of refraction of the titania silicate glass is 1.598. For comparison purposes, the index of refraction of the homogeneous singlet is taken to be this value. In addition, the index polynomial gradient is designed to have a similar base index of refraction, maximum change in index of refraction, and diffusion depth as that which can be obtained in the titania silicate glass.

6.3.2   Homogeneous Design

First, the homogeneous singlet is designed by optimizing the first curvature to minimize spherical aberration while the second curvature is constrained by the required focal length of the lens. The result is shown in Fig. 6.1 (a). A CodeV listing of the lens is given in Appendix B.1. Figure 6.1 (b) shows the ray intercept plots (more commonly referred to as RIM plots) for half field of view angles of 0, 0.7, and 1 degree. The three plots on the left are generated by tracing tangential rays through the system. The horizontal axis is the normalized ray coordinate in the aperture, ρ, which extends from -1 to 1. The vertical axis is the transverse distance between the ray and the paraxial image point, which is given in millimeters. The three plots on right are similar plots but for the sagittal

rays. Thus, for a perfect lens, the vertical displacement is zero for all plots, and therefore any deviation from this axis indicates that there are aberrations present in the lens.

As expected, an analysis of the aberration plots show that this lens is dominated by third order spherical aberration. In particular, this lens shows a maximum deviation of ±200 μm at full aperture which is significantly larger than the diffraction limited spot diameter of 4 μm. Although defocus can be added to the lens to balance some of the spherical aberration and decrease the spot size, it is still not diffraction limited.

6.3.3 Index Polynomial Design

The linear axial gradient is represented by a two term polynomial consisting of the base index of refraction and a linear term in spatial coordinate given by

$$N(z) = N_{00} + N_{01}z \ .$$

(6.1)

For this design, the homogeneous singlet is used as a starting point and the glass material is replaced by a linear axial gradient. An additional flat dummy surface must be inserted between the first and second lens surfaces to act as a reference point for the end of the gradient profile so that it does not extend all the way through the lens. The material after the dummy surface is considered to be homogeneous and its index of refraction must be matched to the index of refraction immediately to the left of the dummy surface. Since the gradient profile is allowed to vary during optimization, care must be taken to ensure that these two values do in fact match.

In this particular design, the first curvature, the gradient coefficient of the first material N_{01}, and the index of refraction of the second material were allowed to vary during optimization while the second curvature was constrained by the required focal length of the lens. The boundary index of refraction for the first material was constrained to be 1.6448; this is the achievable index of refraction (after exchange) for the titania glass used in the diffusion model design in the next section. The thickness of each material was also constrained to be 2 mm.

The final design is listed in Appendix B.2.1. Figure 6.2 (a) shows a layout of the lens where the dummy surface in the middle indicates the depth of the gradient with respect to the front curvature of the lens. The index of refraction profile for the first material is shown in Fig. 6.2 (b). Figure 6.2 (c) shows the ray intercept plot for this lens. As expected, the third order spherical aberration is almost completely eliminated and the remainder is used to balance Petzval field curvature and astigmatism. Furthermore, the on-axis spot size of this lens, 2 μm, is well below the diffraction limit and the full field spot is approximately equal to the diffraction limit.

Thus, the addition of a linear axial gradient to a homogeneous singlet significantly improves the performance of the lens, thereby reducing the spot size to 4 μm from 400 μm and making the lens diffraction limited. The one problem with this type of design (as with any other index polynomial design) is whether or not the index of refraction profile can be fabricated. In many cases, it is difficult to find a glass composition and ion exchange pair that gives a linear index of refraction profile for a specific base index of refraction and Δn. As a result, many trial-and-error experiments are required to manufacture the profile. The index polynomial design is also complicated by the need for an extra non-physical "dummy" surface in the design and several extra constraints are required to match the two lens materials during optimization.
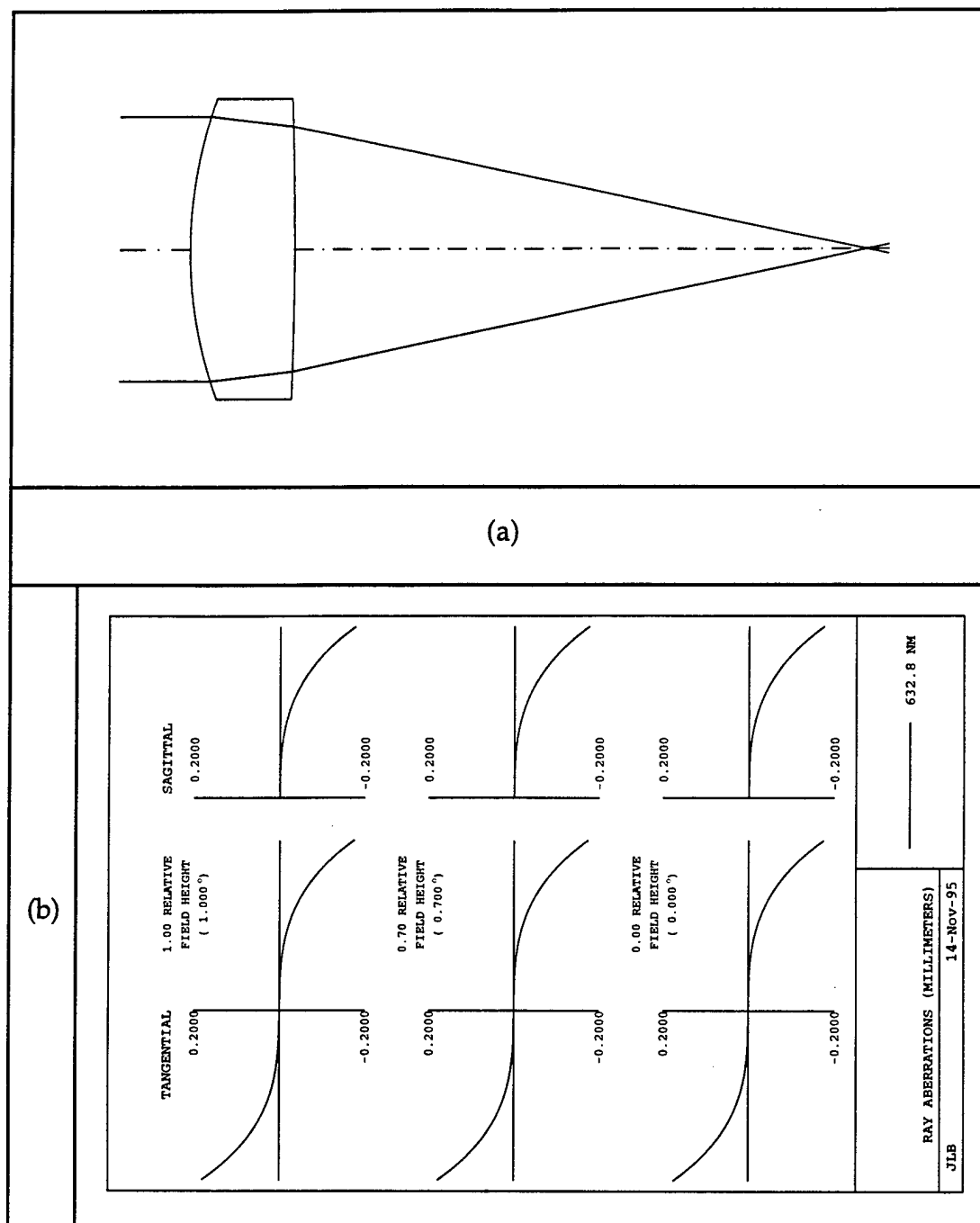
Figure 6.1 Homogeneous design for F/2.5, 25 mm focal length singlet where (a) is the lens layout and (b) is the ray intercept plots for field angles of 0, 0.7, and 1 degree.
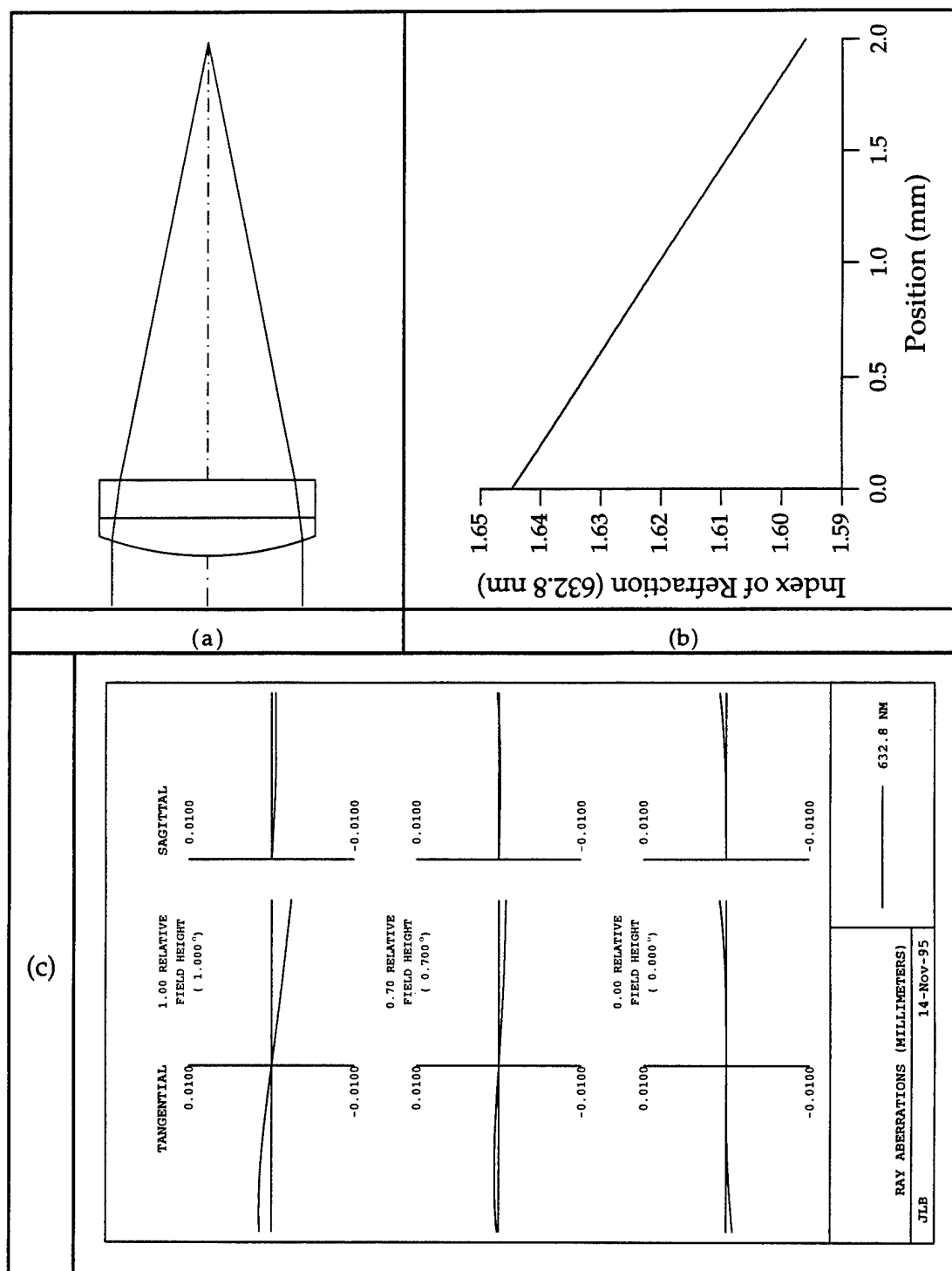
Figure 6.2 Axial gradient index polynomial design for F/2.5, 25 mm focal length singlet where (a) is the lens layout, (b) is the index of refraction profile and (c) is the ray intercept plots for field angles of 0, 0.7, and 1 degree.

6.3.4 Diffusion Model Design

In the second axial gradient design, the gradient-index glass material is specified by the user-defined gradient subroutine instead of the index polynomial. In particular, the titanium glass (RH-1A0068) discussed in Section 5.3 and its values for the concentration dependence of both the diffusion coefficient and the index of refraction are used. A CodeV listing of this lens can be found in Appendix B.2.2, and includes a list of the specific user defined coefficients (C1-C20) in the private catalog section (PVC). Note: this particular specification of the gradient material eliminates the need for a dummy surface.

During optimization, the first curvature and the diffusion time (coefficient C2) were allowed to vary while the second curvature was constrained by the required focal length of the lens. In addition, the thickness after the last surface of the lens was allowed to vary since a paraxial image solve (PIM) cannot be used with user defined gradients. [4] However, a "paraxial" ray can be defined and traced. Then, the thickness after the last surface is constrained during optimization to be the distance at which this ray crosses the axis in order to a find the paraxial image plane for lens evaluation.

Several different solutions were obtained during optimization which had equivalent image quality. Table 6.1 lists the diffusion time, the radius

Diffusion Time (hours)	Radius S1 (mm)	Radius S2 (mm)
4	21.78	-44.33
10	18.54	-70.76
15	17.34	-98.93
20	16.50	-144.52
25	15.12	-1198.65
28.47	14.95	Infinity
40	13.70	145.05

Table 6.1 Axial gradient diffusion model designs for F/2.5, 25 mm focal length singlet for several different diffusion times.
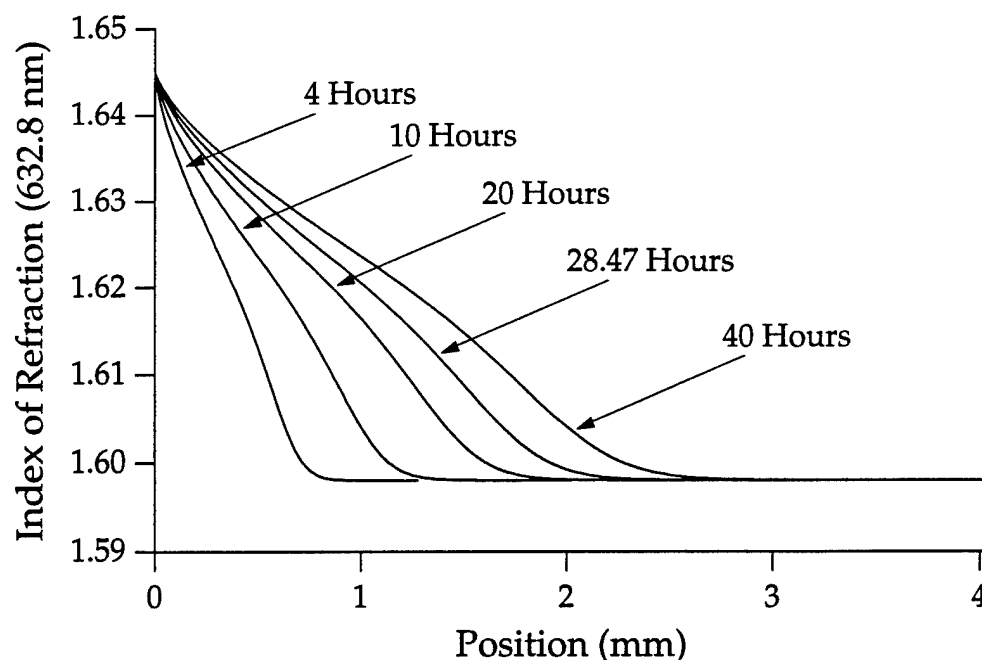
Figure 6.3 Index of refraction profiles for the lens design solutions given in Table 6.1.

of the first surface, and the radius of the second surface for these solutions. In particular, the diffusion time could be changed from 4 hours to 40 hours (with a corresponding change in the curvatures of the lens) and the image quality of the lens maintained. The index of refraction profiles for several of these solutions are shown in Fig. 6.3 demonstrating that as the diffusion time is increased the depth of the gradient profile increases in the lens.

Thus, a trend in lens curvature can be seen as a function of diffusion time (and therefore the depth of the gradient profile). In particular, the radius of the first surface decreases, while the radius of the second surface increases and then after a particular time changes sign. This indicated that a flat backed solution could be achieved. Therefore, in the final design, the radius of the second surface was constrained to be infinity and the lens optimized on diffusion time. The result is also given in Table 6.1 for a diffusion time of 28.47 hours. The lens layout for this solution is shown in Fig. 6.4 (a) and the index of refraction profile is shown in Fig. 6.4 (b).

Figure 6.4 (c) shows the ray intercept plot for this design. (Note: the other designs in Table 6.1 all had similar ray intercept plots.) The addition

of the axial gradient to the homogeneous singlet significantly improves the performance of the lens (reducing the spot size to 20 μm from 400 μm), but, since the profile is not completely linear, the lens is still dominated by spherical aberration. Although this particular lens is not diffraction limited, previous researchers have attained linear profiles in different glass compositions and therefore much better lens performances. [5]

This example illustrates the usefulness of the new diffusion model. First, the diffusion time for a solution with only a single curved surface is easily determined. In addition, a wide range of diffusion times was explored, and it was concluded that for these particular lens specifications, a diffraction limited lens could not be obtained in this glass composition. In the past, several trial and error experiments were required in which, a diffusion was performed, the index profile measured and fit to an index polynomial, and then entered into a lens design program and evaluated. Although some intuition can be gained from previous experiments, this is still a very time-consuming process. Furthermore, the polynomial needed to fit index of refraction profiles like the ones shown in Fig. 6.3 requires a large number of terms (8-10) and is not very accurate, thereby reducing the accuracy of the lens performance evaluation.
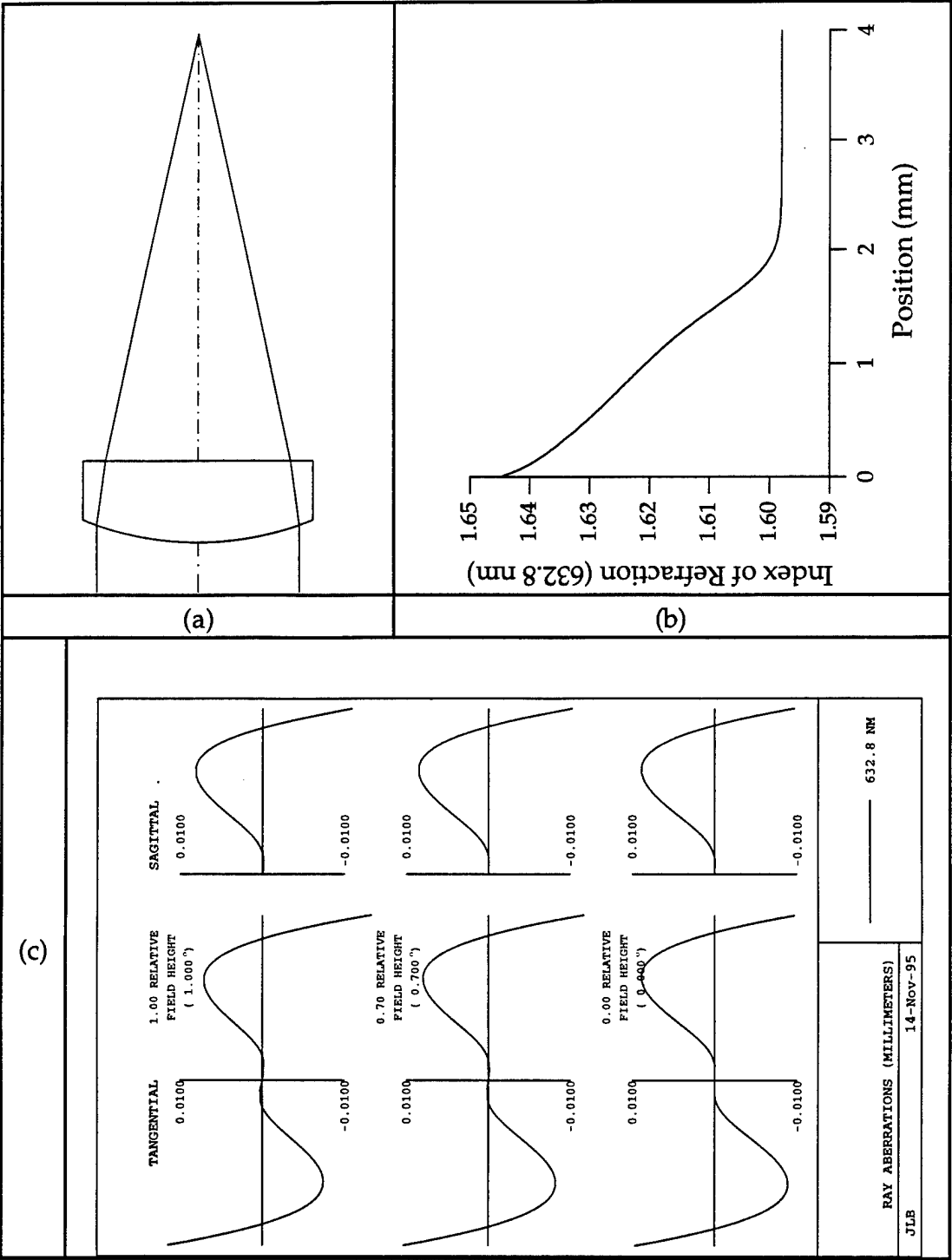
Figure 6.4 Axial gradient diffusion model design for F/2.5, 25 mm focal length singlet where (a) is the lens layout, (b) is the index of refraction profile and (c) is the ray intercept plots for field angles of 0, 0.7, and 1 degree.

6.4 Radial Gradient Focusing Rod

6.4.1 Background

As discussed in Chapter 1, radial gradients with flat surfaces can be used as imaging lenses since the radial gradient profile has the ability to introduce optical power into the lens system. For example, the index of refraction variation is often expressed as an even-ordered polynomial in r, the radial distance from the optical axis, as

$$N(r) = N_{00} + N_{10}r^2 + N_{20}r^4 + \dots \ . \tag{6.2}$$

Then, in a thin lens approximation, the optical power introduced by the gradient can be written as

$$\Phi_{grin} = -2N_{10}t \ , \tag{6.3}$$

where t is the thickness of the element measured along the optical axis.

Rays in long gradient-index imaging rods traverse sinusoidal paths within the material. The height of the ray at positions along the optical axis is given to first order by

$$y(z) = \frac{\theta_0}{\alpha}\sin(\alpha z) + y_0 \cos(\alpha z) \tag{6.4}$$

where

$$\alpha = \sqrt{\left|\frac{2N_{10}}{N_{00}}\right|} \tag{6.5}$$

and y_0 and θ_0 are the initial ray height and slope, respectively. [6] A pitch length, P, is defined as the length required for the rays to complete one full period where

$$P = \frac{2\pi}{\alpha} = \pi\sqrt{\left|\frac{2N_{00}}{N_{10}}\right|} \ . \tag{6.6}$$

Depending on the application, these rods are sold in multiples of pitch length, such as 1/4, 1/2, or 3/4 pitch. [7]

6.4.2 Index Polynomial Design

In this section, a (nominally) 1/4 pitch focusing rod is designed using an index of refraction polynomial for a radial profile given by

$$N(r) = N_{00} + N_{10}r^2 + N_{20}r^4 \qquad (6.7)$$

which has three index polynomial coefficients. The base index of refraction, N_{00}, is chosen to be comparable to that of the alumina silicate glass composition used in the following section for the diffusion model design. The thickness of the rod is set at 40 mm and an approximate starting value for the N_{10} coefficient can be obtained using Eq. (6.11). Therefore, the N_{10} coefficient of the index of refraction profile is set by the power required for the system, but the remaining coefficient, N_{20}, is free for aberration correction. For example, N_{20} can be used to cancel the under-corrected third order spherical aberration of the rod which requires a positive value for N_{20}. [8]

In this design, the lens was optimized for an image distance of 2 mm by allowing the two index coefficients to vary while the thicknesses were kept constant. A CodeV listing of the final lens is given in Appendix B.3.1 which includes the values for the index coefficients. The layout of the lens for this solution is shown in Fig. 6.5 (a) and the index of refraction profile is shown in Fig. 6.5 (b). In particular, a very small N_{20} coefficient (6.415×10^{-7}) is required by the design, such that the final index of refraction profile is very nearly parabolic. In addition, the value for the N_{10} coefficient (-0.001013) is close to the original value calculated with the pitch length equation. Figure 6.5 (c) shows the ray intercept plots for this design and shows that the N_{20} coefficient was used to correct the spherical aberration of the lens. At an image height of 1 mm, the spot size is approximately 4 μm which is much smaller than the diffraction limited spot size (9.5 μm).

227
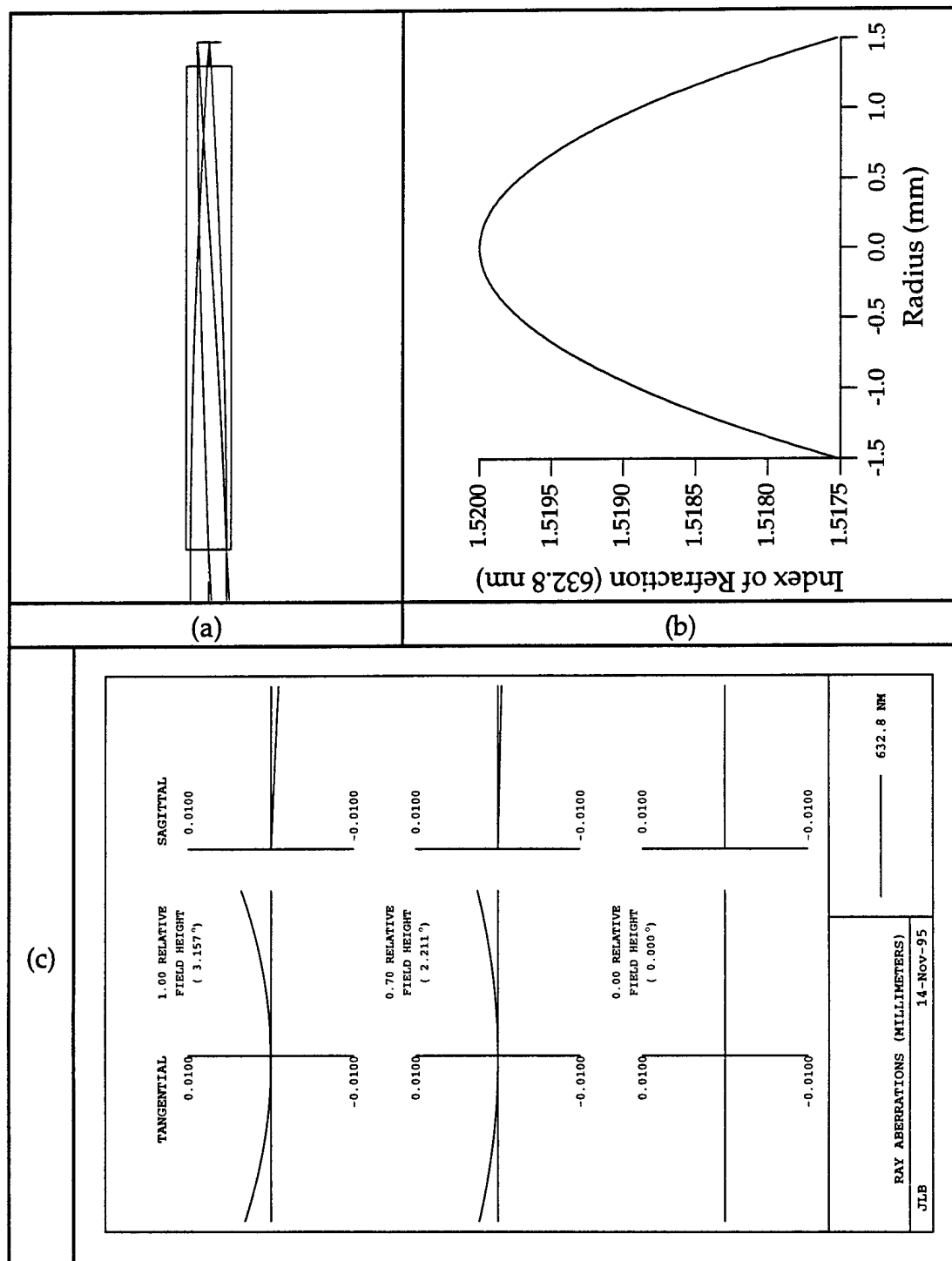
Figure 6.5 Radial gradient index polynomial design for 1/4 pitch, F/6 focusing rod where (a) is the lens layout, (b) is the index of refraction profile and (c) is the ray intercept plots for field heights of 0, 0.7, and 1 mm.

6.4.3 Diffusion Model Design

In the second radial gradient design, the gradient-index glass material is specified by the user-defined gradient subroutine instead of the index polynomial. In particular, an aluminum silicate glass composition (JBGL-16) which was discussed in Section 4.2 and its values for the concentration dependence of both the diffusion coefficient and the index of refraction are used. A CodeV listing of this lens can be found in Appendix B.3.2, and includes a list of the specific user-defined coefficients (C1-C20) used in the design in the private catalog section (PVC).

To determine a good starting solution for the design (and also for a check of the diffusion model design), a series of index of refraction profiles for different diffusion times was generated. Several of these profiles are shown in Fig. 6.6. Then, each profile was fit to a second order polynomial and the contribution to the total Δn calculated. For example, the contribution from N_{10} is given by

$$\frac{\Delta N_{10}}{\Delta N} = \frac{N_{10} r_{max}^2}{N_{10} r_{max}^2 + N_{20} r_{max}^4} \tag{6.8}$$

where r_{max} is the maximum radius of rod (equal to 1.5 mm for this particular design). These contributions are plotted in Fig. 6.7 as a function of diffusion time. Therefore, the diffusion time which should produce a parabolic index of refraction profile (for which the contribution to the total Δn from the N_{10} coefficient is one) is approximately 105 hours. Furthermore, the diffusion time must be increased from this value to obtain the positive N_{20} coefficient required to correct the third order spherical aberration of this lens.

Therefore, the diffusion time (coefficient C2) was allowed to vary during optimization. Also, similar to the axial gradient, the thickness after the last surface of the lens was allowed to vary since a paraxial image solve (PIM) cannot be used with user-defined gradients. However, a "paraxial" ray was defined and the thickness after the last surface was constrained during optimization to be the distance at which this ray crosses the axis to find the paraxial image plane for lens evaluation.

Several different starting points were chosen (for diffusion times ranging from 30 to 150 hours) which all converged to the same solution for a diffusion time of 112.7 hours. The final lens layout is shown in Fig. 6.8 (a) and the index of refraction profile for this design is shown in Fig. 6.8 (b). The ray intercept plots for this design are shown in Fig. 6.8 (c). The lens is not nearly as good as the polynomial design. The reason for this is that a second order polynomial fit to the index of refraction profile yields residual error between them. The profile can be fit significantly better with a higher order polynomial. These higher order coefficients then contribute higher order aberrations to the design which are then balanced with the third order aberrations as shown in Fig. 6.8 (c).

A tolerance of the diffusion time can be examined by investigating a change in the diffusion time to 100 hours and reoptimizing to the paraxial image plane. The result is listed in Appendix B.3.2.2 and shows that the pitch length of the rod has changed by approximately 2 mm. Figure 6.9 (a) shows the ray intercept plot for this design. A diffusion time of 120 hours was also examined and the result is listed in Appendix B.3.2.3. Figure 6.9 (b) shows the ray intercept plot for this design. Thus, in addition to changing the pitch length of the rod, a change in diffusion time of 10 hours increases the spot diameter by almost a factor of ten. Furthermore, both solutions are dominated by spherical aberration but the sign changes as it passes through the diffusion time which gives the minimum spot size solution.

Finally, a different glass composition in this glass composition series was examined. The first glass had a normalized lithium concentration of $\chi=0.5$ while the second glass had an even larger value of $\chi=0.7$. Therefore, it is expected that it should take a longer amount of time to reach a nearly parabolic solution in the second glass composition. As shown in Fig. 6.10, the index of refraction profile which is obtained after optimizing the lens for diffusion time is the same as the one in the first glass composition and in fact gives the same lens performance. However, it takes approximately five hours longer in diffusion time to fabricate the second index of refraction profile.
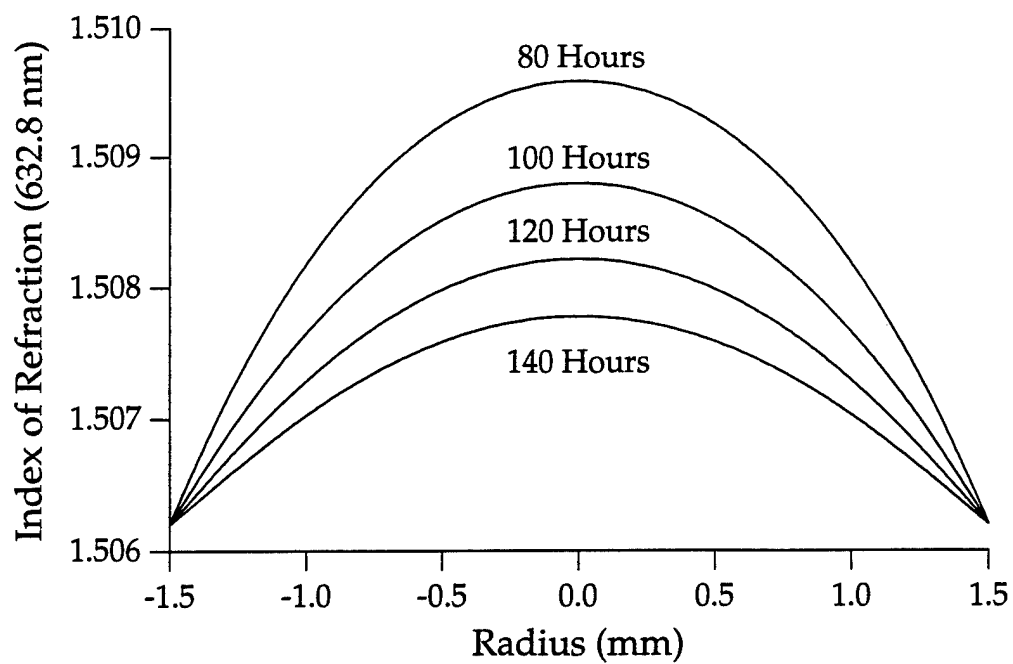
Figure 6.6 Index of refraction profiles for the 1/4 pitch radial gradient focusing rod
calculated for series of different diffusion times.
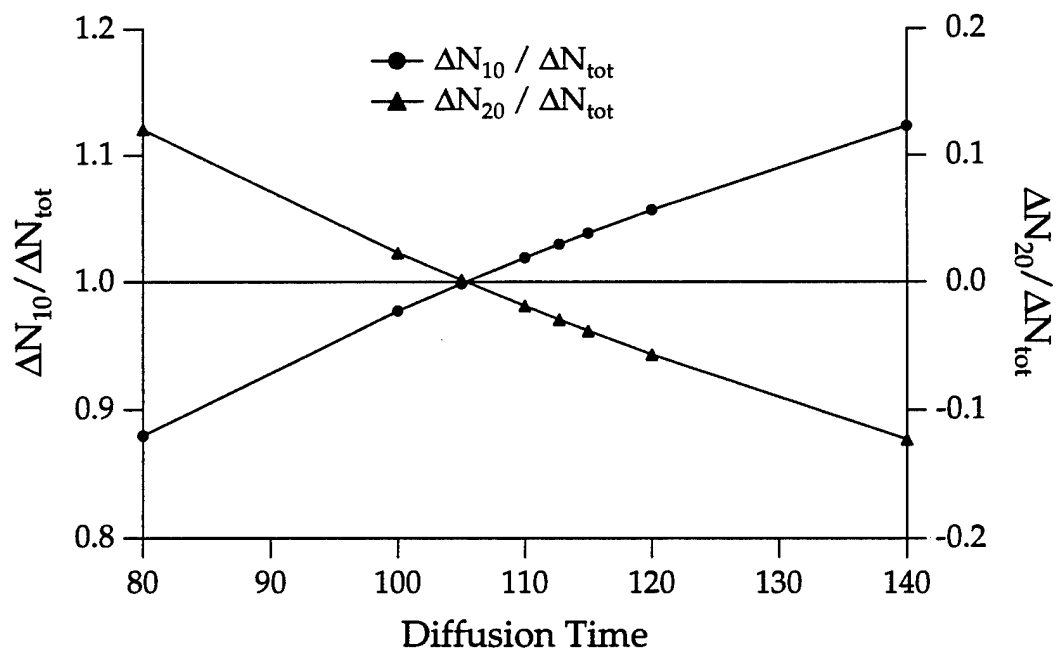
Figure 6.7 Contribution of the index polynomial coefficients to the total Δn as function of
diffusion time.
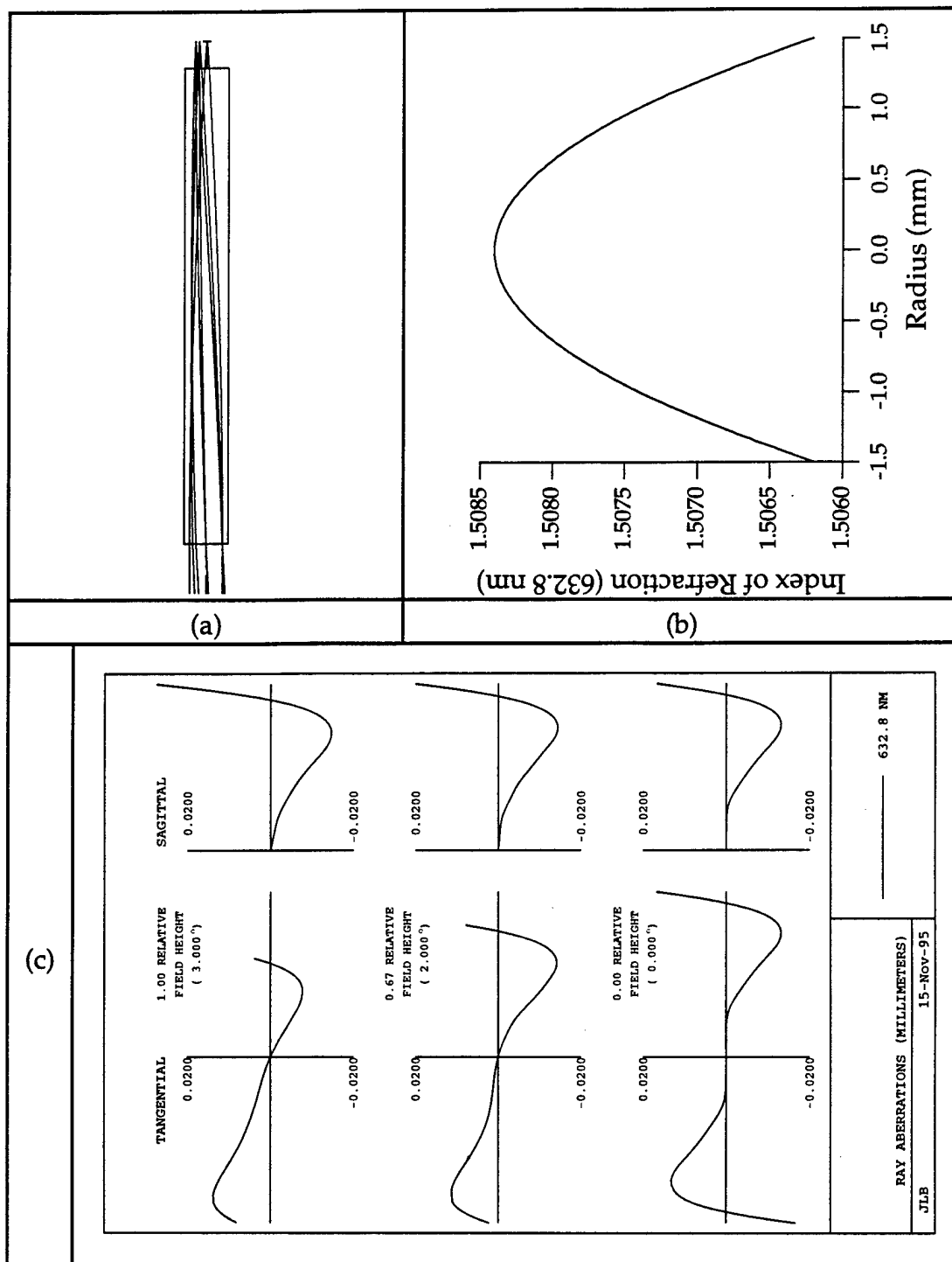
Figure 6.8 Radial gradient diffusion model design for 1/4 pitch, F/6 focusing rod where (a) is the lens layout, (b) is the index of refraction profile and (c) is the ray intercept plots for field heights of 0, 0.7, and 1 mm.
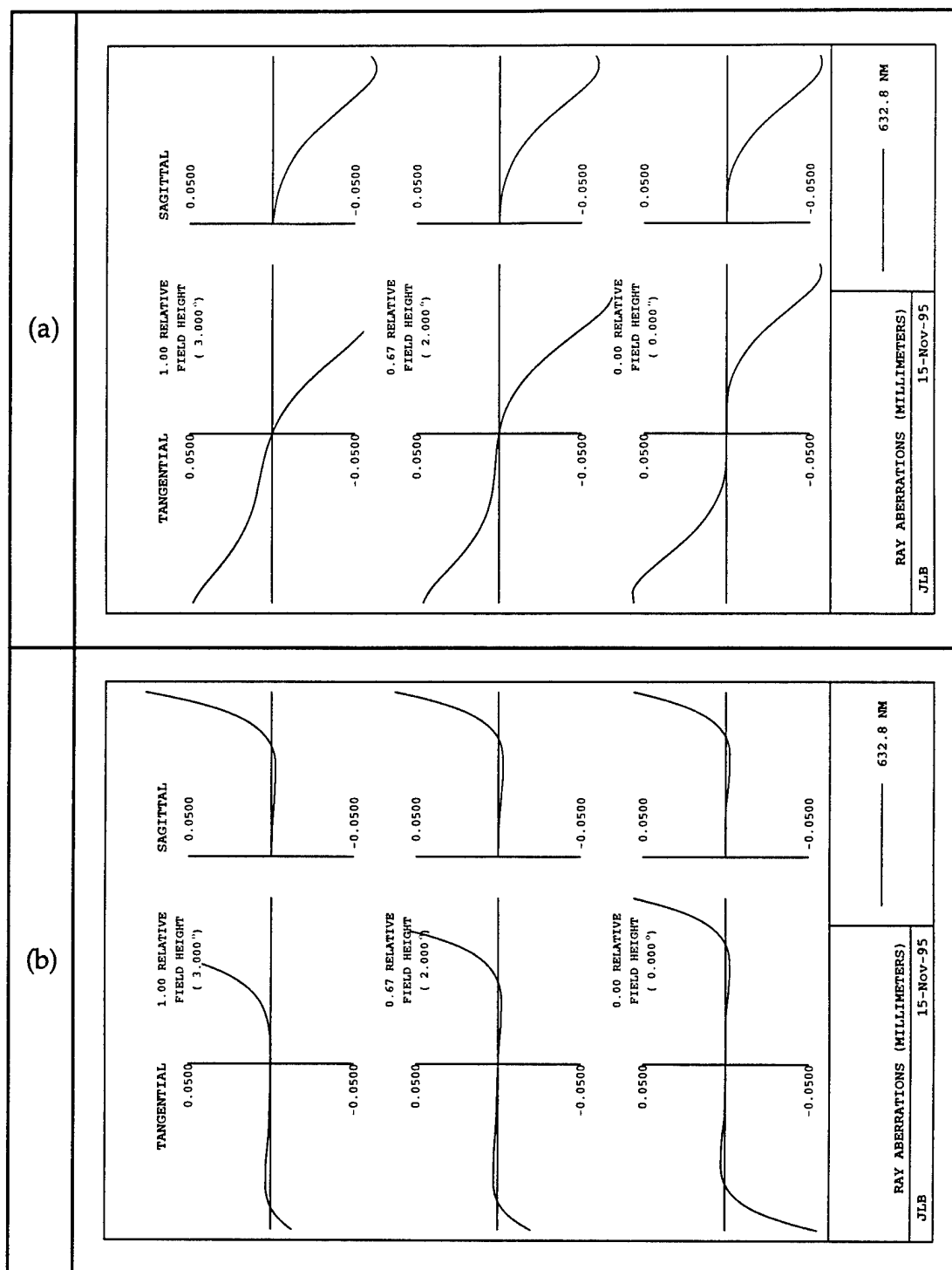
Figure 6.9 Ray intercept plots for radial gradient diffusion model design for 1/4 pitch, F/6 focusing rod where (a) is for 100 hour diffusion time and (b) is for 120 hour diffusion time.
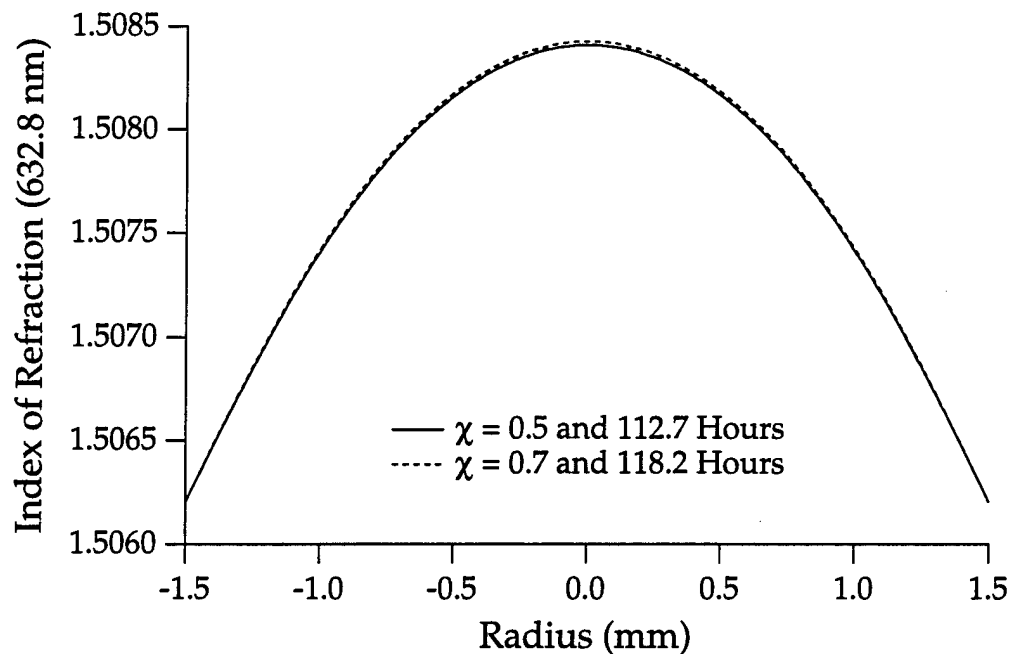
Figure 6.10 Index of refraction profiles for the 1/4 pitch radial gradient focusing rod for two different glass compositions.

6.5 Compact Disc Objective

6.5.1 Introduction

The major commercial application of a compact disk system is the play back of prerecorded music. Audio signals are recorded on optical disks in digital form. The disk's spiral track consists of a series of pits. Each pit has a depth which is approximately a quarter of the wavelength of the incident light. When light falls on an interval between two pits, it is almost completely reflected; when it lands in a pit, interference causes less light to be reflected. Thus, reflectivity sensing optical heads can detect a written mark on a disk from changes in the amplitude of the reflected light.

The high density of information stored on the disk places strict imaging requirements on the compact disk pick-up objective. As the laser scans the disk, the objective must be able to focus the beam into a spot less than a micron in diameter. [9] Aberrations reduce the central intensity of

this spot which makes it more difficult to read information, degrades focus and tracking servo, and may allow crosstalk between adjacent tracks. Thus, it is important that the lens exhibit diffraction limited axial imaging and yet, for this application, still be compact, light-weight, and inexpensive.

Most of the current objective designs can be placed into three general categories—multi-element homogeneous spherical designs, bi-aspherical singlets, and gradient index singlets. Any homogeneous design using only spherical surfaces must have at least three elements to meet the imaging requirements such as in the standard Olympus triplet design. [10] Since any reduction in the mass of the lens makes the control of the optical head easier and less expensive, two alternative singlet designs were developed.

The first alternative uses molding techniques to form biaspheric singlets in both plastic [11,12] and glass [13,14]. Plastic tends to be easier to mold but it can suffer from a thermally induced wavefront distortion. [15] In another approach, gradient-index mediums have been utilized in several different designs of singlets. [16,17,18] Most are radial gradients with spherical surfaces on one or both of the surfaces. Either of the two alternatives provides reduced weight and physical size due to its singlet design, but may add increased production costs or have less environmental stability.

In 1990, a third alternative to the existing systems was designed and fabricated by this author which reduced the number of elements in the conventional homogenous triplet without the use of aspheres or gradient elements with spherical surfaces. [19] The design consists of two elements, the first is a plano-plano radial gradient-index lens and the second is a homogeneous element with spherical surfaces. The index polynomial was used in the design procedure to specify the gradient material and constrain the index of refraction profile so that it could be fabricated using ion exchange. However, since the index polynomial coefficients were unrelated to the specific process parameters, an experimental trial-and-error procedure was used to fabricate the gradient profile. This process took approximately six months and several experiments to complete.

A summary of the previous design of the gradient-index compact disk objective and the results of the gradient-index element fabrication are presented in this section. Furthermore, the design to manufacture procedure used to fabricate this lens is discussed and used to illustrate the type of fabrication process that has been applied to gradient-index lens systems in the past. Then, this same lens system is designed with the diffusion model developed in this thesis and the results of this design are presented. Finally, the two methods (the original design and fabrication procedure and the new design-for-manufacture procedure) are compared.

6.5.2   Background

6.5.2.1   Standard System Requirements

The first-order specifications for a pick-up objective in an optical disk system are given in Table 6.2. A relatively large numerical aperture of at least 0.45 with diffraction limited performance over a small field angle (approximately 1°) is required. "Diffraction limited" in these applications is quantitatively defined by the Marechal criterion. This corresponds to an RMS wavefront error less than 0.07 waves over an image field radius of 75 microns. To satisfy these imaging requirements, a design must correct

Wavelength	780 nm
Numerical Aperture (NA)	0.45 - 0.55
Effective Focal Length (Objective)	< 4.5 mm
Disk Thickness	1.2 mm
Refractive Index of Disk	1.57
Working Distance	> 1.5 mm
RMS Wavefront error (OPD)	< 0.07 λ
Image Field Radius	0.075 mm

Table 6.2 The first-order specifications for a standard pick-up objective found in an optical disk system.

spherical aberration and coma. The effective focal length of the objective need not be constant (only the NA is specified), but it is generally less than 4.5 mm to keep the system compact.

A 1.2 mm thick transparent layer protects the information stored on the disk. This layer is usually a polycarbonate substrate with a refractive index of 1.57. Since the beam must travel through this layer, the design must also correct for the spherical aberration introduced by this disk cover. Furthermore, the working distance between the disk and the objective must be larger than 1.5 mm.

Additional design restrictions were imposed due to fabrication and testing limitations. First, although the laser wavelength commonly used is 780 nm, the design was corrected at 632.8 nm for ease in the measurement of the refractive index profile. Thus, the design was used to prove the principle; but the system must be redesigned for 780 nm for use in an actual compact disk player. Second, because of limits imposed by ion exchange, additional restrictions were set on the gradient's base index and the entrance pupil diameter of the system.

6.5.2.2 Single Wood Lens Solution

At the first stage of design, one might consider a single Wood lens [20], with a radial index profile given by:

$$N(r) = N_{00} + N_{10}r^2 + N_{20}r^4 + N_{30}r^6 + \cdots \tag{6.9}$$

where $N(r)$ is the refractive index of the medium at a radius r from the optical axis, N_{00} is the base index, and N_{10}, N_{20}, N_{30}, etc. are the refractive index coefficients. The significant problem with this design is that although spherical aberration can be corrected by proper optimization of the index coefficients, no remaining degree of freedom exists for coma correction. Thus, the coma makes the field of view too small for use as a compact disk objective.

6.5.2.3 Single Wood Lens with Corrector Element

To add the needed degree of freedom, a curve can be placed on the gradient element, but difficulty in the manufacture of this design can

result from severe tolerances on surface tilts (the surfaces must be aligned to the gradient's axis of symmetry).

A second solution was reported by Caldwell [21]. The design utilizes the fact that a single Wood lens with a parabolic index profile, stop shifted to eliminate coma, is dominated by spherical aberration. This can be corrected by a second thin, powerless (no N_{10} term in the refractive index profile), Wood lens placed at the stop (similar to a Schmidt corrector plate). Because the corrector is thin and placed at the stop, it has little effect on the off-axis aberrations. The performance of this lens is excellent with an RMS wavefront error less than 0.02 λ at an image height of 75 microns. The system is limited only by higher order spherical aberration. Fabrication of this design was considered, but the Δn required by the second element (-0.08) could not be produced in our laboratory.

6.5.3 Design with the Index of Refraction Polynomial

Since the second element in Caldwell's design could not be fabricated, it was replaced with a homogenous element having only spherical surfaces. The resulting design is shown in Figure 6.11. The system has a numerical aperture of 0.45 and a focal length of 4 mm. The aperture stop is located at the first surface and the working distance between the lens and the disk is 2.4 mm. A list of the lens specifications including the index of refraction polynomial coefficients is given in Appendix B.4.1.

The gradient was optimized using three refractive index coefficients N_{20}, N_{30}, N_{40}; N_{10} was not used to keep the element powerless. In the initial design, the homogeneous element was first bent for zero coma. Then the remaining undercorrected spherical aberration introduced by homogeneous lens could be corrected by optimizing the index coefficients of gradient.

In comparison with Caldwell's design, the overall length of the objective is much smaller and has been reduced to less than 3 mm. In addition, during the optimization of the design the best performance was obtained when the two elements were placed in contact with each other. This is due to the fact that the homogeneous singlet contributes more undercorrected spherical aberration than the second Wood lens in

1.0 MM
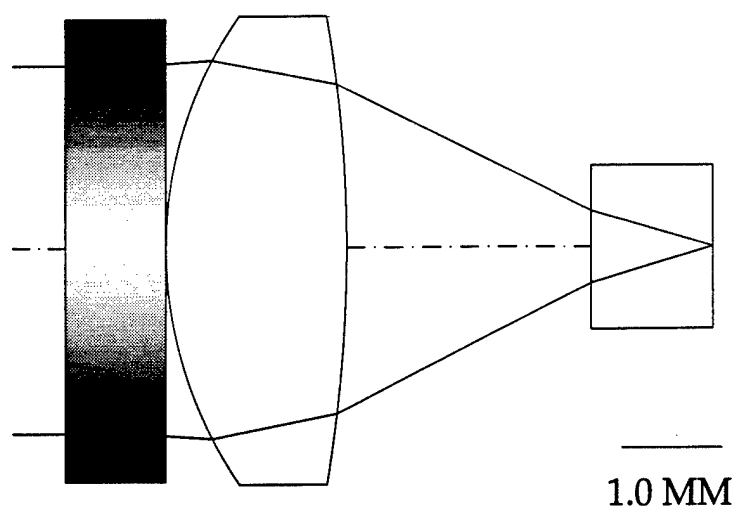
Figure 6.11 Gradient-index compact disk objective designed with the index of refraction polynomial.

Caldwell's design. Thus the stop shift necessary to correct for coma is smaller. The fact that there is no longer any distance between the two elements not only decreases the objective's total length but also makes both alignment and mounting of the lens elements easier.

A high index glass (n_d = 1.8) was chosen for the homogeneous element for shallower curves. The base index of the gradient was chosen after comparing the profile of the first element in Caldwell's design with recently fabricated profiles in a titania flint glass which was developed for ion exchange purposes. [22] This glass has a refractive index of 1.667 and after ion exchange a Δn = 0.02.

The OPD RMS wavefront error versus paraxial image height for this lens is shown in Fig. 6.12. The lens meets the imaging requirements stated earlier. When compared to a homogeneous triplet design, [23] it has better performance on-axis and up to an image height of 75 microns, but beyond this the triplet is better. However, this is not a problem, since the required field of view for this application is only 75 μm.

The thickness of the Wood lens and the entrance pupil diameter of the system were arbitrarily chosen to be 1 mm and 3.6 mm, respectively. However, both of these values can be changed over a certain range and a lens with equivalent performance can be obtained if the index of refraction profile is allowed to vary. For example, the required index of refraction
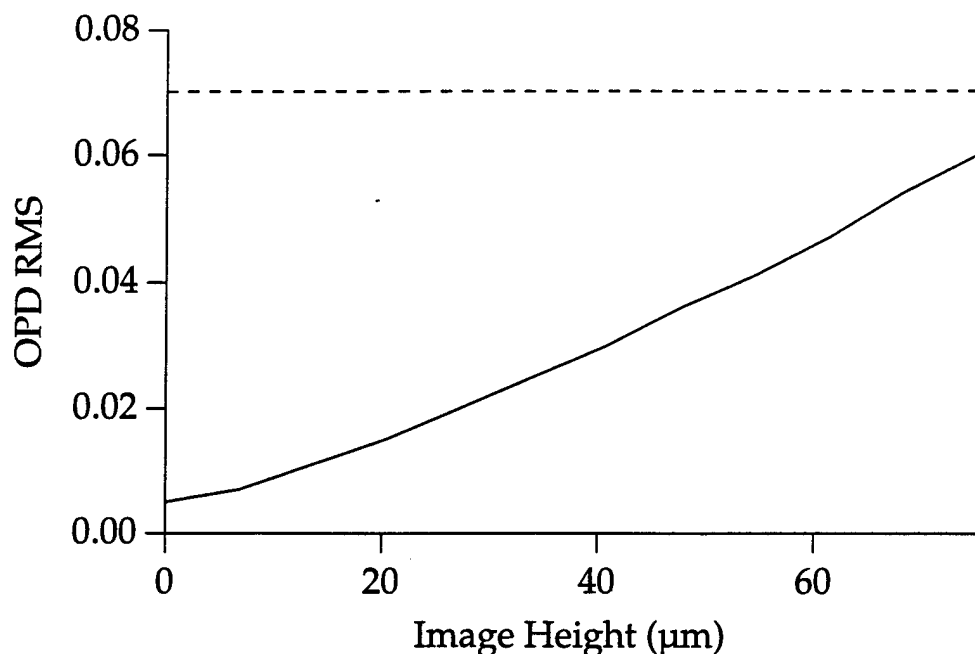
Figure 6.12 OPD for the gradient-index compact disk objective design using a 1 mm thick radial gradient. The Marechal criterion is indicated by the dashed line.

profile for a 1 mm thick, 1.4 mm thick, and 1.8 mm thick design is shown in Fig. 6.13. Similarly, the index of refraction profile for an entrance pupil diameter of 3.6 mm, 3.4 mm, and 3.8 mm is shown in Fig. 6.14.

Thus, an increase in the thickness of the lens decreases the required Δn of the index of refraction profile. Furthermore, as the EPD diameter is increased the "steepness" and overall shape of the profile can be changed. As a result, there exists a large number of index of refraction profiles which give the desired performance and these techniques are used to constrain the index of refraction profile to something that can be fabricated. For example, in the original 1 mm thick design the total change in refractive index is approximately 0.026 over a radius of 1.8 mm. Since this profile is still hard to fabricate in the particular glass composition which was chosen, the thickness of the Wood lens can be increased to 1.8 mm and the design reoptimized. This reduces the required Δn to 0.016 without any changes in the performance of the lens. Thus many solutions exist such that a compromise can be made between lens thickness and entrance pupil diameter and the achievable Δn and shape for the profile.
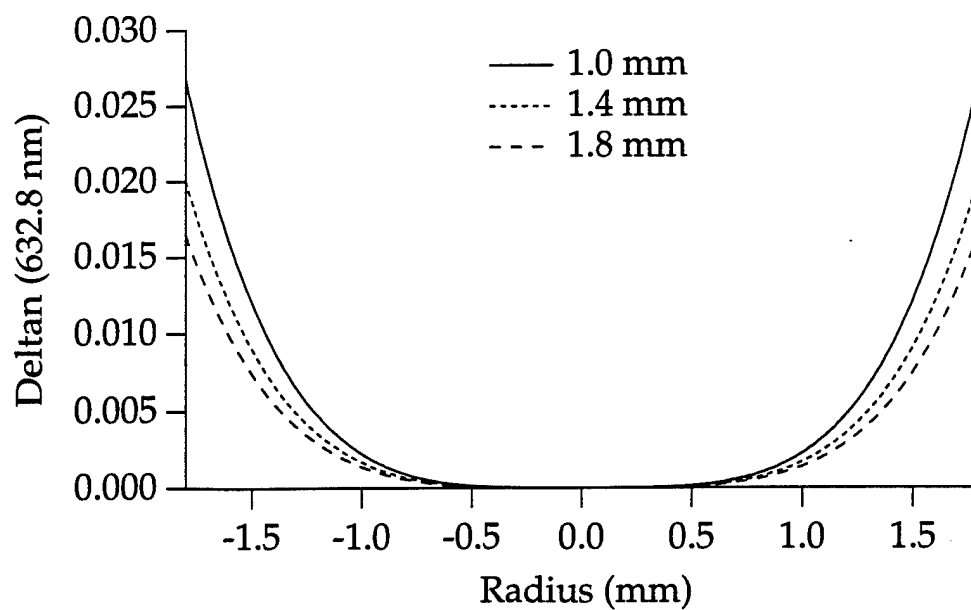
Figure 6.13 Index of refraction profile required for gradient-index compact disk design as a function of lens thickness.
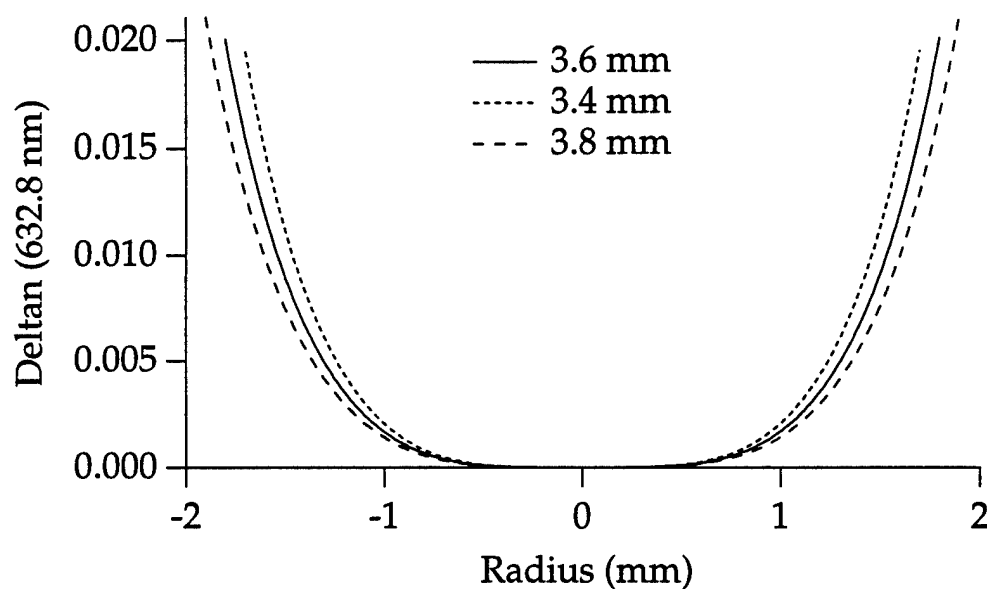
Figure 6.14 Index of refraction profile required for gradient-index compact disk design as a function of entrance pupil diameter.

6.5.4   Fabrication of the Index Polynomial Design

A titania flint glass with a composition of $0.20 \ TiO_2 + 0.10 \ Li_2O$ $+ \ 0.15 \ Na_2O + 0.55 \ SiO_2$ was melted for use as a base glass for the gradient. Then several attempts at fabricating the index profile were made using a lithium for sodium ion exchange in a 40 percent (by weight) lithium chloride, 60 percent calcium chloride salt bath. The diameter of the glass rods used for the diffusion varied from 4.5 - 5.0 mm. The diffusion times ranged from 11 to 24 hrs; the diffusion temperature was set at 550° C. The index of refraction profiles were measured at a wavelength of 0.6328 μm.

Thus a series of diffusion times and rod diameters were tried in an attempt to fabricate the required index of refraction profile. For example, in a 5 mm rod a diffusion time of 24 hours was used in the first fabrication attempt. The measured index of refraction profile from this sample is shown in Fig. 6.15. When compared to the desired profile, the N_{10} term was large. In the second attempt the diffusion time was shortened to 12 hours and the measured index of refraction profile is also shown in Fig. 6.15. Thus, decreasing the diffusion time considerably decreased the N_{10} term making the profile much less parabolic and therefore closer to the desired profile.

Although the general shape of this second profile is close to the desired profile, the homogeneous region in the center of the rod is much smaller for the desired profile. This observation led to several more attempts using glass rods with smaller diameters. For example, shown in Fig. 6.16 are three 12 hour diffusions for different rod diameters from 5.0 mm to 4.5 mm. These profiles are similar to the ones shown in the design section for a variation in the entrance pupil diameter of the system.

After ion exchange, the glass rods had a small devitrified layer on their surface, but this devitrification was not constant for each experiment and varied in thickness from 0.3 to 0.5 mm. Thus, many attempts were required to achieve a suitable index profile because it was difficult to calculate the exact diameter of the rod that was needed. This problem was not eliminated, but could be reduced by using new salts and a new oven. The gradients also had a tendency to crack 1 or 2 days after the diffusion

was finished in approximately 50% of the experiments. This could be caused by excessive stress due to differential thermal expansion from a crystalline layer on the glass host.

The final lens system is given in Appendix B.4.2 and the index of refraction profile is shown in Fig. 4.17. This profile was obtained from a 4.7 mm rod for a diffusion time of 11 hrs 45 min. The optimum design profile is also shown in Fig. 4.17. A comparison between the two profiles shows that the fabricated index profile has the same general shape as the desired profile up to a clear aperture of approximately 3.5 mm. Beyond this the profile is too steep. Therefore, to check the performance of the lens, the index of refraction profile was fitted to an 8th degree polynomial using a least squares fit. These coefficients were then placed back into the original design and the entire design was reoptimized keeping the coefficients constant. The thickness of the gradient had to be increased from 1 mm to 1.6 mm because of the lower Δn in the fabricated profile.

At a numerical aperture of 0.45 the performance of the lens is insufficient as shown by Fig. 4.18. The lens had to be stopped down to a numerical aperture of 0.4 to meet the imaging requirements (also shown in the figure). Thus after many experiments the fabricated design is not quite as good as the original design. In addition, the design to manufacture process took approximately six months to complete; after each experiment the index of refraction profile had to be measured, fit to a polynomial, entered into a lens design program, evaluated, and reoptimized.
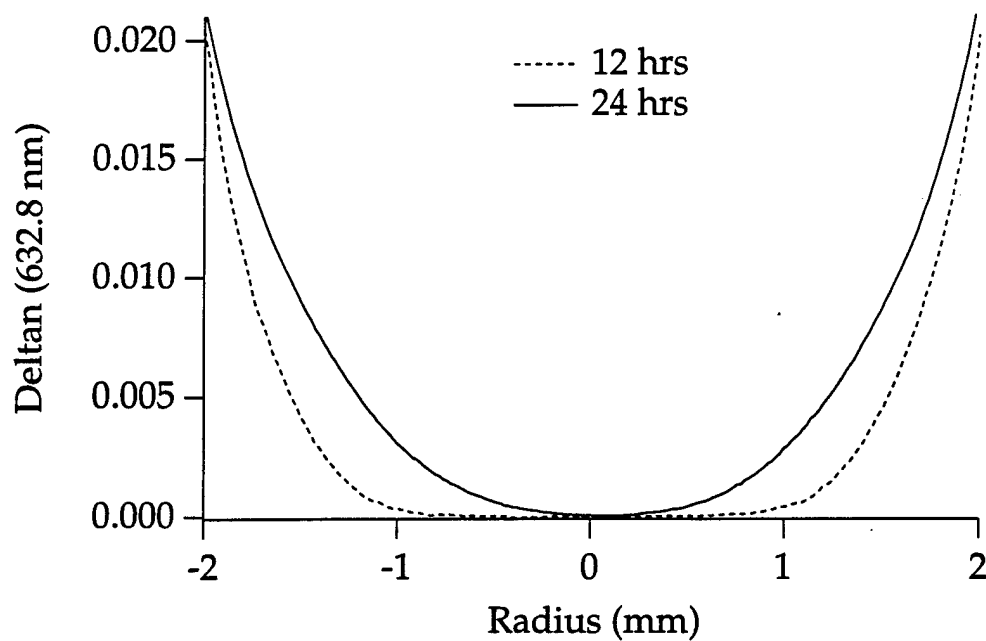
Figure 6.15 Measured index of refraction profiles for the gradient-index compact disk design for two different diffusion times.
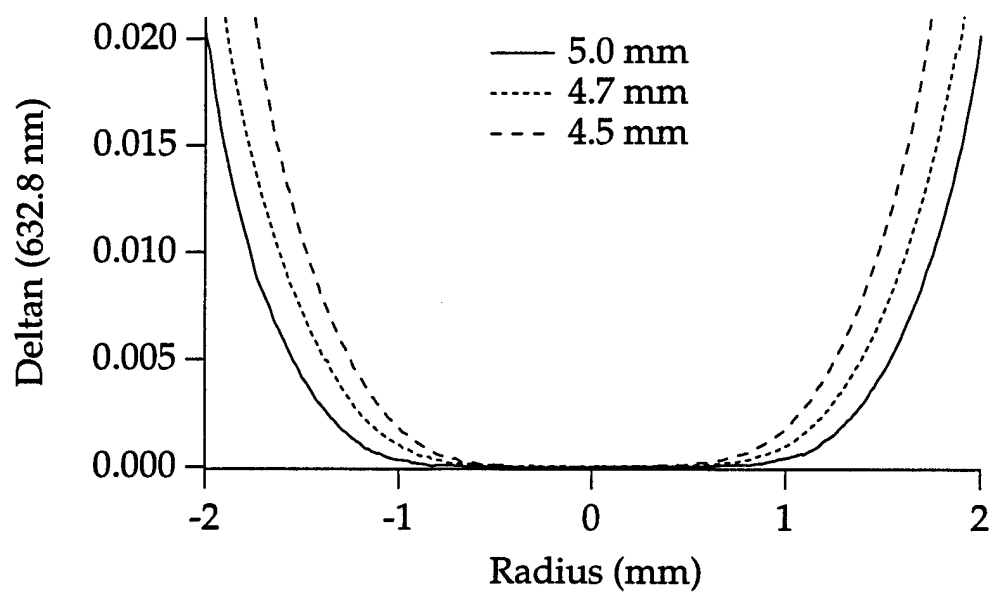
Figure 6.16 Measured index of refraction profiles for the gradient-index compact disk design for three different rod diameters.
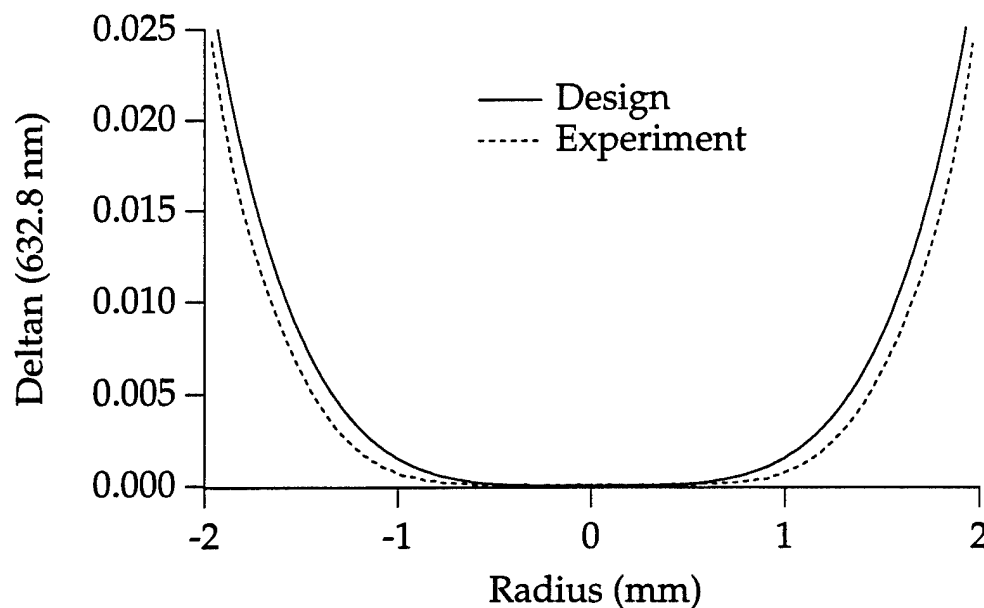
Figure 6.17 A comparison of the final measured index of refraction profile for the gradient-index compact disk with the original index polynomial designed profile.
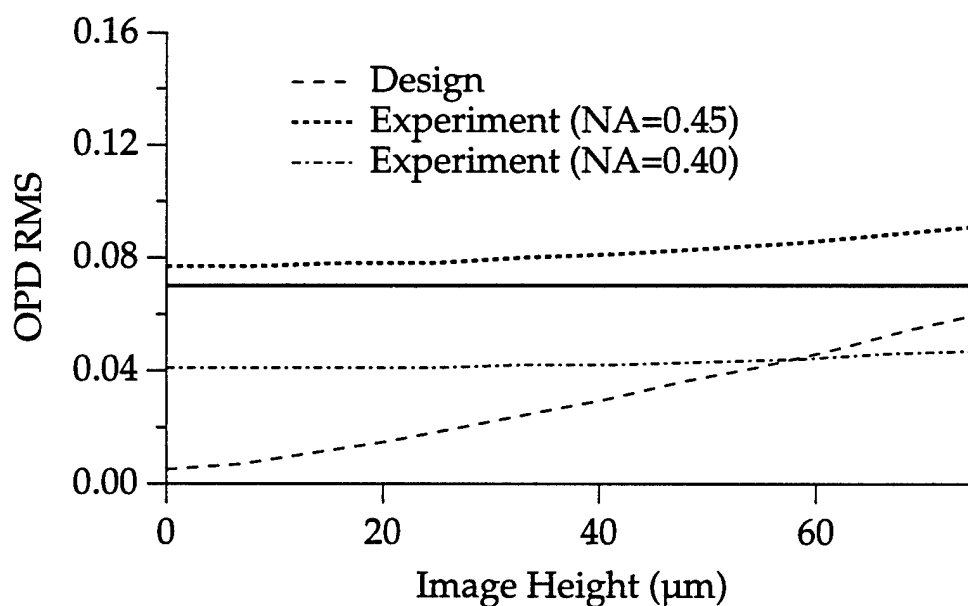
Figure 6.18 OPD as a function of image height for the gradient-index compact disk objective for both the design profile and the experimental profile at a numerical aperture of 0.45 and 0.40. The Marechal criterion is indicated by the solid line.
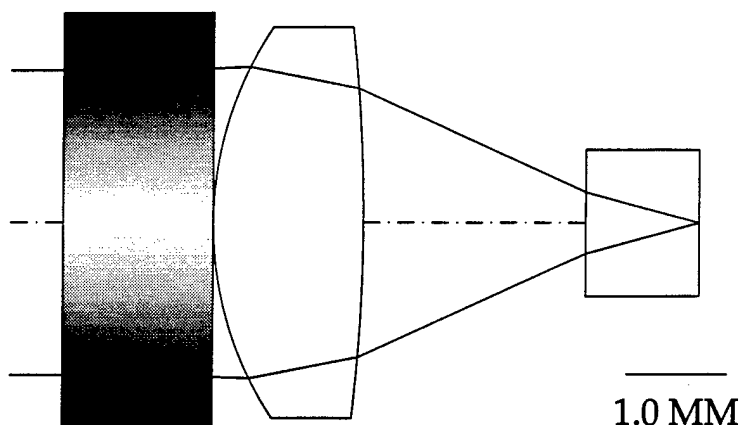
Figure 6.19 Gradient-index compact disk objective designed with the diffusion model.

6.5.5   Design with Diffusion Model

In the second radial gradient design, the gradient-index glass material is specified by the user-defined gradient subroutine instead of the index polynomial. However, the twenty percent titania glass composition used to fabricate the lens in the previous section was not a composition that was studied in this dissertation. Therefore, the measured index of refraction profile from an axial gradient fabricated by Kindred (experiment DSK-42) in a similar glass composition (0.25 Na_2O + 0.20 TiO_2 + 0.55 SiO_2) was used to calculate the concentration dependence of the diffusion coefficient. The measured index of refraction profile, calculation of the diffusion coefficient, and fit to the MQC model are given in Appendix C. In addition, a CodeV listing of the final lens can be found in Appendix B.4.3, and includes a list of the specific user-defined coefficients (C1-C20) used in the design in the private catalog section (PVC).

The curvatures of the homogeneous lens, the thickness of the gradient, and the diffusion time (coefficient C2) were allowed to vary during optimization. The final lens layout is shown in Fig. 6.19 and the index of refraction profile for this design is shown in Fig. 6.20. The index of refraction profile for an index polynomial design with the same gradient thickness and entrance pupil diameter is also shown in Fig. 6.20. Thus,

the diffusion model solution is much closer to the index polynomial design than any of the trial and error experimental profiles in the previous section and it did not take nearly as long to find this solution. In addition, all of the experimental process parameters (such as diffusion time and rod diameter) required to fabricate the gradient are now contained within the design.

The performance of this lens is shown in Fig. 6.21 and shows that the lens meets the original specifications, however, it is not nearly as good as the index polynomial design. This illustrates one of the main problems with index polynomial designs (especially for radial gradient designs which use a large number of polynomial coefficients to specify the profile); an index polynomial design and a manufactured profile can appear to be very similar, however, very small changes in the coefficients of the design profile can improve the performance of the design yet these changes cannot be duplicated in the laboratory. Therefore, the performance of the final lens system is usually worse than the original polynomial design.
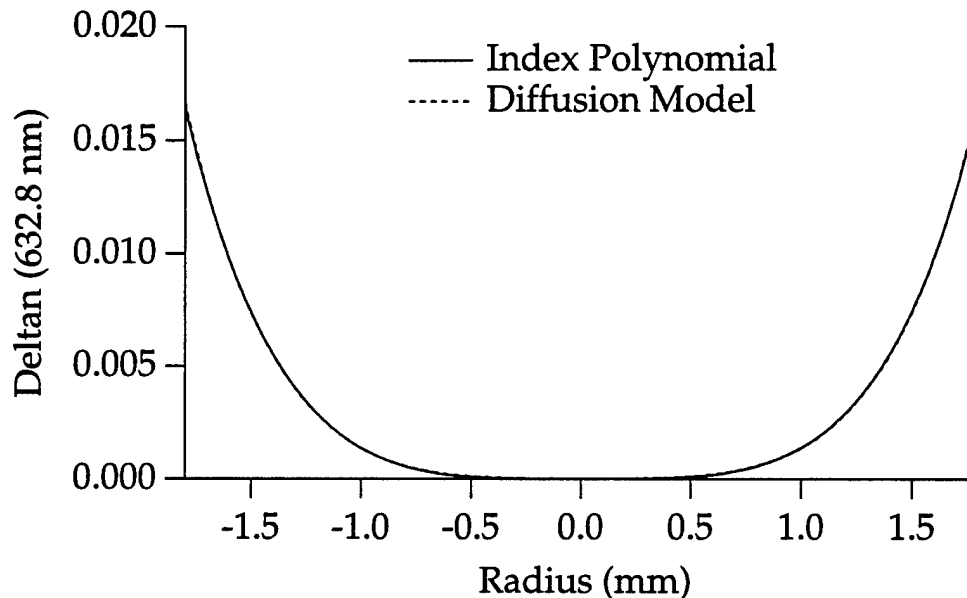
Figure 6.20 A comparison of the index polynomial design profile and the diffusion model design profile for a gradient-index compact disk objective with a 1.84 mm thick gradient element and an entrance pupil diameter of 3.2.
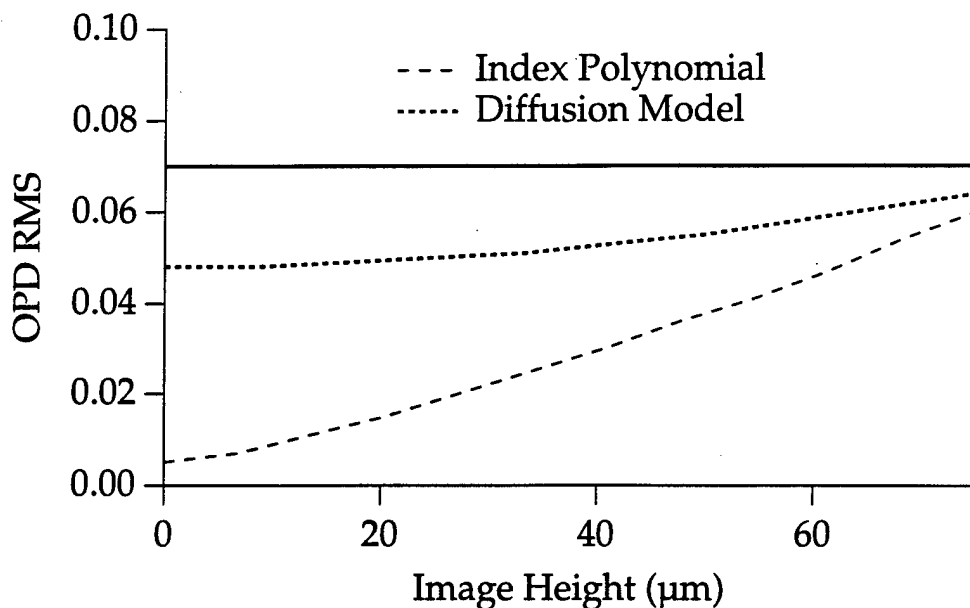
Figure 6.21 OPD as a function of image height for the gradient-index compact disk objective for both the index polynomial design profile and the diffusion model design profile. The Marechal criterion is indicated by the solid line.

6.6 Summary

In the first part of this chapter, a method to link the diffusion model to a lens design program was offered. In particular, a "usergrn" subroutine for CodeV was presented which allows a designer to optimize an index of refraction profile for its Δn, depth, and shape in terms of manufacturing process parameters such as diffusion time. Therefore, a designer can now choose a particular glass composition and explore a range of profiles without spending time designing a lens system that it is either difficult to fabricate or cannot be manufactured.

In the second part of this chapter, the new design method was used for several different types of lens systems. These are an axial gradient singlet, a radial gradient focusing rod, and gradient-index compact disc objective. Furthermore, for each lens system, the old method (using the index polynomial coefficients) and the new method (using manufacturing parameters) of design and optimization were compared and contrasted.

For example, two axial gradient singlets were designed to show the correction of the spherical aberration in a homogeneous singlet through the addition of the gradient. The first gradient design uses a linear axial gradient specified by the index polynomial coefficients, while the second design uses the diffusion model for a titania silicate glass composition to specify the gradient material. In the first design, the addition of linear axial gradient to a homogeneous singlet significantly improved the performance of the lens, thereby reducing the spot size to 4 μm from 400 μm and making the lens diffraction limited.

In the second axial gradient design, the lens system was optimized for diffusion time using the new design method. Several solutions with the same performance were discovered including a solution for which the second surface of the lens was flat. However, the performance of these solutions was not as good as the polynomial design in that the spot size was only reduced to 20 μm from 400 μm, since the index of refraction profile for this particular glass composition is not completely linear and the lens is still dominated by spherical aberration.

This example illustrates the main problem with an index polynomial design and therefore the usefulness of the new diffusion model. From the values of the polynomial coefficients is difficult to determine whether an index polynomial profile can actually be fabricated in a particular glass composition. For example, in many cases, it is difficult to find a glass composition and ion exchange pair that gives a linear index of refraction profile for a specific base index of refraction and Δn. However, using the new diffusion model a wide range of diffusion times was explored, and it was concluded that for these particular lens specifications, a diffraction limited lens could not be obtained in this glass composition. In the past, several trial and error experiments were required in which, a diffusion was performed, the index profile measured and fit to an index polynomial, and then entered into a lens design program and evaluated. Although some intuition can be gained from previous experiments, this is still a very time-consuming process. Furthermore, the polynomial needed to fit index of refraction profiles requires a large number of terms (8-10) and is

not very accurate, thereby reducing the accuracy of the lens performance evaluation.

A similar design procedure was then applied to a radial gradient focusing rod. In the polynomial design, only three index coefficients were used and the resulting index of refraction profile which produced the best performance was nearly parabolic although a small N_{20} coefficient was used to correct the spherical aberration of this lens. The final lens had a spot size of 4 μm at an image height of 1 mm which is much smaller than the diffraction limited spot size of 9.5 μm.

In the diffusion model design, the lens was optimized for diffusion time. In particular, several different starting points were chosen which converged to the same solution of a diffusion time of 112.7 hours. Again, the lens was not nearly as good as the polynomial design. The reason for this is that a second order polynomial fit to the index of refraction profile yields residual error between them, since the profile can be fit significantly better with a higher order polynomial. These higher order coefficients then contribute higher order aberrations to the design which are then balanced with the third order aberrations. Thus, a second problem with the index polynomial design method was revealed. Many of the fabricated profiles require a certain number of coefficients to represent them in a lens design program for an accurate lens evaluation. Often the number of coefficients used in the original design is not enough and furthermore, if they are used it is difficult to constrain them to result in a profile that can actually be manufactured.

The new diffusion model was also used to determine the tolerances for the diffusion time for this design. In particular, the diffusion time was changed and the lens reoptimized to the paraxial image plane. The results showed that for a change in diffusion time of 10 hours, the pitch length of the rod changed by approximately 2 mm and the spot diameter was increased by almost a factor of ten. In the past, tolerances of gradient-index lens systems were done on the index polynomial coefficients and were therefore difficult to relate to the fabrication process parameters. Therefore, this is another example of the usefulness of the new diffusion model for gradient-index lens systems.

Finally, a gradient-index compact disk objective was examined. The design consists of two elements, the first is a plano-plano radial gradient-index lens and the second is a homogeneous element with spherical surfaces. A summary of a previous design which used the index polynomial to specify the gradient material was presented. Furthermore, since the index polynomial coefficients were unrelated to the specific process parameters, the experimental trial-and-error procedure that was needed to fabricate the gradient profile was described. The entire process took approximately six months and several experiments to complete and was used to illustrate the type of fabrication process that has been applied to gradient-index lens systems in the past.

Then, this same lens system was designed with the diffusion model developed in this thesis and the results of this design were presented. In addition, the two methods (the original design and fabrication procedure and the new design-for-manufacture procedure) were compared and contrasted. For example, the diffusion model solution is much closer to the index polynomial design than any of the trial and error experimental profiles and it did not take nearly as long to find this solution. In addition, all of the experimental process parameters (such as diffusion time and rod diameter) required to fabricate the gradient were then contained within the design. However, the performance of this lens showed that the lens met the original specifications, but it is not nearly as good as the index polynomial design. This again illustrates the main problem with index polynomial designs; an index polynomial design and a manufactured profile can appear to be very similar, however, very small changes in the coefficients of the design profile can improve the performance of the design yet these changes cannot be duplicated in the laboratory. Therefore, the performance of the final lens system is usually worse than the original polynomial design.

The example lens systems presented in this chapter demonstrate that the new diffusion model can be used for the design of a variety of optical systems utilizing both axial and radial gradients while guaranteeing that the designs can be manufactured using current ion exchange technology. Furthermore, the new diffusion model allows for studies on the

tolerances of the various diffusion parameters such as diffusion time. Typically, studies of gradient tolerances have utilized the polynomial index of refraction coefficients and have been hard to relate to laboratory parameters. Thus, the new method gives manufacturers information about the tolerances on the process parameters required to fabricate the specific optical systems.

References

1. M. J. Hoppe, "Design of axial gradient singlets utilizing a Fickian diffusion model," M.S. Thesis, University of Rochester, Rochester, NY (1992).

2. N. Haun, "Control of the gradient index profile using sol-gel processes," Doctoral Dissertation, University of Rochester, Rochester, NY (1992).

3. CodeV is a registered trademark of Optical Research Associates, Pasadena, CA.

4. Discussions with CodeV representatives.

5. D. S. Kindred, "Development of new gradient index glasses for optical imaging systems," Doctoral Dissertation, University of Rochester, Rochester, NY (1990), p. 85.

6. E. W. Marchand, *Gradient Index Optics*, Academic Press, New York (1978).

7. Product guide, Nippon Sheet Glass America, Inc., Somerset, New Jersey.

8. D. T. Moore, "Aberration correction using index gradients," M.S. thesis, University of Rochester, Rochester, NY (1970).

9. M. G. Carasso et al., "The compact disc digital audio system," Philips Tech. Rev. 40, 151-156 (1982)

10. A. Goto, "Objective for video disks," United States Patent 4,270,843, June 2, 1981.

11. K. Shintani and S. Kubota, "Evaluation of a Diffraction-Limited Plastic Biaspheric Objective Lens," in *Technical Digest, Conference on Lasers and Electro-Optics* (Optical Society of America, Washington, DC 1984), paper WB2.

12. T. Kiriki, N. Izumiya, K. Sakurai and T. Kojima, "Plastic Aspheric Lens for the Compact Disc System," in *Technical Digest, Conference on Lasers and Electro-Optics* (Optical Society of America, Washington, DC 1984), paper WB3.

13. R. O. Maschmeyer, R. M. Hujar, L. L. Carpenter, B. W. Nicholson, and E. F. Vozenilek, "Optical Performance of a Diffraction-Limited Molded-Glass Biaspheric Lens," Appl. Opt. **22**, 241133 (1983).

14. J. J. M. Braat, A. Smid and M. M. B. Wignakker, "Design and Production Technology of Replicated Aspheric Objective Lenses for Optical Disk Systems," Appl. Opt. **24**, 1853 (1985).

15. J. Braat, "Difraction-Limited Singlet Lenses," Optics News, 21-22 (June 1988).

16. H. Nishi, M. Toyama, T. Yamagishi, K. Fujii and H. Ueno, "Plano-Convex Gradient-Index Singlet," in *Technical Digest, Topical Meeting on Gradient Index Optical Imaging Systems*, Kobe, Japan (1983), paper 2c.

17. Y. Aono, "Optical Design of Pick-Up Objectives with Gradient Index Elements," Micro Opt. News **1**, 126 (1984).

18. K. Kikuchi, S. Ishihara, H. Shimizu, and J. Shimada, "Design of Gradient-Index Sperical Lenses for Optical Pickup System," Appl. Opt. **19**, 1076 (1980).

19. This project was completed for the requirements of an undergraduate senior honor's thesis.

20. E. W. Marchand, *Gradient Index Optics* (Academic, New York, 1978).

21. J. B. Caldwell, "Sol-Gel Methods For Making Radial Gradient-Index Glass," Doctoral Dissertation, University of Rochester, Rochester, NY (1989), p. 157.

22. D. Kindred, J. Bentley, D. Moore, "Axial and Radial Gradients in Titania Flint Glasses," Appl. Opt. **29**, 4036 (1990).

23. H. Nishi, H. Ichikawa, M. Toyama, and I Kitano, "Gradient-Index Objective Lens for the Compact Disk System," Appl. Opt. **25**, 3340 (1986)

Chapter VII
Conclusions

7.1 Concluding remarks

Modern manufacturing methods incorporate fabrication constraints and quality control into the initial product design to create competitive, cost-effective products. Similarly, the research presented in this thesis offers a design-for-manufacture approach to gradient-index lens production. Fabrication parameters are coupled to a lens design program to eliminate the traditional trial-and-error manufacturing process. The new approach allows a lens designer to design a gradient-index optical system in terms of the actual fabrication parameters and then provides a set of experimental specifications to the materials scientist. The result is a much more efficient and cost-effective manufacturing process for gradient-index optical systems.

Previously, the manufacture of gradient-index lens systems was a complicated process since the design methods had been established before many of the current gradient-index materials were available. For example, the index of refraction profile was typically expressed by a general polynomial expansion in optical design. Although this gave some insight to the designers since aberration theories had been developed in terms of

the polynomial coefficients, the resulting design gave no intuition into fabrication. Therefore, once a gradient-index lens had been designed with this representation, the manufacturer had to guess at the diffusion parameters such as time, temperature, and even glass compositions to obtain the required Δn, depth, and profile shape.

As a result, the previous gradient-index design-to-manufacture process was slow and iterative. The designer asked for a particular profile and the manufacturer, after a number of experiments, obtained something similar. In most systems, the difference between the two profiles resulted in a decrease in optical performance and the lens system needed to be reoptimized. The new design usually required a slightly different profile and the entire process was repeated several times, taking several months to complete. A preferable method from a manufacturing standpoint would be to design the lens in terms of the actual fabrication parameters such as time, temperature, and salt/glass composition.

Therefore, a more efficient design-for-manufacture approach is offered by this research and can be divided into three main parts. First, a mathematical model for gradient-index fabrication by ion exchange which uses Fickian diffusion theory was developed. Second, an experimental procedure was developed to test this model against experimental results for several different glass compositions, diffusion times, and temperatures in both axial and radial sample geometries. Third, the model was integrated with a lens design program to allow optimization on diffusion parameters and several sample designs were presented which compared and contrasted the old design procedure (using index polynomial coefficients) with this new method of design. With the completion of this research, a lens designer can now choose from a realistic set of gradient-index glasses and, in turn, generate a complete set of experimental specifications for the production of the gradient.

In summary, a mathematical model for the fabrication of gradient-index materials by ion exchange was formulated in Chapter 2. First, an introduction into Fickian diffusion theory was given which showed how to apply this theory to ion exchange experiments. Then several simple examples were used to demonstrate how manufacturing parameters can

be incorporated into the diffusion equation through the initial condition, the boundary condition, and the diffusion coefficient. Finally, variations in manufacturing parameters (such as diffusion time) were analyzed for their effect on the concentration/index of refraction profile. In particular, these examples showed the importance of the concentration dependence of the diffusion coefficient in determining the final concentration/index of refraction profile in the sample.

In general, the concentration dependence of the diffusion coefficient must be found experimentally for each particular glass/salt pair. Thus, a discussion of the concentration-dependent diffusion coefficient was also given in Chapter 2. First, a well-known form for the concentration dependence of the diffusion coefficient was presented, but the historical treatment of this equation required a time-consuming experimental measurement procedure. Therefore, a new analytic expression for the concentration-dependent diffusion coefficient was derived from statistical thermodynamics. This new theoretical model is called the Modified Quasi-Chemical (MQC) diffusion coefficient and can be used to determine the concentration dependence of the diffusion coefficient from a single ion exchange experiment. In particular, the new expression was shown to be very useful as a fitting function for noisy Boltzmann-Matano calculations of the diffusion coefficient.

Chapter 2 concludes with the development of a numerical routine that incorporates the new diffusion coefficient model, solves the diffusion equation, and calculates concentration profiles based on manufacturing parameters. The routine was formulated so that it could be easily linked to a lens design program to allow optimization of the manufacturing process parameters for a particular design. Thus, a mathematical diffusion model has been realized which, given a set of experimental parameters, can predict future concentration/index of refraction profiles prior to performing the experiment.

In the second part of this research, diffusion model solutions were tested against experimental results for Li^+ for Na^+ and Na^+ for Li^+ diffusions in several different types of glass. A general experimental procedure for testing the model was developed in Chapter 3 and included

glass melting, ion exchange experiments, and the measurement of index of refraction profiles. Furthermore, the mathematical diffusion model developed in Chapter 2 requires an empirical calculation of both the index of refraction and the diffusion coefficient as a function of concentration for each glass composition. Thus, Chapter 3 also determined the experimental procedure for these calculations and included an error analysis for each step in the calculations.

In the next two chapters, empirical diffusion models were developed for a wide variety of glass compositions using this procedure. For example, Chapter 4 examined diffusions in a series of alumina silicate crown glasses with various amounts of alkali and alumina in the homogeneous glass composition. Previous results of $Li^+ - Na^+$ exchange in this type of glass showed that it had favorable ion exchange properties including little or no divitrification and relatively fast diffusion rates. As a result, this type of glass was used to identify the parameters needed to change the mathematical diffusion model developed in Chapter 2 into a working empirical diffusion model. In particular, an empirical calculation of the diffusion coefficient and the index of refraction as a function of concentration was made for several different alumina silicate glass compositions. Ion exchange experiments were conducted in these glasses in both an axial and radial geometry for a range of different temperatures and diffusions times. Finally, the measured index of refraction profiles were compared with the numerical solutions from the diffusion model and were shown to agree to within the experimental error.

In Chapter 5 the diffusion model was then tested for other types of glasses to explore different regions of the glass map and to ultimately determine how well the model conformed to other glass compositions. First, $Li^+ - Na^+$ exchange in a series of alumina borate glasses was examined in axial geometry. The optical properties (such as index of refraction and dispersion) of these glasses are similar to the alumina silicate glasses. However, these glasses use boron as the glass former and they showed large differences in the resulting index of refraction profiles. The diffusion model was tested for both a long and a short diffusion time, at the same temperature, in several different glass compositions of this

series. The numerical solutions from the diffusion model and the measured index of refraction profiles agreed to within the experimental error for the short diffusion time. However, the samples for the longer diffusion time had a large divitrification of the surface of the sample and the diffusion model could not predict these profiles.

The second part of Chapter 5 examined two titanium silicate glass compositions which have a higher index of refraction and are more dispersive than the alumina silicate and alumina borate glasses. The first glass is a simple composition with only three components. The second glass has several additional components to see if the diffusion model can be applied to more complicated glass compositions. Axial diffusions in the two different glass compositions were examined over a relatively large temperature range. An empirical calculation of the diffusion coefficient as a function of concentration and temperature is made for these glasses, and then, the measured index of refraction profiles were compared with the numerical solutions from the diffusion model and agreed to within the experimental error.

Finally, a method to link the diffusion model to a lens design program was offered in the first part of Chapter 6. In particular, a "usergrn" subroutine for CodeV was presented which allows a designer to optimize an index of refraction profile for its Δn, depth, and shape in terms of manufacturing process parameters such as diffusion time. Therefore, a designer can now choose a particular glass composition and explore a range of profiles without spending time designing a lens system that it is either difficult to fabricate or cannot be manufactured.

Then, in the second part of Chapter 6, several example lenses designed with the diffusion model were presented. These were an axial gradient singlet, a radial gradient focusing rod, and gradient-index compact disc objective. For each lens system, the old method (using the index polynomial coefficients) and the new method (using manufacturing parameters) of design and optimization was compared and contrasted. These examples demonstrated that the new diffusion model could be used for the design of a variety of optical systems utilizing both axial and radial gradients while guaranteeing that the designs can be manufactured using

current ion exchange technology. Furthermore, the results from a tolerance study of the diffusion time for one of the systems was presented. Typically, studies of gradient tolerances have utilized the polynomial index of refraction coefficients and have been hard to relate to laboratory parameters. Thus, the new method gives manufacturers information about the tolerances on the process parameters required to fabricate a specific optical system. In conclusion, this research should facilitate the use of a wide range of gradient profiles in lens design with a more efficient and less expensive design-to-manufacture process.

7.2 Suggestions for future research

During this research, Fickian diffusion models were developed to predict the gradient index profiles for ion exchange in three different types of glass in both an axial and a radial geometry. However, only the ion exchange pair of $Li^+ - Na^+$ was investigated. Therefore, other ion exchange pairs, such as $Ag^+ - Na^+$, and even other glass compositions should be investigated and included in the lens design model to give a broader range of index of refraction profiles for the designer to choose from. Furthermore, the diffusion model has only been investigated for a single wavelength, 632.8 nm. Since the designs of most optical systems require evaluation at more than one wavelength, the chromatic dependence of the materials must also be incorporated into the model.

Finally, in the lens designs presented in Chapter 6, only the diffusion time was used as an optimization variable. However, variations in other process parameters such as temperature and glass composition (over the limited range to which a single diffusion coefficient can be applied) should be investigated. Furthermore, experimental techniques such as salt bath poisoning and post-annealing have also been included in the model through the boundary conditions, but the results need to be verified experimentally. For example, initial results with the diffusion model for a radial geometry show that using a post-anneal time (removing the sample from the salt bath and holding it at an elevated temperature) and then a second diffusion time (placing the sample back into the salt bath) results in a much different profile shape than if the sample had been kept in the salt

bath for the same total length of time. Thus, these techniques show great promise for varying the index of refraction profile to obtain better lens performance, but need to be verified experimentally.

Appendix A
Numerical Routines

A.1 Introduction

In this appendix, there are four source code listings for the numerical routines used in this research. In order, these are:

(1)   the Igor Pro™ macro used to calculate the concentration dependence of the diffusion coefficient from a measured index of refraction profile using a Boltzmann Matano calculation,

(2)   the Igor Pro™ user-defined function used to fit the calculated concentration-dependent diffusion coefficient to the Modified Quasi-Chemical (MQC) diffusion coefficient expression,

(3)   the Fortran program used to solve the diffusion equation to predict gradient-index profiles according to the procedure discussed in Chapter 2, and

(4)   the 'usergrn' subroutine for CodeV™ which is based upon the previous program.

A.2 Boltzmann-Matano Diffusion Coefficient Calculation

```
Macro Dofccalc(num, poly_coef, mincon, maxcon, difftime)
    String num, ind_num, con_num, poly_coef, posintp_num, dn_num, pos_num, dofc_num,
        diff_num, intge_num
    Variable/D mincon, maxcon, difftime, minconsc, maxconsc

    ind_num="ind"+num
    con_num="con"+num
    posintp_num="posintp"+num
    dn_num="dn"+num
    pos_num="pos"+num
    dofc_num="dofc"+num
    diff_num="diff"
    intge_num="intge"

    Make/N =300/D/O $ind_num, $con_num
    $con_num = mincon+(maxcon-mincon)*(x/299)
    $ind_num = poly($poly_coef,$con_num)

    Make/N=300/D/O $posintp_num
    $posintp_num=interp($ind_num,$dn_num,$pos_num)
    SetScale/I x mincon,maxcon,"", $posintp_num
    Duplicate/O $posintp_num $diff_num,$intge_num,$dofc_num
    Differentiate $diff_num
    Integrate $intge_num
    $dofc_num=(-1/(2*difftime*100*3600))*(1/1e-7)*$diff_num*$intge_num

End
```

A.3 MQC Diffusion Coefficient Curve Fit Function

```
function/D dofc(w,x)
    wave/D w; Variable/D x
    variable/D sqrtpart,bofzero, bofone, selfdiff,final

    sqrtpart=sqrt(1-4*(x-w[3])*(1-(x-w[3]))*(1-exp(W[2])))
    bofzero=sqrt(1-4*(0-w[3])*(1-(0-w[3]))*(1-exp(W[2])))
    bofone=sqrt(1-4*(1-w[3])*(1-(1-w[3]))*(1-exp(W[2])))
    selfdiff=(w[0]/(1-x*w[1]))
    final=((w[4]/2)*((bofzero*(1-x)+bofone*x)/sqrtpart+(2/w[4]-1)))*selfdiff
    return final
end
```

A.4 Fickian Diffusion Model

```
        PROGRAM USERGRN

        IMPLICIT NONE

        INTEGER L
        INTEGER NPTS
        PARAMETER(NPTS=101)

        REAL*8 COEF(20)
        REAL*8 X(NPTS), NZ(NPTS)

        EXTERNAL PDEDEF, BNDARY, D03PCF

        CHARACTER*50 FNAME

        WRITE(*,*) 'AXIAL=0 OR RADIAL=1'
        READ(*,*) COEF(1)

        WRITE(*,*) 'GLASS CONCENTRATION'
        READ(*,*) COEF(4)

        WRITE(*,*) 'SALT CONCENTRATION'
        READ(*,*) COEF(5)

        WRITE(*,*) 'DIFFUSION TIME'
        READ(*,*) COEF(2)

        WRITE(*,*) 'DEPTH OR RADIUS'
        READ(*,*) COEF(3)

        WRITE(*,*) 'DOFCCOEFS'
        READ(*,*) COEF(6), COEF(7), COEF(8), COEF(9), COEF(10)

        WRITE(*,*) 'nOFCCOEFS'
        READ(*,*) COEF(11), COEF(12), COEF(13), COEF(14), COEF(15)

        CALL DEQSOLVE(COEF,X,NZ)

        WRITE(*, 22)
22      FORMAT('$FILE NAME: ')
        READ(*,9999) FNAME
9999    FORMAT(A50)

        OPEN(UNIT=20, FILE=FNAME, STATUS='NEW')
```

```
        DO 40 L=1, NPTS
           WRITE(20,*) X(L), NZ(L)
40      CONTINUE

        WRITE(20,*) 'AXIAL/RADIAL, DIFFUSION TIME, DEPTH/RADIUS'
        WRITE(20,*) COEF(1), COEF(2), COEF(3)
        WRITE(20,*) 'GLASS CONCENTRATION, SALT CONCENTRATION'
        WRITE(20,*) COEF(4), COEF(5)
        WRITE(20,*) 'DOFC COEFFICIENTS'
        WRITE(20,*) COEF(6), COEF(7), COEF(8), COEF(9), COEF(10)
        WRITE(20,*) 'NOFC COEFFICIENTS'
        WRITE(20,*) COEF(11), COEF(12), COEF(13), COEF(14), COEF(15)

        CLOSE(UNIT=20)


        STOP
        END



        SUBROUTINE DEQSOLVE(COEF,X,NZ)

        COMMON/DOFC/DC1, DC2, DC3, DC4, DC5
        COMMON/BC/CHI0, CHI1
        COMMON/GEO/M

        INTEGER NPDE, M, NPTS, NW, NIW
        INTEGER I, J
        PARAMETER(NPDE=1,NPTS=101, NW=5851, NIW=275)
        INTEGER IW(NIW), ITASK, ITRACE, IND, IFAIL

        REAL*8 COEF(20)
        REAL*8 TS, TOUT
        REAL*8 DC1, DC2, DC3, DC4, DC5
        REAL*8 NC(5), NZ(NPTS)
        REAL*8 CHI0, CHI1
        REAL*8 MAXDEPTH
        REAL*8 U(NPDE, NPTS), X(NPTS), ACC, W(NW)
        REAL*8 SPACE
        REAL*8 CHIVAL, INDVAL

        EXTERNAL PDEDEF, BNDARY, D03PCF

        M = IDINT(COEF(1))
        TOUT = COEF(2)
        DC1 = COEF(6)*0.036D0
        DC2 = COEF(7)
        DC3 = COEF(8)
        DC4 = COEF(9)
        DC5 = COEF(10)
        NC(1) = COEF(11)
```

```fortran
      NC(2) = COEF(12)
      NC(3) = COEF(13)
      NC(4) = COEF(14)
      NC(5) = COEF(15)
      CHI0 = COEF(4)
      CHI1 = COEF(5)
      MAXDEPTH = COEF(3)

      ACC = 5D-4
      TS = 0.0D0
      ITASK = 1
      ITRACE = 0
      IND = 0
      IFAIL = 0

      SPACE = MAXDEPTH/(NPTS-1)
      DO 10 I=1, NPTS
          X(I) = (I-1)*SPACE
          U(1, I) = CHI0
10    CONTINUE

      CALL D03PCF(NPDE,M,TS,TOUT,PDEDEF,BNDARY,U,NPTS,
     *    X,ACC,W,NW,IW,NIW,ITASK,ITRACE,IND,IFAIL)

      DO 20 J=1, NPTS
          CHIVAL=U(1, J)
          CALL INDEVAL(NC, CHIVAL, INDVAL)
          NZ(J)=INDVAL
20    CONTINUE

      RETURN
      END


      SUBROUTINE PDEDEF(NPDE, T, X, U, UX, P, Q, R, IRES)

      IMPLICIT NONE

      COMMON/DOFC/DC1, DC2, DC3, DC4, DC5

      INTEGER NPDE, IRES

      REAL*8 T, X, U(NPDE), UX(NPDE)
      REAL*8 P(NPDE,NPDE), Q(NPDE), R(NPDE)
      REAL*8 DC1, DC2, DC3, DC4, DC5
      REAL*8 BETAN, BETA0, BETA1, THERMO, FUGITA, DOFC


      P(1,1) = 1.0D0
      Q(1) = 0.0D0
```

```fortran
      BETAN = SQRT(1.0-4.0*(U(1)-DC4)*(1.0-(U(1)-DC4))*(1.0-exp(DC3)))
      BETA0 = SQRT(1.0-4.0*(0.0-DC4)*(1.0-(0.0-DC4))*(1.0-exp(DC3)))
      BETA1 = SQRT(1.0-4.0*(1.0-DC4)*(1.0-(1.0-DC4))*(1.0-exp(DC3)))

      THERMO = (DC5/2)*(((U(1)*BETA1+(1-U(1))*BETA0)/BETAN)-1)+1
      FUGITA = DC1/(1-U(1)*DC2)
      DOFC = THERMO*FUGITA

      R(1)=DOFC*UX(1)

      RETURN
      END



      SUBROUTINE BNDARY(NPDE, T, U, UX, IBND, BETA, GAMMA, IRES)

      IMPLICIT NONE

      COMMON/BC/CHI0, CHI1
      COMMON/GEO/M

      INTEGER NPDE, IBND, IRES, M


      REAL*8 CHI0, CHI1
      REAL*8 T, U(NPDE), UX(NPDE), BETA(NPDE), GAMMA(NPDE)

      IF (M.EQ.0) THEN

          BETA(1) = 0.0D0
          IF (IBND .EQ. 0) THEN
              GAMMA(1) = U(1) - CHI1
          ELSE
              GAMMA(1) = U(1) - CHI0
          ENDIF

      ELSE

          IF (IBND .EQ. 0) THEN
              BETA(1) = 1.0D0
              GAMMA(1) = 0.0D0
          ELSE
              BETA(1) = 0.0D0
              GAMMA(1) = U(1) - CHI1
          ENDIF

      ENDIF

      RETURN
      END
```

```
      SUBROUTINE INDEVAL(NC, CHIVAL, INDVAL)

      IMPLICIT NONE

      INTEGER I
      REAL*8 NC(5), CHIVAL, INDVAL

      INDVAL = NC(5)

      DO 200 I=1,4
          INDVAL=CHIVAL*INDVAL + NC(5-I)
200   CONTINUE

      RETURN
      END
```

A.5 'Usergrn' Subroutine for CodeV

The specific details of how to link the usergrn subroutine with CodeV can be found in the reference manuals. However, the parameters that must be defined by the subroutine are listed below:

brind   The index of refraction at the polar tangent plane of the usergrn surface; the C0 coefficient of the material. (Input)

coef(20)   Array of coefficients, C1 through C20, entered by the user in CodeV to describe the manufacturing process parameters for the system. (Input)

s(3)   Array for the x, y, and z coordinates of the ray. (Input)

rindx   Parameter set by the subroutine to the index of refraction at the ray position specified by s(3). (Output)

xngran(3)   Array set by the subroutine to the product of the index of refraction and its derivative with respect to the x, y, and z directions at the ray position specified by s(3). (Output)

The usergrn subroutine is then accessed in CodeV through a private catalog entry which specifies a user-defined gradient by entering the values for brind (C0) and the set of 20 coefficients (C1-C20). Each coefficient must be defined for each wavelength in the design. If the value for a particular coefficient is not specified, it is assumed to be zero. This information along with the ray coordinates is sent to the user-defined subroutine which calculates the index of refraction and the derivative of the index profile (in each direction) at that particular ray position. Therefore, it is important to know what each coefficient is, whether it can be varied in an optimization routine, and finally, what constraints, if any, must be imposed.

The user-defined subroutine listed in this appendix is based on the diffusion model program from the previous section. In this particular subroutine, the coefficients are defined as:

C0: the polar tangent plane index of refraction; this is the same as brind,

C1: specifies either an axial gradient (0) or a radial gradient (1), where a value other than 0 or 1 returns an error,

C2: diffusion time in hours,

C3: either the diffusion depth for an axial gradient or the radius of the cylinder for a radial gradient in millimeters,

C4: initial ion concentration in the glass sample,

C5: the maximum ion concentration that the glass sample can attain after diffusion.

C6-10: used to specify the MQC Diffusion Coefficient as a function of normalized concentration, χ,

$$D = \left[\frac{c}{2}\left(\frac{\chi\beta'(\chi=1)+(1-\chi)\beta'(\chi=0)}{\beta'} - 1 \right) + 1 \right]\frac{D_B}{1-\chi\alpha} \quad (A.1)$$

and

$$\beta' = \sqrt{1 - 4(\chi - \chi_0)\left[1 - (\chi - \chi_0)\right]\left(1 - e^\rho\right)} \quad (A.2)$$

where

C6: self-diffusion coefficient, D_B,
C7: mobility ratio, α,
C8: interaction energy term, ρ,
C9: peak position shift, χ_0, and
C10: cation-cation coordination number, c.

C11-15: used to specify the index of refraction as a function of normalized concentration, χ, for

$$n(\chi) = n_0 + n_1\chi + n_2\chi^2 + n_3\chi^3 + n_4\chi^4, \qquad (A.3)$$

where

    C11: base index of refraction, n_0,
    C12: index of refraction coefficient, n_1,
    C13: index of refraction coefficient, n_2,
    C14: index of refraction coefficient, n_3,
    C14: index of refraction coefficient, n_4.

C16-20: are additional coefficients which can be used for special experimental conditions, including post-anneal time, a second diffusion time after the post-anneal, and for time-dependent boundary conditions.

The appropriate coefficients can then be allowed to vary in a optimization routine to improve the performance of the lens. For example, to vary the diffusion time, the gradient control code for coefficient C2 is set to zero and the lens is optimized. During this process, each time that CodeV changes the value of C2, the diffusion equation is solved and the solution stored in an array. This array is then used to determine the index of refraction profile for the gradient at that particular diffusion time.

```fortran
      SUBROUTINE  USERGRN(KERROR,BRIND,COEF,S,RINDX,XNGRAN)

      IMPLICIT NONE

      INTEGER KERROR
      INTEGER M, NPTS
      PARAMETER(NPTS=251)

      REAL*8  BRIND, COEF(20), S(3), RINDX, XNGRAN(3)
      REAL*8  RAYDEP,LAST_TIME,LAST_TM2,LAST_TM3,LAST_TM4,LAST_TM5
      REAL*8  LAST_TM6, NZ(NPTS)
      REAL*8  SPACE, PREZ, PREZCK
      REAL*8  NZA, NZB, DELTAN, GRADX
      SAVE  LAST_TIME,LAST_TM2,LAST_TM3,LAST_TM4,LAST_TM5,last_tm6,NZ

      M = IDINT(COEF(1))

      IF (M.EQ.0) THEN
          RAYDEP = S(3)
      ELSEIF (M.EQ.1) THEN
          RAYDEP = DSQRT((S(1))**2 + (S(2))**2)
      ELSE
          KERROR = 1
      ENDIF

      IF (RAYDEP.GT.COEF(3)) THEN
          KERROR=1
      ENDIF

      IF (COEF(2).NE.LAST_TIME) THEN
          LAST_TIME = COEF(2)
          CALL DEQSOLVE(COEF,NZ)
      ELSEIF (COEF(4).NE.LAST_TM2) THEN
          LAST_TM2=COEF(4)
          CALL DEQSOLVE(COEF,NZ)
      ELSEIF (COEF(3).NE.LAST_TM3) THEN
          LAST_TM3=COEF(3)
          CALL DEQSOLVE(COEF,NZ)
      ELSEIF (COEF(5).NE.LAST_TM4) THEN
          LAST_TM4=COEF(5)
          CALL DEQSOLVE(COEF,NZ)
      ELSEIF (COEF(16).NE.LAST_TM5) THEN
          LAST_TM5=COEF(16)
          CALL DEQSOLVE(COEF,NZ)
      ELSEIF (COEF(17).NE.LAST_TM6) THEN
          LAST_TM6=COEF(17)
          CALL DEQSOLVE(COEF,NZ)
      ENDIF

      SPACE = COEF(3)/(NPTS-1)
```

```
PREZ = IDINT(RAYDEP/SPACE)
PREZCK = PREZ*SPACE


IF (PREZCK.EQ.RAYDEP) THEN
    IF (PREZCK.EQ.0) THEN
        RINDX=NZ(PREZ+1)
        GRADX=0.0
    ELSEIF (RAYDEP.EQ.COEF(3)) THEN
        NZB=NZ(PREZ)
        NZA=NZ(PREZ+1)
        DELTAN = NZA - NZB
        GRADX = DELTAN/SPACE
        RINDX = NZB + DELTAN*(RAYDEP/SPACE-PREZ)
    ELSE
        NZB=NZ(PREZ)
        NZA=NZ(PREZ+2)
        DELTAN = NZA - NZB
        GRADX = DELTAN/(2*SPACE)
        RINDX = NZB + DELTAN*(RAYDEP/(2*SPACE)-PREZ)
    ENDIF
ELSE
    NZB = NZ(PREZ+1)
    NZA = NZ(PREZ+2)
    DELTAN = NZA - NZB
    GRADX = DELTAN/SPACE
    RINDX = NZB + DELTAN*(RAYDEP/SPACE-PREZ)
ENDIF

IF (M.EQ.0) THEN
    XNGRAN(1) = 0.0D0
    XNGRAN(2) = 0.0D0
    XNGRAN(3) = RINDX*GRADX
ELSE
    IF (RAYDEP.EQ.0) THEN
        XNGRAN(1) = 0.0D0
        XNGRAN(2) = 0.0D0
        XNGRAN(3) = 0.0D0
    ELSE
        XNGRAN(1) = RINDX*GRADX*S(1)/RAYDEP
        XNGRAN(2) = RINDX*GRADX*S(2)/RAYDEP
        XNGRAN(3) = 0.0D0
    ENDIF
ENDIF

RETURN
END
```

```
SUBROUTINE DEQSOLVE(COEF,NZ)

COMMON/DOFC/DC1, DC2, DC3, DC4, DC5
COMMON/BC/CHI0, CHI1, CHI2, ALPHA
COMMON/GEO/M

INTEGER NPDE, M, NPTS, NW, NIW
INTEGER I, J
PARAMETER(NPDE=1,NPTS=251, NW=23101, NIW=1025)
INTEGER IW(NIW), ITASK, ITRACE, IND, IFAIL

REAL*8 COEF(20)
REAL*8 TS, TOUT
REAL*8 DC1, DC2, DC3, DC4, DC5
REAL*8 NC(5), NZ(NPTS)
REAL*8 CHI0, CHI1, CHI2, ALPHA
REAL*8 MAXDEPTH
REAL*8 U(NPDE, NPTS), X(NPTS), ACC, W(NW)
REAL*8 SPACE
REAL*8 CHIVAL, INDVAL

EXTERNAL PDEDEF, BNDARY, D03PCF

M = IDINT(COEF(1))
TOUT = COEF(2)
DC1 = COEF(6)*0.036D0
DC2 = COEF(7)
DC3 = COEF(8)
DC4 = COEF(9)
DC5 = COEF(10)
NC(1) = COEF(11)
NC(2) = COEF(12)
NC(3) = COEF(13)
NC(4) = COEF(14)
NC(5) = COEF(15)
CHI0 = COEF(4)
CHI1 = COEF(5)
CHI2 = COEF(16)
ALPHA = COEF(17)
MAXDEPTH = COEF(3)

ACC = 5D-4
TS = 0.0D0
ITASK = 1
ITRACE = 0
IND = 0
IFAIL = 0
```

```
         SPACE = MAXDEPTH/(NPTS-1)
         DO 10 I=1, NPTS
            X(I) = (I-1)*SPACE
            U(1, I) = CHI0
10       CONTINUE

         CALL  D03PCF(NPDE,M,TS,TOUT,PDEDEF,BNDARY,U,NPTS,
     *   X,ACC,W,NW,IW,NIW,ITASK,ITRACE,IND,IFAIL)

         DO 20 J=1, NPTS
            CHIVAL=U(1, J)
            CALL INDEVAL(NC, CHIVAL, INDVAL)
            NZ(J)=INDVAL
20       CONTINUE

         RETURN
         END


         SUBROUTINE PDEDEF(NPDE, T, X, U, UX, P, Q, R, IRES)

         IMPLICIT NONE

         COMMON/DOFC/DC1, DC2, DC3, DC4, DC5

         INTEGER NPDE, IRES

         REAL*8 T, X, U(NPDE), UX(NPDE)
         REAL*8 P(NPDE,NPDE), Q(NPDE), R(NPDE)
         REAL*8 DC1, DC2, DC3, DC4, DC5
         REAL*8 BETAN, BETA0, BETA1, THERMO, FUGITA, DOFC


         P(1,1) = 1.0D0
         Q(1) = 0.0D0

         BETAN = SQRT(1.0-4.0*(U(1)-DC4)*(1.0-(U(1)-DC4))*(1.0-exp(DC3)))
         BETA0 = SQRT(1.0-4.0*(0.0-DC4)*(1.0-(0.0-DC4))*(1.0-exp(DC3)))
         BETA1 = SQRT(1.0-4.0*(1.0-DC4)*(1.0-(1.0-DC4))*(1.0-exp(DC3)))

         THERMO = (DC5/2)*(((U(1)*BETA1+(1-U(1))*BETA0)/BETAN)-1)+1
         FUGITA = DC1/(1-U(1)*DC2)
         DOFC = THERMO*FUGITA

         R(1)=DOFC*UX(1)

         RETURN
         END
```

```fortran
      SUBROUTINE BNDARY(NPDE, T, U, UX, IBND, BETA, GAMMA, IRES)

      IMPLICIT NONE

      COMMON/BC/CHI0, CHI1, CHI2, ALPHA
      COMMON/GEO/M

      INTEGER NPDE, IBND, IRES, M

      REAL*8 CHI0, CHI1, CHI2, ALPHA
      REAL*8 T, U(NPDE), UX(NPDE), BETA(NPDE), GAMMA(NPDE)

      IF (M.EQ.0) THEN

          BETA(1) = 0.0D0
          IF (IBND .EQ. 0) THEN
              GAMMA(1) = U(1) - CHI1
          ELSE
              GAMMA(1) = U(1) - CHI0
          ENDIF

      ELSE

          IF (IBND .EQ. 0) THEN
              BETA(1) = 1.0D0
              GAMMA(1) = 0.0D0
          ELSE
              BETA(1) = 0.0D0
              GAMMA(1) = U(1)-(CHI2+(CHI1-CHI2)*exp(-ALPHA*T))
          ENDIF

      ENDIF

      RETURN
      END

      SUBROUTINE INDEVAL(NC, CHIVAL, INDVAL)

      IMPLICIT NONE

      INTEGER I
      REAL*8 NC(5), CHIVAL, INDVAL

      INDVAL = NC(5)

      DO 200 I=1,4
          INDVAL=CHIVAL*INDVAL + NC(5-I)
200   CONTINUE

      RETURN
      END
```

Appendix B
Lens Listings

B.1 Homogeneous Singlet

	RDY	THI	GLA	CCY	THC	GLC
OBJ:	INFINITY	INFINITY	AIR	100	100	
STO:	16.40372	4.000000	'homo'	0	100	
2:	-153.30149	22.718702	AIR	0	PIM	
> IMG:	INFINITY	0.000000		100	100	

SPECIFICATION DATA

EPD	10.00000		
DIM	MM		
WL	632.80		
REF	1		
WTW	1		
INI	JLB		
XAN	0.00000	0.00000	0.00000
YAN	0.00000	0.70000	1.00000
VUY	0.00000	0.00000	0.00000
VLY	0.00000	0.00000	0.00000

PRIVATE CATALOG

PWL	632.80
'homo'	1.598000
GRC	100
URN	0.100000

REFRACTIVE INDICES

GLASS CODE		632.80
'homo'	1.598000	
URN	0.100000	

SOLVES
 PIM

INFINITE CONJUGATES

EFL	25.0000
BFL	22.7187
FFL	-24.7559
FNO	2.5000
IMG DIS	22.7187
OAL	4.0000
PARAXIAL IMAGE	
HT	0.4364

ANG   1.0000
ENTRANCE PUPIL
DIA   10.0000
THI   0.0000
EXIT PUPIL
DIA   10.0986
THI   -2.5278

B.2 Axial Gradient Singlet

B.2.1   Index Polynomial design

	RDY	THI	GLA	CCY	THC	GLC
OBJ:	INFINITY	INFINITY	AIR	100	100	
STO:	16.12000	2.000000	'ax1'	0	100	
2:	INFINITY	2.000000	'homo'	100	100	
> 3:	INFINITY	22.512548	AIR	100	PIM	
IMG:	INFINITY	0.000000		100	100	

SPECIFICATION DATA
EPD   10.00000
DIM   MM
WL   632.80
REF   1
WTW   1
INI   JLB
XAN   0.00000   0.00000   0.00000
YAN   0.00000   0.70000   1.00000
VUY   0.00000   0.00000   0.00000
VLY   0.00000   0.00000   0.00000

PRIVATE CATALOG
PWL   632.80
'homo'   1.596013
GRC   0
URN   0.100000
'ax1'   1.644800
GRC   100
URN   0.100000
URN C1   -0.2439E-01
GRC   0

REFRACTIVE INDICES
GLASS CODE   632.80
'ax1'   1.644800
URN   0.100000
URN C1   -0.2439E-01
'homo'   1.596013
URN   0.100000

SOLVES
 PIM

INFINITE CONJUGATES
 EFL   25.0000
 BFL   22.5125
 FFL   -25.0000
 FNO   2.5000
 IMG DIS   22.5125
 OAL   4.0000
 PARAXIAL IMAGE
 HT   0.4364
 ANG   1.0000
 ENTRANCE PUPIL
 DIA   10.0000
 THI   0.0000
 EXIT PUPIL
 DIA   10.0000
 THI   -2.4875

B.2.2   *Diffusion Model design*

	RDY	THI	GLA	CCY	THC	GLC
OBJ:	INFINITY	INFINITY	AIR	100	100	
STO:	14.95000	4.000000	'ax2'	0	100	
> 2:	INFINITY	20.706491	AIR	100	0	
IMG:	INFINITY	0.000000		100	100	

SPECIFICATION DATA
 EPD   10.00000
 DIM   MM
 WL   632.80
 REF   1
 WTW   1
 INI   JLB
 XAN   0.00000   0.00000   0.00000
 YAN   0.00000   0.70000   1.00000
 VUY   0.00000   0.00000   0.00000
 VLY   0.00000   0.00000   0.00000

PRIVATE CATALOG
 PWL   632.80
 'ax2'   1.598000
 GRC   100
 UDG   0.100000
 UDG C2   0.2847E+02
 GRC   0
 UDG C3   0.6000E+01
 UDG C5   0.1000E+01

UDG C6   0.1486E+00
UDG C7   0.6460E-01
UDG C8   -0.2022E+01
UDG C9   -0.2269E+00
UDG C10   0.4400E+01
UDG C11   0.1598E+01
UDG C12   0.1115E+00
UDG C13   -0.1123E+00
UDG C14   0.4765E-01

No solves defined in system

INFINITE CONJUGATES
  EFL   25.0000
  BFL   22.4419
  FFL   -25.0000
  FNO   2.5000
  IMG DIS   20.7065
  OAL   4.0000
  PARAXIAL IMAGE
  HT   0.4364
  ANG   1.0000
  ENTRANCE PUPIL
  DIA   10.0000
  THI   0.0000
  EXIT PUPIL
  DIA   10.0000
  THI   -2.5581

B.3 Radial Gradient Focusing Lens

B.3.1   Index Polynomial design

	RDY	THI	GLA	CCY	THC	GLC
OBJ:	INFINITY	INFINITY	AIR	100	100	
STO:	INFINITY	40.000000	'rad1'	100	100	
> 2:	INFINITY	2.000000	AIR	100	100	
IMG:	INFINITY	0.000000		100	100	

SPECIFICATION DATA
  EPD   3.00000
  DIM   MM
  WL   632.80
  REF   1
  WTW   1
  INI   JLB
  XIM   0.00000   0.00000   0.00000
  YIM   0.00000   0.70000   1.00000
  VUY   0.00000   0.00000   0.00000

VLY   0.00000   0.00000   0.00000

APERTURE DATA/EDGE DEFINITIONS
  CA
  CIR S1   1.500000
  CIR S2   1.500000

PRIVATE CATALOG
  PWL   632.80
  'rad1'   1.520000
  GRC   100
  URN   0.100000
  URN C10   -0.1013E-02
  GRC   0
  URN C20   0.6415E-06
  GRC   0

REFRACTIVE INDICES
  GLASS CODE   632.80
  'rad1'   1.520000
  URN   0.100000
  URN C10   -0.1013E-02
  URN C20   0.6415E-06

No solves defined in system

INFINITE CONJUGATES
  EFL   18.1318
  BFL   2.0000
  FFL   -2.0000
  FNO   6.0439
  IMG DIS   2.0000
  OAL   40.0000
  PARAXIAL IMAGE
  HT   1.0000
  ANG   3.1568
  ENTRANCE PUPIL
  DIA   3.0000
  THI   0.0000
  EXIT PUPIL
  DIA   27.1977
  THI   -162.3813

B.3.2   Diffusion Model design

B.3.2.1 Optimal Diffusion Time

	RDY	THI	GLA	CCY	THC	GLC
OBJ:	INFINITY	INFINITY	AIR	100	100	
STO:	INFINITY	40.000000	'rad2'	100	100	

| 2: | INFINITY | 2.270358 | AIR | 100 | 0 |
| > IMG: | INFINITY | 0.000000 | | 100 | 100 |

SPECIFICATION DATA

EPD	2.80000		
DIM	MM		
WL	632.80		
REF	1		
WTW	1		
INI	JLB		
XAN	0.00000	0.00000	0.00000
YAN	0.00000	2.00000	3.00000
VUY	0.00000	0.20000	0.40000
VLY	0.00000	0.00000	0.00000

APERTURE DATA/EDGE DEFINITIONS

CA		
CIR S1	1.500000
CIR S2	1.500000

PRIVATE CATALOG

PWL	632.80
'rad2'	1.519800
GRC	100
UDG	0.100000
UDG C1	0.1000E+01
UDG C2	0.1127E+03
GRC	0
UDG C3	0.1500E+01
UDG C4	0.5000E+00
UDG C6	0.1236E+00
UDG C7	0.3000E+00
UDG C8	-0.1503E+01
UDG C9	0.6740E-01
UDG C10	0.1087E+02
UDG C11	0.1506E+01
UDG C12	0.3070E-01
UDG C13	-0.1277E-01
UDG C14	0.1155E-01

No solves defined in system

INFINITE CONJUGATES

EFL	6.5154
BFL	-5.4089
FFL	4.1611
FNO	2.3269
IMG DIS	2.2704
OAL	40.0000
PARAXIAL IMAGE	
HT	0.3415

```
ANG        3.0000
ENTRANCE PUPIL
DIA        2.8000
THI        0.0000
EXIT PUPIL
DIA        0.1001
THI        -5.1759
```

B.3.2.2 Diffusion Time of 100 Hours

	RDY	THI	GLA	CCY	THC	GLC
OBJ:	INFINITY	INFINITY	AIR	100	100	
STO:	INFINITY	38.000000	'rad2'	100	100	
2:	INFINITY	2.009389	AIR	100	0	
> IMG:	INFINITY	0.000000		100	100	

```
PRIVATE CATALOG
PWL        632.80
 'rad2'    1.519800
GRC        100
UDG        0.100000
UDG C1     0.1000E+01
UDG C2     0.1000E+03
UDG C3     0.1500E+01
UDG C4     0.5000E+00
UDG C6     0.1236E+00
UDG C7     0.3000E+00
UDG C8     -0.1503E+01
UDG C9     0.6740E-01
UDG C10    0.1087E+02
UDG C11    0.1506E+01
UDG C12    0.3070E-01
UDG C13    -0.1277E-01
UDG C14    0.1155E-01
```

B.3.2.3 Diffusion Time of 120 Hours

	RDY	THI	GLA	CCY	THC	GLC
OBJ:	INFINITY	INFINITY	AIR	100	100	
STO:	INFINITY	40.000000	'rad2'	100	100	
2:	INFINITY	3.263100	AIR	100	0	
> IMG:	INFINITY	0.000000		100	100	

```
PRIVATE CATALOG
PWL        632.80
 'rad2'    1.519800
GRC        100
UDG        0.100000
UDG C1     0.1000E+01
UDG C2     0.1200E+03
```

```
UDG C3     0.1500E+01
UDG C4     0.5000E+00
UDG C6     0.1236E+00
UDG C7     0.3000E+00
UDG C8     -0.1503E+01
UDG C9     0.6740E-01
UDG C10    0.1087E+02
UDG C11    0.1506E+01
UDG C12    0.3070E-01
UDG C13    -0.1277E-01
UDG C14    0.1155E-01
```

B.3.2.4   Optimal Diffusion Time for Different Glass Composition

	RDY	THI	GLA	CCY	THC	GLC
OBJ:	INFINITY	INFINITY	AIR	100	100	
STO:	INFINITY	40.000000	'rad2'	100	100	
2:	INFINITY	2.201738	AIR	100	0	
> IMG:	INFINITY	0.000000		100	100	

```
PRIVATE CATALOG
  PWL       632.80
  'rad2'    1.519800
  GRC       100
  UDG       0.100000
  UDG C1    0.1000E+01
  UDG C2    0.1182E+03
  UDG C3    0.1500E+01
  UDG C4    0.7000E+00
  UDG C6    0.1236E+00
  UDG C7    0.3000E+00
  UDG C8    -0.1503E+01
  UDG C9    0.6740E-01
  UDG C10   0.1087E+02
  UDG C11   0.1506E+01
  UDG C12   0.3070E-01
  UDG C13   -0.1277E-01
  UDG C14   0.1155E-01
```

B.4 Gradient-Index Compact Disk Objective

B.4.1   Index Polynomial Design

	RDY	THI	GLA	CCY	THC	GLC
OBJ:	INFINITY	INFINITY		100	100	
> STO:	1.0000E+10	1.000000	'rad1'	100	100	
2:	INFINITY	0.000000		100	100	
3:	3.94708	1.800000	SFL6_SCHOTT	0	100	
4:	-13.37989	2.428661		0	0	

| 5: | INFINITY | 1.200000 | 'disk' | 100 | 100 |
| IMG: | INFINITY | 0.000000 | | 100 | 100 |

SPECIFICATION DATA

EPD	3.60000		
DIM	MM		
WL	632.80		
REF	1		
WTW	1		
INI	JLB		
XAN	0.00000	0.00000	0.00000
YAN	0.00000	0.70000	1.10000
VUY	0.00000	0.00000	0.00000
VLY	0.00000	0.00000	0.00000

APERTURE DATA/EDGE DEFINITIONS
CA
CIR S1   1.850000

PRIVATE CATALOG

PWL	632.80
'rad1'	1.666940
GRC	100
URN	0.100000
URN C20	0.2178E-02
GRC	0
URN C30	0.2576E-04
GRC	0
URN C40	0.2767E-04
GRC	0
'disk'	1.573654

REFRACTIVE INDICES

GLASS CODE	632.80
'rad1'	1.666940
URN	0.100000
URN C20	0.2178E-02
URN C30	0.2576E-04
URN C40	0.2767E-04
SFL6_SCHOTT	1.798837
'disk'	1.573654

No solves defined in system

INFINITE CONJUGATES

EFL	6.2946
BFL	1.1980
FFL	-3.1611
FNO	1.1111
IMG DIS	1.2000
OAL	5.2287

PARAXIAL IMAGE
HT   0.0768
ANG   1.1000
ENTRANCE PUPIL
DIA   3.6000
THI   0.0000
EXIT PUPIL
DIA   4.5553
THI   -6.7671

B.4.2   Fabricated Index Polynomial Design

	RDY	THI	GLA	CCY	THC	GLC
OBJ:	INFINITY	INFINITY		100	100	
STO:	1.0000E+10	1.600000	'rad1'	100	0	
2:	INFINITY	0.000000		100	100	
> 3:	3.65384	1.600000	SFL6_SCHOTT	0	0	
4:	-17.95210	2.367131		0	0	
5:	INFINITY	1.200000	'disk'	100	100	
IMG:	INFINITY	0.000000		100	100	

SPECIFICATION DATA
EPD   3.20000
DIM   MM
WL   632.80
REF   1
WTW   1
INI   JLB
XAN   0.00000   0.00000   0.00000
YAN   0.00000   0.70000   1.00000
VUY   0.00000   0.00000   0.00000
VLY   0.00000   0.00000   0.00000

APERTURE DATA/EDGE DEFINITIONS
CA
CIR S1   1.800000

PRIVATE CATALOG
PWL   632.80
'rad1'   1.664000
GRC   100
URN   0.100000
URN C10   -0.9292E-03
GRC   100
URN C20   0.1689E-02
GRC   100
URN C30   -0.1560E-03
GRC   100
URN C40   0.4994E-04
GRC   100

'disk'   1.573654

REFRACTIVE INDICES
  GLASS CODE   632.80
'rad1'   1.664000
URN   0.100000
URN C10   -0.9292E-03
URN C20   0.1689E-02
URN C30   -0.1560E-03
URN C40   0.4994E-04
SFL6_SCHOTT   1.798837
'disk'   1.573654

No solves defined in system

INFINITE CONJUGATES
  EFL   6.1240
  BFL   1.1848
  FFL   -2.7804
  FNO   1.2161
  IMG DIS   1.2000
  OAL   5.5671
  PARAXIAL IMAGE
  HT   0.0679
  ANG   1.0000
  ENTRANCE PUPIL
  DIA   3.2000
  THI   0.0000
  EXIT PUPIL
  DIA   4.4788
  THI   -7.3865

B.4.3   Diffusion Model Design

	RDY	THI	GLA	CCY	THC	GLC
OBJ:	INFINITY	INFINITY		100	100	
> STO:	1.0000E+10	1.837553	'rad2'	100	0	
2:	INFINITY	0.000000		100	100	
3:	3.94411	1.800000	SFL6_SCHOTT	0	100	
4:	-11.61496	2.334947		0	0	
5:	INFINITY	1.200000	'disk'	100	100	
IMG:	INFINITY	0.000000		100	100	

SPECIFICATION DATA
  EPD   3.20000
  DIM   MM
  WL   632.80
  REF   1
  WTW   1
  INI   JLB

XAN	0.00000	0.00000	0.00000
YAN	0.00000	0.70000	1.00000
VUY	0.00000	0.00000	0.00000
VLY	0.00000	0.00000	0.00000

APERTURE DATA/EDGE DEFINITIONS
CA
CIR S1   1.850000

PRIVATE CATALOG
PWL   632.80
'rad2'   1.666940
GRC   100
UDG   0.100000
UDG C1   0.1000E+01
UDG C2   0.7951E+01
GRC   0
UDG C3   0.1900E+01
UDG C4   0.4000E+00
UDG C5   0.1000E+01
UDG C6   0.1220E+00
UDG C7   -0.2394E+00
UDG C8   -0.1271E+01
UDG C9   -0.2709E+00
UDG C10   0.9859E+01
UDG C11   0.1632E+01
UDG C12   0.1418E+00
UDG C13   -0.2056E+00
UDG C14   0.1970E+00
UDG C15   -0.7828E-01
'disk'   1.573654

REFRACTIVE INDICES
GLASS CODE   632.80
SFL6_SCHOTT   1.798837
'disk'   1.573654
'rad2'   1.666940
UDG   0.100000
UDG C1   0.1000E+01
UDG C2   0.7951E+01
UDG C3   0.1900E+01
UDG C4   0.4000E+00
UDG C5   0.1000E+01
UDG C6   0.1220E+00
UDG C7   -0.2394E+00
UDG C8   -0.1271E+01
UDG C9   -0.2709E+00
UDG C10   0.9859E+01
UDG C11   0.1632E+01
UDG C12   0.1418E+00
UDG C13   -0.2056E+00

UDG C14	0.1970E+00
UDG C15	-0.7828E-01
'disk'	1.573654

No solves defined in system

INFINITE CONJUGATES
EFL	6.2946
BFL	1.4292
FFL	-2.6189
FNO	1.1111
IMG DIS	1.2000
OAL	5.9725

PARAXIAL IMAGE
HT	0.0768
ANG	1.1000

ENTRANCE PUPIL
DIA	3.6000
THI	0.0000

EXIT PUPIL
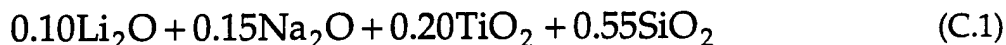| DIA	5.5206
THI	-8.2236

Appendix C
Titania Silicate Glass

C.1 Introduction

In this appendix, the concentration dependence of the diffusion coefficient for the glass composition given by

$$0.10\text{Li}_2\text{O} + 0.15\text{Na}_2\text{O} + 0.20\text{TiO}_2 + 0.55\text{SiO}_2 \qquad \text{(C.1)}$$

is calculated from an experimental axial index of refraction profile using a Boltzmann-Matano technique. The result is then fit to the MQC diffusion coefficient model for use in the diffusion model to predict the index of refraction profile for the compact disk objective design presented in Chapter 6.

C.2 Diffusion Coefficient Calculation

This particular glass composition is not one which was studied in an axial geometry by this author for diffusion modeling and was only used to make the radial gradients presented in Chapter 6. Therefore, an index of refraction profile measured by Kindred from experiment DSK-42 was used to calculate the concentration dependence of the diffusion coefficient for Li^+ for Na^+ exchange. The measured index of refraction profile is shown in Fig. C.1.

The index of refraction as a function of concentration data presented in Chapter 5 is used to change the index of refraction profile to a concentration profile. The calculated diffusion coefficient is then shown in Fig. C.2 along with the MQC fit to the data. The particular coefficients for this fit are listed in Table C.1.

Note: although the temperature for this diffusion was nominally 550 °C it was only read from the oven controller and not measured with a thermocouple. Therefore, the diffusion times obtained with a diffusion model which uses this axial experiment may be incorrect. Furthermore, the glass composition is slightly different the actual glass composition
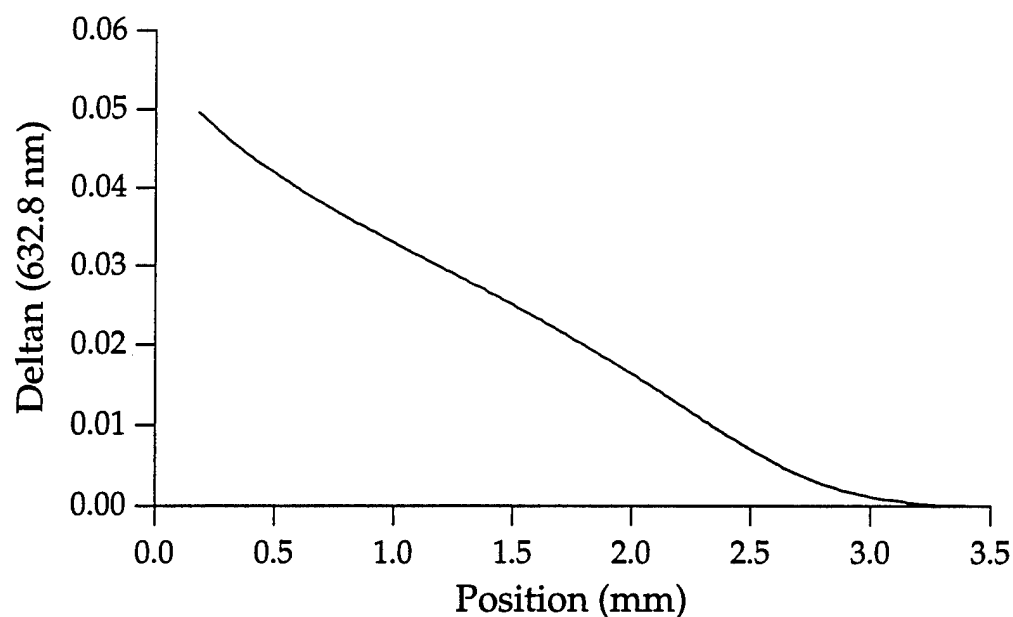
used in the fabrication of the gradient for the compact disk objective. For a more accurate representation of the diffusion process, a new axial experiment is needed at a measured temperature and in the correct glass composition.

Figure C.1 Measured index of refraction profile for experiment DSK-42 for a 72 hour Li^+ for Na^+ diffusion at 550 °C in the glass 0.25 Na_2O + 0.10 TiO_2 + 0.55 SiO_2.
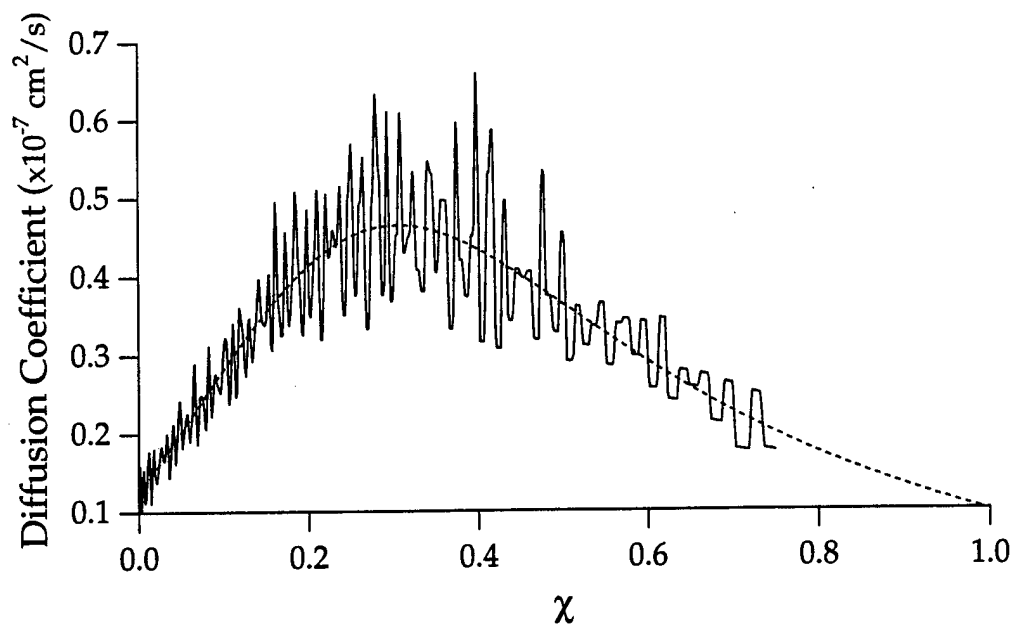
Figure C.2 Calculate diffusion coefficient for experiment DSK-42 for a 72 hour Li$^+$ for Na$^+$ diffusion at 550 °C in the glass 0.25 Na$_2$O + 0.10 TiO$_2$ + 0.55 SiO$_2$. The MQC diffusion coefficient fit is also shown.

Exp. #	x Li$_2$O	D$_B$	α	ρ	χ_0	c
DSK-42	0.0	0.1220	-0.2394	-1.2706	-0.2709	9.86

Table C.1 MQC fit parameters for the concentration dependent diffusion coefficient for experiment DSK-42 in the glass composition 0.25 Na$_2$O + 0.20 TiO$_2$ + 0.55 SiO$_2$.